Investigation of the use of Electro Active Polymer as a Paediatric VAD Driver

Moutaz Hamdan

Supervisor: Prof. Terence Gourlay

Department of Biomedical Engineering
University of Strathclyde
This thesis is submitted in accordance with the regulations governing the award of the Degree of Doctor of Philosophy in Biomedical Engineering
2017

Declaration of Authenticity and Author's Rights:

This thesis is the result of the author's original research. It has been composed by the author and has not been previously submitted for examination which has led to the award of a degree.

Signed:

Date:

Acknowledgments

I would like genuinely to thank my supervisor Professor Terry Gourlay for his advice, support and help throughout my time here at the University of Strathclyde. His wealth of experience and knowledge in the cardiovascular area guided me to produce this piece of work. Without his vision, the project could not have begun.

I would also like to express my thanks to the Biomedical Engineering staff for their support during my PhD in all workshops and labs.

Special thanks to my parents Adnan and Inaam, who gave all that they can and helped me to achieve this degree.

Thanks to my siblings Asmaa, Hiba, Mouaz, Salam, and their families for their support and encouragements over the years of my study.

Also, special thanks for Dr Taja and Mr AL Bali for their great support for the whole of my life.

Thanks to all my friends in Glasgow, and back home in Syria for their support and encouragements.

Abstract

Background

Heart failure is one of the principal causes of death and disability. The causes of heart failure are many, and a number of technologies have been developed to address this issue by providing support to the failing heart, both as a permanent solution and as a bridge to recovery. These options are called Mechanical Circulatory Support Devices, a particular branch of these devices is the Ventricular Assist Devices, which have been under intense development over the recent years offering a promising solution for this major problem. However, these devices are still bulky, and heavy designed to support failing hearts in the adult population. On the other hand, little has been done in recent times on the development of implantable solutions for heart failure or insufficiency in children. There are many reasons for this, but primarily the relatively small number of children requiring these procedures, the challenges associated with growth, and the lack of physical space for such implantable circulatory support technologies in children are fundamental limitations to the development and deployment of these technologies.

Aims of the project

The primary purpose of this project was to investigate the development of a new miniaturised self-power VAD that is suitable for paediatrics implantation. This project suggested the use of the newly developed Artificial Muscles to create a mesh that envelops the heart and works as an external assisting circulation mechanism. The same materials could be used to generate electricity when deformed, which can be used to power the proposed device. Critically, the project was to focus on optimising the materials with regard to their operating efficiency to ascertain whether they represent a viable option for VAD production.

Materials and Methods

A full review of the current available Artificial Muscles was performed to choose the most suitable type for this project. Then different fabrication protocols were developed to make IPMC Artificial Muscles using platinum and palladium coatings. A series of characterization tests were conducted on the fabricated Ionic Polymeric Metal Composites (IPMC) to ensure

their quality. Finally, the mechanical and electrical properties were tested and compared with the proposed device requirements.

Results

The review of Artificial Muscles showed that IPMC would be the best candidate to use in this application. The characterisation tests showed as well that the produced IPMC Artificial Muscles were fabricated to the same standards as those commercially available, and the reported by other investigators. However, these materials showed very low mechanical output with high electrical power consumption, which made them far from practical and not suitable for the proposed application. On the other hand, IPMCs showed promising results as an option to generate electricity to power low consumption implantable devices.

Keywords

Heart

Paediatrics

Cardiovascular

Electro Active Polymers

Artificial Muscles

Ventricular Assists Devices

Mechanical Circulatory Support Devices

Blocking Force

Tip Displacement

Power Harvesting

Surface Resistance

Polymers

Ionic Polymer Metal Composites

Table of Contents

List of Tables

List of Figures

List of Abbreviations

Alternative Current (AC)

Analogue to Digital Converter (ADC)

Arterial Septal Defect (ASD)

Beats Per Minute (BPM)

Bi-Ventricular Assist Device (BiVAD)

Bridge To Decision (BTD)

Bridge To Recovery (BTR)

Bridge To Transplant (BTT)

Carbon NanoTube (CNT)

Cardiopulmonary Bypass (CPB)

Conductive Polymers (CP)

Congenital Heart Disease (CHD)

Coronary Artery Disease (CAD)

Data Acquisition (DAQ)

Destination Therapy (DT)

Dielectric Elastomer (DE)

Digital to Analogue Converter (DAC)

Dimethylformamide (DMF)

Direct Current (DC)

Electroactive Ceramics (EAC)

Electro-Active Polymer (EAP)

Electromyography (EMG)

Electrorheological Fluid (ERF)

Extracorporeal Membrane Oxygenation (ECMO)

Inferior Vena Cava (IVC)

Integrated Circuit (IC)

Intensive Care Unit (ICU)

Intra-Aortic Balloon Pump (IABP)

Ionic Polymer Metal Composite (IPMC)

Ionic Polymeric Gel (IPG)

Latissimus Dorsi (LD)

Left Ventricular Assist Device (LVAD)

Liquid Crystal Elastomer (LCE)

Material Testing System (MTS)

Mechanical Circulatory Support Devices (MCSD)

Muscle Energy Converter (MEC)

Muscle Powered Cardiac Assist Device (MCAD)

National Instruments (NI)

Pneumatic Artificial Muscles (PAM)

Proton Exchange Membrane (PEM)

Pulmonary Artery Pressure (PAP)

Right Atrium (RA)

Right Ventricular Assist Device (RVAD)

Root Mean Square (RMS)

Scanning Electron Microscope (SEM)

Shape Memory Alloy (SMA)

Skeletal Muscle Ventricle (SMV)

Superior Vena Cava (SVC)

Tetralogy Of Fallot (TOF)

Ultraviolet (UV)

Ventricular Assist Devices (VAD)

Ventricular Septal Defect (VSD)

Water Uptake (WUP)

Thesis Outline

Chapter 1 introduces the anatomy of the heart, coronary arteries, and the blood circulation system in general. Then it moves to describe the cardiovascular diseases that affect the heart and lead to end stage heart failure. The final part of this chapter describes the available options of Mechanical Circulatory Support Devices.

Chapter 2 details the objectives and the concept of the project. Then it explains the history, types, and properties of Artificial Muscles. Finally, it lists the proposed solutions and hypothesis to create a VAD from Artificial Muscles.

Chapter 3 starts with determining the requirements of proposed devices. Then explains the primary investigation phase of IPMC Artificial Muscles. After that, it moves to detail the process of making IPMC samples and their electrical driver.

Chapter 4 lists all the tests conducted on IPMC Artificial Muscles to evaluate their properties. These tests are surface scanning, measuring thickness, measuring water uptake, measuring surface resistance, electrical power consumption, displacement, and blocking force.

Chapter 5 describes the use of IPMC for power harvesting and sensing.

Chapter 6 discusses and explains the results of the proposed device.

Chapter 7 concludes finding of the project.

Chapter 8 describes the limitations that were faced during the project.

Chapter 9 lists the future development of the proposed device.

Chapter 1
Background

1. *Physiological Background*

1.1 Introduction

Heart transplantation is still the gold standard for patients suffering from end-stage heart failure. According to the World Health Organization, one in 33 infants born has one or more congenital anomaly, some of these patients require surgical intervention in their first month of life (Hines 2013). In the USA alone, more than 9,000 infants are born with congenital heart problems annually, just 400 of them will have their chance to get a new heart (Fynn-Thompson and Almond 2007). The cost of cardiovascular diseases and stroke in the United States is estimated at more than $300 billion a year (Shahinpoor 2010). Due to the shortage of donors (Mitamura 2015), and the high risk of rejection of the donated heart, Mechanical Circulatory Support Devices (MCSD) are used to support the patient's heart while a long-term solution is considered. In the last three decades, mechanical support devices have been the focus of considerable development activity, offering a broad range of solutions for patients with end-stage heart failure as a bridge to decision (BTD), bridge to transplant (BTT), bridge to recovery (BTR), or finally as a destination therapy (DT) for the whole life (Timms 2011, Sabashnikov, Mohite et al. 2014).

Until recently, the most popular and reliable solution for this problem was using venoarterial Extracorporeal Membrane Oxygenation (ECMO). ECMO can offer full cardiac support that can be applied rapidly. On the other hand, it can be implemented only for a short time, over a few days in most cases, with a few weeks being the extreme range of deployment (Fynn-Thompson and Almond 2007). Centrifugal pumps are also used as an extracorporeal circuit in infants and children, supporting them from a few days to a few weeks. Under both treatment modalities, patients are confined to the Intensive Care Unit (ICU) setting (Potapov, Stiller et al. 2007).

More advanced mechanical support devices are the Ventricular Assist Devices (VAD), which can help the patient's heart longer than ECMO. VADs can be divided into several categories depending on the flow, place of implantation and the supporting system that can offer to the heart (Potapov, Stiller et al. 2007).

1.2 Anatomy of the Heart

2.1 The Heart

The heart is the most important working muscular organ in all living creatures, playing a significant role in providing oxygenated blood and nutrients to all of the living cells. In humans, the heart is located in the anterior chest wall directly posterior to the sternum. Connected to it are the great blood vessels, the aorta, the vena cava, the pulmonary arteries, and pulmonary veins, as shown in **Figure 1.1** and **Figure 1.2**. The healthy adult's heart measures around 12.5 cm in length, and it has a mass between 250 g and 350 g. The adult's heart usually beats between 60 and 100 times a minute, while the baby's heart may beat up to 190 times a minute. During an average lifetime, the human heart will beat more than three billion times, pumping more than 160 million litres of blood (Martini F. 2011). On average, each day the human's heart pumps 7,500 litres of blood and beats 100,000 times (Shahinpoor 2010).

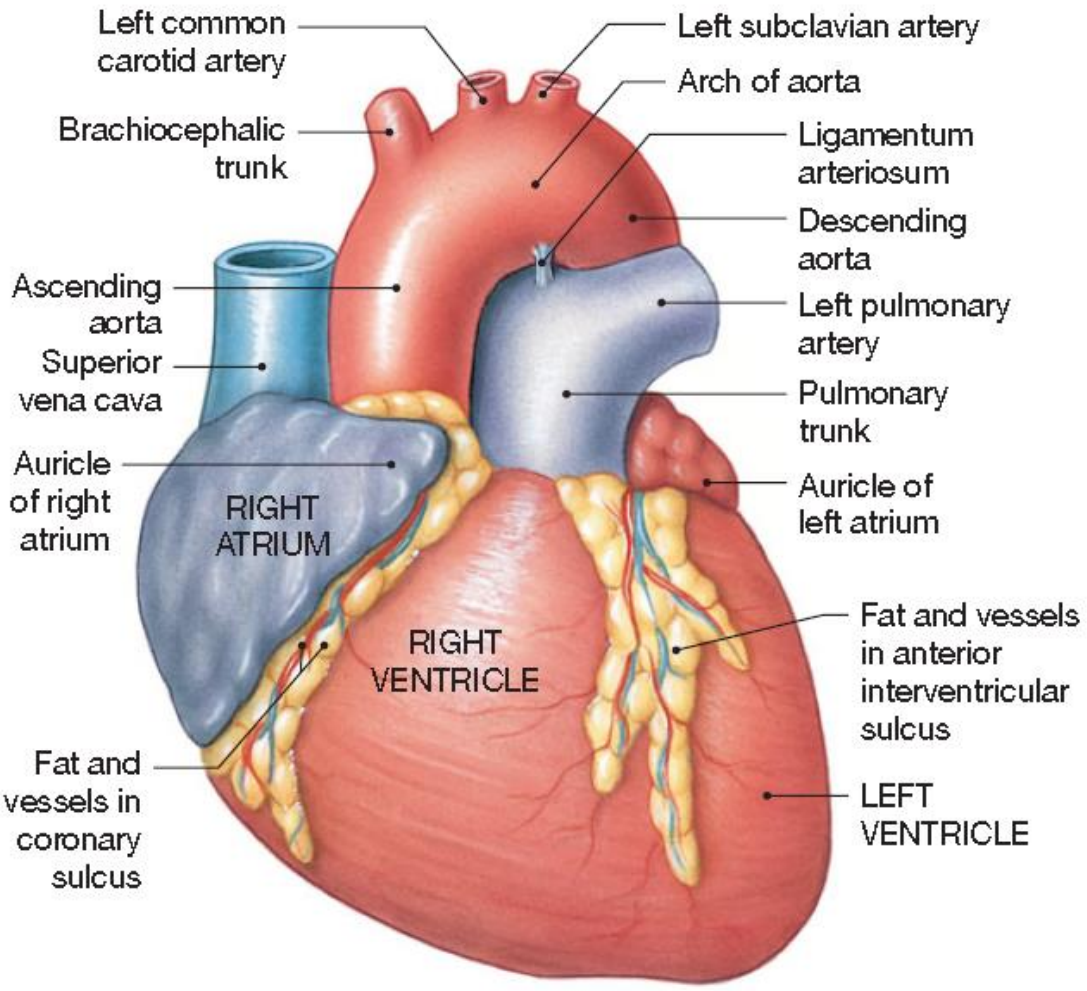

Figure 1.1 The Heart (Martini F. 2011)

The wall of the heart consists of three primary layers, the Epicardium, the Myocardium, and the Endocardium. The first layer covering the outer surface of the heart is the Epicardium; this layer consists of an exposed mesothelium and an underlying layer of loose areolar connective tissue, which is connected with the second layer. The second layer is the Myocardium, which is the primary muscular layer forming the atria and ventricles. This layer consists of concentric layers of cardiac muscle tissue; it also contains blood vessels and nerves. The third layer is the Endocardium, which covers all the inner surfaces of the heart including the valves. The thickness of the heart wall is not equal in all heart chambers; the left ventricle has a thicker wall which enables it to pump the large systemic circuit through the body at a high arterial pressure (Martini F. 2011).

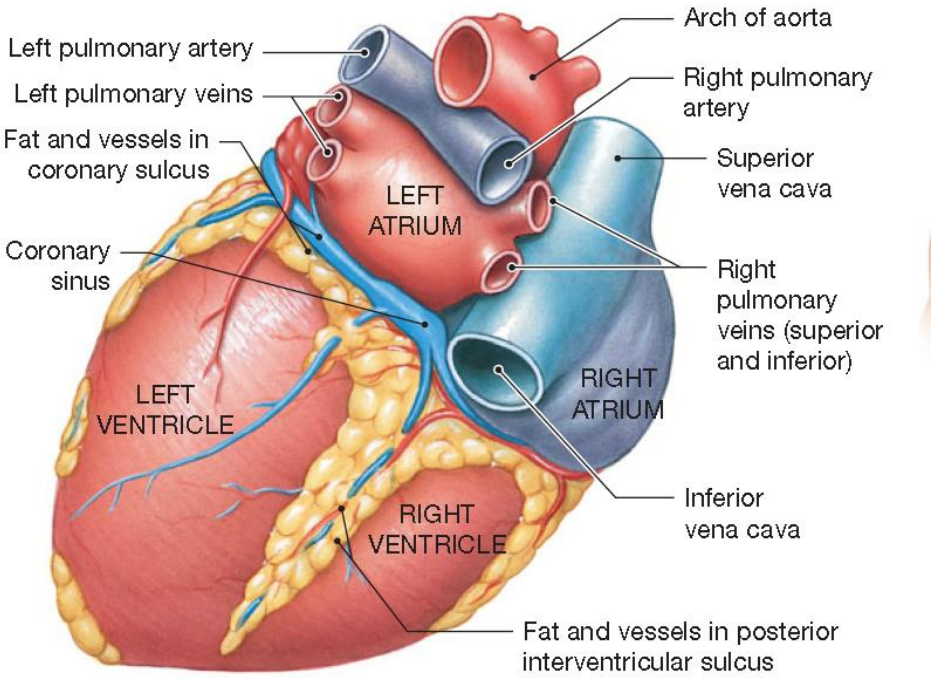

Figure 1.2 The Heart (Martini F. 2011)

The heart consists of four main chambers: two ventricles and two atria, as shown in **Figure 1.3**. The right atrium is located on the top right side of the heart, receives the deoxygenated blood from all parts of the body through the Superior Vena Cava (SVC) and the Inferior Vena Cava (IVC), and is connected to the right ventricle through the tricuspid valve. The left atrium is located on the top left side of the heart, receives all oxygenated blood from the left and right lungs through the pulmonary veins and delivers this blood to the left ventricle through the mitral valve. The right ventricle is located on the right bottom side of the heart, receives the deoxygenated blood from the right atrium and pumps it to the left and right pulmonary

arteries through the pulmonary valve to the left and right lungs. The left ventricle, which is normally the largest chamber of the heart, is located on the left bottom side of the heart, receives the oxygenated blood from the left atrium and pumps it to the whole body throughout the aortic valve and the aorta. The aorta is then divided into several branches to cover all parts of the human body. A thick muscular wall called the septum separates the right side and the left side of the heart. In each heartbeat, the right side of the heart pumps the same amount of blood into the lungs and the left side of the heart into the body. Commonly, physicians refer to the right atrium and right ventricle as the right heart, and the left atrium and the left ventricle as the left heart (Martini F. 2011).

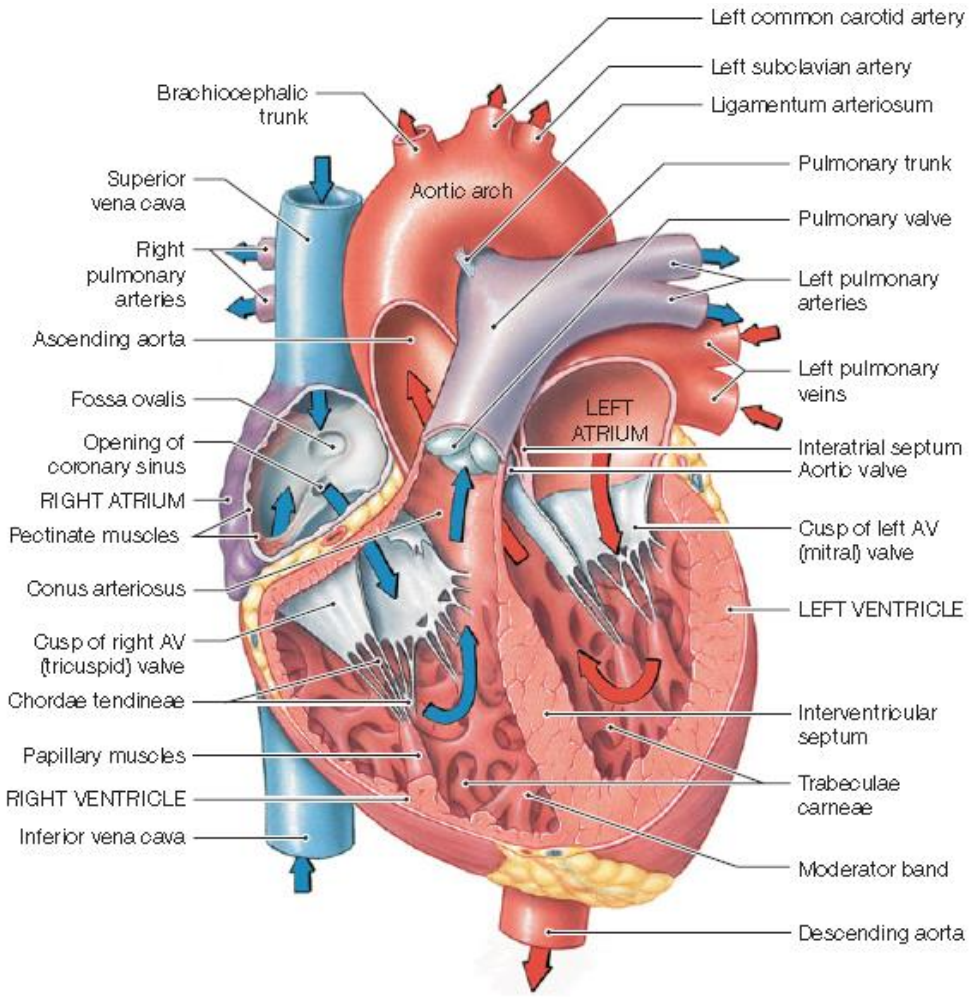

Figure 1.3 Heart Valves (Martini F. 2011)

2.2 The Coronary Circulation

Since the heart is a continuously working pump, it requires a constant energy supply. The coronary circulation, which supplies the heart and its muscular cells with the oxygen, provides this energy and nutrients needed and removes all the waste products. Interestingly, the first

function of the heart is to supply nutrients to itself. The coronary circulation, shown in **Figure 1.4**, consists of the left and right coronary arteries, which are branched from the ascending aorta. Also the cardiac veins, which are connected to the right atrium near the base of the inferior vena cava. The coronary circulation is crucial; any blockage to this circulation, even partially blockage, will cause a reduction in the cardiac performance and can result in a heart attack. This blockage in the coronary circulation system is called a Coronary Artery Disease (CAD)(Martini F. 2011).

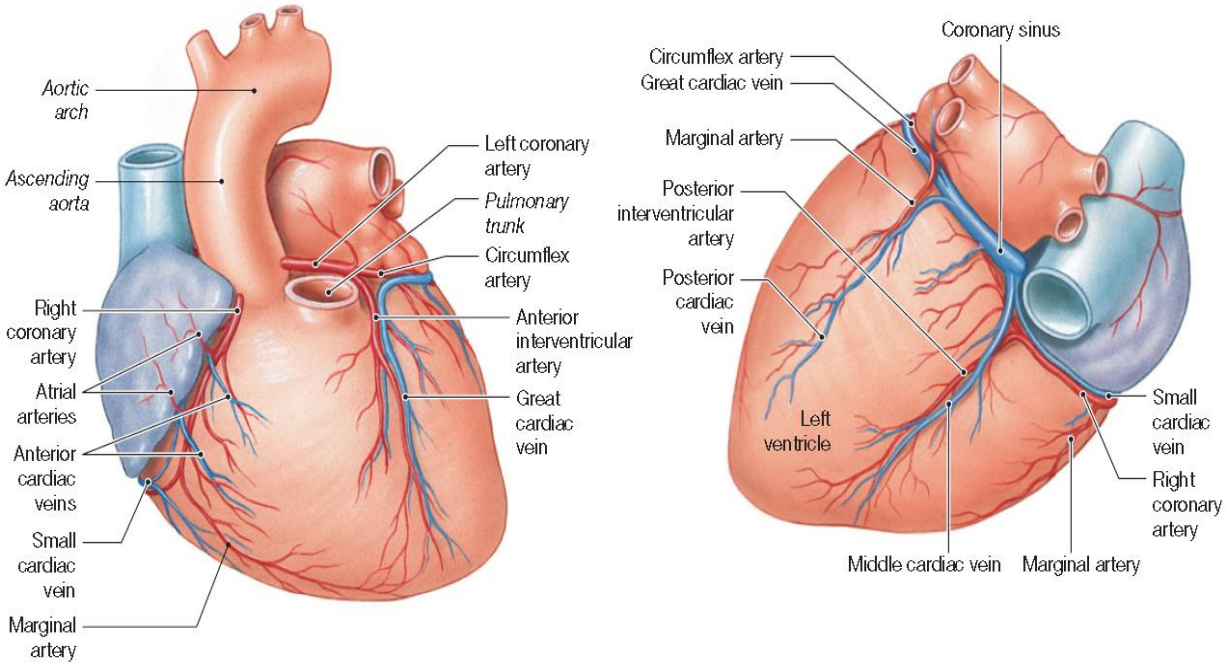

Figure 1.4 The Coronary Circulation (Martini F. 2011)

2.3 The Blood Circulatory System

The blood circulatory system, shown in **Figure 1.5**, consists of the heart and two blood circuits connected with it: the pulmonary circuit, and the systemic circuit. In the pulmonary circuit, the deoxygenated blood from all parts of the body is collected in the right side of the heart and then pumped to the lungs, where gaseous exchange occurs, deoxygenated blood is converted to oxygenated blood, and redirected to the left side of the heart. In the systemic circuit, the oxygenated blood is pumped from the left side of the heart to all parts of the body to supply the tissues with oxygen and nutrients needed for their various functions, and to collect the metabolic waste products from all living cells. Following this, the deoxygenated blood is returned to the right side of the heart to complete the circuit(Martini F. 2011).

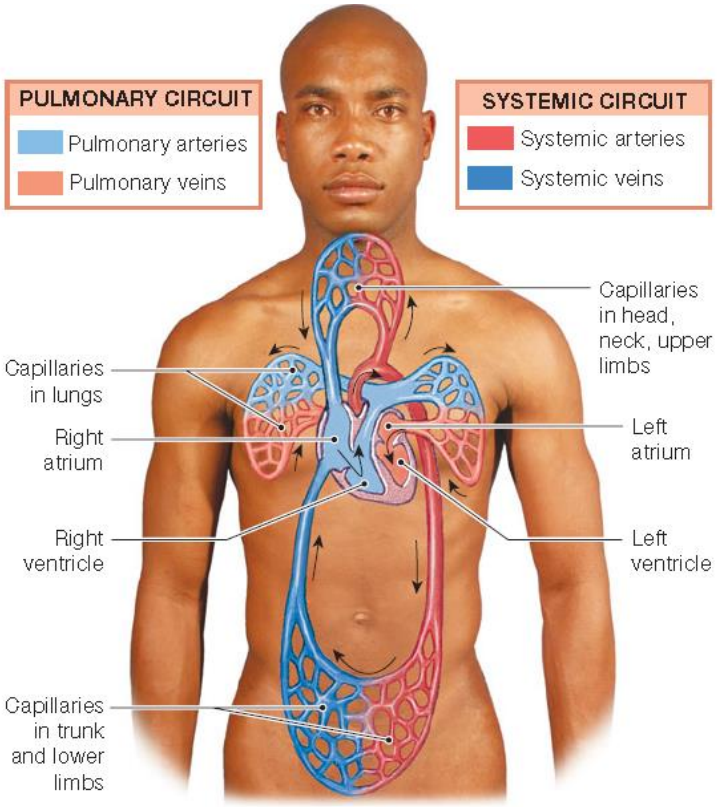

Figure 1.5 The Blood Circulatory System (Martini F. 2011)

2.4 The Embryonic Heart

There are several phases of fetal heart development. The first phase is Tube Formation, between 15 and 20 days, where the heart has a shape of two bent tubes and begins to beat. The second phase is Looping, between 21 and 28 days. In this stage, distinct chambers start to appear, the left and right ventricles became more evident. The third phase is Atrial Septation, between 34 and 50 days. Here, the septum grows from the ventral wall of the atrium and forms a ridge on the posterior wall of the atria. The fourth phase is Outflow Tract Septation between 35 and 56 days. In this stage, the outflow tract begins as a single tube connected with the ventricles, by the end of this stage the aorta and the pulmonary outflow are separated and attached to the left and right ventricles respectively. The fifth phase is Ventricular Septation, between 38 and 45 days, in this phase, the separation between the ventricles is completed (Yeung 2007). Development of an embryonic heart is a very complicated process, any small change during this process can cause congenital heart disease of the fetus.

2.5 Paediatric Cardiovascular System:

Paediatric patients fall into the followings categories shown in **Table 1.1**:

Neonates	A baby within 44 weeks of age from the date of conception
Infants	A child of up to 12 months of age
Child	1 to 12 years
Adolescent	13 to 16 years

Table 1.1 Paediatric age range (Macfarlane 2006)

In neonates, the myocardium is less contractile, causing the ventricle to be less compliant and less able to generate tension during contraction. That is why they have a higher heart rate compared to the other groups (Macfarlane 2006). **Table 1.2** shows the changes in heart rate and blood pressure in the paediatric range.

Age	Heart rate (BPM)	Blood Pressure (mm Hg)
Preterm	130	120-170
Newborn	120	100-170
1-11 months	120	80-160
2 years	110	80-130
4 years	100	80-120
6 years	100	75-115
8 years	90	70-110
10 years	90	70-110
14 years boy	80	60-100
14 years girl	85	65-105
16 years boy	75	55-95
16 years girl	80	60-100

Table 1.2 Heart rate and blood pressure in the paediatric range (Macfarlane 2006)

1.3 Cardiovascular Diseases

2.1 Congenital Heart Disease

Congenital Heart Disease (CHD) is any defect or change in the structure of the healthy heart and the primary vessels connected with it, which appears directly after birth. The chance of having congenital heart disease is 6 in 1000 births and occurs in similar frequencies in each part of the world within all ethnic groups (Kenny and Stuart 2009).

Depending on the direction of blood flow through intracardiac shunts, congenital heart disease can be classified into different types. Blood flowing from left side to the right side of the heart is called acyanotic defect. Arterial Septal Defect (ASD) is an example of the acyanotic defect, where the blood flows from the left atrium to the right atrium. The oxygenated blood in the left atrium is mixed with the deoxygenated blood in the right atrium, which causes an increased volume load on the right atrium. The other case when the blood is flowing from the right side to the left side of the heart is called a cyanotic defect. The most common example is Tetralogy of Fallot (TOF), where the right ventricle outflow tract is narrowed. In TOF, the deoxygenated blood in the right ventricle faces a significant resistance to flow into the pulmonary artery, and as a result, blood then follows the lower resistance path which is the Ventricular Septal Defect (VSD) and flows to the aorta without undergoing gaseous exchange in the lungs. Some children may suffer from both cases together; this case is called mixed lesion CHD or complex CHD (Woodward 2011).

Infants with complex CHD may suffer from poor nutrition due to their poor appetites, which can have a substantial effect on their healthy growth. Unrepaired CHD in the early stages of life increases the risk of morbidity and mortality due to underlying cardiopulmonary compromises (Woodward 2011).

2.2 Myocardial Dysfunction

Children suffering from myocardial dysfunction can be streamed into one of two clinical approaches; a bridge to recovery in reversible dysfunction cases, and a bridge to heart transplantation in more severe cases. Paediatric patients suffering from reversible myocardial dysfunction can be treated with a Mechanical Circulatory Support Device (MCSD) as a bridge to recovery. Reversible myocardial dysfunction includes postcardiotomy myocardial dysfunction, acute myocarditis, or acute post-transplant rejection. Children with end-stage

congenital heart disease and prolonged graft rejection after heart transplantation are candidates for long-term support with MCSDs as a bridge to transplantation or in other cases as a destination therapy (Chang and McKenzie 2005).

2.3 Cardiopulmonary Resuscitation

MCSDs are used to rescue the patient's heart after the failure of conventional resuscitation. All cardiac intensive care units should be able to support the patient with an MCSD, in this case, in a matter of a few minutes (Chang and McKenzie 2005).

2.4 Preoperative Stabilisation

MCSDs are used to support paediatric patients with cardiovascular collapse, or severe hypoxemia before any surgical intervention is undertaken. Some cases that are considered under this situation are pulmonary hypertensive crises, total anomalous pulmonary venous connection, tetralogy of Fallot with the absence of pulmonary valve, or Ebstein's anomaly (Chang and McKenzie 2005).

2.5 Acute Respiratory Distress Syndrome

Extracorporeal Membrane Oxygenation (ECMO) is the primary option for parenchymal lung disease in paediatrics. Patients with congenital heart disease are more prone to develop parenchymal lung disease before or after their cardiac surgery. ECMO is used for a few weeks to support patients suffering from parenchymal lung disease, allowing more time for the lungs to recover (Chang and McKenzie 2005).

2.6 Malignant Dysrhythmias

In some rare cases, patients who fail conventional aggressive medical therapy for continuous tachydysrhythmias may be suitable for a short-term support with MCSDs. Patients in this case, may suffer from lethal arrhythmias associated with myocardial disease, supraventricular tachycardia, ventricular tachycardia, or junctional ectopic tachycardia (Chang and McKenzie 2005).

2.7 Profound Cyanosis

Paediatric patients diagnosed with cyanosis need to be corrected. MCSDs can be used to support these patients on a case-by-case basis. Some alternative options could be possible to help patients with cyanosis, but MCSDs are used if all the previous options fail (Chang and McKenzie 2005).

2.8 Dilated Cardiomyopathy

Cardiomyopathy disease is a disease that affects the heart's muscle or in other words the wall of the heart. Cardiomyopathy includes abnormal changes in the size of the heart chambers, the wall thickness, or abnormalities in heart functions such as systolic or diastolic dysfunctions. Dilated cardiomyopathy is the most common type of cardiomyopathy in the world, in this case, the left ventricle or the ventricles are enlarged and contract very weakly (Jefferies and Towbin 2010).

1.4 Mechanical Circulatory Support Device (MCSD)

The first report of MCSD use was in 1967 when Dr Debakey used a left atrial- axillary artery ventricular assist device in a teenager's heart to recover him from postcardiotomy failure after mitral valve replacement. This was the first successful use of MCSD and the patient recovered after six months (Fynn-Thompson and Almond 2007).

The use of centrifugal pump systems started in the 1970s, supporting infants and children in their early age (<6 kg). This type of treatment had excellent reports at that time, but also it has the same problems with as ECMO, such as non-pulsatile blood flow and a short support time (Fynn-Thompson and Almond 2007).

During the early 1990s, VAD systems emerged in greater numbers and configurations. Extracorporeal systems have been used in medium size children, and the results were generally encouraging. Some problems arose with the use of VAD systems, including those associated with thrombogenicity. However, the development of VADs advanced and had been developed to the degree of use in infants and small children, offering both pulsatile and continuous blood flow modalities. Despite the huge advancement achieved in this field, there remains a compromise between clinical need and safety in the use of VADs in the paediatric domain with none yet meeting the ideal criteria (Fynn-Thompson and Almond 2007, Timms 2011).

The fundamental purpose of MCSD is to save the patient's life in emergency cases. They are primarily used to support the patient's heart for short periods, but the following devices have been developed to help the patient for longer periods.

MCSDs are divided into three main groups

- Extracorporeal Membrane Oxygenation (ECMO).
- Centrifugal Pumps.
- Ventricular Assist Devices (VADs).

1.5 Extracorporeal Membrane Oxygenation (ECMO)

ECMO is the first solution used to support children suffering from heart failure. Lack of alternatives and the long time experience in applying ECMO as a treatment for respiratory and heart failure make ECMO the leading approach at present. The first child to have ECMO support was a nine years old boy in the late 1980s, reported by Dr Denton Cooley. This boy was supported for 12 hours until a suitable donor was found. This case was the beginning of the use of MCSDs in paediatric patients and has opened all the options for researchers in this field (Frazier, Bricker et al. 1989).

The ECMO circuit as shown in **Figure 1.6** below consists of the following components:

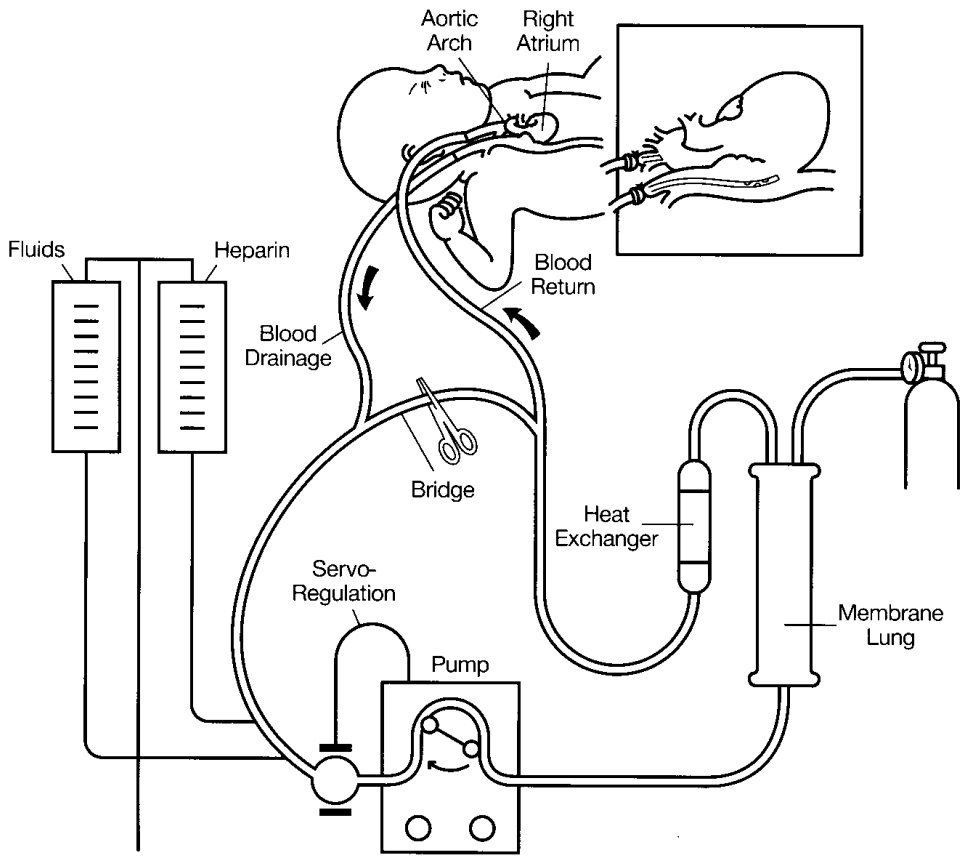

Figure 1.6 ECMO circuit (Lodge, Antunez et al. 2012)

- **Blood Pump:** Gravity drainage is responsible for flowing the blood from the patient's Right Atrium (RA) to a blood reservoir before the pump, the pump then pumps the blood from the reservoir to the other components. It could be a centrifugal pump or roller head pump (Palanzo, El-Banayosy et al. 2013).
- **Oxygenator:** or the artificial lung, where the blood status will change from deoxygenated into oxygenated blood. This oxygenator is connected to an external oxygen gas source to keep the gaseous exchange running.
- **Heat Exchanger:** is applied to maintain the blood temperature at a fixed point.
- **Tubing Set:** a set of tubes and cannulas that are used to connect the patient's heart with the other components. Special cannulas are used depending on the type of support applied on the patient. Some cannulas are directly applied to the heart while others are applied peripherally.
- **Monitoring System:** control and monitor all the components and the parameters, such as blood flow and temperature. Provide the user also with the appropriate alarms.

Due to the presence of the oxygenator, it can also offer support for the lungs when the heart disease is associated with hypoxia or pulmonary hypertension. ECMO is an option that can offer a cardiac support alone, pulmonary support only, or a combination of both. In children, the primary cause of using ECMO is a failure to recover from cardiopulmonary bypass (CPB) after cardiac surgery or in the case of fulminant myocarditis (Amodeo, Brancaccio et al. 2010).

ECMO is associated with several complications due to the large artificial surface area of contact between the circuit and patient's blood, which requires a high level of anticoagulation. Some of these complications are thromboembolic and bleeding. Using cannulas can also cause some problems, such as infection due to the open chest, and immobilisation. The continuous non-pulsatile flow could also be a possible cause of end-organ failures, such as kidneys and liver, besides the neurological complications. Short term support could be considered as one of the limitations in using ECMO, where it can be applied just for few weeks maximum (Fynn-Thompson and Almond 2007). These problems caused ECMO patients to have a high mortality, with a 50% chance of survival and discharge from the hospital (Jeewa, Manlhiot et al. 2010). On the other hand, ECMO still has some advantages, such as supporting both heart and lung at the same time, biventricular support, quick and

easy installation, accommodation of neonatal size limitations, inexpensive compared to the other solutions, and the large international neonatal and paediatric experience (Lodge, Antunez et al. 2012).

2.1 Centrifugal Pumps

This system is very similar to ECMO, but without the oxygenator and heat exchanger, it is also used for a short-term support. The system consists of a centrifugal pump, control console, and a set of tubes that connect the patient's heart with the pump. A non-pulsatile flow is provided by a vortex technology, where an impeller rotates at speeds between 1,000 and 4,000 RPM to create a flow of 5 - 6 L/min (Potapov, Stiller et al. 2007). Blood enters from the centre of the pump and leaves from the side; blood path is shown in **Figure 1.7**.

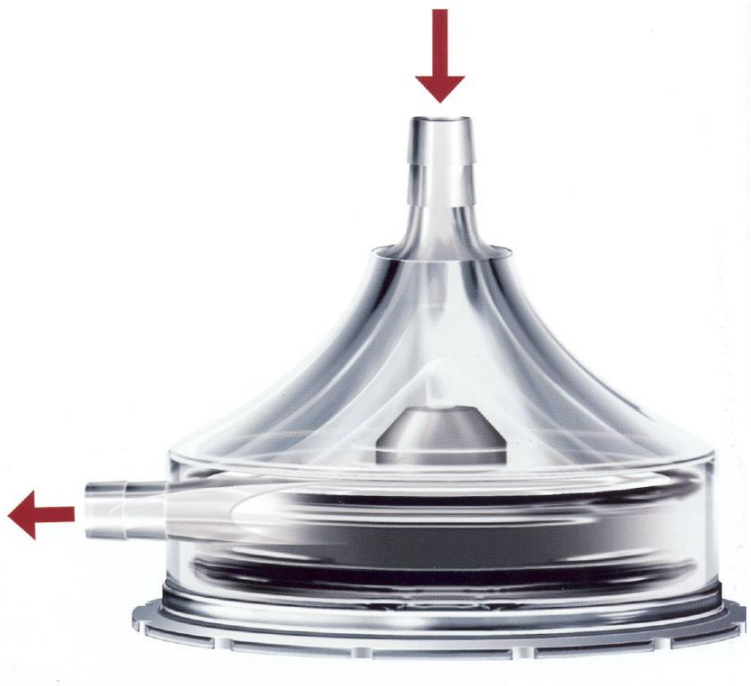

Figure 1.7 Centrifugal Pump (Adachi and Fraser 2011)

The main advantage of this system is the low priming volume of the pump and short length of the tubing system, which allows its use in small patients <10kg (Del Nido, Duncan et al. 1999). Centrifugal pumps also show lower rates of haemolysis compared with other types of MCSDs (Kosaka, Yada et al. 2013, Yasui, Kosaka et al. 2013), and their design is still under development to improve the haemocompatibility level (Amaral, Gross-Hardt et al. 2013). Several reports have described the successful use of centrifugal pumps in supporting a broad range of paediatric cardiac diseases(Inoue, Nishimura et al. 2011). It is also a relatively inexpensive choice, and much easier for transporting the patient compared to

ECMO(Potapov, Stiller et al. 2007). However, the cannulation system is not very stable and this could be considered as a problem by not allowing the patient to move. The patient's movement is restricted unlike the VAD, which offers some degree of freedom. Infection still exists in this system but to a lesser extent than ECMO. Anticoagulation substances are needed due to the contact between the blood and the artificial surface of the pump and tubes(Lodge, Antunez et al. 2012).

Figure 1.8 Bio Medicus Centrifugal Pump (Adachi and Fraser 2011)

Several products have been used in practice, such as Bio-Pump (Medtronic Bio-Medicus, Minneapolis, MN), as shown in **Figure 1.8**, Capiox (Terumo, Ann Arbor, MI, USA) and Rotaflow (Maquet, Rastatt, Germany). The pump chamber is available with a variety of different sizes to cover a broad spectrum of patients; small priming volume pumps are specially produced for infants (Baldwin and Duncan 2006).

2.2 Ventricular Assist Device (VAD)

1.5.2.1 *Introduction to VADs*

The third option available for children with heart failure is using VAD. These devices have been in use since the 1990s. For adult patients, VADs are very successful with BTT, BTR, and DT. In contrast, for paediatric patients, VADs are still behind, and new technologies are still under research to develop a suitable paediatric VAD (Fumoto, Shiose et al. 2014, Padalino, Bottio et al. 2014). VADs have several advantages over ECMO, such as pulsatile flow, which leads to a better tissue perfusion, and patients do not need to be totally paralysed. Also, VADs

can offer some degree of freedom for the patient where he/she can move and allow physical rehabilitation(Gandhi 2009). **Figure 1.9** shows an example of an adult VAD.

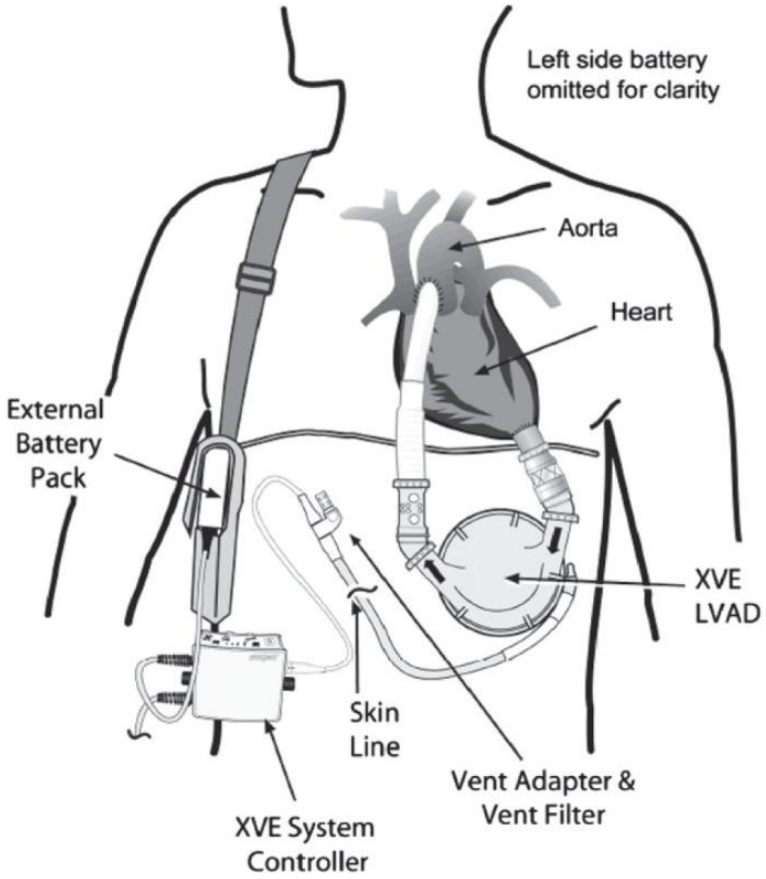

Figure 1.9 HeartMate XVE (Thunberg, Gaitan et al. 2010)

VADs can be divided into several categories depending on their outflow pattern, duration of support, the mechanism of the pump, and the connection between the device and the patient.

According to the **outflow pattern,** VADs can be divided into a pulsatile flow and a continuous flow:

- **Pulsatile Flow:** the blood flows in series of pulses, like the blood flow produced by a normal heart. **Figure 1.10** shows an example of a pulsatile flow VAD driven by compressed air.

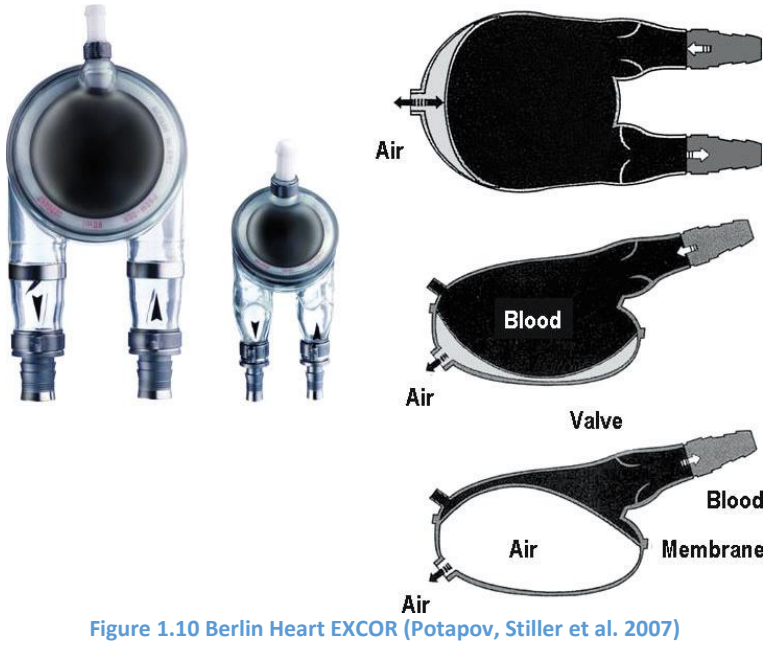

Figure 1.10 Berlin Heart EXCOR (Potapov, Stiller et al. 2007)

- **Continuous Flow:** the blood flows continuously in this type of VAD using axial flow pumps or centrifugal pumps, as shown in **Figure 1.11**. This type has several advantages, such as a small size pump, no need for a compliance chamber, no need for valves, low power consumption, and much quieter than the pulsatile flow pumps.

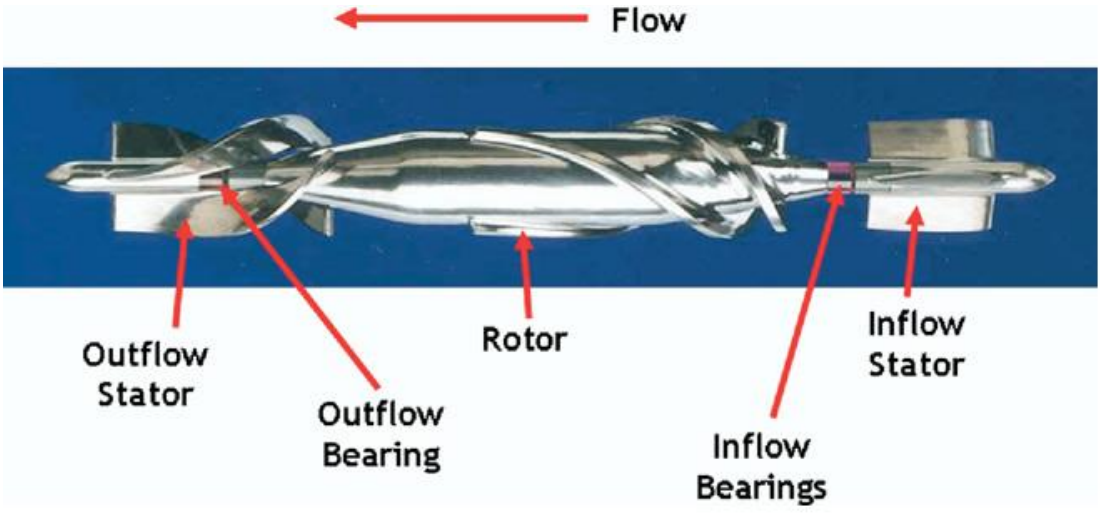

Figure 1.11 HeartMate II (John 2008)

According to the **duration of support,** VADs can be divided into short-term support and long-term support:

- **Short Term Support:** In this category, the devices are used to support the heart for a few days, usually less than 30 days. They are applied until the decision is made, transplantation is ready, or heart is recovered. Mainly, those devices are placed outside the patient's body.
- **Long Term Support:** these devices can be used for months or even years, mostly applied as a destination therapy and are entirely implantable inside the patient's body.

According to the **mechanism of the pump,** VADs can be divided into positive displacement pumps, axial flow pumps, and centrifugal pumps (Garbade, Bittner et al. 2011):

- **Positive Displacement Pumps:** they are also called the first generation VADs, these pumps have a pulsatile outflow. The pump is driven either pneumatically by compressed air, or electrically by an electric motor. **Figure 1.12** shows an example of the pulsatile VAD.

Figure 1.12 Thoratec IVAD (Timms 2011)

- **Axial Pumps:** also called the second generation VADs. These pumps have a continuous outflow, as shown in **Figure 1.13**.

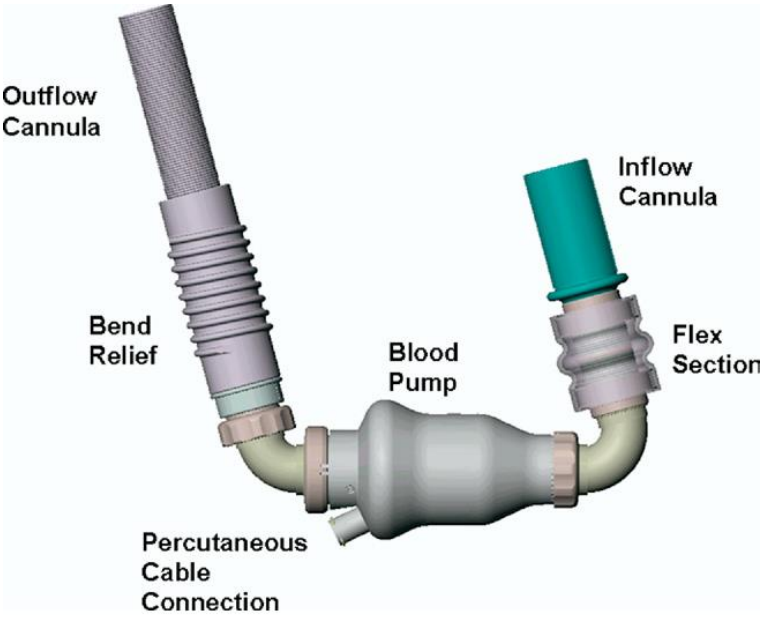

Figure 1.13 HeartMate II (John 2008)

- **Centrifugal Pumps:** the new generation of VADs are using magnetically levitated impellers with centrifugal pumps, as shown in **Figure 1.14**. This type is still under development.

Figure 1.14 HVAD (Garbade, Bittner et al. 2011)

According to the **support system applied on the heart,** VADs can be divided into RVAD, LVAD, and BiVAD:

- **Right Ventricular Assist Device (RVAD):** support the right ventricle.
- **Left Ventricular Assist Device (LVAD):** support the left ventricle.
- **Bi-Ventricular Assist Device (BiVAD):** support both left and right ventricles, it could be called a total artificial heart, as shown in **Figure 1.15**.

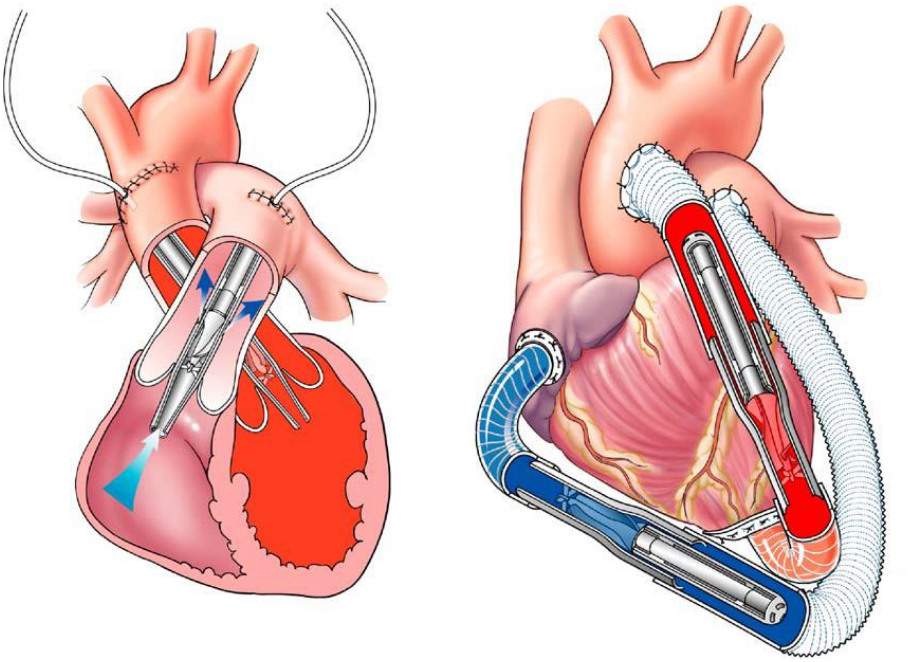

Figure 1.15 PediPump (Baldwin and Duncan 2006)

According to the **connection between the device and the patient**, VADs can be divided into extracorporeal (paracorporeal) devices and intracorporeal devices:

- **Extracorporeal Devices:** those VADs are placed outside the patient's body. They need special care, and the patient should stay in the ICU all the time. Mainly used as a short term support systems. **Figure 1.16** shows an Extracorporeal VAD placed outside the patient's body.

Figure 1.16 Toyobo LVAS (Masuoka, Katogi et al. 2008)

- **Intracorporeal Devices:** those VADs are entirely implantable inside the patient's body, apart from the external power source and the controller connected to the patient through a percutaneous cable, as shown in **Figure 1.17**.

Figure 1.17 PediaFlow (Noh, Antaki et al. 2008)

The last classification is the most important one in many ways as it represents the ideal VAD solution, the one which is in-dwelling and renders the patient independent of the ICU setting over prolonged periods of time.

1.5.2.2 *VADs Classifications*

1.5.2.2.1 VADs Generations

1.5.2.2.1.1 First Generation VADs

The first-generation design is based on a pulsatile positive displacement pump. This engineering design consists of an internal blood chamber, two mechanical or biological valves to maintain unidirectional blood flow, and two grafts for inflow and outflow. The pump is either driven pneumatically by an external compressed air source, or by an electric mechanical actuator driven by an internal electric motor. These following devices are big, heavy, noisy, and they need large percutaneous cables, which incorporates an air vent line to equalise the atmospheric pressure in the motor chamber. There is also a high incidence of mechanical failure associated with long-term support. All these limitations restrict the use of

the first generation VADs for young children and are not suitable for paediatric patients (Pagani 2008, Jaquiss and Imamura 2011).

1.5.2.2.1.2 Second Generation VADs

The second-generation design is based on continuous flow rotary pumps, which are suspended on contact bearings. These VADs contain two main parts, the rotor and the stator, beside two grafts for inflow and outflow. The rotor is pivoted on two mechanical bearings at each end of the rotor spindle, with the spinning of the rotor achieved by magnetic coupling with the motor placed in the stator part (Stanfield and Selzman 2013). A thin percutaneous cable exits the body and connects the device to an external electrical power source and a system controller. The second generation VADs are much smaller, lighter, and quieter than the first generation. This allows them to be implantable in small size patients and adults, and suitable for medium and long term support (Pagani 2008).

1.5.2.2.1.3 Third Generation VADs

The third-generation design is based on continuous flow rotary pumps, which are suspended on noncontact bearings system. This design is very similar to the second-generation devices, except for the bearing mechanism. The pump consists of two parts (the stator and the rotor), the latter part being suspended magnetically within the stator part. This levitation force could be either passive (depending on permanent magnets), or active (generated by an electrical current passing through a coil). In both cases, this technique helps in reducing the power consumption. These noncontact bearings mitigate the risk of flow stagnation, thrombus formation, heat generated by friction, and mechanical wear (Pagani 2008, Miera, Potapov et al. 2011, Boehning, Timms et al. 2013, Kim, Ishiyama et al. 2013).

The first, second, and third generation VADs are listed in **Table 1.3** below:

First Generation	Second Generation	Third Generation
HeartMate I	HeartMate II	HeartMate III
Thoratec Implantable VAD (IVAD)	Micromed DeBakey VAD Child/ Heart Assist 5	Berlin Heart Incor
Thoratec PVAD	Infant and Child Size Jarvik 2000 VAD	PediaFlow
Berlin Heart EXCOR	Circulite Micro VAD	PediPump
MEDOS HIA-VAD	Abiomed Impella cVAD Tandem Heart	Toddler VAD
Novacor LVAS	Pediatric pVAD	CorAide
Abiomed Biventricular Support 5000	Pediatric Cardiac Assist System pCAS	Levacor VAD
Abiomed AB 5000	Cardio Flow PQ	Dura Heart
Penn State PVAD		VentrAssist
Toyobo NCVC LVAS		Heart Ware Ventricular Assist Device HVAD
		Levitronix PediVAS
		Tiny Pump
		Levitronix CentriMag Blood Pumping System

Table 1.3 VADs Generations

1.5.2.2.2 Intracorporeal and Extracorporeal VADs

Extracorporeal pumps are the first VADs used to support paediatric patients, offering less mobility restriction than ECMO, and longer time than previous options. This type of VAD is used for short to medium term support until heart recovery or transplantation (Jaquiss and Imamura 2011). The patient with extracorporeal VAD should stay at the hospital all the time for monitoring. The location of the VAD outside the body allows easy monitoring of the blood flow and helps in observing any thrombus formation; any mechanical failure could be directly noticed and solved immediately. The main disadvantage is the high risk of infection due to the large tubes needed to connect the pump with the patient's heart; two tubes for single

ventricular support, and four tubes for biventricular support. Particular care is required to keep these tubes clean and sterile at the skin entry sites.

The other type of VAD is the intracorporeal VAD, where the pump is fully implanted inside the patient's body, either intraventricular or extraventricular, depending on the size of the pump and the patient. This type can provide both short-term or long-term support. Unlike the extracorporeal VADs, there is no need for any external motor or air compressor; the intracorporeal pump is just connected to a small controller and a set of rechargeable batteries through a thin percutaneous cable. This small percutaneous cable helps to reduce the risk of infection. Patients with intracorporeal VADs are mobile and tend to leave the hospital after implantation. Intracorporeal and Extracorporeal VADs are listed in **Table 1.4** below:

Intracorporeal VADs	**Extracorporeal VADs**
HeartMate I	Thoratec PVAD
HeartMate II	Berlin Heart EXCOR
HeartMate III	MEDOS HIA-VAD
Berlin Heart Incor	Abiomed Biventricular Support 5000
Thoratec Implantable VAD (IVAD)	Abiomed AB 5000
PediaFlow	Penn State PVAD
Micromed DeBakey VAD Child/ Heart Assist 5	Levitronix CentriMag Blood Pumping System
Infant and Child Size Jarvik 2000 VAD	Levitronix PediVAS
PediPump	Tandem Heart
Toddler VAD	Pediatric pVAD
CorAide	Pediatric Cardiac Assist System pCAS
Levacor VAD	Cardio Flow PQ
CircuLite Micro VAD	Toyobo NCVC LVAS
Dura Heart	Tiny Pump
VentrAssist	
Novacor LVAS	
Heart Ware Ventricular Assist Device HVAD	
Abiomed Impella cVAD	

Table 1.4 Intracorporeal and Extracorporeal VADs

1.5.2.2.3 Continuous Flow and Pulsatile Flow

Pulsatile flow or positive displacement pumps are the first generation VAD's pumps. Pulsatile flow pumps are either pneumatically or electrically driven pumps. Pneumatic pumps need an external compressed air source to push the diaphragm, while the electrical pumps have an electrical motor to drive the pusher plate (Huang, Yang et al. 2013). Those pumps are enormous, which make them unsuitable for small patient sizes. They need a large vent line for the pusher plate chamber, which increases the risk of infection. On the other hand, this type of pump has a simple control system and can be adjusted very easily to accommodate the patient's need for everyday activities (Fukamachi and Smedira 2005).

The vast majority of VADs available for paediatric patients are continuous flow pumps; there are two types as previously described, the axial pumps and the centrifugal pumps. Both axial and centrifugal pumps have almost the same design; a rotor impeller is generating the flow. In the axial flow, the impeller is in the same line of the inflow and outflow tubes, whereas in the centrifugal pump the inflow cannula is in the top of the pump and the outflow one is coming from the side of the pump. Centrifugal pumps have the advantage of less ventricular suction which reduces the risk of left ventricular collapse(Fukamachi and Smedira 2005).

In general, continuous flow pumps have the following benefits: small, quiet, no need for valves, no need for vent lines, a thin driveline or percutaneous cable, and very low power consumption. The very complicated control mechanism, inability to respond to the flow rate needed by the patient and the unknown outcomes of non-pulsatile flow are the main disadvantages of continuous flow pumps(Fukamachi and Smedira 2005). In another study, patients with continuous flow pumps showed lower Pulmonary Artery Pressure (PAP) than the patients with pulsatile flow pumps (Ozturk, Engin et al. 2013).

Continuous flow and pulsatile flow VADs are listed in **Table 1.5** below:

Continuous Blood Flow VADs	**Pulsatile Blood Flow VADs**
HeartMate II	HeartMate I
HeartMate II	Thoratec PVAD
Berlin Heart Incor	Berlin Heart EXCOR
PediaFlow	MEDOS HIA-VAD
Micromed DeBakey VAD Child/ Heart Assist 5	Abiomed Biventricular Support 5000
Levitronix CentriMag Blood Pumping System	Abiomed AB 5000
Infant and Child Size Jarvik 2000 VAD	Thoratec Implantable VAD (IVAD)
Levitronix PediVAS	Penn State PVAD
PediPump	Novacor LVAS
Tandem Heart	Toyobo NCVC LVAS
Toddler VAD	Paediatric Cardiac Assist System pCAS
Paediatric pVAD	Cardio Flow PQ
Abiomed Impella cVAD	
Heart Ware Ventricular Assist Device HVAD	
VentrAssist	
Dura Heart	
Tiny Pump	
CircuLite Micro VAD	
Levacor VAD	
CorAide	

Table 1.5 Continuous Flow and Pulsatile Flow VADs

1.5.2.3 *VAD Limitations for Children*

1.5.2.3.1 Size

The anatomical space available for VAD implantation in paediatric patients is one of the greatest challenges. Firstly, this area is tiny at the time of birth, so the VAD should be a miniature pump that can fit into this small volume. Secondly, this small space is not fixed in size. The infant will start to grow up and the previous miniature pump will not be suitable, and VAD replacement surgery is associated with high risk of mortality. Therefore, a miniature modular system could be the best possible solution for paediatric patients.

1.5.2.3.2 Power

All implantable paediatric VADs, which are available now, need power to run the pump; this power is provided by rechargeable batteries connected to the pump through a percutaneous cable. This cable is associated with a high risk of infection and limits the ability of the patients to move and practice their usual daily activities (Schima, Stoiber et al. 2013). One elegant solution to VAD power is to receive power inductively from an external power source and store it in a battery inside the body or ideally to generate its power from a source inside the patient's body.

1.5.2.3.3 Mechanism of Control

The most advanced generation of VAD's is based on continuous blood flow design, using either axial flow or centrifugal pumps. In both cases, blood flow is not measured directly but is estimated from the operating parameters of the pump, such as the pump speed and pressure drop. The absence of this kind of blood flow monitor makes the control of the pump very complicated, especially when the body requires various amounts of cardiac output due to the different daily activities. The available techniques are expensive and very complex, and only a few VADs have a flow probe to measure the exact blood flow, and very few VADs have the ability to remotely monitor the patients (Pektok, Demirozu et al. 2013). Therefore, a secure, remote, cheap and accurate technique is required to monitor the blood flow and to control the pump performance.

1.5.2.3.4 Haemocompatibility and Infections

Infection is a clinically adverse effect associated with the patient with VADs. This could happen for several reasons, such as reduced immune response caused by the damage of

leukocytes during VAD support (Chan, Hilton et al. 2013). The blood contacting side of the VAD is made of artificial materials, which are considered as foreign material for the blood cells. This will increase the risk of bleeding when patients are taking anticoagulation (Pieri, Agracheva et al. 2014), or in other cases thrombus formation (Capoccia, Bowles et al. 2013, Egger, Maas et al. 2013).

1.5.2.3.5 Price

The cost of implanting a paediatric VAD is around $150,000 including the surgery and hospital accommodation. This huge sum of money is due to the expensive extra costs in developing and manufacturing paediatric VADs, but is also due to the small quantity of paediatric patients compared with the adults. A novel affordable material could be the possible solution to overcome this problem (Mulloy, Bhamidipati et al. 2013).

1.5.2.4 *The Ideal VAD for Paediatric Applications*

The primary purpose of current VAD research is to develop a fully implantable independent that fulfils the following criteria:

- **Durable:** this VAD should stay for the whole life with the patient.
- **Reliable:** since the device is implanted inside the patient's chest, there should be minimal chance of any type mechanical failure.
- **Adequate flow:** VAD should provide enough cardiac output to keep organs functioning perfectly.
- **Quiet:** VAD should be completely silent while running.
- **Small and lightweight:** since this VAD is designed for small children, size and weight are the major parameters, which should be noticed carefully.
- **Modular system:** the system should be capable of providing cardiac support across a wide range of patient sizes, ranging from neonates to young adults.
- **Immunologically inert:** should not cause any type of immunological complications, which may affect other organs.
- **Resistant to infection:** should be totally sterile.
- **Resistant to thrombosis:** thrombus formation is very dangerous and could cause problems for other organs.
- **No need for anticoagulation:** no bleeding problems in future.

- **Fully implantable:** no need for a percutaneous power cable or vent line.
- **No external power source:** no need to carry sets of batteries all the time, the new power supply could be inside the body.
- **Easy to operate:** easy in implantation, does not need complicated equipment in implanting or running.
- **Cost effective and affordable:** all patients could afford it, by using cheap materials.
- **Forgettable:** patient should not notice that he/she is connected to a VAD.

1.5.2.5 *Future VADs*

1.5.2.5.1 Minimally Invasive VAD

The improved technologies in developing new VADs have made it possible to reduce the size of the current VADs compared with the first generation ones. These developments result in the possibility of using minimally invasive surgeries for the implantation, explantation, and exchange of VADs. Minimally invasive surgeries reduce the risk of postoperative complications after full sternotomy, such as bleeding, sternal instability, wound infections, and right heart failure (Rojas, Avsar et al. 2015).

1.5.2.5.2 Integrated Power Source for VAD

All implantable VADs have an external power source system placed outside the patient's body, connected with the implantable pump through a small percutaneous cable. This technique has solved some problems but not all of them, with infection remaining the primary cause of morbidity and mortality for patients with implantable VADs. The restriction of movement with this type of power system prohibits some activities, such as swimming (Trumble 2011). Therefore, there is a need to look for an integrated power source, which either can be totally implanted inside the patient's body, such as nuclear power, or can be generated inside the body from the muscles or the metabolic activities.

1.5.2.5.3 Muscle Power Source

Using muscle to produce power is one of the earliest methods used to generate power inside the human body. Several muscles have been studied for this cause; the most appropriate muscle for generating power is the Latissimus Dorsi (LD). This muscle is moving continuously with breathing, so it is considered as the non-stopping muscle. A unique device called Muscle Energy Converter (MEC) is connected with the muscle and used to convert the contractile

energy of the muscle into hydraulic power. This type of integrated power source VAD is called Muscle Powered Cardiac Assist Device (MCAD). Muscle power was found to be able to produce energy up to 1.37 J, which is enough to run a VAD at a 60 BPM heart rate or below (Trumble, Melvin et al. 2008, Trumble 2011). The diaphragm could also be used to generate power during breathing. The flat sheet of transducers can be placed on the diaphragm, and its continuous movement could be converted to an electric current that can run the VAD. A similar approach is the use of a Skeletal Muscle Ventricle (SMV), which can be configured to assist the heart by filling during systole phase, and ejecting during diastole phase. The method provides counterpulsation support same as Intra Aortic Balloon Pump (IABP) (Ramnarine, Capoccia et al. 2006).

1.5.2.5.4 Piezoelectric Source

Piezoelectric crystals are used to convert the mechanical power to electrical power, or vice versa. This technique is very well known in the medical field especially for ultrasound and physiotherapy. Stress applied on the moving bones can be implemented to a piezoelectric crystal to generate electric power. This requires the continuous moving of the bones, which is not achieved during sleeping or resting. This source could be used to partially power the VAD (Ming, Zhu et al. 2005, Lewandowski, Kilgore et al. 2009).

1.5.2.5.5 Thermal Gradient Source

The thermal gradient between the internal body temperature and the surface temperature could also be a possible source of electric power. This power source has been used previously to power a wristwatch. The main problem with this type is that the thermal gradient is not stable. This changes between summer and winter and it is suitable just for cold countries not for hot countries (Lewandowski, Kilgore et al. 2009).

1.5.2.5.6 Internal Fuel (metabolic) Source

The primary source of energy for all muscles is glucose, where the body is using this substance to store the energy (Martini F. 2011). This source can be used to generate power by using special sensors inside the body. This will require the patients to be more careful about their diet. More studies are needed to focus on this technique and decide if this source is sufficient to run an implantable blood pump.

1.5.2.5.7 Nuclear Power Source

Nuclear power is a small, continuous, durable, and clean source of energy. On the other hand, it needs continuous cooling and a thick housing for shielding, which make it hefty and not suitable for portable applications. Some early studies used nuclear power to operate a total artificial heart and failed for the earlier reasons. A small, lightweight, and self-cooled nuclear reactor could be the future option for implantable devices.

1.5.2.5.8 Soft Robotic Sleeve Supports Heart Function

Soft robotics are constructed from a combination of elastomers, fibres, and other filler materials, which make them suitable for human interaction. By combining the soft robotics design with a simple controlling mechanism, they can achieve complex motions, mimicking the motion of the heart. (Roche, Horvath et al. 2017) Reported creating an implantable soft robotic sleeve to provide circulatory support for a patient with a failing heart. This design is implanted around the heart, offering support for the cardiac muscle instead of replacing it, without getting in contact with the blood, which will eliminate the risk of blood clotting or infection.

This robot mimics the motion of the cardiac muscle by providing twisting and compression motions as shown in **Figure 1.18**. An ECG signal or pacemaker from the patient's heart is used to trigger the soft Pneumatic Artificial Muscles (PAM). During systolic phase, PAMs will be pressurised causing them to contract. While in the diastolic phase, they will be decompressed causing them to extend. The device monitors and records heart rate, pulmonary artery pressure, flow rate, and ascending aortic pressure. Ecoflex 00-30 silicone is used to fabricate the soft robotic actuators because of their large strains and elastic modulus values, which are very close to the heart muscle. A hydrogel cushion between the device and the heart is used to reduce friction and minimise inflammation.

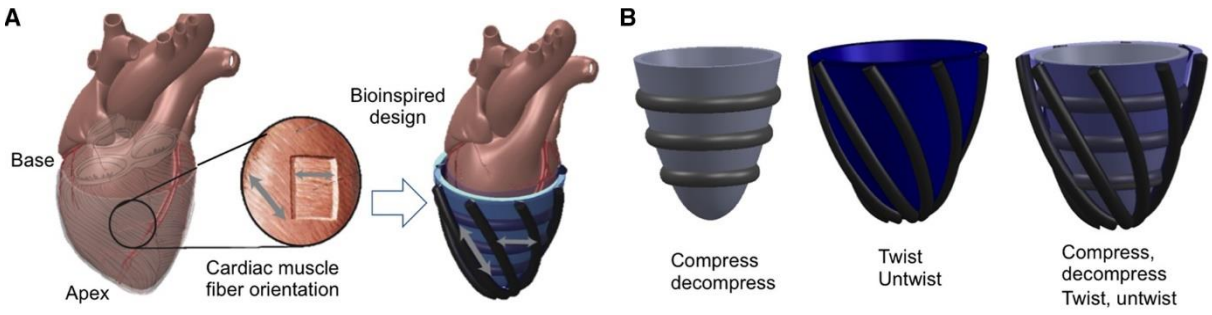

Figure 1.18 Soft Robotic Sleeve (Roche, Horvath et al. 2017)

In vitro, the device was tested using a simplified synthetic silicone heart, showing 68 ml volumetric displacement under twisting motion, and 84 ml under circumferential. The next stage of testing was in vivo, where it was implanted inside a pig with a heart failure. The soft robotic showed 88% restoration of cardiac output when 21 PSI pressure was applied at 80 BPM for 200 mSec per cycle. The device is still under improvement, and there are still many aspects of developing, such as biocompatibility, long-term mechanical properties, controlling, sensors, and miniaturising the system.

Chapter 2

Device Concept

2. *Device Concept*

2.1 Introduction

This chapter explains the theory behind the device concept, starting with objectives of the proposed device, and its concept. Then, explaining in details the theory of Artificial Muscles, their properties, types, limitations, and applications. Finally, this chapter will detail the three proposed solutions and the hypothesis.

2.2 Objectives

This thesis will explain the process of the development of a Ventricular Assist Device using Electro Active Polymers for paediatric use.

The objectives of this project are:

- Review the IPMC actuators and decide which one is suitable for creating a VAD.
- Make IPMC materials in the lab.
- Test the mechanical properties of the IPMC.
- Test the electrical properties of IPMC.
- Verify the ability of IPMC to generate electricity.
- Design and build a VAD made from IPMC.
- Test the performance of the VAD.

2.3 Concept

The new proposed device is based on the idea of creating a thin elastic membrane around the heart, which is custom formed to match the epicardium shape of the heart for each patient. This proposed device will completely envelop the heart, without any direct contact with the patient's blood, generating a compression force to support the failing heart. This device will be powered by an internal power source inside the patient's body.

2.4 Artificial Muscle

Actuators that are responsive to an external stimulus and have several characteristics in common with natural muscles are called Artificial Muscles. Their ability to generate motions is used in many application, such as mechatronics, robotics, automation, biomedical engineering, haptics, biotechnology, fluidics, optics, and acoustics (Carpi, Kornbluh et al. 2011).

2.1 History of the Material

Polymeric materials have many attractive properties, such as lightweight, easy to manufacture, cheap, fracture tolerance, thin, can take different shapes, soft, and pliable. These features make polymeric materials suitable for various applications (Bar-Cohen 2004, Biddiss and Chau 2006, Madden 2006).

Since the early discovery of polymeric materials, it has been known that certain types of polymers could change shape in response to an external stimulant, inducing a slight strain. The early discovery of this reaction could be tracked back to 1880 when Roentgen conducted an experiment on a strip of natural rubber (Roentgen 1880). Roentgen recognised the volume change of the dielectric material when an electric field is applied.

Polymeric materials were considered as passive materials, but later on, more stimulus methods were applied and tested. Polymeric materials could be stimulated using electrical, chemical, thermal, pneumatic or magnetic stimulations. This discovery changes the face of polymeric materials from passive elements into smart structures that could be utilised in many applications such as actuation and sensing (Bar-Cohen 2004, Mirfakhrai, Madden et al. 2007).

Further studies and tests were carried on these polymer sheets; the main focus was to investigate the response of these sheets to an electrical stimulus. From the beginning of the 1990s, these polymer sheets were found to be able to change their shape and size if an electric current is applied, they can induce strains exceeding 100%. On the other hand, if a mechanical deformation is applied then they can produce an electrical output. This type of material is called Electro-Active Polymer (EAP). EAP is the material that undergoes shape change in response to electric stimulation and acts rather like natural muscles (Sareh and Rossiter 2013). Polymers responding to electric fields, and reactive (faradic) conducting polymers are collectively known as electroactive polymers since annual SPIE conferences in 1999 (Otero, Martinez et al. 2012).

Those properties attracted the scientists to study them and discover more about EAP. Since EAP was very close to human muscles, they were called Artificial Muscles. EAP can be used in many fields such as biomimetic, robotics and other biomedical applications (Bar-Cohen 2004, Bar-Cohen and Zhang 2008).

2.2 Biological Muscles

To understand and model EAP properly, we need to compare it with natural human muscles. Natural muscles are biological organs that have been developed to transform chemical energy into mechanical energy and heat (Otero, Martinez et al. 2012). They are made from a series of muscle cells that are specialised for contraction. Biological muscles can be divided into three main categories; skeletal muscles, cardiac muscles, and smooth muscles. Skeletal muscles are organs made from skeletal muscle tissues, connective tissues, nerves, and blood vessels. Their main task is to move our bodies by pulling bones, based on a controlling nerve signal, making it possible for humans to walk. Cardiovascular muscles are found in the heart; their job is to push the blood into the cardiovascular system. While the smooth muscles are found in the digestive system, their job is to push food into the digestive tract and regulate the diameter of small arteries (Martini F. 2011).

Muscle cells are composed of a series of fascicles (bundles of fibres) covered by a dense collagen layer called epimysium. These bundles are separated by connective tissues fibres called the perimysium. Each bundle is made of a series of cylindrical shape muscle fibres, or muscle cells. Each muscular cell measures between 10 and 100 μm in diameter, and a few cm lengthwise, as shown in **Figure 2.1**. Human muscles are designed to change length; extend and contract. The movement mechanism is driven by a reversible hydrogen bonding between two proteins; actin and myosin. These muscles can produce a huge lifting force in a concise period (Martini F. 2011).

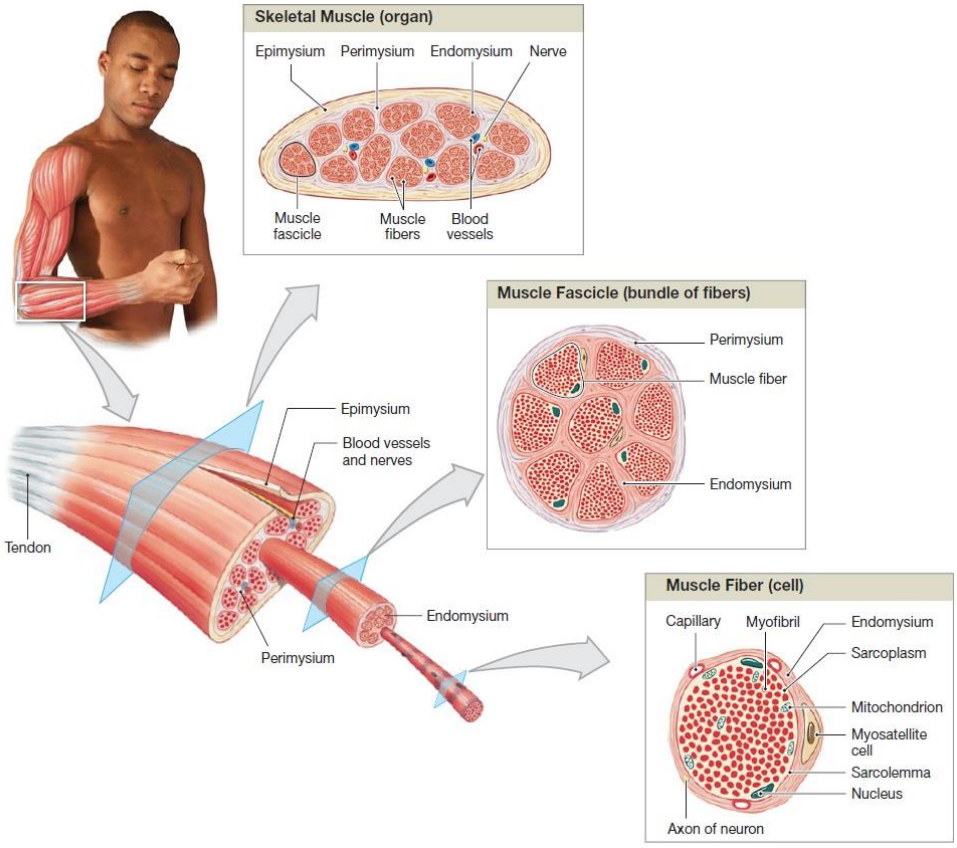

Figure 2.1 The organisation of skeletal muscle (Martini F. 2011)

2.3 Non-Electrically Deformable Polymers

Polymers can be activated by different kinds of stimulus, other than an electric field. They have the ability to memorise a shape or deformation and to return to their original shape when appropriately stimulated. This stimulus could be chemical, photovoltaic, or thermal changes in the surrounding environment of the polymers, which will trigger a response in the polymeric materials and cause them to change their shape or properties (Rossiter, Takashima et al. 2012).

2.4.3.1 *Chemically Activated Polymers*

Chemo-mechanical behaviour in polymers can be traced back in the late 1940s when (Katchalsky 1949) discovered a contractile polymeric gel. Certain polymers are very sensitive to the pH level in their solution, and they can expand or contract in response to the change of the pH. Increasing the acidity level of the solution will cause the polymer gel to contract because of the increase of the hydrogen ion concentration. While in alkaline solutions, the polymer gel will expand due to the decrease of the hydrogen ions (Bar-Cohen 2004).

2.4.3.2 *Light Activated Polymers*

Researchers in polymers that respond to change in the light density reported in the 1970s. (Aviram 1978) Indicated that a polymeric gel made of poly (N, N-dimethyl glutamanilide) could expand up to 35% under UV illumination (Bar-Cohen 2004).

2.4.3.3 *Magnetically Activated Polymers*

Magnetically activated polymeric gels, which are also called ferrogels, are chemically cross-linked polymer networks. These gels will swell under the effect of a magnetic field due to the movement of their particles in the direction of the magnetic field (Bar-Cohen 2004).

2.4.3.4 *Thermally Activated Polymers*

It has been proven that heat is the most widely used stimulus in environmental polymer actuator systems, as it can be applied directly and efficiently on materials without energy conversion. Certain polymer gels response to the change in the temperature by changing their volume (Hu and Chen 2011). Hirokawa and Tanaka first reported this experiment in 1984 (Hirokawa, Tanaka et al. 1984). The gels went through a phase transition in the range of 20^{o}C to 40^{o}C, causing the gel to contract and produce a force up to 100 kPa in a very short period of 20-90 Sec (Bar-Cohen 2004).

2.4 Properties of EAPs

EAP can generate more than 300% strain, which is much higher than the rigid, fragile Electroactive Ceramics (EAC). Compared with Shape Memory Alloy (SMA), EAP has a higher response time, lower density, and better resilience. Also, EAP consumes less power than the other rivals do. On the other hand, EAP has limitations in mechanical force and robustness compared with SMA and EAC (Yambe, Amae et al. 2001, Bar-Cohen 2004).

Table 2.1 shows a comparison between EAP, SMA, and EAC.

Property	EAP	SMA	EAC
Actuation strain	Over 300%	<8% short fatigue life	Typically 0.1-0.3%
Force (MPa)	0.1-40	200	30-40
Reaction Speed	µsec to min	msec to min	µsec to sec
Density	1-2.5 g/cc	5-6 g/cc	6-8 g/cc
Drive Voltage	1-7 v for ionic EAP and 10-150 v/µm for electric EAP	5 V	50-800 V
Consumed Power	m-watt	watt	watt
Fracture Behaviour	Resilient, elastic	Resilient, elastic	Fragile

Table 2.1 Comparison between EAP, SMA and EAC (Bar-Cohen 2004)

EAPs, are resilient, fracture tolerant, noiseless actuators that can be made miniature, low mass, inexpensive and consume low power. Many characteristics of soft EAPs including pliability, scalability, low weight, silent operation and relatively large actuation strain, make them well suited for robotic applications (Sareh and Rossiter 2013).

2.5 Types of EAPs

EAP can be divided into two main groups based on the type of electrical stimulation: Electric and Ionic. Electric EAP includes Ferroelectric, Electrostrictive Graft, and Liquid Crystalline polymers. The electric field (Coulomb Force) drives this group, they require a high voltage >150 V/µm close to the breakdown level, and they can hold their displacement under a DC voltage (Bar-Cohen, Bao et al. 2002). Ionic EAP includes Gels, Polymeric Metal Composites, Conductive Polymers, Carbon Nanotubes. These polymers are driven by the mobility or diffusion of ions, they require a low driving voltage as 1-5 V. However, they need to be kept wet, and it is challenging to maintain their displacement under a DC voltage (De Luca, Digiamberardino et al. 2013).

2.4.5.1 *Electric EAPs*

Electric EAPs are driven by an electric field, or a Coulomb Force, also known as dry EAP or field activated EAP. This type has several advantages, such as holding the induced displacement

under activation of a DC voltage, achieving high actuation strains and stresses, fast response, and has a long lifetime (Carpi, Kornbluh et al. 2011). Also, this type has a greater mechanical energy density, and they can be operated in air with no major constraints. On the other hand, they require a high activation field, typically up to the order of 100 V/µm (Bar-Cohen 2004, De Luca, Digiamberardino et al. 2013).

Table 2.2 shows the advantages and disadvantages of the Electric EAP:

Advantages	Disadvantages
• Exhibits high mechanical energy density. • Induces relatively large actuation forces. • Can operate for a long time in room conditions. • Exhibits rapid response (mSec) • Can hold strain under DC Activation.	• Independent of the voltage polarity, it produces mostly monopolar actuation due to associated electrostriction effect. • Requires high voltages (~100 MV/m). Recent development allowed for a fraction of the field in the Ferroelectric EAP.

Table 2.2 Advantages and Disadvantages of Electric EAP (Bar-Cohen 2004)

Electric EAPs are listed below:

2.4.5.1.1 Ferroelectric Polymers

Piezoelectric effects were discovered in 1880 by Pierre and Paul-Jacques Curie when they found that applying a force at certain axes on a certain crystal a voltage could be recorded on the surface of the crystal. On the other hand, if an electric current is applied to these crystals, then they will sustain an elongation (Madden, Vandesteeg et al. 2004).

This phenomenon is called Ferroelectricity and is found in non-centre symmetric materials only. In other words, Ferroelectrics are non-conducting crystals or dielectric materials that exhibit a spontaneous electric polarisation (Bar-Cohen 2004). These polymers have a high Young's modulus in the range of 1-10 GPa, which makes them offer high mechanical energy density. On the other hand, these polymers need a high-applied AC field (~200 MV/m) which can be very dangerous, and it is very close to the dielectric breakdown (Bauer, Fousson et al. 2002, Bar-Cohen 2004).

2.4.5.1.2 Electrets

Electrets are the materials that retain their electrical polarisation after being subjected to a strong electrical field. The positive charges within the materials will be permanently oriented alongside the electric field, while the negative charges will be oriented on the opposite side. These electrets can be made from polymers, ceramics, or wax, where the molecules will be randomly distributed at the beginning, and then an electric field is applied which will cause the molecules to hold a permanent polarisation(Bar-Cohen 2004, Marchese, Katzschmann et al. 2015).

2.4.5.1.3 Dielectric Elastomers (DEs)

Dielectric Elastomers are a particular class of non-conductive rubber-like solids that have a low elastic stiffness and dielectric constants; they were first developed in the early 1990s (Vertechy, Frisoli et al. 2012, Carpi, Anderson et al. 2015). These Dielectric Elastomers can produce a large actuation strain under the effect of an electrostatic field (Bar-Cohen 2004, Brochu and Pei 2010). Because of their performance, simplicity, and easy availability, the interest in developing DEs has continued to grow, which makes them suitable for a range of applications from haptic devices to energy harvesting (McKay, O'Brien et al. 2010, Wang, Cai et al. 2012).

2.4.5.1.4 Electrostrictive Graft Polymers

First developed in NASA Langley Research Centre in 1998, which shows a considerable strain when subjected to an electric field. This material consists of two components; a flexible backbone macromolecule, and a grafted polymer that forms a crystalline structure. The main advantage is the ability to produce a relatively high electromechanical power density, and high processability (Cheng, Xu et al. 2002, Bar-Cohen 2004).

2.4.5.1.5 Electrostrictive Papers

Papers are made from a group of fibres that are connected with each other to make a single sheet. This passive sheet of paper could be converted into a smart material if it could be combined with electroactive properties. Such as EAP has been produced by (Kim and Seo 2002) where two silver laminated sheets of paper were bonded with a silver electrode placed on the outside surface. Upon applying a voltage to the electrode surface, the paper produced a bending motion, depending on the level of voltage applied, the frequency, and the shape of

the voltage wave. This new material has many applications, such as active sound absorbing material, flexible speakers, and smart shape control devices (Bar-Cohen 2004).

2.4.5.1.6 Liquid Crystal Elastomer (LCE) Materials

These materials were first developed at Albert-Ludwigs University in Germany. They have the properties of piezoelectric materials and can be activated by inducing Joule heating (Finkelmann, Kock et al. 1981). The actuation procedure of the material requires phase change between nematic and isotropic phase during a very short period, in less than a second. The reverse process takes a long time, around 10 seconds, and requires cooling for the material to expand to its initial shape. The mechanical properties of the LCE can be controlled by the liquid crystalline phase selection, density of crosslinking, the flexibility of the polymer backbone, the coupling between the backbone and liquid crystal group, and the external stimuli. The main advantage of the LCE lies in its uniaxial response to an external activation, such as temperature, light or electric fields (Bar-Cohen 2004, Madden, Vandesteeg et al. 2004).

2.4.5.2 *Ionic EAPs*

Ionic EAPs (Gels, Polymer Metal Composites, Conductive Polymers, and Carbon Nanotubes) involve mobility or diffusion of ions. This type is driven by diffusion of ions, and they require an electrolyte for the actuation mechanism. The main advantage is that they require low voltage for activation around 1-2 Volts (Carpi, Kornbluh et al. 2011). On the other hand, they are slower and produce smaller energy density compared with Electric (De Luca, Digiamberardino et al. 2013).

Table 2.3 shows the advantages and disadvantages of Ionic EAP:

Advantages	Disadvantages
• Natural bi-directional actuation that depends on the voltage polarity. • Some ionic EAP like Conducting Polymers have a unique capability of biostability. • Requires low voltage.	• Requires using an electrolyte. • Electrolysis occurs in aqueous systems at >1.23 V. • Require encapsulation or protective layer to operate in open air conditions. • Low electromechanical coupling efficiency. • Except for CPs and NTs, ionic EAPs do not hold strain under DC voltage. • Slow response (fraction of a second). • Bending EAPs induce a relatively low actuation force. • High currents require rare earth electrodes such as gold or platinum. • Except for CPs, it is difficult to produce a consistent material (particularly IPMC).

Table 2.3 Advantages and disadvantages of Ionic EAP (Bar-Cohen 2004)

2.4.5.2.1 Ionic Polymeric Gels (IPG)

Ionic Polymeric Gels are crosslinked polymers, that have been developed in the late 1980s and early 1990s in the USA, Japan, and Italy (Carpi, Kornbluh et al. 2011). These polymeric gels are activated by changing the environmental parameters, such as temperature, or pH level. They will swell in alkaline solutions and get denser in acidic solutions. This change in the pH level can be controlled electrically, which will make IPG behave and look like Artificial Muscles. They can produce a strong actuation force that could match the force generated from a biological muscle (Schreyer, Gebhart et al. 2000, Bar-Cohen 2004, Choe, Kim et al. 2006).

During activation, the IPG will bend, as the cathode side becomes more alkaline, while the anode side becomes more acidic. This movement happens as a result of ion diffusion through the multilayered gel, which means the response will be very slow. For example, expanding and shrinking an IPG from 6x6 to 3x3 occurred over a period of 20 minutes, which make these gels very slow for many functions and far away from practical applications. Besides that, the large actuation caused the electrodes to damage, which results in a failure of the actuator after 2 or 3 cycles (Schreyer, Gebhart et al. 2000, Bar-Cohen 2004).

2.4.5.2.2 Conductive Polymers (CP)

Conductive Polymers are made from two layers of polymers, such as polypyrrole or polyaniline, with an electrolyte in between them. The actuation mechanism functions via the revisable counter-on insertion and expulsion during redox cycling. When a voltage is applied to both polymers, oxidation occurs at the anode side, and reduction occurs at the cathode side. This will cause the H^+ ions to move from the anode to the cathode through the electrolyte to balance the electric charge that is applied. The increased concentration of H^+ ions will cause the cathode to swell, while the decreased concentration of H^+ will cause the anode side to shrink. This will result in the CP sandwich bending towards the anode side. The thickness of the polymers plays an important role in controlling the speed of actuation; the thinner the layers, the faster the response, but on the other hand, the CP will produce lower force. The CP requires low voltage to be activated (in the range of 1-5 V), speed and force density both increase with increasing the voltage (Bar-Cohen 2004, Madden, Vandesteeg et al. 2004, Fang, Tan et al. 2008).

2.4.5.2.3 Carbon NanoTube (CNT)

(Baughman, Cui et al. 1999) First introduces Carbon Nanotubes with diamondlike mechanical properties as a form of EAP in 1999. The carbon- carbon bond between the carbon atoms are suspended in the electrolyte, and the change in the bond length is responsible for the actuation mechanism. The electrolytes form an electric double layer surrounding the carbon nanotubes and play a major role in injecting significant charges that affect the balance of the carbon-carbon bonds and cause these bonds to change their length. These small changes in carbon-carbon bond levels are rendered into macroscopic movements and results in CNT extensions (Bar-Cohen 2004, Kosidlo, Omastova et al. 2013). The CNT can produce a higher mechanical stress and a higher work per cycle than any other previous EAP. Since carbon

offers a high thermal stability, CNT can be used in applications at a high temperature that could reach up to 1000^{o}C. The main disadvantages facing CNT are the high production cost and the difficulty in mass production (Bar-Cohen 2004, Hu, Chen et al. 2010).

2.4.5.2.4 Electrorheological Fluids (ERF)

Electrorheological Fluids experience a large change in their viscosity levels when subjected to electricity. These fluids are made from two components; a suspension base fluid and small particles size 0.1-100 μm. Winslow first reported ERF in 1949, and the electrorheological effect is called the Winslow effect (Winslow 1949). The change in ERF viscosity is believed to happen because of the difference in dielectric constant between the base fluid and the particles. When an electric field is applied, the particles will form a chain in the same direction of the field because of the dipole moment. This chain will change the properties of the ERF, such as the viscosity and the yield stress, allowing the ERF to change its appearance from a liquid state into a more viscoelastic like a gel. The response time is very short between these two states, in the range of milliseconds. These properties make the ERF suitable for many hydraulic applications, such as shock absorber, active damper clutches, adaptive gripping devices, and variable flow pumps (Bar-Cohen 2004, Glaser, Caccese et al. 2011, Must, Vunder et al. 2014).

2.4.5.2.5 Ionic Polymer Metal Composites (IPMC)

IPMC is an EAP that bends in response to an electric stimulus, because of the movement of the cations in the polymer network. They were first reported in the early 90s when different groups of researchers in Japan and the United States started testing the electroactive characteristics of the IPMC (Bar-Cohen 2004, De Luca, Digiamberardino et al. 2013).

IPMC is the product of combining ionic polymer with a conductive medium such as a metal. It can produce a significant mechanical deformation when an electric current is applied; it has been reported that IPMC could generate a blocking force in the range 1 mN/V to 10 mN/V (De Luca, Digiamberardino et al. 2013). As well, it can produce an electrical output when a dynamic mechanical deformation is applied. It can be used both as an actuator and as a sensor at the same time (Shahinpoor and Kim 2001, Kruusamäe, Brunetto et al. 2011). IPMC can generally produce a bending motion towards one side. Recently, some new techniques can produce more complexed deformations, where different sections of IPMC are controlled

separately to produce such a complicated motion (Chen and Tan 2010, Riddle, Jung et al. 2010, Feng and Liu 2014).

There are several types of polymer base used to make IPMC; the most famous ones are Nafion (perfluorosulfonate, made by DuPont), and Felmion (perfluorocarboxylate, made by Asahi Glass, Japan). Both membranes provide channels for the movement of the positive ions when the voltage is applied, which will result in the bending action (Shahinpoor 2003, Bar-Cohen 2004). **Figure 2.2** shows a schematic structure of IPMC.

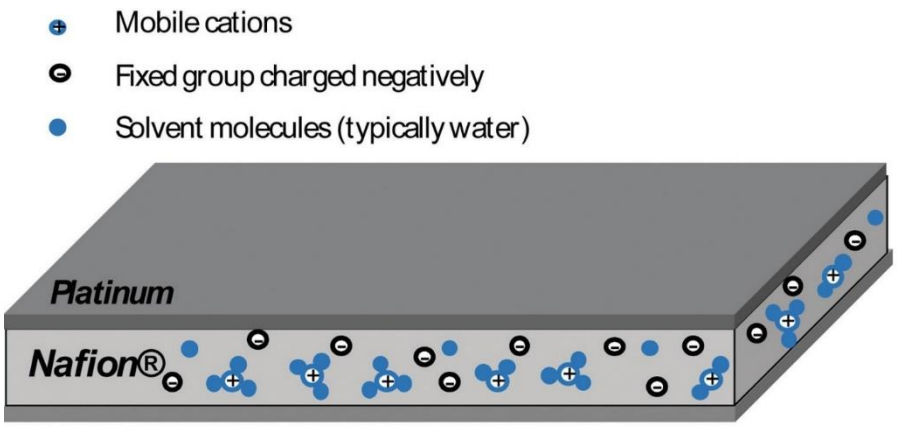

Figure 2.2 Schematic Diagram of IPMC (De Luca, Digiamberardino et al. 2013)

IPMC displacement depends on the chemical composition and structure of the backbone of ionic membrane. The morphology of the metal electrodes, the nature of the cations, the level of hydration (Nemat-Nasser 2002, Kikuchi, Sakamoto et al. 2011), and the surrounding environmental conditions affect the actuation performance of the IPMC (Punning, Must et al. 2015). The movement of water molecules inside the membrane matrix is believed to be the main driver of the actuation mechanism, where water appears on the surface of the expansion side and disappears on the surface of the contraction side. The electrophoresis - like internal ion- water movement is responsible for creating effective strain for actuation. Water leakage through the porous platinum electrode reduces the electromechanical conversion efficiency, similar to a leaky hydraulic jack (Shahinpoor and Kim 2001, Kim and Shahinpoor 2003, Park, Kim et al. 2010). **Figure 2.3** shows an explanation of how IPMC actuates.

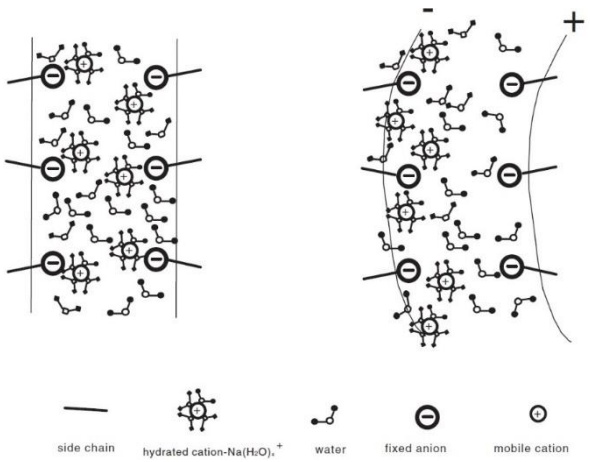

Figure 2.3 Schematic diagram of how IPMC actuates (Shahinpoor and Kim 2001)

Manufacturing of an IPMC starts with an ionic polymer with ion exchanging capability, which is then chemically treated with an ionic salt solution of a metal (gold, platinum, palladium, or others) and then chemically reduced to yield ionic polymer metal composites (Shahinpoor and Kim 2001, Shahinpoor 2005). The type of metal used in making IPMC will play an important role in the electromechanical properties of the IPMC actuator. IPMC requires low voltage to be active, in the range of 1-10 V, as shown in **Figure 2.4**. Previous tests found that IPMC will provide a large actuation at low frequencies lower than 1 Hz, and their response will decrease by increasing the frequency (Bar-Cohen 2004, Brufau-Penella, Puig-Vidal et al. 2007).

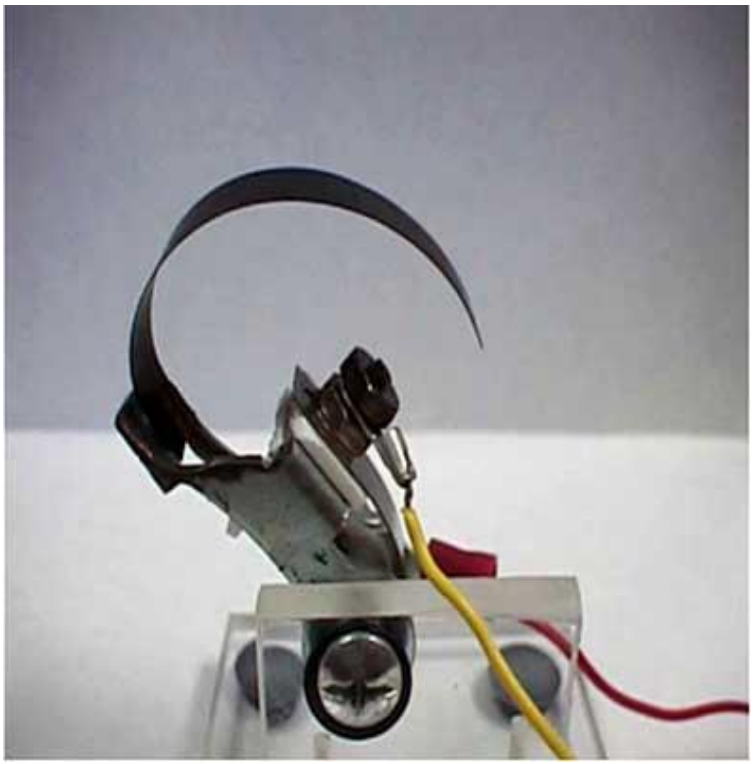

Figure 2.4 Deformation of IPMC strip (10x 80x0.34 mm) under 4 V DC (Shahinpoor 2010)

IPMC advantages can be summarised as the following (Lumia and Shahinpoor 2008):

- Low actuating voltage.
- Flexible and compliant material (Young's Modulus 200 MPa).
- It can be cut to micro size without loss in actuation and sensing properties.
- Fast response (microseconds to seconds).
- Lightweight.
- Ability to actuate at sub-zero temperatures (Paquette, Kim et al. 2005).

2.6 EAP Limitation

2.4.6.1 *Mechanical Power Generated*

Mechanical power generated from EAP is linked to different factors, such as the thickness of the actuator, the voltage applied and the frequency. The surrounding environment also plays a major role in the EAP behaviour. Some EAP performs better in wet conditions, such as Ionic EAP.

2.4.6.2 *Lifespan*

EAPs have different lifespans depending on the type and the applications. Electric EAP has a longer lifespan compared with Ionic, as the Ionic EAPs need to be hydrated to function properly.

2.4.6.3 *Reaction Time*

Not all EAPs react at the same rate. The actuation mechanism of some EAPs depends on ion movement, which needs some time for the ion to move between the electrodes. Usually the reaction time is in the range of few seconds. This has a significant effect on the response time.

2.4.6.4 *Cost*

EAPs are still in the development stage and at the moment only a handful of companies are producing them. They are not fully commercialised yet, as many types of EAPs are still under tests and developments at research centres. These make the materials difficult to source and very expensive to be used in many applications.

2.4.6.5 *Fabrication Procedure*

EAPs are still in their early stage of research and development. This means EAPs are custom made, which will take a long time to order some samples from the current EAPs providers.

Some fabrication procedures might take weeks to reach the desired thickness of EAP. Also, any small mistake during this procedure will have an effect on the final product.

2.7 Applications of EAP

Since the early discovery of EAPs, they have been used in many fields as actuators and sensors, from basic robotic applications to more advanced medical devices. Here are some of these applications:

2.4.7.1 *Wearable Haptic Interface*

Body worn systems have been under investigation recently. They enable the possibility of monitoring people anywhere and anytime and provide feedback as well as to the person using them. Their applications vary from healthcare, well-being, lifestyle, protection, and safety. (De Rossi, Carpi et al. 2011, Carpi, Frediani et al. 2012) Developed a new textile integrated glove, which can provide sensing and feedback at the same time. This glove is made from two types of electroactive polymers; the actuator part is made from piezoresistive rubber, while the sensing part is made from a dielectric elastomer. This glove will be able to monitor, classify hand gestures, and provide vibration feedback for the user.

2.4.7.2 *Tunable Lens*

Different applications require the use of one lens with the ability to change focus, such as consumer electronics (cameras, mobile phones, and surveillance systems), medical devices (video endoscopy), and optical communication systems (optical fibre components) (Hanley, Gun'ko et al. 2014). Many techniques have been used to develop such a lens, where a lens made from smart material could respond to mechanical, electrical, thermal and chemical stimulation. (Carpi, Frediani et al. 2011) Reported the use of dielectric elastomer to create a tunable lens. This new lens is made of a fluid-filled elastomeric lens integrated with an annular elastomeric actuator working as artificial muscle-like the human eye, **Figure 2.5** shows a comparison between the natural human eye and the new tunable lens. When electrically activated, the Artificial Muscle (elastomeric actuator) deforms the lens and changes the focal length resulting in changing the focus of the lens. This new design is small in size, light, silent, does not overheat, and has low power consumption (Carpi, Frediani et al. 2012).

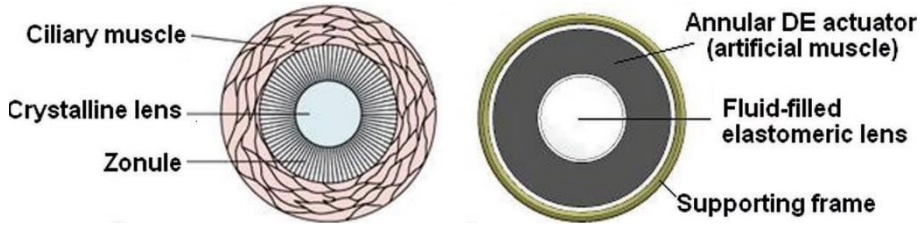

Figure 2.5 Comparison between the human lens and the bio-inspired lens (Carpi, Frediani et al. 2011)

2.4.7.3 *Braille Display*

Previously, piezoelectric ceramics were used in refreshable Braille display pages, where a group of actuators will push the Braille dots to create a word. The big size, the fragility of the piezoelectric ceramics, plus the high cost of the actuators make it very limited to develop a cheap and small refreshable Braille display system. One solution to this problem is the use of EAP instead of piezoelectric ceramics. (Ren, Liu et al. 2008) Reported using Ferroelectric EAP to create a refreshable Braille display. The design is shown in **Figure 2.6**, where the EAP actuators are connected to the Braille pins and pushed up based on a word to display. The new model is more compact, light, cheaper to manufacture, and able to produce a full page of refreshable Braille display.

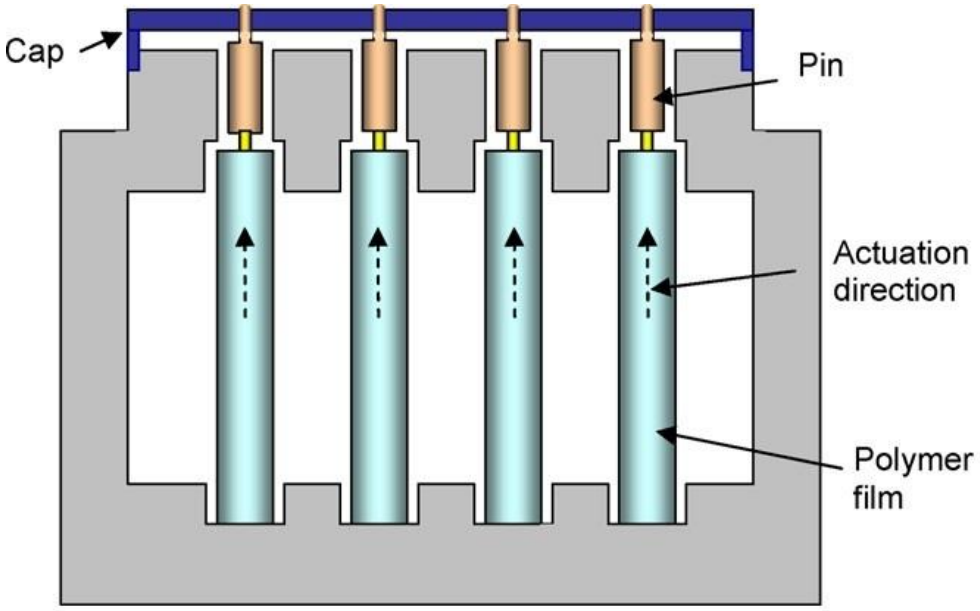

Figure 2.6 Schematic diagram of the proposed EAP Braille cell using the compact (Ren, Liu et al. 2008)

2.4.7.4 *Robotic Micro-Gripper*

Micro-grippers can be found in many fields, such as handling small components precisely or moving fragile living cells. EAPs offer the best solution to create a gripper that can handle both rigid and flexible objects, and move them precisely to the required position (McDaid, Aw

et al. 2011). (Alici and Huynh 2006) Used conducting polymers to create a three fingers gripper (10x1x0.2 mm). The gripper was able to lift a 30 mg object under 1 V of activation as shown in **Figure 2.7**. The main drawback of this design was the low speed of response and nonlinearity of the actuation. (Deole, Lumia et al. 2008) Used IPMC as well to create a microgripper, finger size were 5x1x0.2 mm. This design was able to lift objects up to 16 mg.

Figure 2.7 Conducting Polymer Gripper (Alici and Huynh 2006)

To obtain a faster response (Lumia and Shahinpoor 2008), used IPMC to create their version of a two fingers micro-gripper, measuring 5x1x0.2 mm. The shape of the design has a large base leading to the micro-gripper finger. The large base was designed for a better electrical conductivity, which leads to a more powerful and faster response. This micro-gripper was able to lift a 15 mg solder ball under a 2V signal. (Jain, Datta et al. 2010, Jain, Datta et al. 2011) Also reported using IPMC to make a two fingers micro-gripper, 30x6x0.2 mm. The IPMC fingers were able to move 14 mm and creating a force of 10 mN, which make them able to lift a weight up to 10 mg. More advanced tasks can also be produced by a multi fingers IPMC micro-gripper, like moving objects in large surface areas and placing them accurately (Jain, Majumder et al. 2013, Jain, Datta et al. 2014)

2.4.7.5 *Micropumps*

Micropumps are essential parts in any microfluidic system and lap on chip technologies. The need for a controlled micro flow of gases or liquids has led to the use of EAPs as a heart of micropumps (Simon, Jager et al. 2009, Santos, Lopes et al. 2010). (Nguyen, Goo et al. 2008) Used IPMC actuators in their flap valve micropump design. This design is based on a flexible

IPMC supported diaphragm as shown in **Figure 2.8**, which gave the actuator a large displacement and improve the pump performance. The pump was able to produce a 760µl/min flow, and maximum back pressure of 1.5 kPa when a 3 V driving signal was applied at 3 Hz.

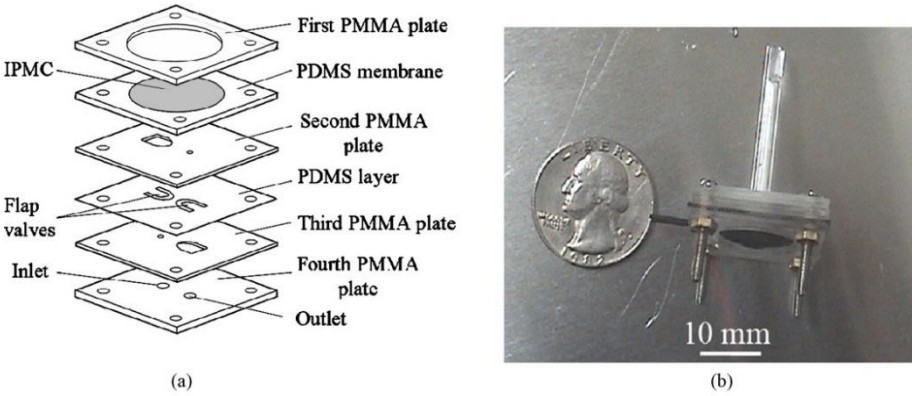

Figure 2.8 The IPMC micropump with a flexible support design: (a) structure of the micropump with six stacked layers and (b) photograph of the fabricated micropump (Nguyen, Goo et al. 2008)

2.4.7.6 *Jellyfish Robot*

Currently, many biomimetic robotics have the ability to move, fly, or walk based on motors. With the recent developments of EAPs, they could replace the motors and build an EAP-based robot. (Yeom and Oh 2009) Developed a new jellyfish robot based on using curved strips of Ionic Polymer Metal Composite. This study focused on making curved non-electric plating IPMC, building a Jellyfish robot, and then test this robot in water. The robot consists of Jellyfish legs, which are the IPMC actuators, and electrical connection components. **Figure 2.9** shows the final design of multi strips of IPMC connected in a shape of Jellyfish. This Jellyfish robot could travel upward with a velocity of 0.057 mm/s and 0.045 mm/s under 1 Hz and 2Hz signal respectively. The thrust force was also measured under the same frequencies, 0.87 gf and 0.544 gf respectively.

Figure 2.9 Jellyfish Robot (Yeom and Oh 2009)

2.4.7.7 *Artificial Cilia*

A more advanced movement could also be produced by EAPs. (Sareh, Rossiter et al. 2012) Demonstrated how to build a cilium using IPMC and produce a very complexed actuating. In simple IPMC, the actuator bends towards the negative electrode producing a curved shape actuator, while a cilium produces a more complexed curvature with multiple curving points. In this study, a low voltage-based actuator was developed from IPMC to replicate the movement of a biological Cilium. **Figure 2.10** shows the artificial IPMC cilium with its multiple twisting points; the arrows refer to the electrical contacts points.

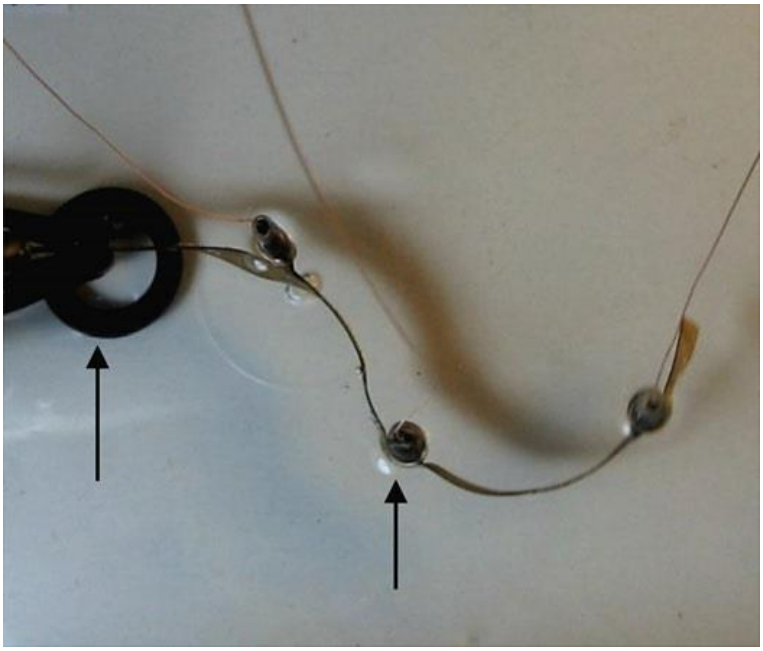

Figure 2.10 Artificial IPMC Cilium (Sareh, Rossiter et al. 2012)

2.4.7.8 *Hand Prosthesis*

Recently, there have been lots of research on using robots for limbs rehabilitation, making assistive devices for arms, hands, and legs. Most of these devices are using heavy mechanical components, like motors with complicated electronics. However, these assistive devices are very bulky, heavy and expensive, which make them unsuitable for many situations. Therefore, Artificial Muscles could be used as the main actuator in these devices (Biddiss and Chau 2006, Jain, Datta et al. 2010, Jain, Datta et al. 2014). (Lee, Jung et al. 2006) Used IPMC Artificial Muscle to create an artificial hand prosthesis which was controlled by the human muscle signal Electromyography (EMG). Four strips of IPMC were made of different thickness between 178 µm and 800 µm and then placed on a holder similar to the hand's shape. The EMG signal was receded from flexor carpi ulnaris and the extensor carpi ulnaris muscles, then used as a guide to change the driving voltage of the IPMC strips. **Figure 2.11** shows the layout of the IPMC hand prosthesis and how it could move based on the hand movement. On the left side the hand is in none state, while the right side the hand is in flexion state.

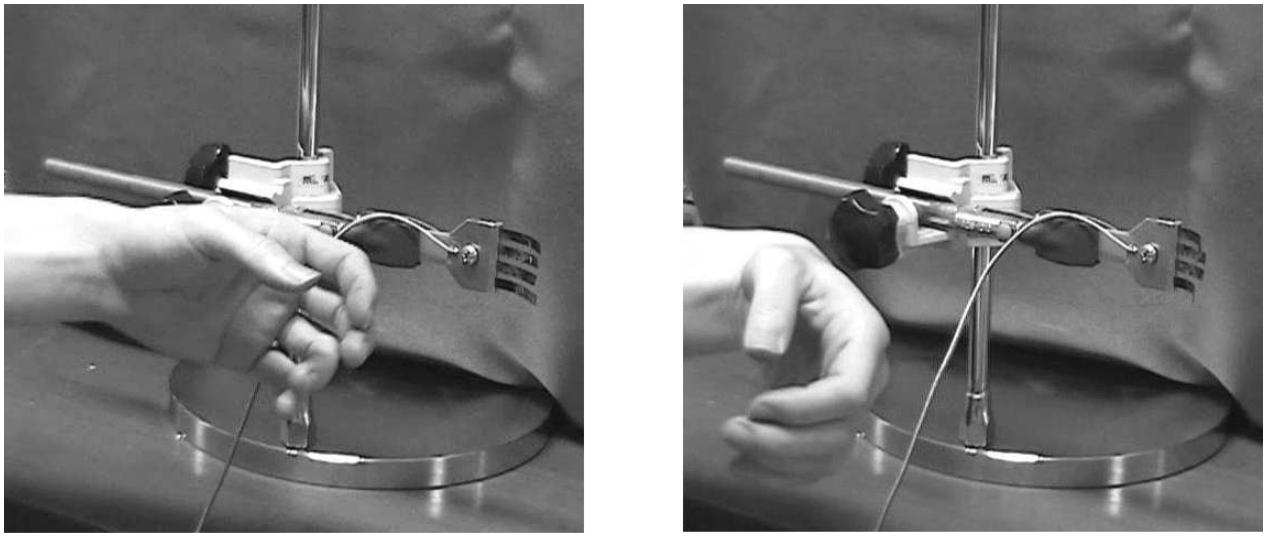

Figure 2.11 IPMC Hand Prosthesis (Lee, Jung et al. 2006)

2.4.7.9 *Medical Devices*

There is a continuous need to improve new technologies for minimally invasive therapies, where tiny and accurate movements are necessary for robotic surgeries, or scanning endoscope (Yoon, Reinhall et al. 2007). The use of EAPs has increased recently in this field, due to their interesting properties. Conducting Polymers (CP) are perfect candidates, they can be used in various applications, such as micro-anastomosis connector, steerable guide wires and catheters, and balloon catheter (Jager 2013).

In teleoperation surgeries, the key parameter is how to measure the force applied on the object accurately, and how to gauge the softness of that object. IPMC is an excellent martial for this application, as it could be used for actuation and sensing at the same time. (Bonomo, Brunetto et al. 2008) Designed a new small tactile sensor that can measure the softness of an object. This design can be applied in both medical surgeries, and in aerospace as well. The prototype as shown in **Figure 2.12** consists of two IPMC strips. The first one is the actuator, and the second one is the sensor. When sinusoidal voltage is applied to the actuator, it will vibrate, and it will push the sensor towards the object under testing. The sensor will deform and generate a voltage, which is reordered and then used to measure the object's stiffness.

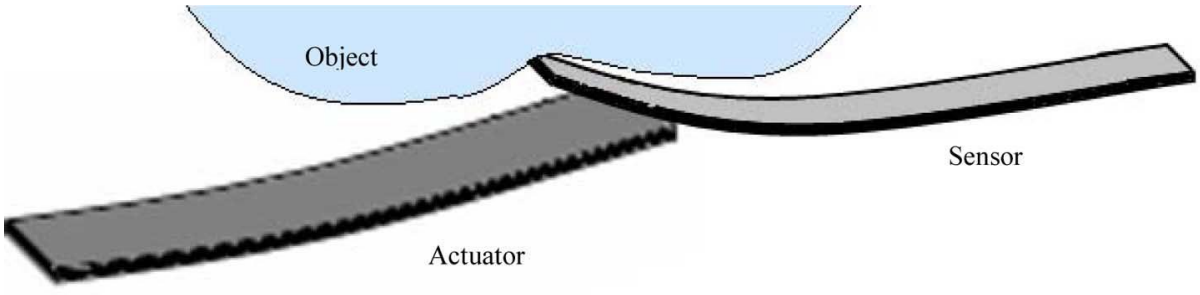

Figure 2.12 IPMC Tactile Sensor (Bonomo, Brunetto et al. 2008)

(Li, Kim et al. 2011, Moeinkhah, Rezaeepazhand et al. 2014) Reported using IPMCs in a helical shape to create an active biomedical stent. The stent was fabricated through thermal treatment of an IPMC strip helical coiled on a glass rod and then put in 90^{o}C water for 1 hour. This IPMC helical stent could show not only bending motions but also torsional and longitudinal motions as well. The movement of the stent can be controlled by changing the pitch, the diameter, the width of the stent, as well as the voltage applied, and the frequency. **Figure 2.13** shows the stent in (a) expanding state, (b) neutral state, and (c) contracting state.

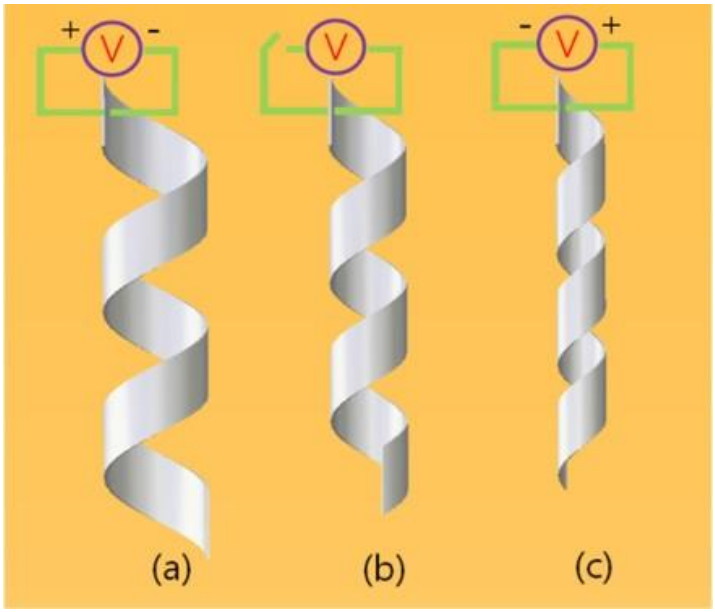

Figure 2.13 IPMC Helical Stent (Li, Kim et al. 2011)

(Liu, Wang et al. 2014) Used a new approach to create a silicone tube with four IPMC actuators that have a multi-degree of freedom, as shown in **Figure 2.14**. This new design was prepared for use in minimally invasive surgeries.

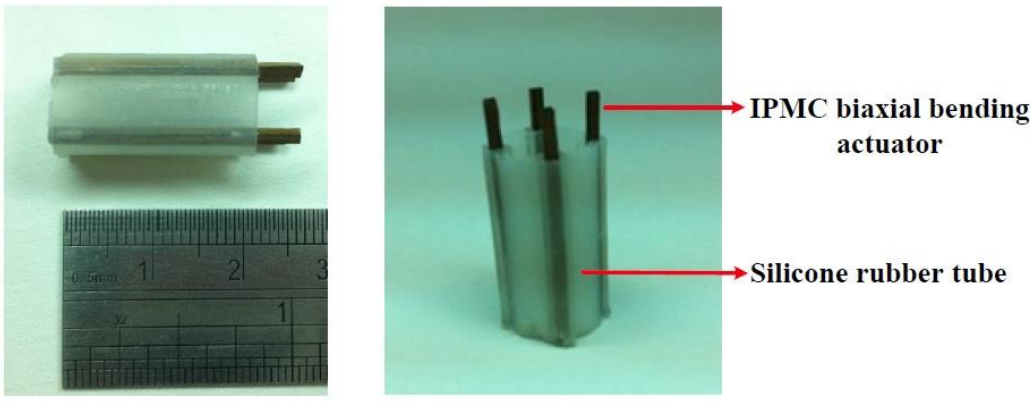

Figure 2.14 Fabricated IPMC-embedded tube showing four embedded IPMC biaxial bending actuators (Liu, Wang et al. 2014)

(HEGDE, BUCH et al. 2004) Explained the use of EAP to create a cardiac supporting apparatus in their patent. The proposed apparatus is based on two heart's coverings made from biologically compatible materials, covering the heart partially and connected with each other through EAP actuators. The actuators are oriented in a way that upon activation they will pull the two covering towards each other and create an assistive force for the heart to push the blood. The design is shown in **Figure 2.15** where 100 is the apparatus, 104 the patient's body, 108 the heart, 106 constraint device, 110 the heart's coverings, 112 the size adjustment

mechanism, 114 and 116 the EAPs actuators, 118 the controller, 120 and 122 sensors, 124 power source, 126 transducer.

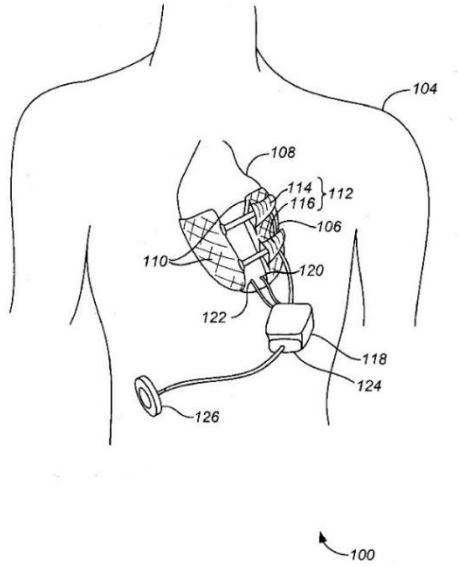

Figure 2.15 EAP Cardiac Apparatus (HEGDE, BUCH et al. 2004)

(Shahinpoor and Kim 2005, Shahinpoor 2009, Shahinpoor 2010) Suggested using IPMC to make a heart compression/assist device. This device was based on three IPMC fingers, each with 2 mm thickness and plated with 24-carat gold, mounted on a base and surrounding the heart. Upon activation, these IPMC fingers will contract and apply a gentle force on the outer wall of the heart, enhancing the blood circulation and assisting the weak heart. The design is shown in **Figure 2.16**, where 42 is the patient's body, 5 the heart, 3 IPMC fingers, 30 the base of the device, 10 a wire, 46 the rib cage, 12 power supply, and 44 abdomen. IPMCs were chosen because of their flexibility, and softness, which can apply enough gentle force to the heart without damaging the ventricle.

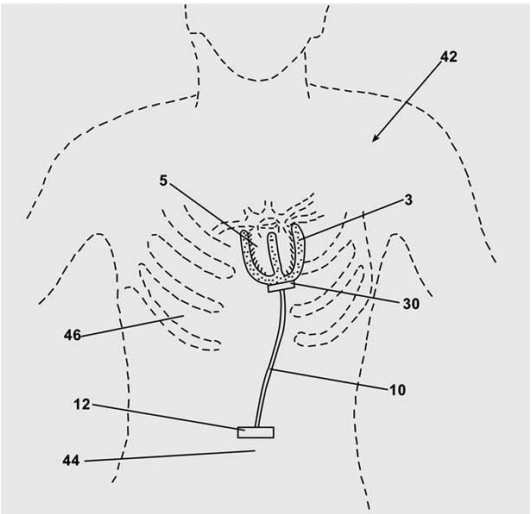

Figure 2.16 Three Fingers IPMC VAD (Shahinpoor 2010)

2.5 Proposed Solutions

Most of the available devices in the VAD field focus on creating a pump, either internal or external, and using it parallel to the heart. These devices are big bulky and not suitable for all patients. In addition, they are in direct contact with the blood, which causes blood cell damage, blood clots, and leads to more serious risks of thromboembolism in the circulatory system. Several studies focused on improving the biocompatibility of the material in contact with blood to minimise the mentioned risks (Kobayashi, Ohuchi et al. 2005).

In this thesis, a new approach is suggested, where this method will help the heart in its job, and assist the heart during the contraction phase. The proposed device is based on a thin mesh made from a smart material that fits around the patient's heart. This structure can change its shape; contracts and expands based on a controlling signal. The movement of the device will produce a mechanical force to assist the heart to contract, which will generate enough pressure inside the heart's chambers, and will lead to a normal blood flow in the body. The main advantage of this newly proposed device is that the blood will not be in contact with any foreign surface, unlike any other previous VADs, where blood will be exposed to a high risk of coagulation, and patients should use anticoagulations for their whole life (Lowe, Hughes et al. 1999). This proposed device will eliminate this risk by keeping the blood circulating inside the normal blood vessels without contacting any artificial surface.

Our approach is to use Electro-Active Polymer (EAP) as a smart material, in particular, IPMC, to design and test this new VAD. IPMCs have unique characteristics making them the ideal solution for this design, such as their excellent chemical stability, good mechanical strength, remarkable thermal stability, and very high electrical conductivity. This new device has a unique shape that can fit around the wall of the heart, and occupy a minimum space around the heart; all the other components will be installed in the rib cage and the abdomen area. By using smart materials, like EAP, this device can expand and suits the different sizes of the heart. Additionally, this new VAD has a very low power consumption; this will allow us to apply some techniques to harvest energy from inside the patient's body, eliminating the need to use a percutaneous power cable.

Here in this thesis, three solutions are suggested to solve this problem:

2.1 VAD powered directly from IPMC placed on the diaphragm

The first solution suggests creating a VAD made from IPMC actuators and power this VAD directly from another sheet of IPMC that is placed on the diaphragm. The continuous movement of the diaphragm will constantly activate the IPMC actuator, which will produce electrical power that is used to run the VAD. **Figure 2.17** shows the proposed option where 1 is the patient, 2 the heart, 3 the IPMC mesh around the heart, 4 the controlling device, 5 the wires, 6 the diaphragm, and 7 IPMC sheets to harvest electrical power.

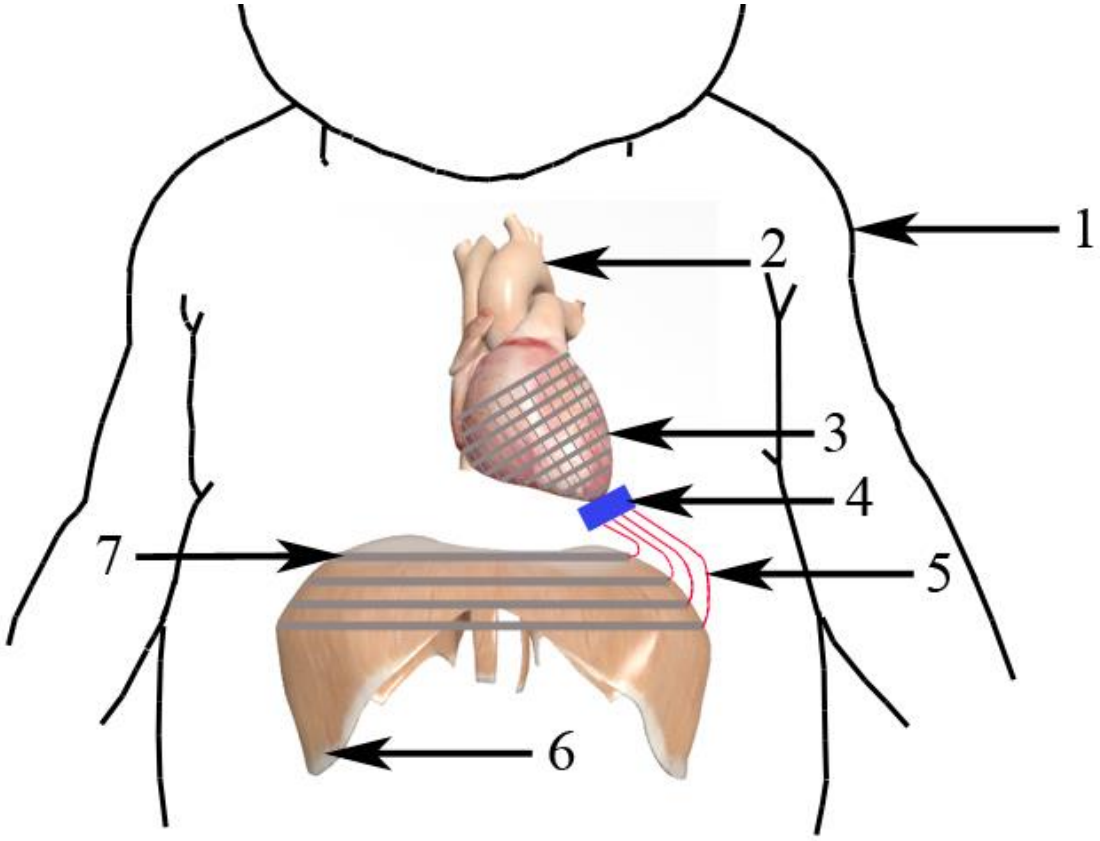

Figure 2.17 Proposed solution option 1

2.2 VAD powered from a battery charged from IPMC placed on the diaphragm

If the first solution is not producing sufficient electrical energy directly to run the VAD, then we can use an internal battery to run the VAD and use the sheet of IPMC placed on the diaphragm to charge the battery. **Figure 2.18** shows the proposed option where 1 is the patient, 2 the heart, 3 the IPMC mesh around the heart, 4 the controlling device, 5 the wires, 6 the battery, 7 IPMC sheets to harvest electrical power, and 8 the diaphragm.

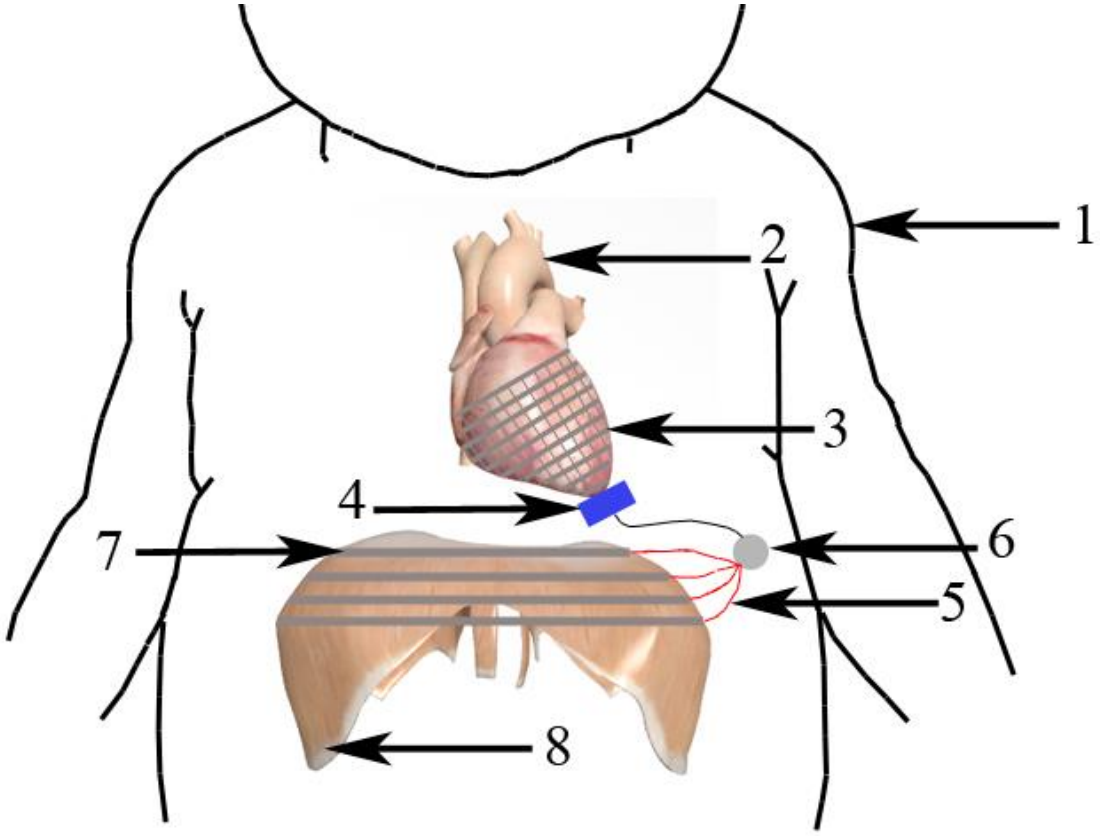

Figure 2.18 Proposed solution option 2

2.3 VAD powered from a battery charger transcutaneously

The final option is to use an internal battery to run the VAD that can charge transcutaneously without any cable connection. **Figure 2.19** shows the proposed option where 1 is the patient, 2 the heart, 3 the coil, 4 the wires, 5 the battery, 6 the controlling device, and 7 IPMC mesh around the heart.

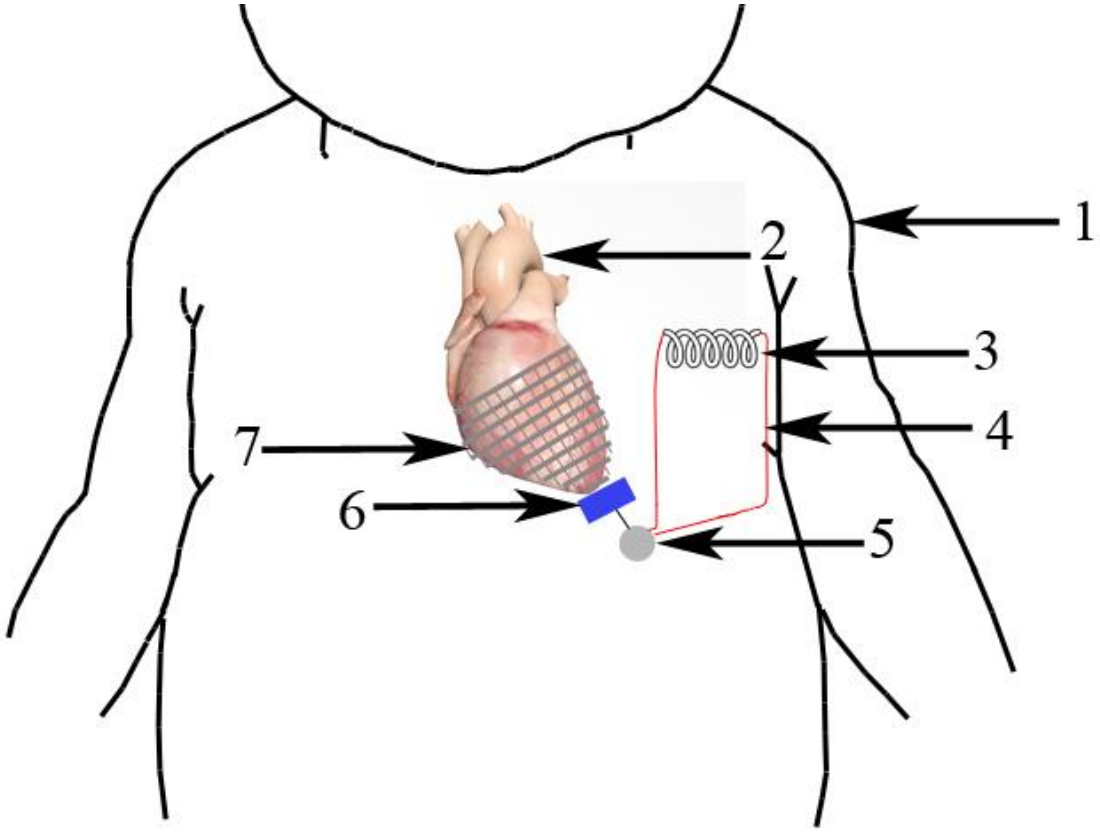

Figure 2.19 Proposed solution option 3

2.4 Properties of the Proposed Device

2.5.4.1 *Self-Powered*

All previous VADs require an external power source to keep the VAD running; this requires having a percutaneous cable to connect the VAD with the external power supply. Therefore, the proposed device should be self-powered from an internal power supply that can generate power from inside the patient's body, or to transfer the power wirelessly and store it in an internal battery inside the patient's body without any need for cables coming out of the patient's skin.

2.5.4.2 *Small Size*

In paediatrics, their heart is very small, and there is not enough room around the heart to insert any implants. For this reason, the proposed device should be as small as possible to fit in this space without affecting the other organs.

2.5.4.3 *Ability to Grow*

The heart's size is not fixed; it changes its size over the growing period from infancy to adulthood. The proposed device should fit the heart during the growth stage without any need to replace the VAD with a bigger size one.

2.5.4.4 *Control the Rhythm*

The heart contraction cycle consists of different phases, where each part of the heart contracts at a specific time. The proposed device should follow the same heart contraction cycle to produce the same blood flow pattern.

2.6 Hypothesis

In this thesis, two main hypotheses are suggested:

We can use IPMC to generate enough mechanical power to force the heart to contract.

We can use IPMC to generate electricity to charge a battery.

2.7 Summary

This chapter explained the theory behind the proposed device, and the listed the proposed solution with the hypothesis. The next chapter will account for the development of the proposed device and explains all the experiments.

Chapter 3

Device Development

3. *Device Development*

3.1 Introduction

This chapter will discuss the requirements of the proposed device regarding force, displacement, and frequency. Then it will explain step by step the development of the IPMC actuators that are used to make the proposed device.

3.2 Device Requirements

The idea of applying external mechanical force on the heart has been under research for a few decades, mainly using pneumatic power (Lowe, Hughes et al. 1999). While this has been the most common approach, some challenges are associated with it. Principally, related to the need for an external driving mechanism that is both bulky and represents an infection hazard. The solution proposed in this present work suggests a more miniaturised solution with no major concerns to the external environment. The proposition is to employ IPMC actuator to apply a mechanical force on the wall of the heart, which will maintain the pulsatile blood flow without the use of an air compressor.

2.1 Compressing Force

The first criterion in the design is to know how much compression force this proposed device needs to generate to facilitate the compression of the heart. Assuming the left ventricle has a conical shape, and the applied force is uniform on the surface, then the pressure inside the ventricle can be calculated using equation (3.1), where **P** is the pressure in (Pa), **F** is the force in (N), and **A** is the surface area in (m^2)

$$P = \frac{F}{A} \quad (3.1)$$

3.2.1.1 *Size of the Left Ventricle*

Assuming the left ventricle has a conical shape as shown in **Figure 3.1**.

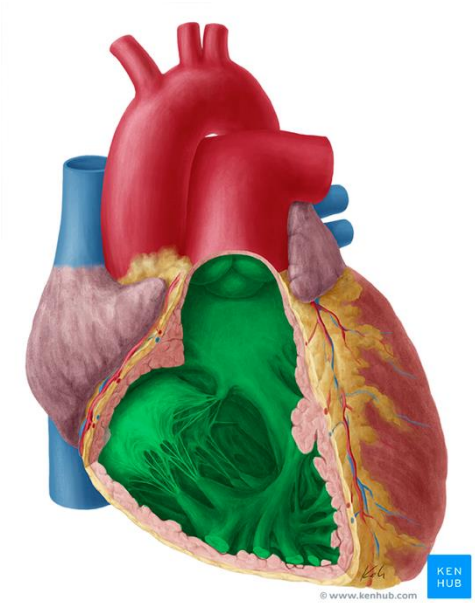

Figure 3.1 Anatomy of the Left Ventricle (HUB 2017)

The lateral surface area can be calculated using the following equation:

$$A = \pi \times r \times \sqrt{r^2 + h^2} \quad (3.2)$$

Where **r** is the radius of the base of the cone, and h is the height of the cone, as shown in **Figure 3.2**.

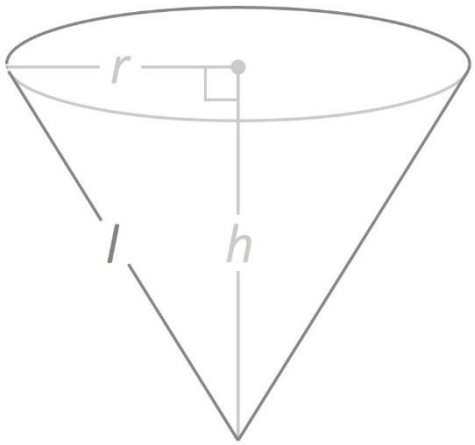

Figure 3.2 Lateral surface area of a cone

The base of the cone represents the width of the left ventricle, which varies between diastole and systole, and also changes a lot depending on the age of the patient. The maximum width of the left ventricle will be at the end of the diastole phase when the heart is fully expanded. Therefore, it will be considered as the width where the proposed device is applying the compressing force.

In the paediatric domain, the width of the left ventricle at the end of the diastole phase is D=1.425 cm, and the length is h=2.6 cm when accurate measurements are taken at birth (Sharland and Allan 1992).

While in the adult domain, the left ventricle measures D=5 cm in width at the end of the diastole phase (Gibson, Becher et al. 2014), and h=9.5 cm in length (Støylen, Mølmen et al. 2016).

From equation (3.2):

Lateral surface area of a paediatric= 6 cm^2 = 6x10^{-4} m^2

Lateral surface area of an adult = 29.4 cm^2 = 29.4x10^{-4} m^2

3.2.1.2 *Pressure Inside the Left Ventricle*

For a healthy heart stroke, the pressure inside the ventricle needs to reach a certain level; this pressure level is linked to the patient's size, age, and physical requirements. The adult blood pressure inside the left ventricle will oscillate between 0 and 120 mm Hg during each cardiac cycle, as shown in **Figure 3.3** (Martini F. 2011). The heart beats around 60-70 BPM, and the left ventricle pumps around 70 ml of blood each beat (Shahinpoor 2010). While in paediatrics, the left ventricle blood pressure could reach a maximum of 170 mm Hg and then gradually decreases to 100 mm Hg at the age of 16 years (Macfarlane 2006).

To use the pressure values in equation (3.1), they should be converted to Pa:

Paediatric maximum left ventricle blood pressure= 170 mm Hg = 22664.8 Pa

Adults maximum left ventricle blood pressure= 120 mm Hg = 15998.7 Pa

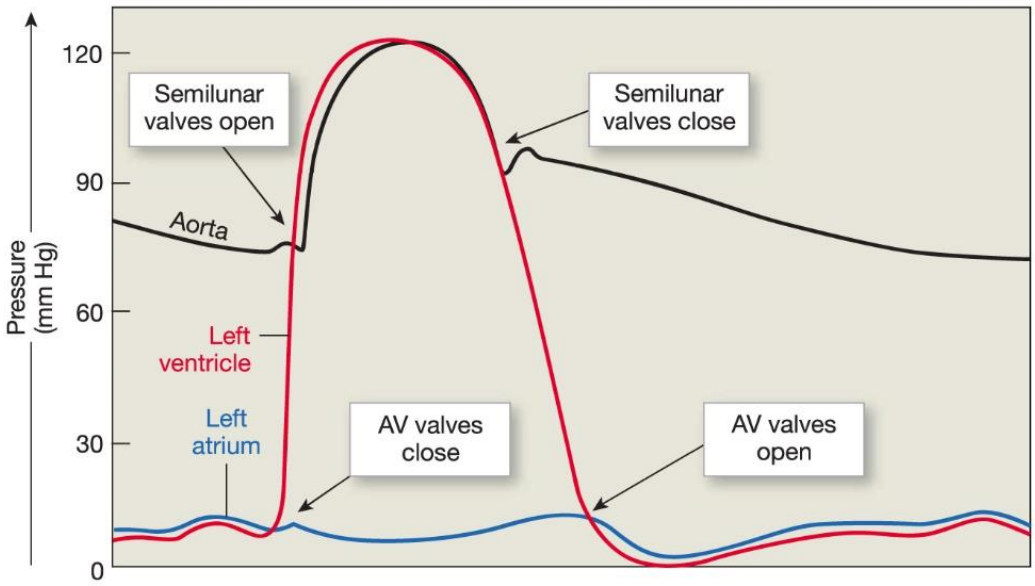

Figure 3.3 Ventricular Blood Pressure in Adults (Martini F. 2011)

3.2.1.3 *Force*

This force represents the approximate external force needed to get a healthy heart stroke. In other words, the proposed device should at least match this force to get the desired blood pressure inside the ventricle and maintain a healthy blood flow.

Then, from equation (3.1), the force can be calculated for both paediatrics and adults:

$$F = P \times A \quad (3.3)$$

For paediatrics:

$$F = 22664.8 \times 6 \times 10^{-4} = 13.6 \text{ N}$$

For adults

$$F = 15998.7 \times 29.4 \times 10^{-4} = 47 \text{ N}$$

The previous values give an idea of the minimum approximate external mechanical force that should be applied to the heart to maintain a healthy pulsatile blood flow.

Heart's wall elasticity and the ventricle thickness are also other aspects that should be considered when finalising the design. These parameters should be included in the design to determine the exact amount of force needed for each patient. In this study, the focus is on the main parameters, which are the size of the ventricle and the ventricle pressure.

2.2 Displacement

In systolic phase the heart contracts, which makes the left ventricular diameter smaller than the diastolic phase. Therefore, the proposed device should contract to the same diameter.

In adults, the left ventricle end systolic diameter varies between 2 cm to 4 cm depending on the physical requirements of the body (Talley and O'Connor 2009), which means the proposed device should be able to shrink its dimension by 20% to 50% from its original form.

2.3 Frequency

Normal heart rate represents the working frequency of the proposed device. The paediatric heart pumps at a rate of 130 BPM at birth and decreases towards 60 BPM with growth. Therefore, the proposed device should cover a range from 130 BPM to 60 BPM, which means roughly the range between 1 Hz to 2 Hz.

2.4 Summary

Table 3.1 summarises all the required parameter of the proposed device:

Parameter	Range
Compressing force	13.6 N to 47 N
Displacement	20% to 50%
Frequency	1 Hz to 2 Hz

Table 3.1 Device requirements

3.3 Primary Investigation Phase

The practical phase of the project started by looking at the current suppliers of IPMC Artificial Muscles to evaluate their mechanical and electrical properties. As this type of material is still in its infancy stage, and they are not available commercially, the search moved towards research centres and universities that have experience with EAP. Four pieces of platinum coated IPMC Artificial Muscles were bought from Environmental Robots Incorporated (Bangor, Maine, USA), measuring (0.5x3 cm) and thickness of 0.2 mm on 15/3/2013. To drive the IPMC, they came with a variable voltage/frequency power supply and dynamic signal generator, which is powered by a 9 V battery. This signal generator generates a square wave and can change the output frequency from (0-20 Hz), and the output voltage from (0-8 V), as shown in **Figure** 3.4.

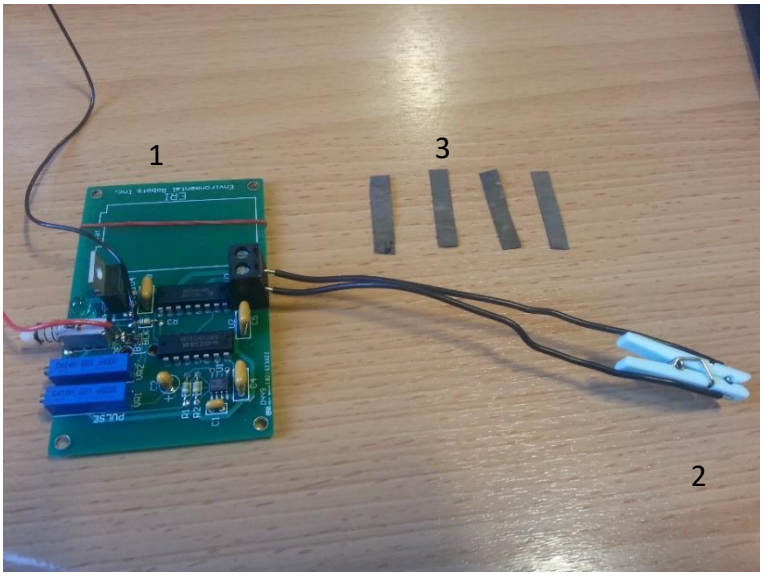

Figure 3.4 IPMC Artificial Muscles from (Bangor, Maine, USA) 1- signal generator, 2-alligator clip, 3- IPMC strips.

Towards the end of the project for further comparison, two samples were bought on 27/4/2016. The first was Gold plated IPMC measuring 35x42x2 mm, and the other was 5x30x0.2 mm platinum plated.

2.1 Primary Bench Test

IPMCs showed a noticeable mechanical response when an electric current was applied to the strips, under both dry and wet conditions. In the dry conditions, where the samples were left to dry for a few hours on the bench, IPMCs showed a short time of actuation before it stopped, around 56 seconds. While in the wet conditions, where they were soaked in water for a couple of minutes before testing. IPMCs showed a longer duration of actuation than in the dry conditions. Higher voltages, more than 7 volts, caused the materials to heat up and left some burn marks on both sides of the strip under the alligator clip. IPMCs showed a shorter duration of actuation at high frequencies in both wet and dry conditions; **Figure 3.5** below shows IPMC in the bending stage.

Figure 3.5 IPMC bending

The materials showed promising responses to an electric stimulus under different voltages, frequencies and testing conditions. Therefore, they have the potential for further studies to quantify their mechanical and electrical properties.

2.2 Challenges

To quantify the mechanical and electrical properties of IPMC, more samples were needed with a variety of shapes, thicknesses, and coating metals. As these IPMCs were still produced in research centres and universities, the cost of buying them was extremely expensive. The cost of the previous beginner kit was $584. To make things more complicated, most of the IPMCs are custom made, and they have to be pre-ordered weeks in advance. For those reasons, the project focus moved to the next step, which is to fabricate IPMC in the lab.

3.4 Fabrication of IPMC

Ionic Polymer Metal Composites (IPMC) are currently the best-known type of EAPs, and they have the largest spectrum of applications, especially in biomimetic robotics (Must, Kaasik et al. 2015). It is now well known and documented that ionic polymers with a conductive metal can exhibit a significant deformation when electrically activated. Conversely, a dynamic strain of IPMC produces a dynamic voltage across the polymeric membrane (Shahinpoor and Kim 2001). When IPMC is hydrated, the positive ions can move freely inside the polymeric matrix, while the negative ions are fixed with the carbon chain of the polymer. When an electric field is applied, the positive ions will move towards the cathode side, while the negative ions will stay fixed in place. This will cause the membrane to expand at the cathode side and contract at the anode side, which will lead the membrane to bend to the anode side (Chen, Um et al. 2011).

The fabrication method of IPMCs starts with a polymeric membrane with an ion exchange capability (often called ionomers), which is then coated with a metallic layer on both sides, as shown in **Figure 3.6** (Shahinpoor and Kim 2000). Mechanical and electrical properties of IPMC are determined by the type of polymer, thickness of polymer, the metal particles, and the fabrication method (Kim and Shahinpoor 2003). For example, a thin IPMC creates a larger displacement, while a thick one produces a larger blocking force (Trabia, Hwang et al. 2016).

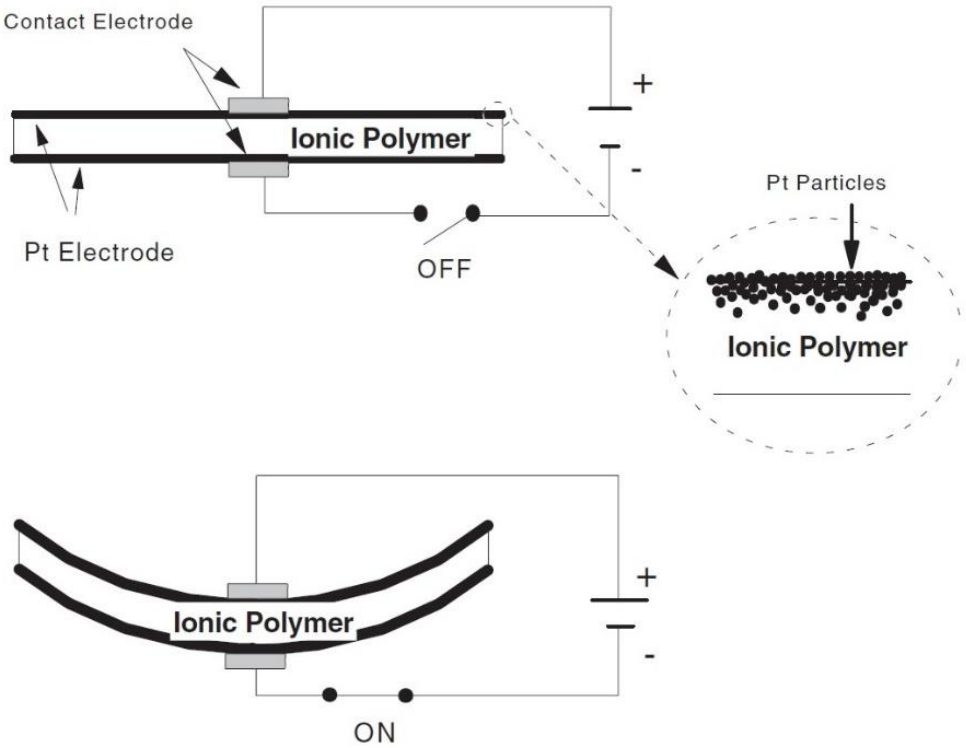

Figure 3.6 Schematic diagram of IPMC Artificial Muscle (Shahinpoor and Kim 2001)

2.1 Ion Exchange Membranes

Ion exchange membranes are designed and synthesised to selectively pass ions of single or multiple charges, which means ions are mobile within the materials of the membrane. There are several commercial ion exchange membrane manufacturers, including Aqualitics, Asahi Chemicals, Asahi Glass, DuPont, W L Gore, Ionics, Solvay, Sybron, Tokuyama, Membranes Internationals Inc., and fuMA Tech (Park, Palmre et al. 2014). The most common used ion exchange membranes to make IPMC are Nafion from DuPont, Neosepta from Tokuyama, Aciplex from Asahi Chemicals, and Flemion from Asahi Glass. (Kim and Shahinpoor 2003). In this project, Nafion from DuPont is considered as the base polymer for IPMC.

Nafion from DuPont (perfluorinated membrane) is one of the most common used ion exchange material, the chemical structure of Nafion is shown in **Figure 3.7**. Developed in the 1960s by DuPont and commercialised in the 1970s, Nafion is widely used for Proton Exchange Membrane (PEM) fuel cells and water electrolysers. The membrane performs as a separator and solid electrolyte in a variety of electrochemical cells that requires the membrane to selectively transport cations across the cell junction (DuPont 2009, Bahramzadeh and Shahinpoor 2014).

Table 3.2 list all the properties of Nafion 117

Property	Value
Thickness	170 µm
Water uptake capacity	Up to 30% at room temperature
Volume expansion	12-15%

Table 3.2 Representative properties of Nafion 117 (Kim and Shahinpoor 2003)

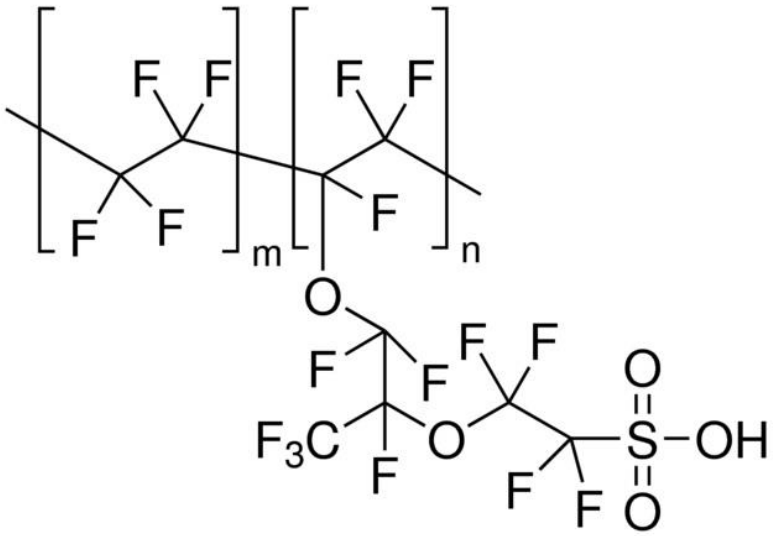

Figure 3.7 Chemical Structure of Nafion (DuPont 2009)

Polymeric membrane preparation methods:

Readymade: this method is considered the easiest one to make IPMC, where the polymer is bought in sheets, and ready to start the plating process directly. This approach is suitable to create regular shapes. On the other hand, this option is associated with a high cost. For example, buying 8×10 inches Nafion membrane would cost £429.

Hot Pressing: this method starts with single sheets of Nafion membrane and stacks them on top of each other to achieve a thicker membrane. The main advantage of this approach is that it can control the thickness of the final membrane by changing the number of layers stacked on top of each other. The membranes will be placed between two hot press plates, heated up to 180^{o}C for 20 minutes, and then pressed with a medium pressure 50 MPa for 10 minutes (Lee, Han et al. 2006).

Electrospinning: this method is used to manufacture very thin large-scale membranes. Polymer pellets are dissolved in appropriate solution to prepare the desired Nafion mixture (Põldsalu, Mändmaa et al. 2015). The electrospinning system consists of a high voltage generator, a micro syringe pump, a stainless steel collecting roller wrapped with aluminium foil, and a plastic syringe with a stainless steel needle. The syringe is filled with a Nafion solution, and then the needle is connected to the high voltage generator, while the collecting roller is attached to the ground. The voltage applied between the needle and the roller is between 10-13.5kV, and the distance between them is 10 cm. This procedure can produce a very thin membrane in the range of 20 µm (Lee and Yoo 2011)

Spraying: Nafion is available in different forms; one of them is water dispersion, which gives the opportunity to make IPMC in unique shapes. Water dispersion also allows mixing Nafion with other polymers for various reasons. (Trabia, Hwang et al. 2016) Reported creating IPMC actuators from water dispersion Nafion using an airbrush, and then chemically coat with platinum, as shown in **Figure 3.8**. The Nafion spray membrane has a thickness of 300 µm, and the final actuator showed almost identical characteristics to the commercial IPMC.

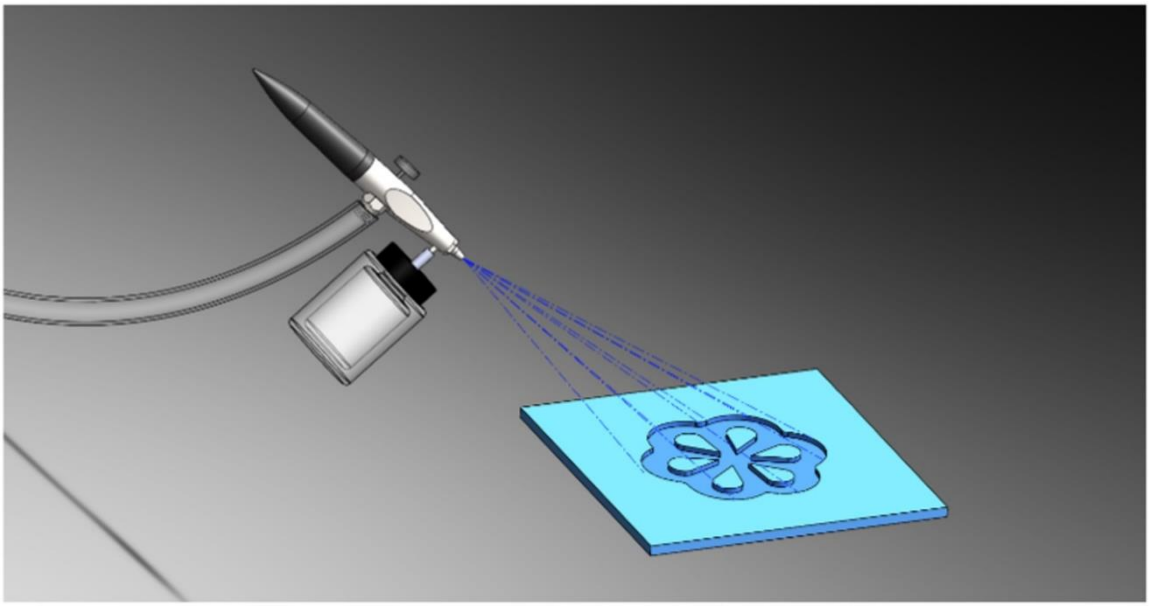

Figure 3.8 Water dispersion Nafion (Trabia, Hwang et al. 2016)

Casting: this method is used to obtain certain shapes of IPMC. The membrane is prepared from blended polymers, depending on the application, and then dissolved in Dimethylformamide (DMF) to form a polymeric solution. This solution is then poured into the mould to get the desired shape. After a curing process, the membrane will be ready for the plating process. The main disadvantage of this method is producing many micro and macro

cracks in the membrane during drying. On the other hand, this approach is suitable for producing very thick membranes, up to 2 mm (Panwar, Cha et al. 2012, De Luca, Digiamberardino et al. 2013, Panwar, Ko et al. 2013, Hwang, Palmre et al. 2015, Zhao, Wang et al. 2015). Also, this technique could be used to cast multi-layers of Nafion on top of each other, which is a handy tool to produce a layer by layer configurations (Lee, Yoo et al. 2014). Membranes with different properties could be cast separately and then combined by hot pressing to produce one thick membrane with multi-layers (Liu, Ghaffari et al. 2012)

2.2 Non-Electric Plating Protocol

Many groups have developed their fabrication protocol of IPMC, which produced IPMC actuators suitable for different applications (Chen, Um et al. 2011, De Luca, Digiamberardino et al. 2013). In general, all these protocols follow almost the same structure, which involves two main steps: first is the initial compositing process, and then the surface electroding process (Park, Jung et al. 2008). The initial compositing process requires an appropriate metal salt such as platinum $Pt(NH_3)_4HCl$ in the context of chemical reduction processes (Kim and Shahinpoor 2002), palladium $Pd(NH_3)_4Cl_2$ (Kim and Kim 2008, Liu, Wang et al. 2014, Zhao, Wang et al. 2015), nickel (Fang, Ju et al. 2007), gold (Zadin, Krasheninnikov et al. 2015), or silver $AgNO_3$ (Chung, Fung et al. 2006). Platinum is the preferred metal because it is largely immune to corrosion, and allows the use of high driving voltages without causing damage to IPMC actuators (Malone and Lipson 2006). Other methods of plating such as electroplating, physical deposition, and electrochemical deposition were also reported (Jeon, Yeorn et al. 2008).

The principle of the compositing process is to metallise the inner surface of the polymer by a chemical reduction means such as $LiBH_4$ or $NaBH_4$. The ionic polymer membrane is soaked in a salt solution to allow platinum-containing cations to diffuse through via the ion-exchange process. Later, a proper reducing agent, such as $LiBH_4$ or $NaBH_4$, is introduced to metallise the polymer. The primary reaction for the platinum composite is shown in equation (3.4) (Shahinpoor, Bar-Cohen et al. 1998)

$$NaBH_4 + 4[Pt(NH_3)_4]^{2+} + 8HO^- \rightarrow 4Pt^0 + 16\ NH_3 + NaBO_2 + 6H_2O \quad (3.4)$$

In this stage, the metallic platinum particles are not homogeneously formed across the membrane but concentrate predominantly near the interface boundaries, and only buried

few microns deep in the membrane. Therefore, the second step is applied, where multiple reducing agents are introduced to continue the reducing process and enhance the surface roughness (Shahinpoor and Kim 2001). **Figure 3.9** shows the difference between the first and the second stage of the IPMC fabrication.

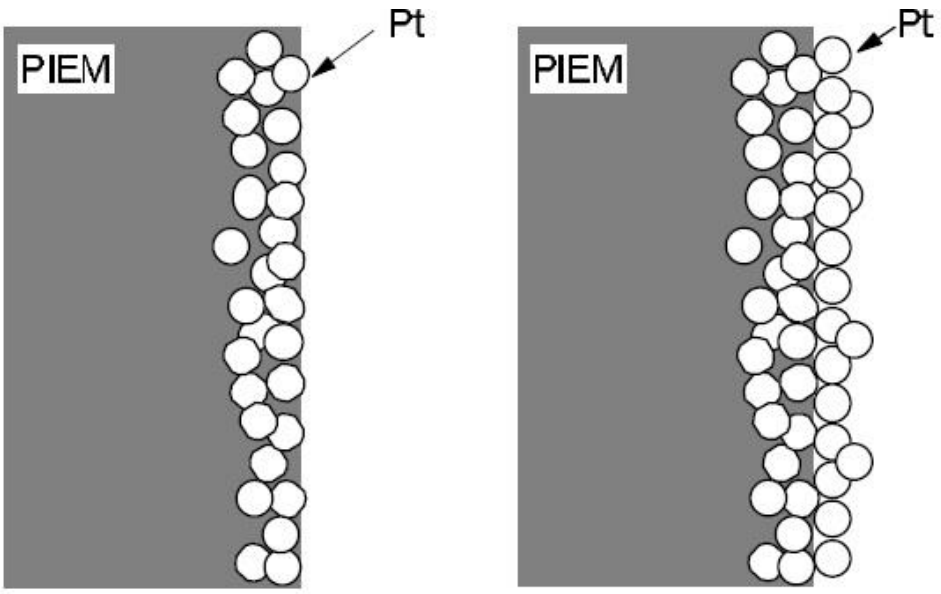

Figure 3.9 IPMC preparation process: left after the initial compositing process, right after the surface electroding process (Shahinpoor and Kim 2001)

The first and second steps could be repeated a few times to reach the desired thickness of electrodes on the IPMC surface as shown in **Figure 3.10**

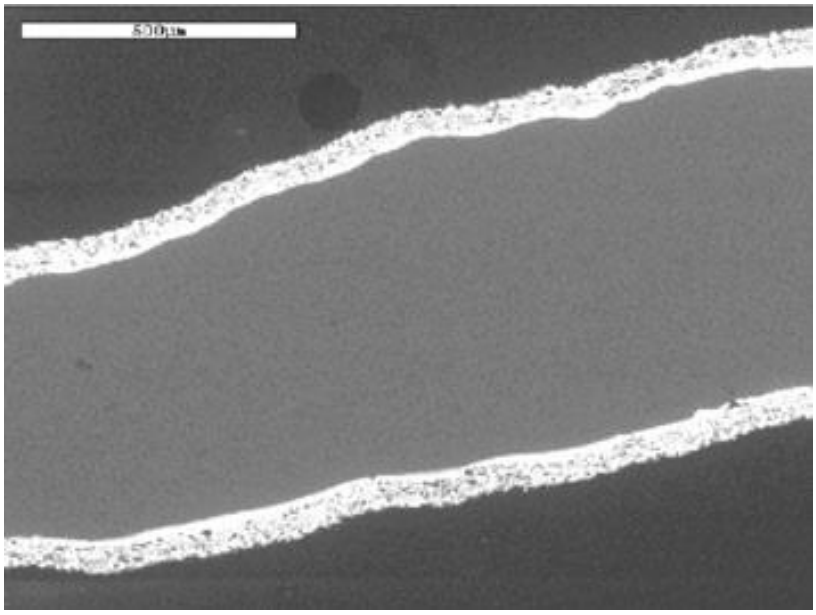

Figure 3.10 Cross section of IPMC showing the two electrodes and the Nafion membrane in the middle (Kim and Shahinpoor 2003)

All materials used in IPMC fabrications were bought from (Sigma-Aldrich, UK), including the Nafion 117 membrane and the chemicals, as shown in **Figure 3.11**.

Figure 3.11 Chemicals used to make IPMC

Table 3.3 shows a list of all the materials used during these experiments:

No	Item
1	Nafion.TM. 117 membrane 0.007 inch thick
2	HCl (Hydrogen chloride)
3	$(Pt(NH_3)_4\ Cl_2)$ (Tetra-amine platinum chloride hydrate)
4	$Pd(NH_3)_4Cl_2{\cdot}H_2O$ (Tetra-ammine palladium(II) chloride monohydrate)
5	NH_4OH (Ammonium hydroxide)
6	$NaBH_4$ (Sodium borohydride)
7	$H_2NOH.HCl$ (Hydroxylamine hydrochloride)
8	$H_2NNH_2.H_2O$ (Hydrazine monohydrate)
9	NaOH (Sodium hydroxide)

Table 3.3 Materials used to make IPMC samples

The method utilised in this project contains the following the major steps, as shown in **Figure 3.12**:

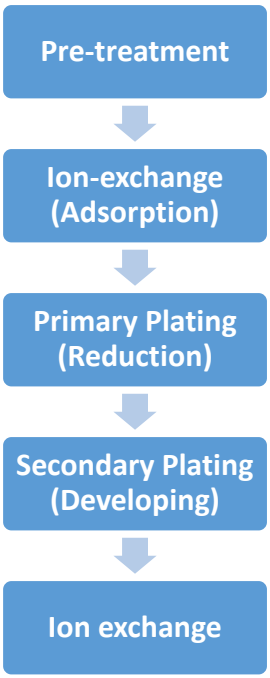

Figure 3.12 IPMC Fabrication process

Pre-treatment: At this step, the surface of the Nafion 117 membrane will be prepared to receive the metal ions. The membrane is shown in **Figure 3.13**.

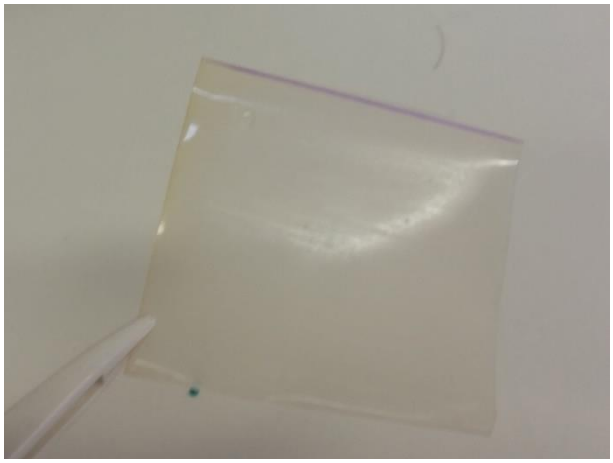

Figure 3.13 Nafion 117 membrane before surface treatment

It includes surface treatment of the polymer using sandpaper, which will increase the surface area. Very fine sandpaper is used (Norton 600A). Then, the membrane will be cleaned in an ultrasound bath (Fisher Scientific, Germany) for 10 minutes to remove any residuals, as shown in **Figure 3.14**.

Figure 3.14 Ultrasound water bath

After that, the membrane will be boiled in 2.4N HCl solution for 30 minutes to remove any impurities and ions in the membrane, using a hot water bath (Grant Instruments, Cambridge UK) as shown in **Figure 3.15**.

Figure 3.15 Hot water bath

Finally, boiled in water to remove acid and to completely swell the membrane. **Figure 3.16** shows the Nafion 117 membrane at the end of this stage.

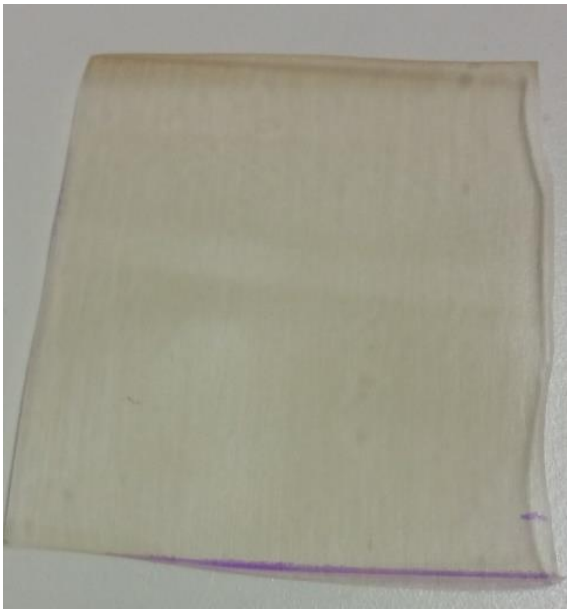

Figure 3.16 Nafion 117 after the surface preparation

Ion-exchange (Adsorption): Primary coating includes soaking the membrane in the platinum complex ($[Pt(NH_3)_4]Cl_2$ or $[Pt(NH_3)_6]Cl_4$) solution or any other metal salt solution, such as palladium or gold. The solution should contain more than 3 mg of Pt per cm^2 membrane area to cover the membrane with Pt completely. An Excess amount of the Pt solution is preferable. Then, the membrane is kept in the solution at room temperature for one night, while stirring at a low speed. **Figure 3.17** shows the Nafion 117 membrane at the end of this stage.

Figure 3.17 Nafion 117 membrane after the Ion-exchange stage.

Primary Plating (Reduction): Reducing step includes reducing the metal particles placed on the surface of the membrane, using some strong reducing agents, such as sodium borohydride $NaBH_4$. The amount of the reagent should be proportional to the area of the

membrane. In the sequence of addition, the temperature is raised from 40°C to 60°C gradually, while stirring at a medium speed. At the end of this stage, a black layer of fine Pt particles should be deposited only on both surfaces of the membrane; **Figure 3.18** shows the membrane at the end of this stage with a black layer covering its surface.

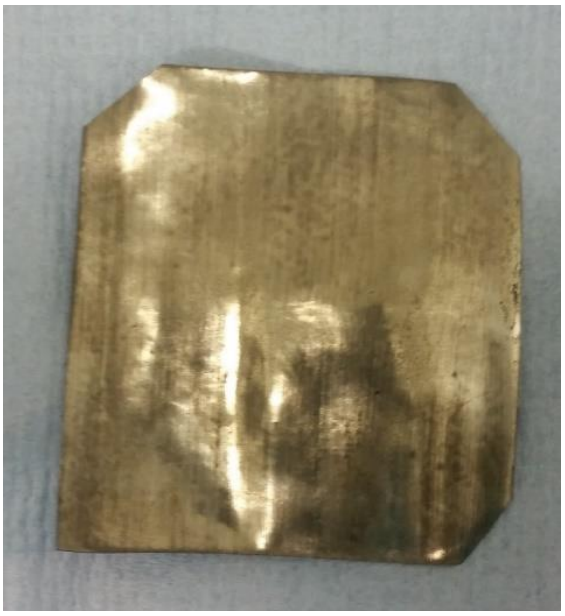

Figure 3.18 Nafion 117 after the Primary Plating stage

Secondary Plating (Developing): The amount of platinum deposited by the 1st plating (reduction process) is only less than 0.9 mg/cm^2, which depends on the ion exchange capacity, the thickness of the membrane, and the structure of the Pt complex. An additional amount of platinum is plated by the developing process on the deposited Pt layer. The Secondary coating stage includes soaking the membrane again in Pt solution and adding reducing agents. Plating amount is determined by the content of Pt in the solution. Both hydroxylamine hydrochloride (NH_2OH-HCl) and hydrazine monohydrate ($H_2NNH_2.H_2O$) are used as reducing agents during the developing process, while raising the temperature from 40°C to 60°C gradually; **Figure 3.19** shows the Nafion 117 membrane at the end of this stage.

Figure 3.19 Nafion 117 membrane after the Secondary Plating stage

Ion exchange: The final stage includes rinsing the membrane with water, and boiling in dilute hydrochloric acid to remove the ammonium cation in the membrane. After washing with water, H^+ in the composite can be exchanged for any cation by immersing in a solution of the chloride salt of the cation; the final IPMC is shown in **Figure 3.20**

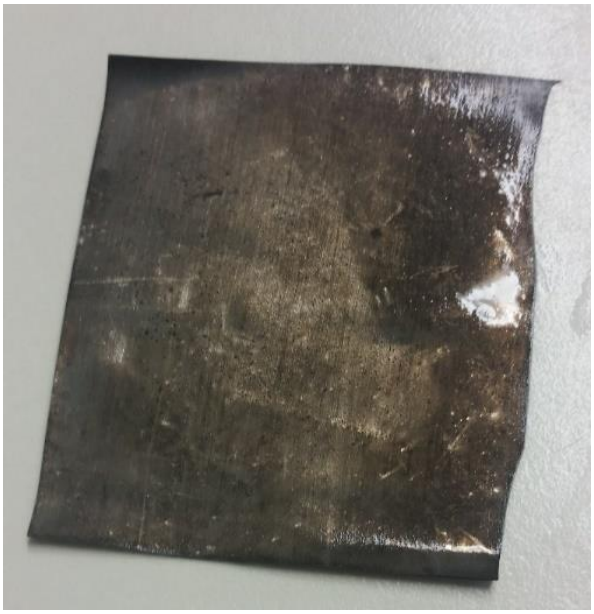

Figure 3.20 Final IPMC

The last setup of the IPMC fabrication is shown in **Figure 3.21**.

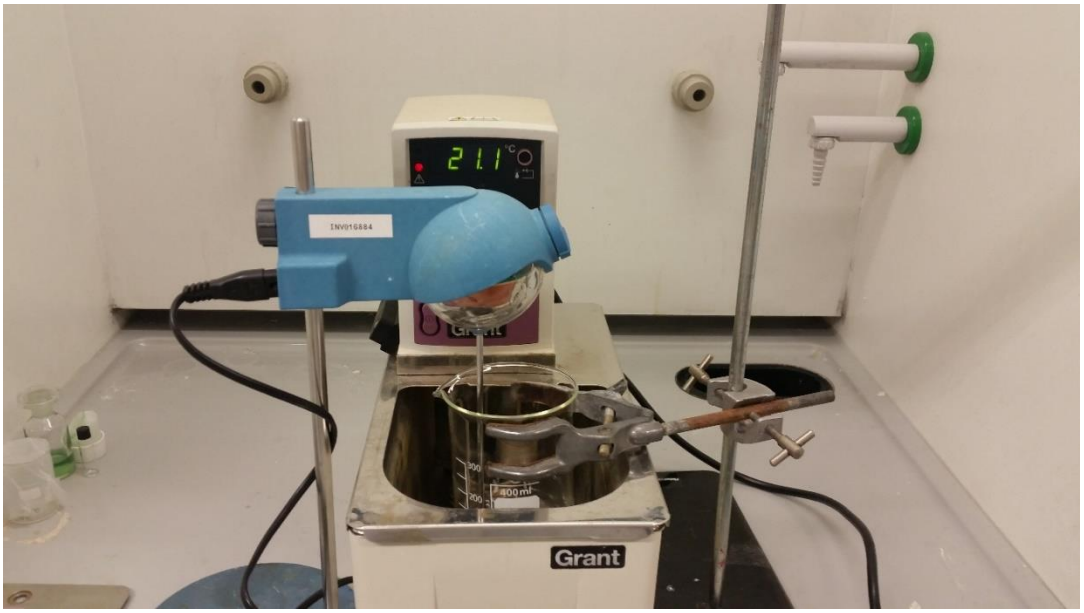

Figure 3.21 The full experiment setup

Table 3.4 summarise all the steps in IPMC fabrication:

1		*Pre-treatment* This is to roughen the surface of Nafion 117 to improve the surface adhesion by sandblasting. *Thermal treatment* This refers to thermal treatments in the oven for making the curved Nafion membrane.
2	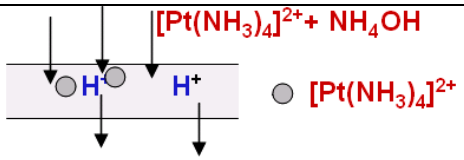	*Adsorption* This is for exchanging the hydrophilic ion clusters (H+) with the platinum complex cations overnight.
3	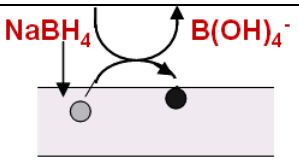	*Reduction (initial compositing)* This is for making platinum cations penetrate into the Nafion film in depth.
4	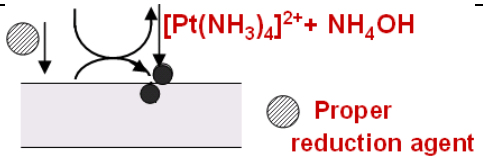	*Secondary plating (surface electroding)* This is for developing platinum layers on the primary plating surface to improve the electrical conductivity of the electrodes by the reduction method.
5	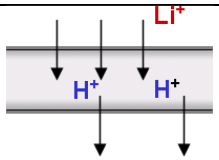	*Ion exchange* This is to exchange H+ in the IPMC membrane with other counter ions such as Li+ or Na+.

Table 3.4 Fabrication process of curved IPMC actuators (Yeom and Oh 2009)

2.3 Protocol Development

The manufacture of IPMC can be optimised to obtain the maximum force or displacement by changing some parameters during the manufacturing process. These parameters are water bath temperature, concentration of the metal salt, type of the metal salt, and repetition of secondary plating.

In this study, eight different protocols were used to make IPMC samples; all protocols followed almost the same structure which was reported by (Shahinpoor and Mojarrad 2002, Kim and Shahinpoor 2003, Yu, Shen et al. 2007, De Luca, Digiamberardino et al. 2013). Protocol **A** used platinum for plating, with two phases of secondary plating. Protocol **B** also used platinum for plating, and two steps of the secondary plating and treated only once with NaOH at the end of the process. Protocol **C** followed the same steps, the only change was increasing the temperature very slowly during the primary and secondary plating. Protocol **D** used platinum for plating; the membrane was treated with HCl only once at the end of the secondary plating. Protocol **E** used palladium and platinum both for plating. Protocol **F** used platinum for plating, repeating the primary plating twice before moving to the secondary step. Protocol **G** used palladium only for plating. Protocol **H** used platinum for plating, repeated the primary and secondary plating twice. The detailed protocols are all listed in the appendices (section 11.1). **Table 3.5** lists all the protocols with the plating metal used.

Protocol	Plating metal
A	platinum
B	platinum
C	platinum
D	platinum
E	palladium and platinum
F	platinum
G	palladium
H	platinum

Table 3.5 IPMC fabrication protocols with the plating metal type

2.4 Results

In this project, 11 IPMC samples were prepared from different protocols. All samples started with 2x2 inch of Nafion 117 and then cut into smaller sizes for testing 5x35 mm, (surface area

of 1.75 cm^2). At the end of this stage, two groups of IPMC were ready for the surface, mechanical, and electrical tests. The first group was the commercial samples as shown in **Table 3.6**:

Sample No	Coating
Commercial 1	platinum
Commercial 2	platinum
Commercial 3	platinum
Commercial 4	platinum
Commercial 5	platinum
Commercial 6	gold

Table 3.6 Commercial IPMC samples

The second group was the Strathclyde IPMC samples fabricated at the Department of Biomedical Engineering, Strathclyde University as shown in **Table 3.7**:

Sample No	Protocol No	Coating
Strathclyde 1	H	platinum
Strathclyde 2	G	palladium
Strathclyde 3	F	platinum
Strathclyde 4	E	platinum + palladium
Strathclyde 5	E	platinum + palladium
Strathclyde 6	D	platinum
Strathclyde 7	C	platinum
Strathclyde 8	B	platinum
Strathclyde 9	A	platinum
Strathclyde 10	A	platinum
Strathclyde 11	A	platinum

Table 3.7 Strathclyde IPMC samples fabricated at the Department of Biomedical Engineering, Strathclyde University

During the different stages of fabrication of Strathclyde sample 1 and 2, small fragments were taken from the membrane for further comparison under the SEM, as follows:

Fragment	Stage
1	Before the first immersion of the membrane in the metallic solution (Adsorption).
2	After the first immersion the membrane in the metallic solution (Adsorption).
3	After the first primary plating (Reduction)
4	Before the second immersion the membrane in the metallic solution (Adsorption).
5	After the second immersion the membrane in the metallic solution (Adsorption).
6	After the second primary plating (Reduction)
7	After the first secondary plating (Developing)
8	After the second secondary plating (Developing)

Table 3.8 Fragments taken during the fabrication stages

All samples then were stored in deionised water waiting for the mechanical and electrical tests, as shown in **Figure 3.22** and **Figure 3.23**

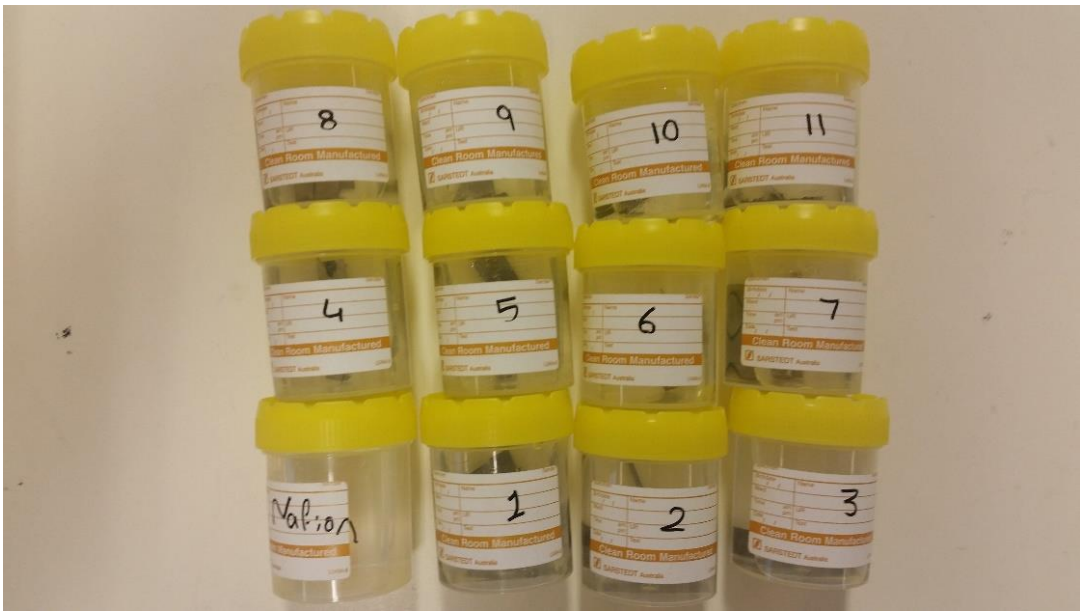

Figure 3.22 Strathclyde Fabricated IPMC samples

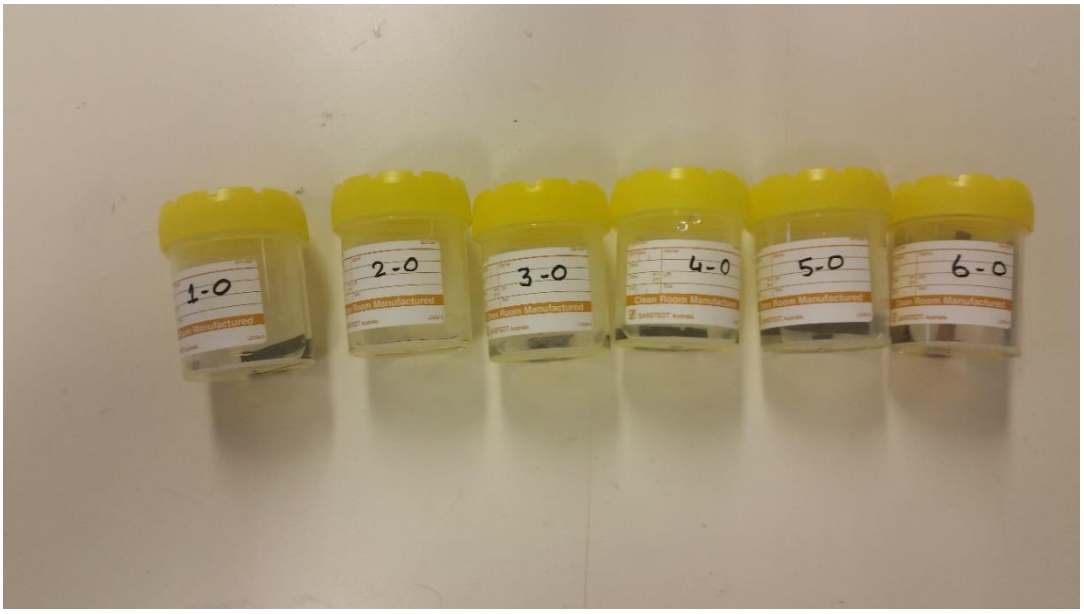

Figure 3.23 Commercial IPMC samples

2.5 Summary

At the end of this stage, two groups of IPMC samples were ready for characterisations. The first was the 11 Strathclyde IPMC samples prepared in the Department of Biomedical Engineering, Strathclyde University, and the second was the 6 Commercial IPMC samples bought from Environmental Robots Incorporated (Bangor, Maine, USA). Both groups will undergo a series of tests to evaluate their properties.

3.5 IPMC Driver

The actuation of IPMC depends on the electrical signal applied across the membrane. Therefore, the signal's shape, amplitude, frequency, and current all should be accurately controlled to optimise the movement of IPMC actuators.

The original sample bought from Environment Robotics Inc. (Bangor, Maine, USA) came with a basic function generator that can produce a square wave based on a 555 digital timer IC, with the ability to control the frequency and the amplitude, as shown in **Figure 3.4**. This function generator ran on a 9 V battery and was not able to provide sufficient current for testing. Therefore, it was not suitable for this study, and a new function generator with the ability to provide a high current was developed.

The ideal IPMC driver should be able to:

- Generate sine wave, square wave, and triangle wave.
- Adjust the amplitude between 0-10 V.
- Adjust the frequency between 0-2 Hz.
- Provide a driving current up to 2 A.

The first design was based on a voltage-controlled oscillator IC (XR-2209), which can generate triangle and square wave output. Both voltage and frequency of the generated signals were controlled by a potentiometer. The output of this IC was linked to an electrical current amplifier (OPA548T) (Yu, Shen et al. 2007, Vunder, Itik et al. 2014), which can provide a driving current up to 3 A; **Figure 3.24** shows the function generator. The main disadvantage of this design was the low accuracy in controlling the amplitude and the frequency of the generated signal. The output was connected to an oscilloscope to adjust the parameters all the time, so this option was abandoned.

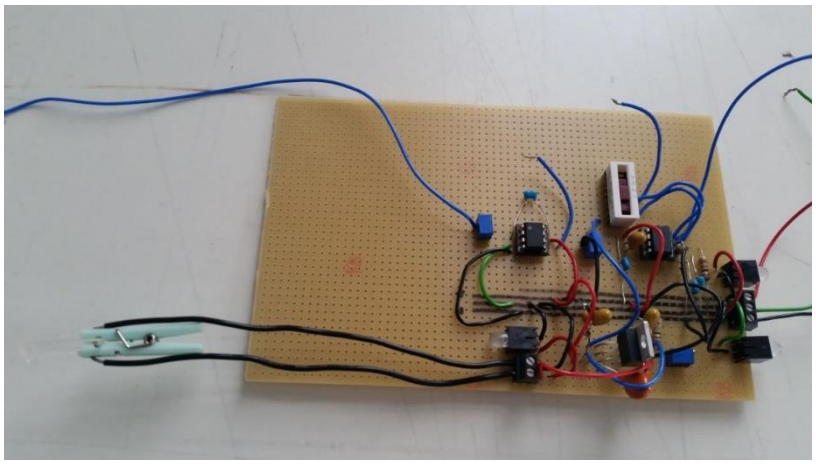

Figure 3.24 First design function generator

The second option was based on a signal generator (TG550, Aim TTi, USA), as shown in **Figure 3.25**, and the output was then connected to a current amplifier circuit using OPA548T. This option was more accurate than the previous one and was able to provide a sine wave, square wave, and tringle wave. This option lacks the ability to record the generated signal for further comparisons, so it was also abandoned.

Figure 3.25 Second design function generator

The third option was a computer based function generator, using Lab View 2015, DAQ system (NI USB 6225), and a current amplifier (OPA548T). Lab View was used to generate, control the signal parameters, and record the generated signal, while the DAQ system (16 bits ADC) was used as a Digital to Analogue Converter (DAC) at a rate of 1000 sample per second. Finally, the analogue signal was fed to the current amplifier and then applied to the IPMC actuator. **Figure 3.26** shows the current amplifier and the DAQ system.

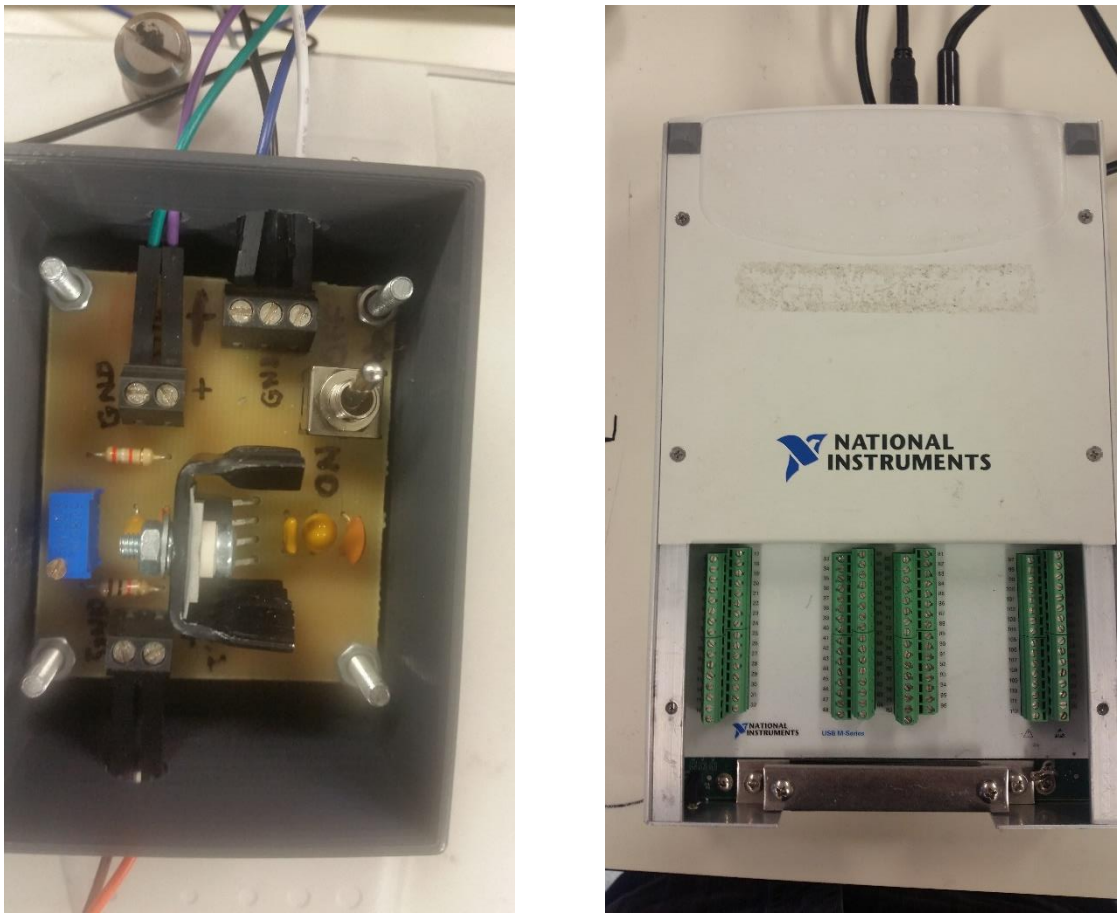

Figure 3.26 Current amplifier on the left, DAQ system on the right

Based on previous studies, the best signal to drive IPMC and obtain the highest response in displacement and blocking force is a square wave (Yu, Shen et al. 2007). Therefore, the square wave signal was used to test the IPMC actuators, with the amplitude of 0-10 V, and the frequency of 0-2 Hz. **Figure 3.27** shows a block diagram of the different stages of the IPMC controller.

Figure 3.27 Block diagram of IPMC driver

3.6 Summary

This chapter listed the requirements of the proposed device, explained the various stages of making the IPMC actuators, and finally showed the development of the IPMC driver electronic circuit. The next three chapters will focus on testing the surface topography, mechanical, and electrical properties of the IPMC samples.

Chapter 4
IPMC System Characterisation

4. *IPMC System Characterisation*

4.1 Introduction

This chapter will detail the different tests used to check the characterisation of the IPMC samples. The first group of tests (Surface tests, Thickness, Water uptake, and Surface Resistance) are used to test the quality of the fabricated Strathclyde IPMC and compare them with the Commercial IPMC samples, while the second group (Electrical Power Consumption, Displacement, and Blocking Force) are used to evaluate the IPMC as actuators to make the proposed device.

4.2 Surface Tests

Surface tests focus on the topography of the surfaces of the electrode, and the cross section of the actuator. The electrode surface shows an indication of the homogeneity of the metallic particles, which relates to the surface resistance, while the cross section test illustrates the penetration of the metallic particles inside the structure of the membrane. This is used as an indicator of the quality of the tested IPMC samples.

2.1 Experiment Setup

In this study, the Hitachi Scanning Electron Microscope (SEM) (tabletop scan 1000, Hitachi, Japan) was used to scan the surface of the IPMC actuators. SEM can scan the surface of a sample with a focused beam of electrons and produce an image of the surface's topography. SEM may also provide information about the chemistry and crystalline structure of the sample. In most applications, a particular area of the sample will be selected for scanning; this area could range from 1 cm to few microns in width. SEM will produce a 2D image of the chosen area with a magnification force from 20X up to 30,000X. Figure 4.1 shows the SEM used in this study.

Figure 4.1 Hitachi tabletop scan 1000 SEM

To prepare IPMC samples for scanning, a small fragment of the actuator was cut, placed on a sample holder and then placed inside the SEM vacuum chamber. **Figure 4.2** shows the holder on the left and the sample ready for scanning on the right.

Figure 4.2 The sample holder on the left and the sample ready for scanning on the right.

2.2 Top Surface Test

This test focuses on the electrode's surface morphology and the distribution of the deposited electrode metal particles on the surface of the membrane. The surface of the IPMC usually appears to be rough and cracked with discrete islands. This is believed to happen because of

the swelling of the polymeric membrane and bubbles during the reduction processes. This has a huge effect on the surface resistance of the IPMC (Park, Kim et al. 2007, Kim and Kim 2008). To improve the surface morphology, Kim used palladium as a buffer layer between the membrane and platinum, which showed a huge difference in the appearance of the surface of the electrode, and reduced the surface resistance from 3.3 Ω/□ to 1.2 Ω/□. **Figure 4.3** shows a comparison between two IPMC samples, the left one without Pd where the surface appeared cracked, and the sample with Pd on the right, where the surface seemed to be smoother and more homogeneous.

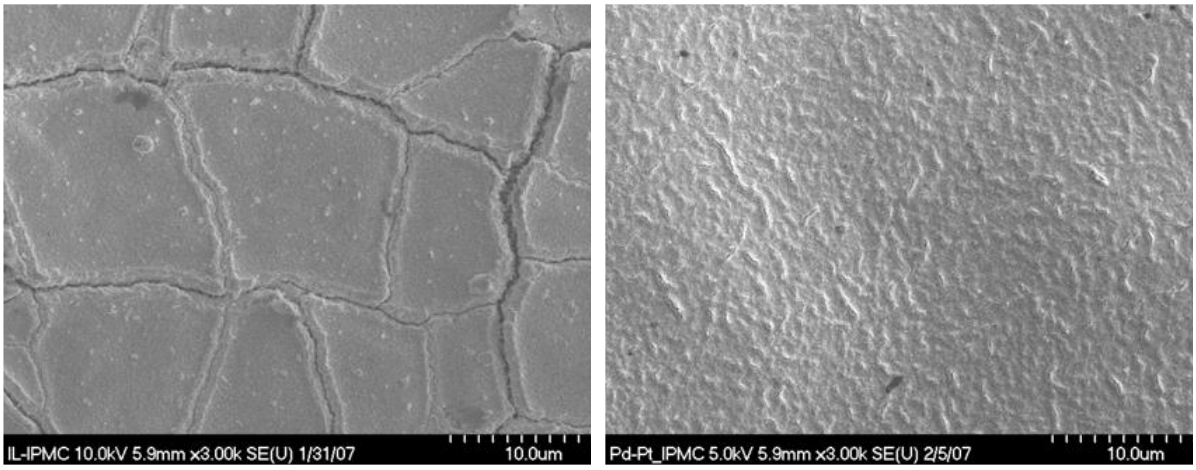

Figure 4.3 SEM images of IPMC without Pd on the left and with Pd on the right

All samples were scanned under different magnifications (200x, 2000x, 3000x, 6000x, 8000x, and 1000x) to obtain a clear perspective of the surface morphology. In the next section, a few examples are shown, and the rest of the photos can be found in the Appendices section (11.3).

4.2.2.1 *Results*

Figure 4.4 shows all top surface scanning images of the Commercial 5 IPMC under 6 different magnifications.

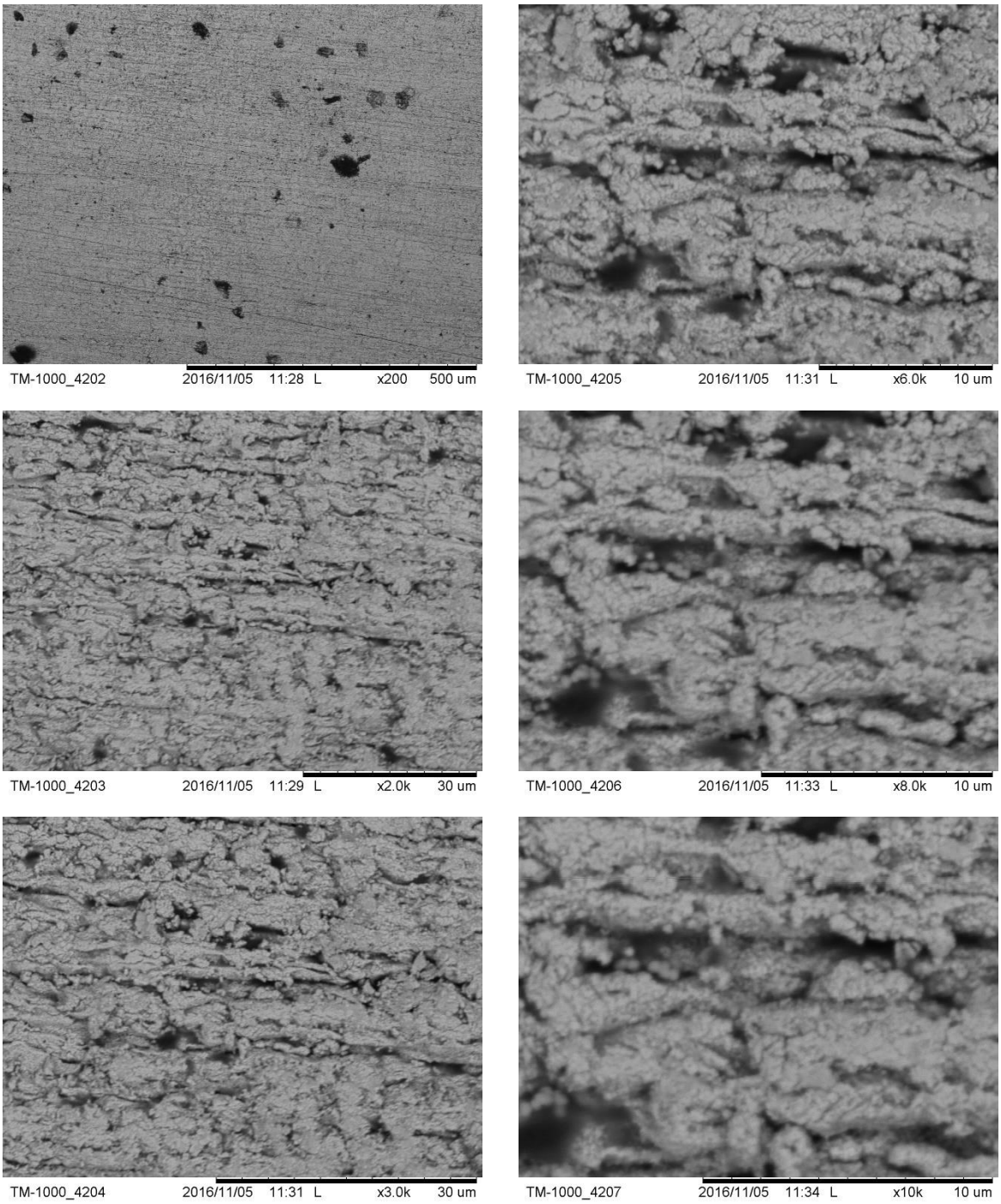

Figure 4.4 SEM images of the Commercial 5 IPMC

Figure 4.5 shows all top surface scanning images of the Strathclyde 3 IPMC under 6 different magnifications.

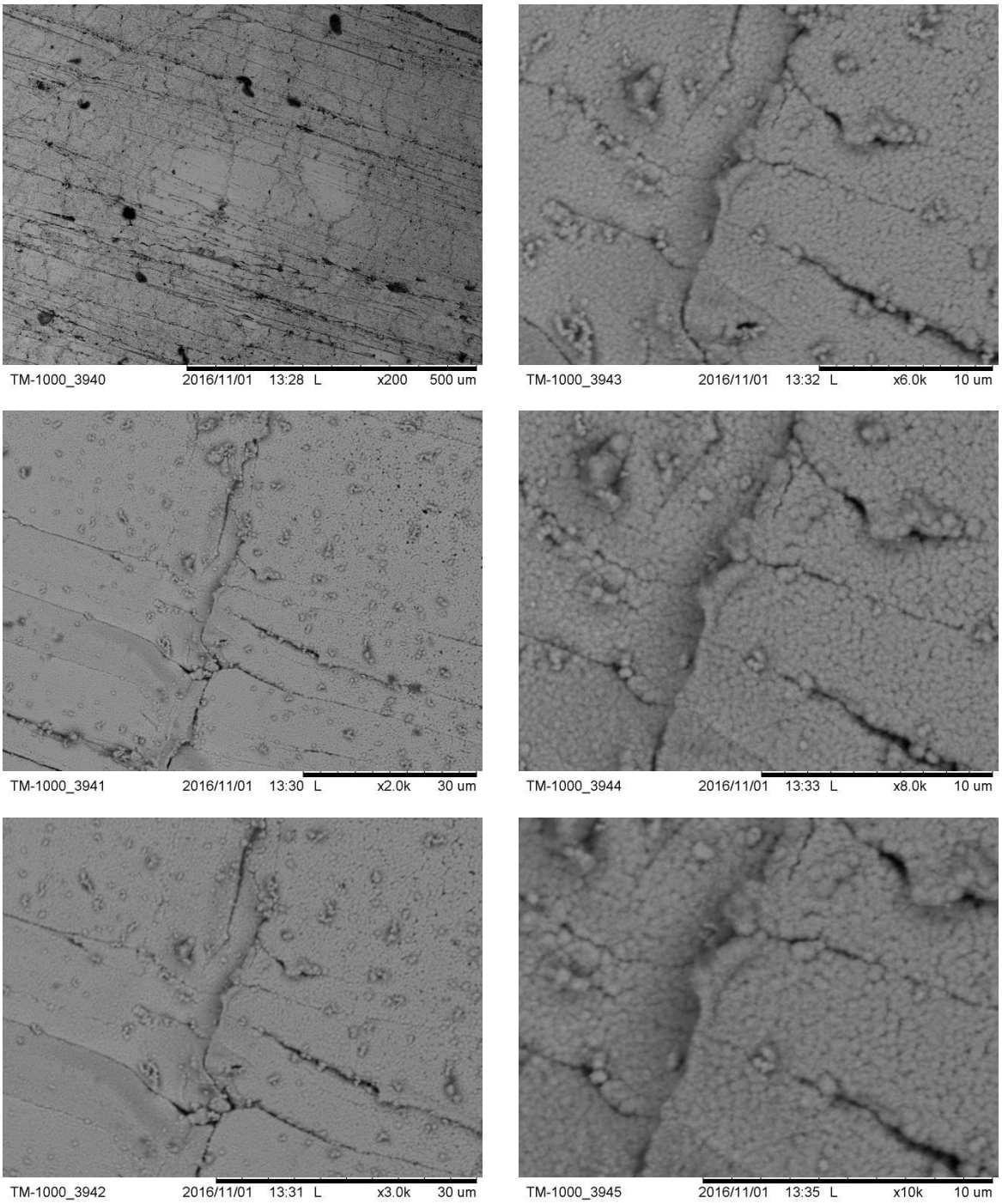

Figure 4.5 SEM images of the Strathclyde 3 IPMC

Figure 4.6 shows all top surface scanning images of the Strathclyde 5 IPMC under 6 different magnifications.

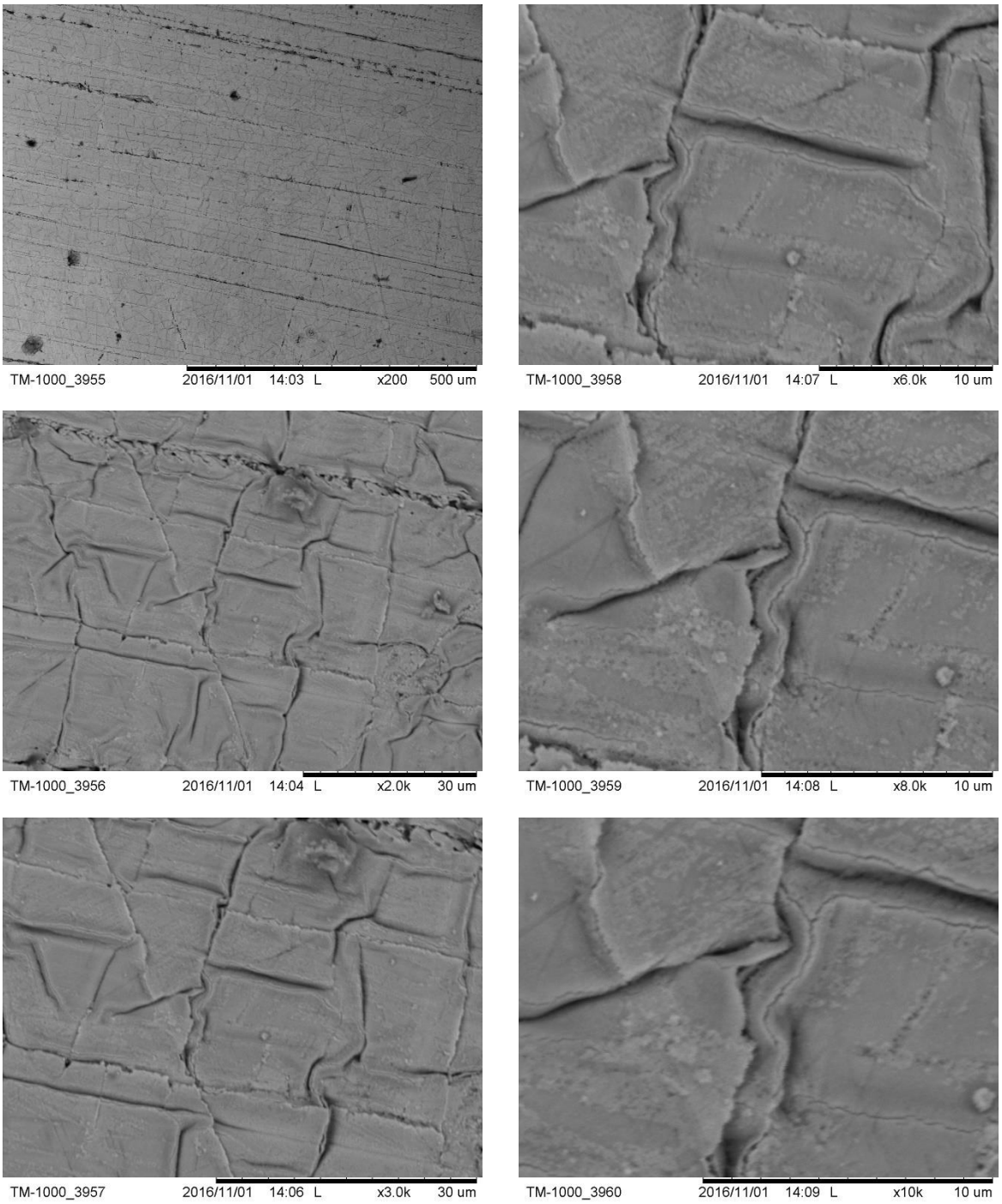

Figure 4.6 SEM images of the Strathclyde 5 IPMC

Figure 4.7 shows all top surface scanning images of Strathclyde 11 IPMC under 6 different magnifications.

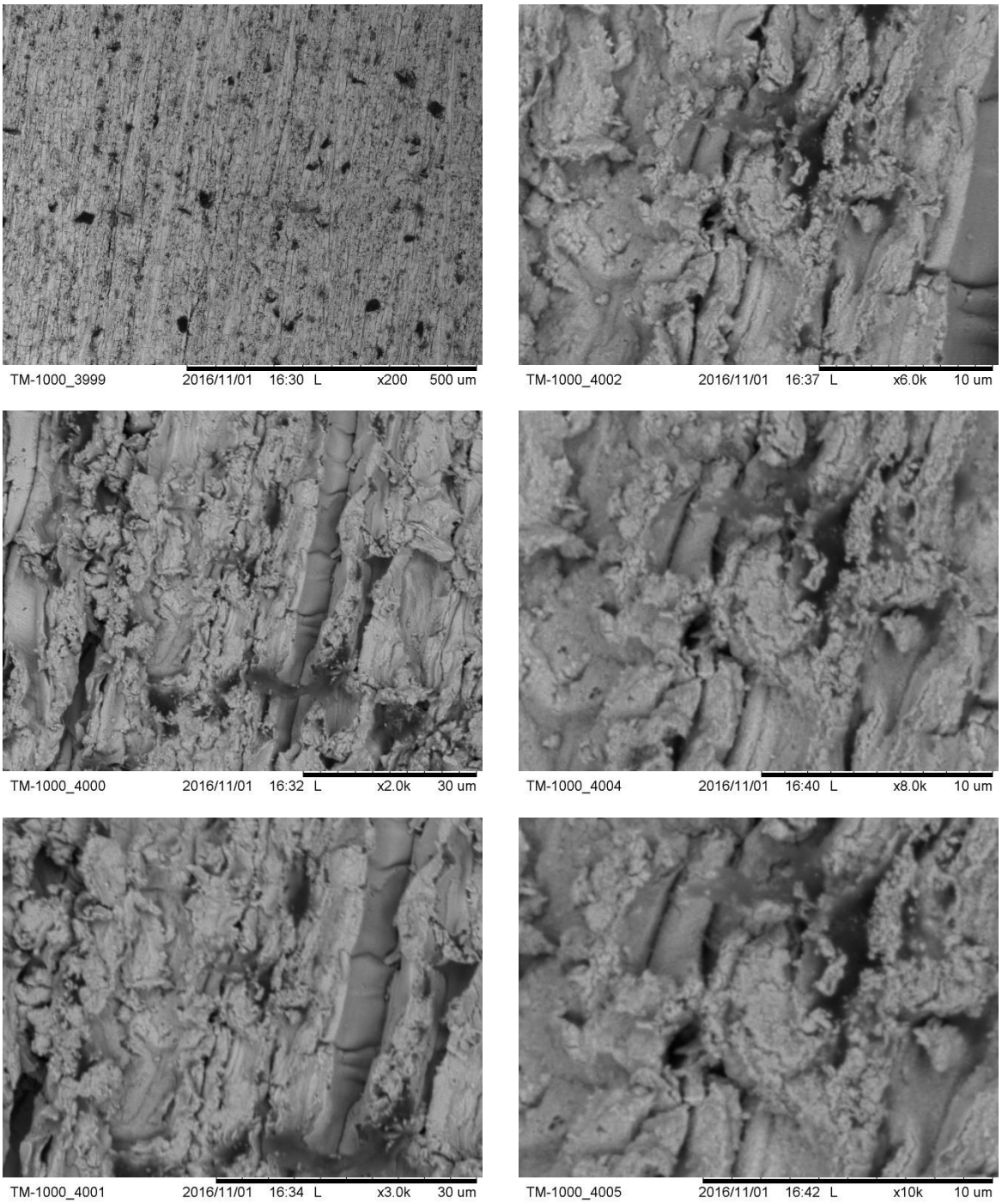

Figure 4.7 SEM images of the Strathclyde 11 IPMC

4.2.2.2 *Summary*

The SEM images of the surfaces gave a clear indication of the quality of the IPMC fabrication. The first fabricated Strathclyde samples (Strathclyde 11, and Strathclyde 5) appeared to have a rough surface with clear islands on the electrode surface. This problem has disappeared in the most recent Strathclyde samples (Strathclyde 3), which have a smoother surface with no sign of cracks or islands on the surface of the electrode, similar to the Commercial 5 images. The rest of the top surface images can be found in the Appendices section (11.3).

2.3 Cross Section Test

This test focuses on the penetration of the metallic particles inside the matrix of the polymeric membrane. The base membrane has a thickness of 170 μm. Usually, the thickness of Pt particles deposited on the surface is between 7 and 9 μm (Nguyen, Lee et al. 2007, Nguyen and Yoo 2007, Yu, Shen et al. 2007). The thickness can be increased by repeating the plating process many times. **Figure 4.8** shows a scanned image of the IPMC cross section.

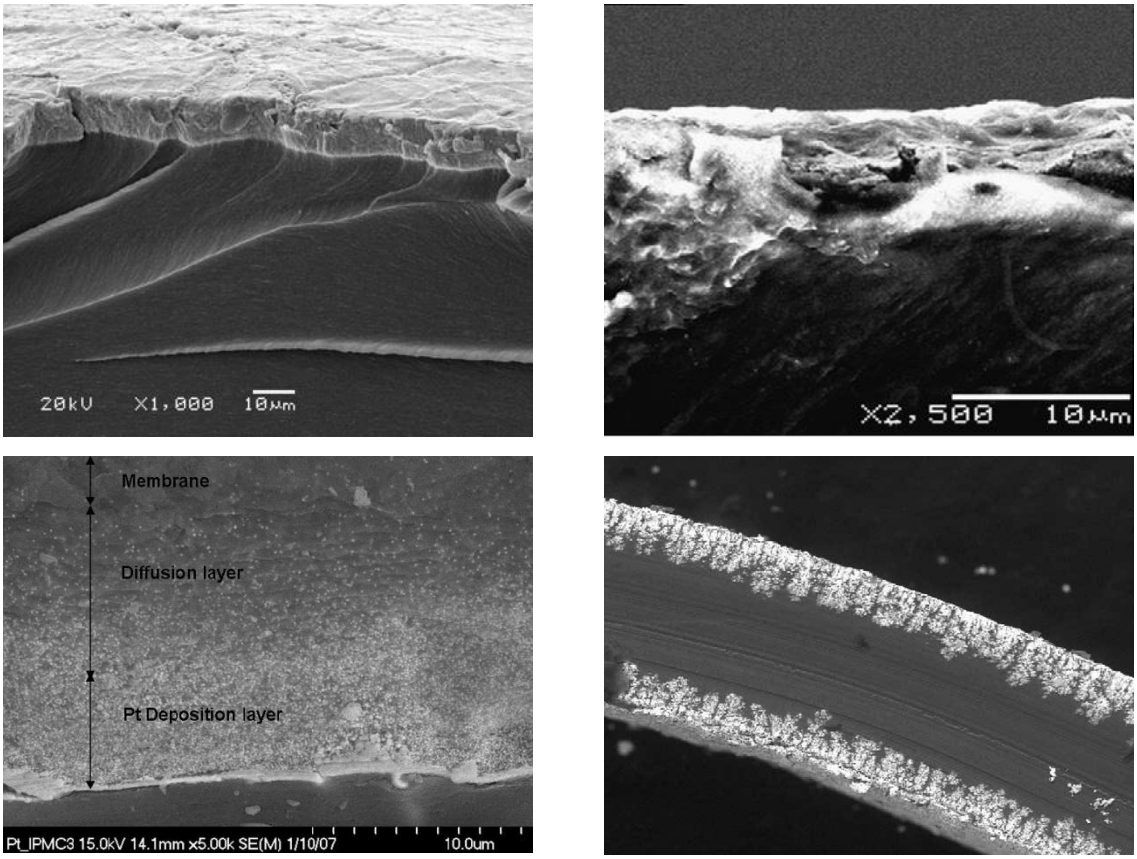

Figure 4.8 Cross section of IPMC top left (Yu, Shen et al. 2007), top right (Nguyen and Yoo 2007), bottom left (Park, Kim et al. 2007), bottom right (Shahinpoor 2003)

4.2.3.1 *Results*

A few examples of the cross section images are shown here, while the rest could be found in the Appendices section (11.4).

Figure 4.9 shows the cross section scanning images of the Commercial 3, 4 and 6 IPMCs under 2 different magnifications.

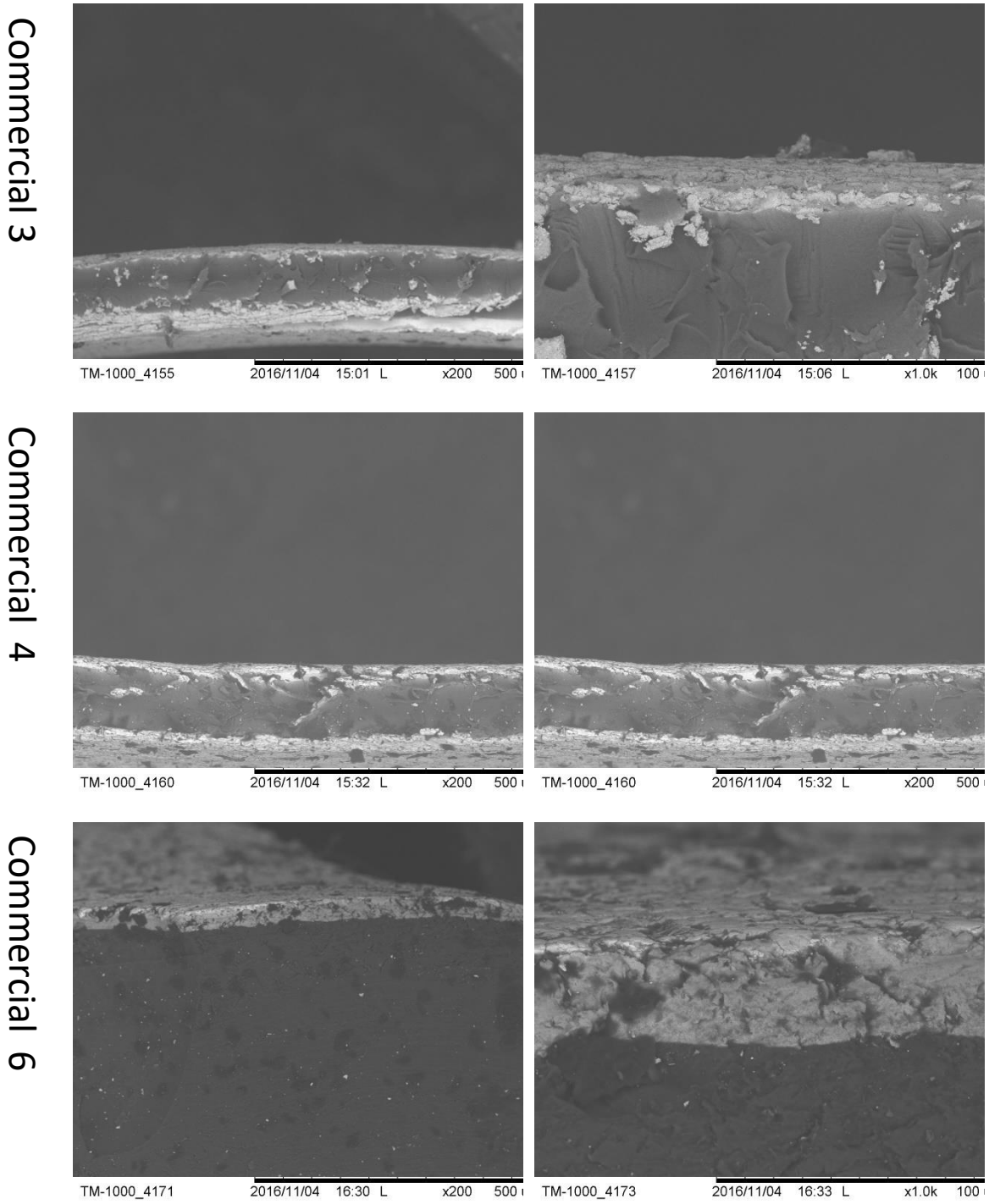

Figure 4.9 Cross Section SEM images of the Commercial IPMCs

Figure 4.10 shows the cross section scanning images of the Strathclyde 1, 6, and 11 IPMCs under 2 different magnifications.

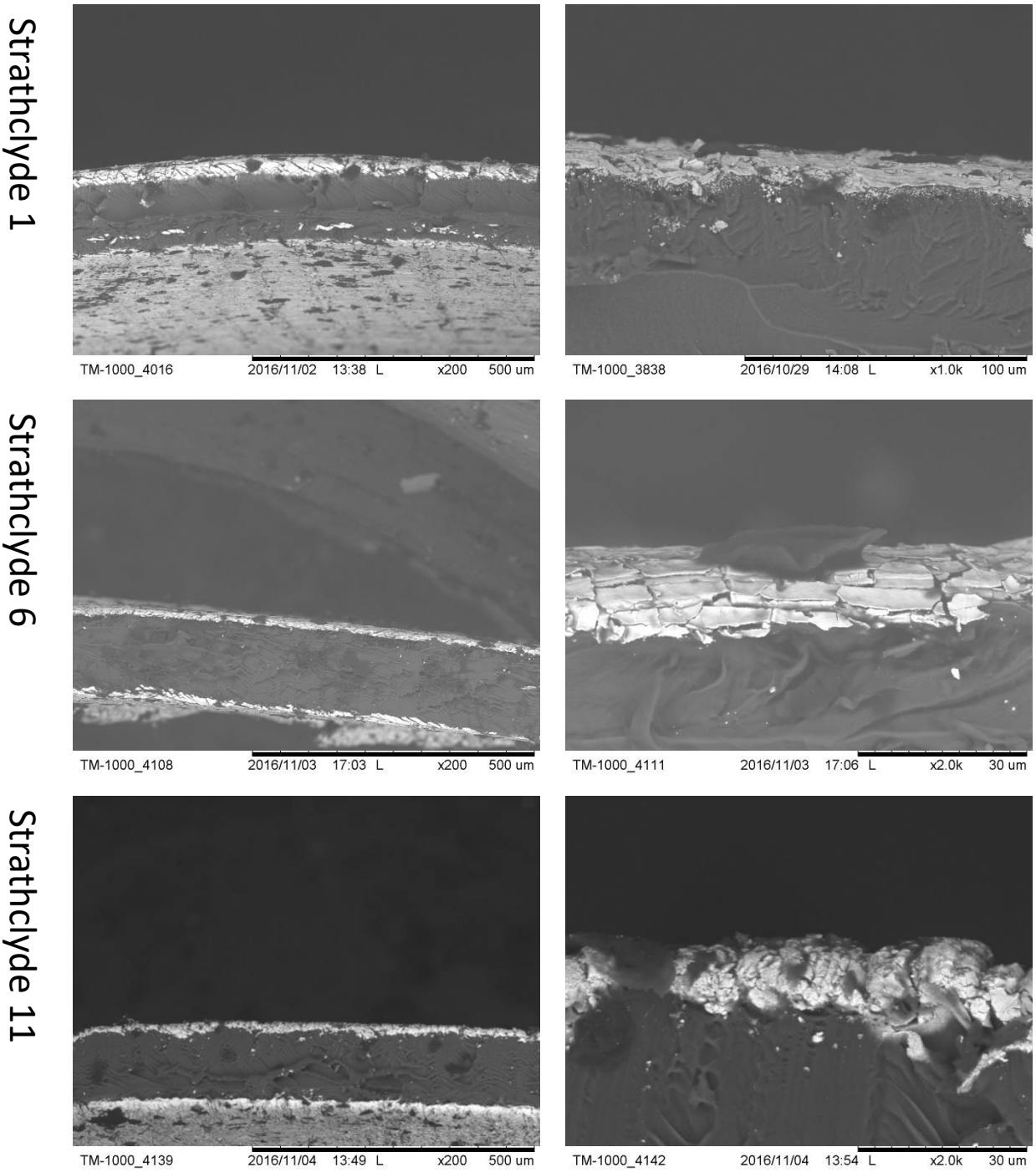

Figure 4.10 Cross Section SEM images of the Strathclyde IPMCs

Figure 4.11 and **Figure 4.12** show the cross section scanning images of the Strathclyde IPMC sample 2 at the different stages of fabrication under 2 different magnifications.

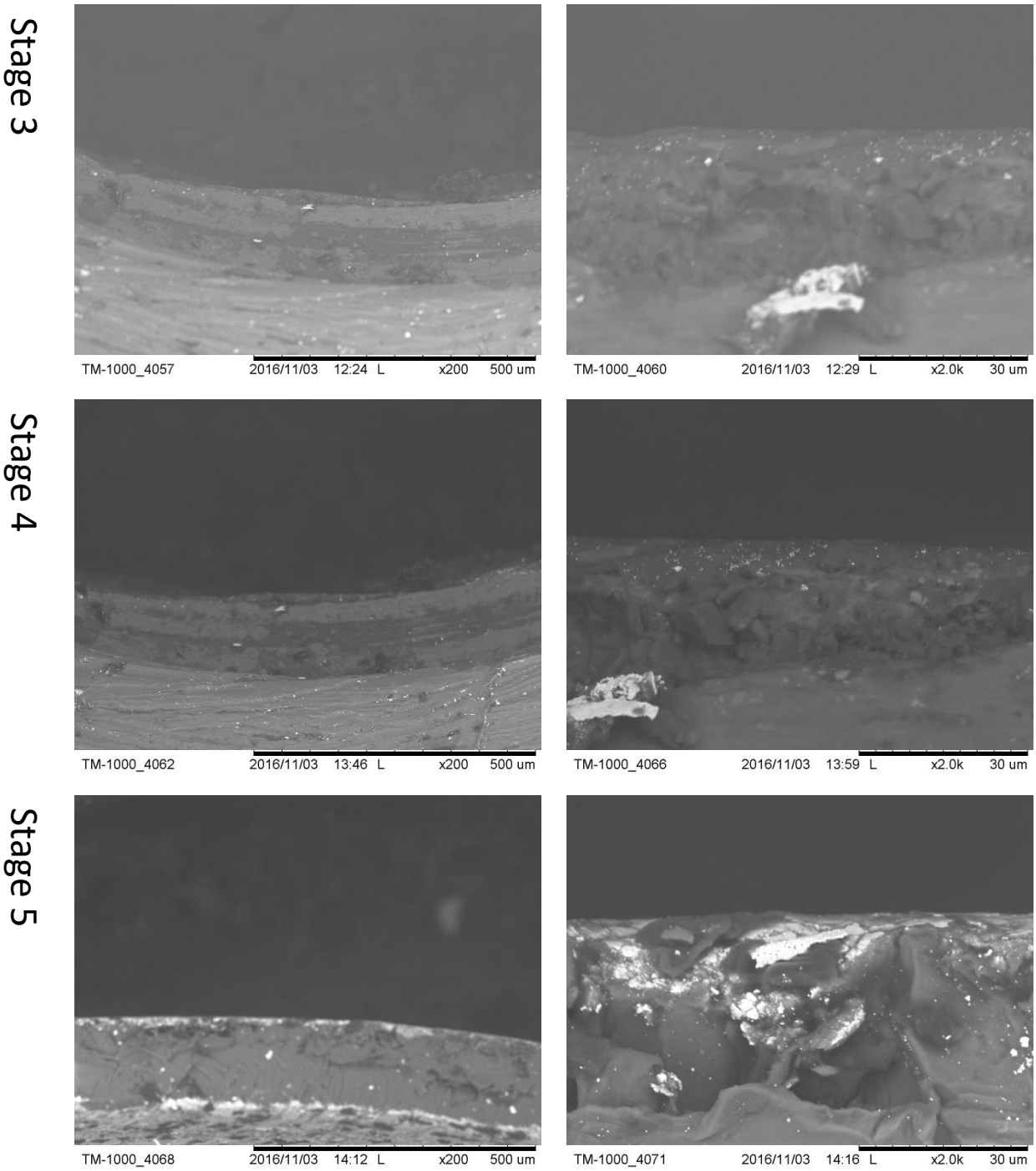

Figure 4.11 Cross Section images of Strathclyde 2 IPMC

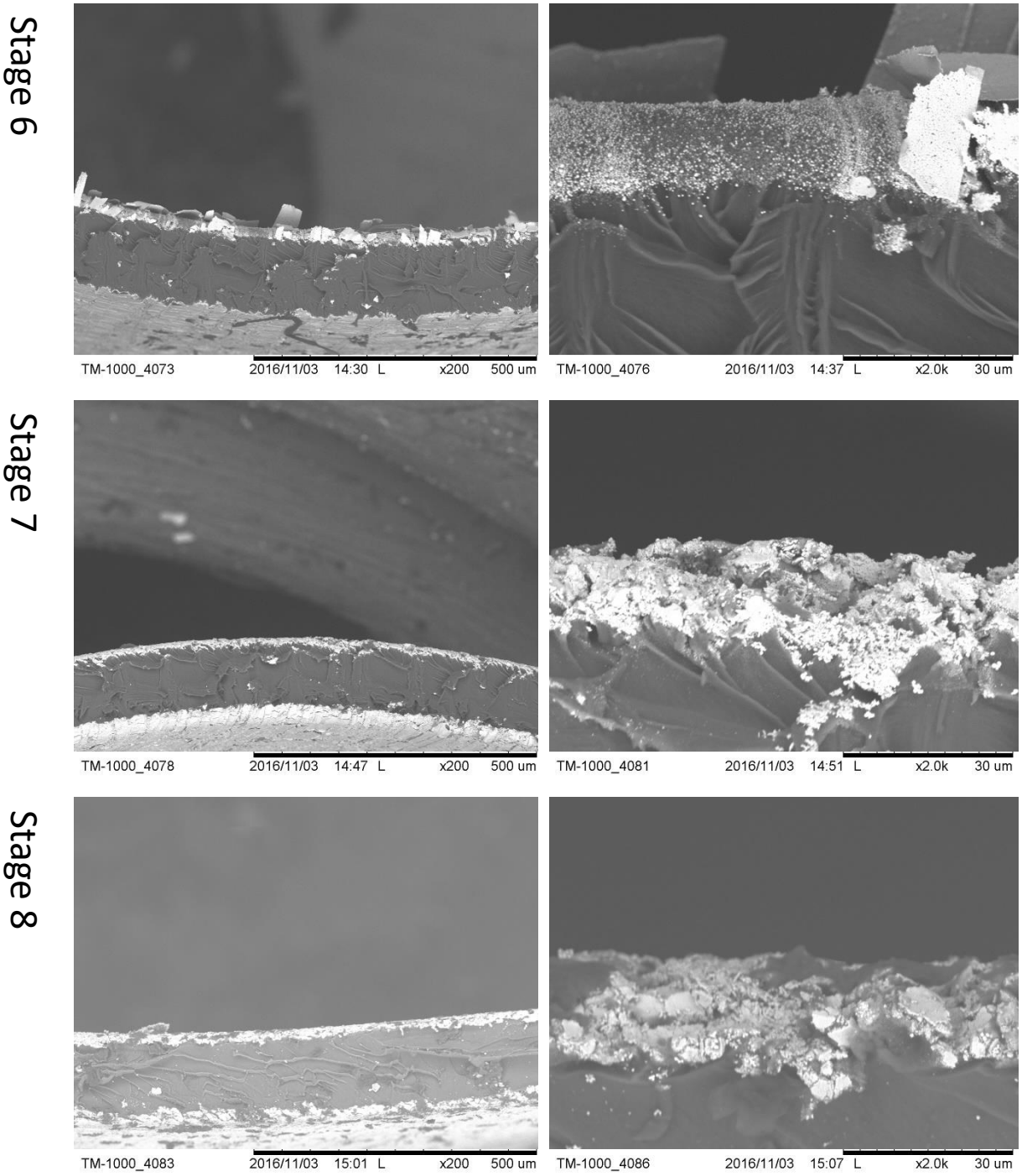

Figure 4.12 Cross Section images of Strathclyde 2 IPMC

4.2.3.2 *Summary*

This test gave an indication of the development of the thickness of the electrode during the fabrication of Strathclyde IPMC. These images are used in the next test to measure the thickness of the electrode.

4.3 IPMC Thickness

All samples started from the same base membrane (Nafion 117), which has a thickness of 170µm. During the different plating process, the metal particles were deposited on the surface and created the electrode layer. Some particles also penetrated inside the matrix of the membrane. The thickness of the electrode and the depth of penetration are critical parameters, and they have a huge reflect of the IPMCs behaviour when electrically stimulated.

2.1 Experiment Setup

All samples were left to dry for 24 hours before measuring the thickness using an electronic micrometer (resolution 1 µm). Three readings were taken from each sample, at different places on the surface of the IPMC actuator. After that, the average value and the standard error were calculated. **Figure 4.13** shows the electronic micrometer.

Figure 4.13 Electronic micrometer

Since the thickness of the base membrane was known, the thickness of the metal particles deposited on top of the membrane on each side could be calculated using equation (4.1).

$$\text{Electrode thickness on top of the Nafion} = \frac{\text{total IPMC thickness} - \text{Nafion thickness}}{2} \qquad (4.1)$$

Cross section images from the previous test were analysed using image processing software (ImageJ) to measure the total thickness of the electrode. Five readings were taken from each image and then the average, and the standard error were calculated. The same method was used to measure the development of the total electrode thickness during the different fabrication stages of Strathclyde 1 and 2.

Finally, the depth of the metal particles inside the membrane can be calculated from equation (4.2):

Particles penetration = Total Thickness of the Electrode - Electrode Thickness on top of the Nafion (4.2)

2.2 Results

Figure 4.14 shows the total thickness of the IPMC measured using the micrometer. The thickness of Commercial 6 was 2045 µm, it was removed from the graph to make it easier for comapariosn.

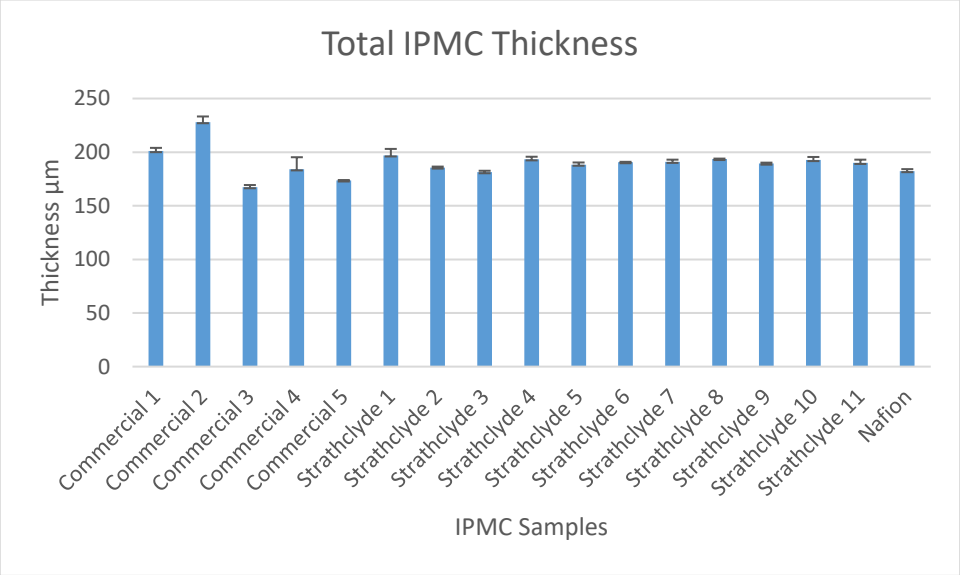

Figure 4.14 Total Thickness of the IPMC samples

Figure 4.15 shows the total electrode thickness measured using the SEM images and ImageJ

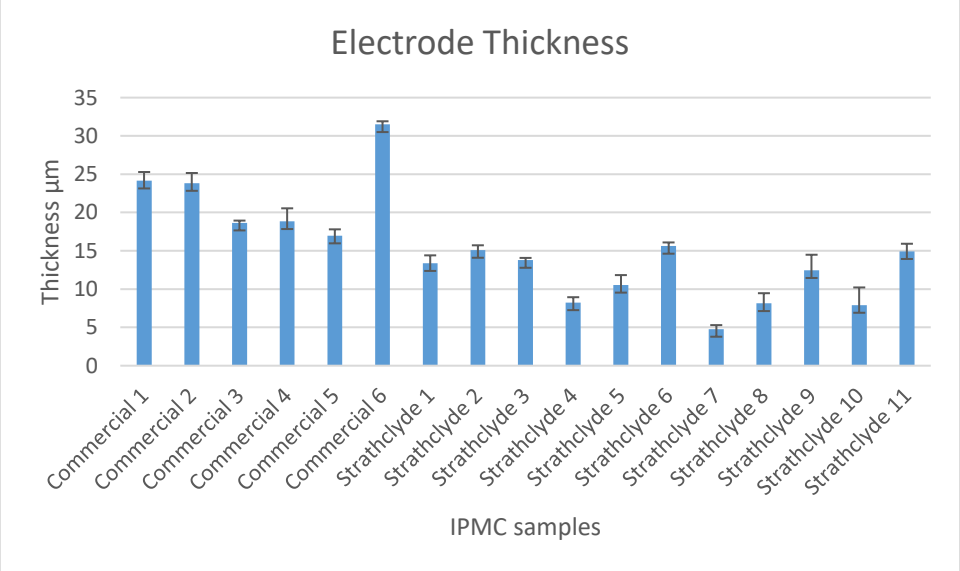

Figure 4.15 Total Electrode thickness of IPMC samples

Figure 4.16 shows the electrode thickness development of Strathclyde 1 during the fabrication stages, measured using the SEM images and ImageJ.

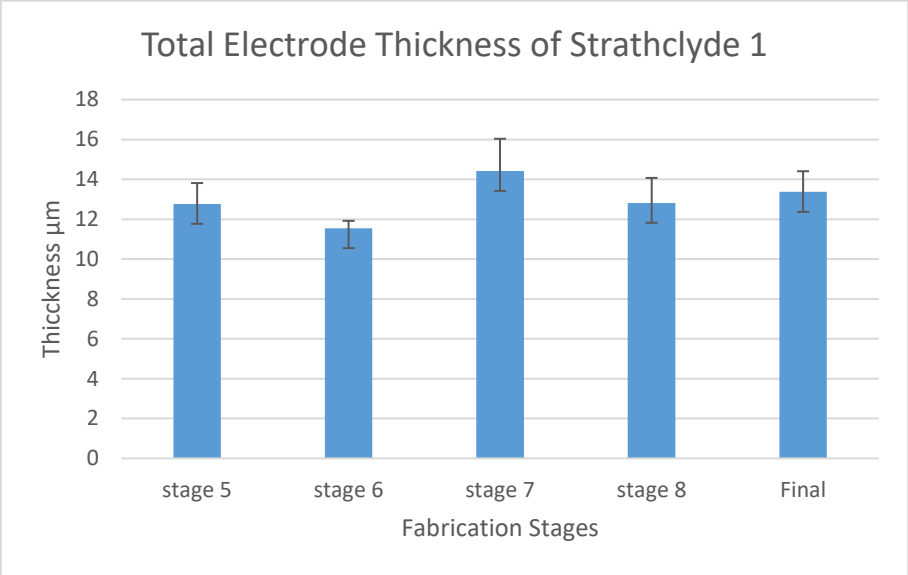

Figure 4.16 Total electrode thickness development of Strathclyde 1

Figure 4.17 shows the electrode thickness development of Strathclyde 2 during the fabrication stages, measured using the SEM images and ImageJ.

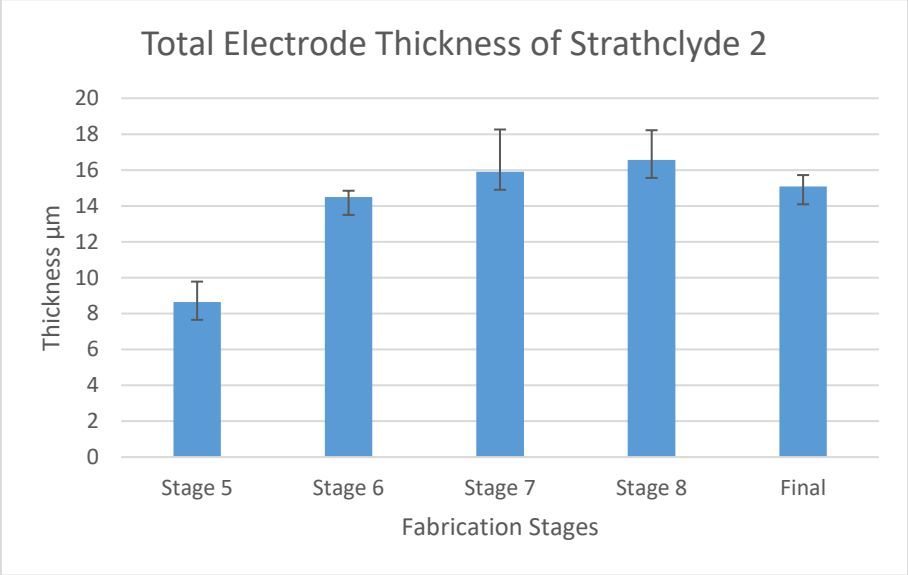

Figure 4.17 Total electrode thickness development of Strathclyde 2

Figure 4.18 shows the metal particle penetration inside the membrane. The values were calculated from equation (4.2).

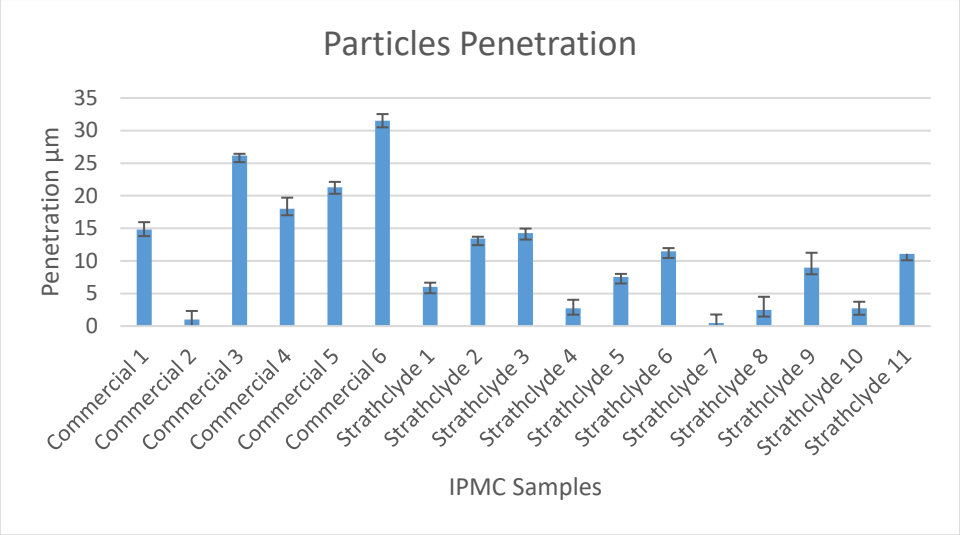

Figure 4.18 Metal particles depth inside the membrane

2.3 Summary

All the results are in the normal range. IPMC total thickness is around 200 µm, metal particles penetration is in the range of 5-7 µm, as described in the literature (section 4.22.3). This indicated that all IPMC samples were fabricated properly. The changes in the electrode thickness of Strathclyde 1 and Strathclyde 2 at the different fabrication stages showed a slight increase in thickness in stages 7 and 8 before dropping a little at the final thickness in stage 8. This could be because of weakly attached particles to the surface, where were lost in the last stage. Regarding the depth of the metallic particle penetration inside the membrane, Strathclyde Samples showed less penetration than the Commercial Samples, which suggested the Commercial sample might have a slightly different fabrication protocol that allowed the metal particles to penetrate deep in the membrane.

4.4 Water Uptake

The actuation mechanism in IPMC relies on the movement of the water molecules through the hydrophilic channels inside the matrix of the polymeric membrane (Gong, Tang et al. 2009). Therefore, IPMC required being hydrated all the time to keep actuating. Water Uptake (WUP) is defined as the water holding capacity of the IPMC, which can be calculated by measuring the difference in weight between a dry and wet IPMC (Inamuddin, Khan et al. 2015). Nafion 117 has a WUP of 48% (Trabia, Hwang et al. 2016), which is one of the reasons why it is used in IPMCs. During the fabrication process, the WUP of Nafion decreases because

of the electrode layers covering the surface of the membrane. The final IPMC can reach a WUP of 16.7% (Inamuddin, Khan et al. 2015)

There are three important mechanisms for water loss: water leakage from the surface of the electrode, natural evaporation, and water loss due to electrolysis. For example, Nafion IPMC lost nearly 70% of its water after 5 minutes of actuation (Nguyen, Lee et al. 2007).

When an electric field is applied across the membrane, the IPMC will start to actuate, and water will be noticed appearing on the cathode side of the electrode, which will lead to some water evaporating and the IPMC will dry out and then stop (Shahinpoor and Kim 2002). That is why the IPMC should have a high WUP values to keep actuating longer. One solution for this issue, is a better platinum particles penetration inside into the ionic polymer membrane with a smaller particle size (Shahinpoor and Kim 2002). Another option is using rubber coatings to cover the IPMC to prevent water from evaporating (Richardson, Levesley et al. 2003, Lee, Lee et al. 2005).

To measure WUP, the samples first were dried for 24 h and weighed. Then, the samples were soaked in deionised water for another 24 h at room temperature to completely hydrate. Excess water drops were removed and samples were weighed again (Panwar, Lee et al. 2012, Park, Palmre et al. 2014)

2.1 Experiment Setup

All samples were tested in both dry and wet conditions. For the wet conditions, they were left in containers full of deionised water and left for 24 hours at room temperature to hydrate fully, while in the dry conditions, they were left for 24 hours on the bench between paper towels to dehydrate fully. All tests were carried out using a Lab Balance (Fisher Brand PS-60, UK) with a resolution of 0.1 mg, as shown in **Figure 4.19**. Three measurements were taken each time, and then the average and the standard error were calculated.

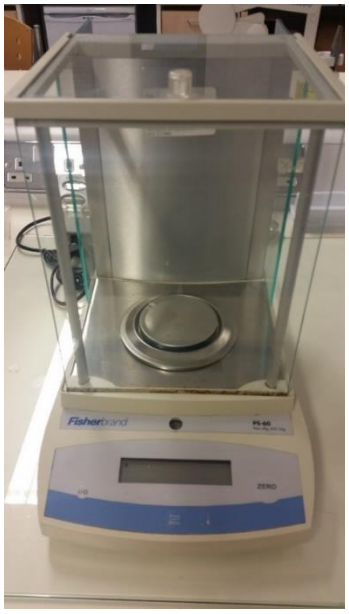

Figure 4.19 Balance used to weigh the IPMC samples

Both water uptake in mg and percentage were calculated using the following equations:

$$WUP\ (mg) = Wet\ Weight - Dry\ Weight \quad (4.3)$$

$$WUP\% = \frac{Wet\ Weight - Dry\ Weight}{Wet\ Weight} \times 100 \quad (4.4)$$

2.2 Results

Table 4.1 lists all the dry and wet weights of the IPMC samples:

IPMC	Dry (mg)	Wet (mg)
Commercial 1	83.80	97.40
Commercial 2	90.73	112.10
Commercial 3	71.63	87.37
Commercial 4	66.67	80.73
Commercial 5	85.07	103.00
Commercial 6	735.10	914.73
Strathclyde 1	108.10	125.70
Strathclyde 2	84.97	110.27
Strathclyde 3	100.67	119.80
Strathclyde 4	126.80	152.07
Strathclyde 5	84.20	104.80
Strathclyde 6	80.47	94.57

Strathclyde 7	90.83	110.47
Strathclyde 8	104.27	126.33
Strathclyde 9	105.57	126.47
Strathclyde 10	82.73	97.17
Strathclyde 11	106.87	126.53
Nafion 117	82.00	104.57

Table 4.1 Dry and wet weight of IPMC samples

Figure 4.20 shows a comparison between dry and wet weight of the IPMC samples in mg, Commercial 6 was removed for an easier comparison.

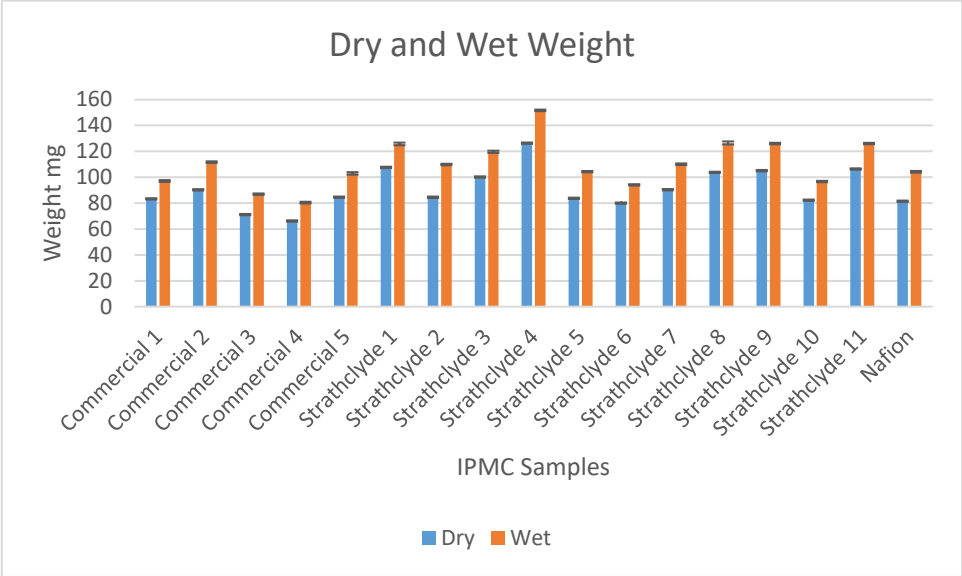

Figure 4.20 Dry and wet weight of IPMC Samples

Figure 4.21 shows the water uptake in mg of the PMC samples in mg, apart from Commercial 6 which was 179.63 mg.

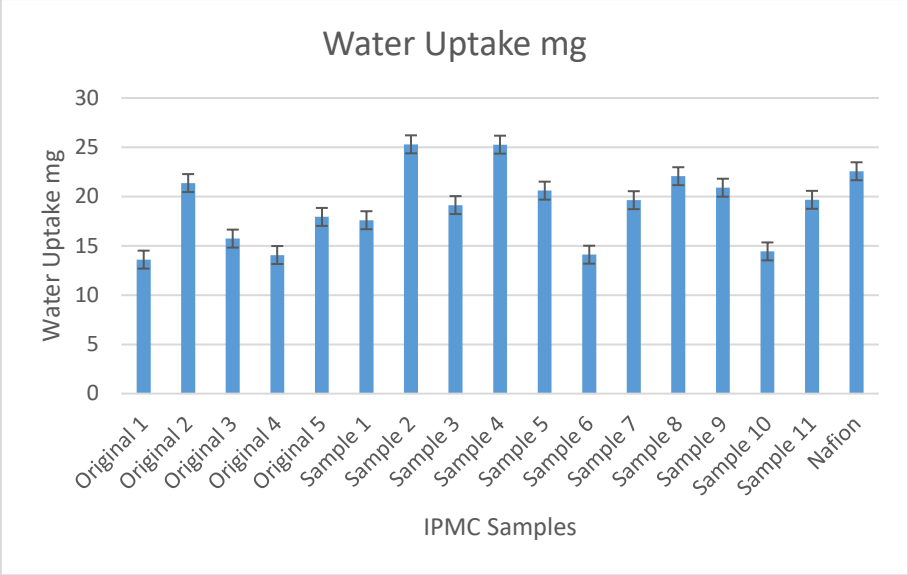

Figure 4.21 Water Uptake in mg of IPMC Samples

Figure 4.22 shows the percentage of water uptake of all IPMC samples

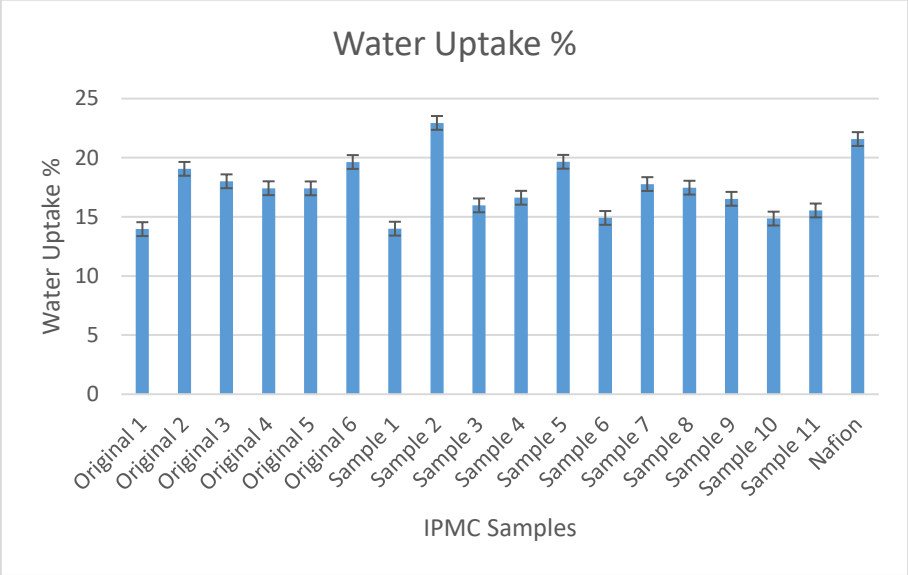

Figure 4.22 Water Uptake Percentage of IPMC Samples

2.3 Summary

This test was conducted to measure the WUP percentage of all fabricated samples, and compare it with the results found in the literature. The results were very close between the two groups; the Strathclyde IPMCs and the Commercial IPMCs. WUP values were between 14% and 22%, which match the 16.7% value found in a previous study. This showed again that the fabricated samples were fabricated successfully.

4.5 Surface Resistance Test

Sheet resistance is a vital parameter and indicates the quality of the electrodes. The sheet resistance R_s is defined as the electrical resistance per a square unit of the membrane (Instruments 2001, Panwar, Cha et al. 2012).

The non-electric plating procedure involves treatment of the membrane at an elevated temperature, which causes the membrane to crack and results in increasing the surface resistance. To avoid this problem, (Johanson, Punning et al. 2008) used Cu to treat IPMC after plating. This method was used to improve the conductivity of the IPMC and prevent the surface of the membrane from cracking. Besides that, the relationship between metal particles penetration within the polymer and the surface resistance is critical. It is also noticed that samples with low surface resistance tend to produce larger blocking force (Kim and Shahinpoor 2003).

There are two main methods to measure the surface resistance or (sheet resistivity). The first method used a Four-point surface resistivity device such as Guardian Model SRM-232, (Kim and Shahinpoor 2003, Põldsalu, Mändmaa et al. 2015). This device operates by passing a calibrated constant current source of 4.53 mA through the two outer tips of the 4-point probe. This current develops a voltage across the two inner probe tips, which is directly proportional to the surface resistivity. The device shows the results in Ω/□. (Kim and Kim 2008) Used this method to measure the surface resistance, 3.3 Ω/□ for the Pt coated IPMC, and 1.2 Ω/□ for Pd/Pt coated IPMC. **Figure 4.23** shows the principle of the four-point measurement resistance device.

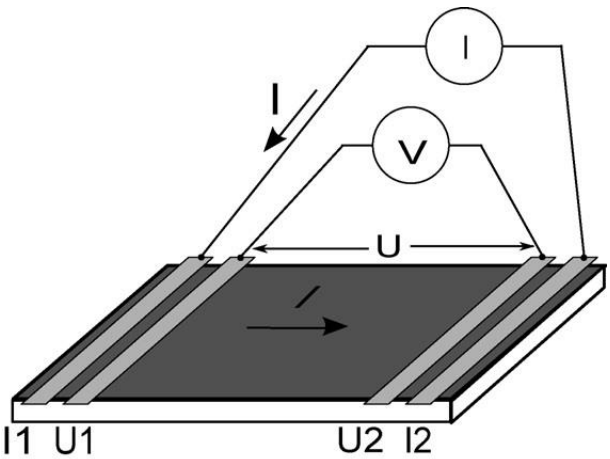

Figure 4.23 Four-point surface resistivity device (Punning, Kruusmaa et al. 2007)

The other method to measure the resistance used a multimeter, with a distance of 1 cm between the probes, as shown in **Figure 4.24**. This method is suitable for small samples, and present the surface resistance in Ω/cm. (Panwar, Kang et al. 2011) Used this method and recorded a surface resistance of 2.5 Ω/cm, (Trabia, Hwang et al. 2016) Recorded 2 Ω/cm, and (Hwang, Palmre et al. 2015) also found the surface resistance to be 2 Ω/cm of their samples.

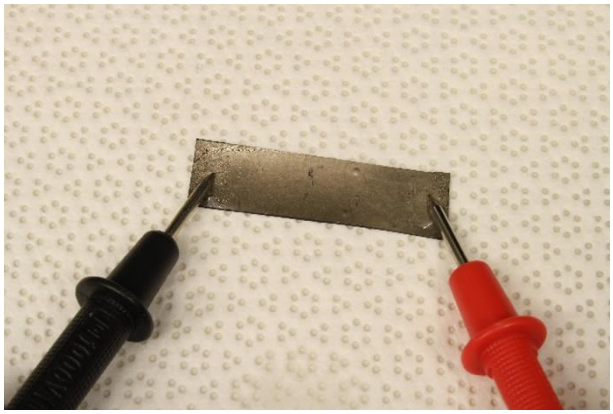

Figure 4.24 Point to point surface resistance (Trabia, Hwang et al. 2016)

2.1 Experiment Setup

In this test both methods were used, the square method and the point to point one. The square method was used during the fabrication process, as there was enough space to place the testing square on top of the membrane and obtain some readings in different locations. The testing square was made of a 2x2 cm of polypropylene and had two metal plates on two opposite sides only, which were connected to a multimeter. To measure the surface resistance, the testing square was placed on top of IPMC surface in different locations to obtain the average resistance. **Figure 4.25** shows the testing square.

Figure 4.25 Surface resistance testing square

The point to point method was used after cutting the IPMC into equal strips. This method used a multimeter only with the probes are 1 cm apart from each other. Three reading were taken on each side of the IPMC sample, and then the average and the standard error were calculated. All surface resistance tests were conducted under dry conditions.

2.2 Results

Figure 4.26 shows the surface resistance per cm of the IPMC samples.

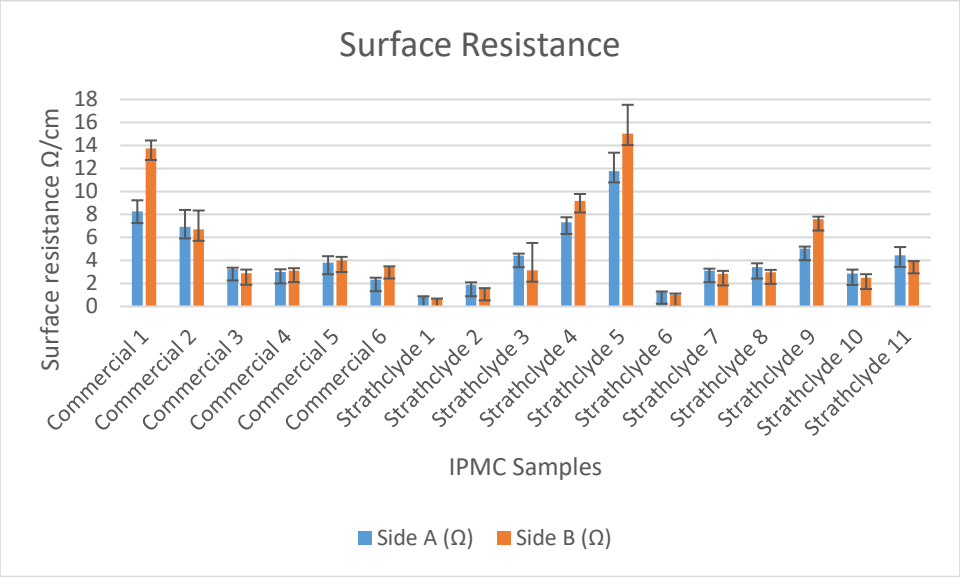

Figure 4.26 Surface resistance side A and B of IPMC samples

Figure 4.27 shows the changes in surface resistance of Strathclyde 1 during fabrication stages.

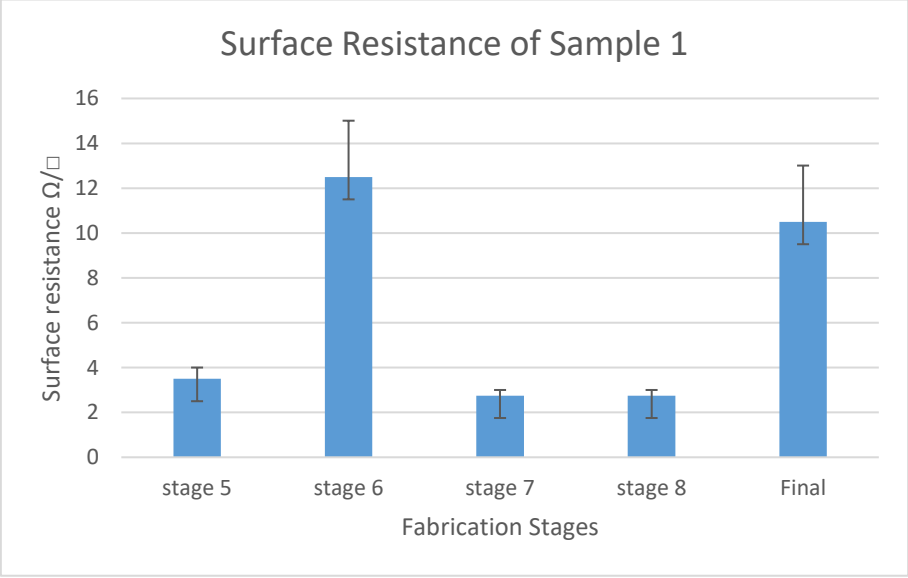

Figure 4.27 Surface resistance of Strathclyde 1

Figure 4.28 shows the changes in surface resistance of Strathclyde 2 during fabrication stages.

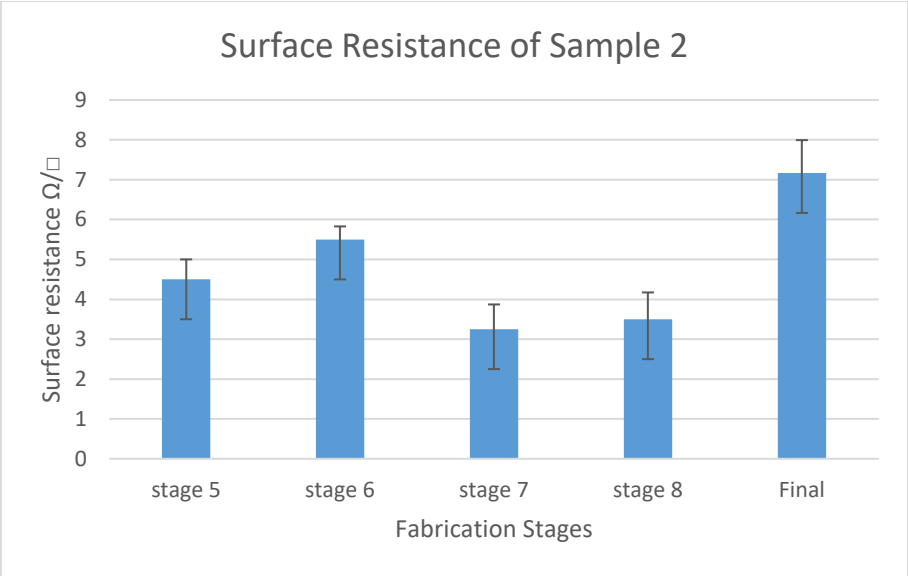

Figure 4.28 Surface resistance of Strathclyde 2

2.3 Summary

In general, both tests showed low surface resistance per cm and per square. Some samples such as Strathclyde 5, and Strathclyde 9 have a different surface resistance on each side. The results of the resistance per cm were a little bit over what was found in previous studies, most of the values were between 2 Ω/cm and 8 Ω/cm. This was taken in consideration when testing the mechanical and electrical properties.

4.6 Electrical Power Consumption

One of the most severe drawbacks of IPMC application is their high-current consumption. One option to reduce the energy consumption is to improve the properties of the materials, using materials that need lower energy to operate. Another option is to enhance the controlling signal using a modulated controlling signal (Punning, Anton et al. 2005).

2.1 Experiment Setup

This test focused on the electrical power consumed by the IPMC samples, which gave an idea of how much power is needed to run the proposed device. As previously explained, the proposed device is made of IPMC strips, which should be powered either directly from a power-harvesting device or through a battery. In both cases, there is a need to measure and decide how much electrical power is required to run the device.

Each IPMC sample was placed between an alligator holder, which applied a 6V, square wave across the IPMC, as shown in **Figure 4.29**.

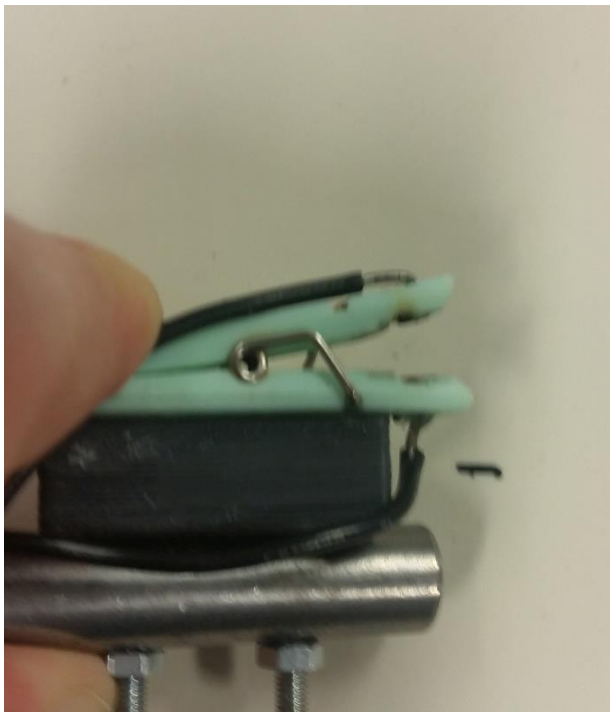

Figure 4.29 IPMC alligator holder

IPMCs were tested under different frequencies (0.05, 0.5,1, and 2 Hz), using the IPMC driver described in (section 3.5). The current passing through the IPMC was measured using a multimeter and recorded. Total power consumption was calculated using the equation (4.5)

$$P = V \times I \quad (4.5)$$

Where **V** is the applied voltage (6V), **I** is the measured current in (A), and **P** is the consumed power in (W).

To achieve a better understanding of all the samples and for an easier comparison, the previous results were used to calculate the current consumption per weight, current consumption per surface area, power consumption per surface area, and power consumption per weight.

2.2 Results

Figure 4.30, **Figure 4.31**, **Figure 4.32**, and **Figure 4.33** show the maximum current consumption in mA at 0.05 Hz, 0.5 Hz, 1 Hz, and 2 Hz respectively.

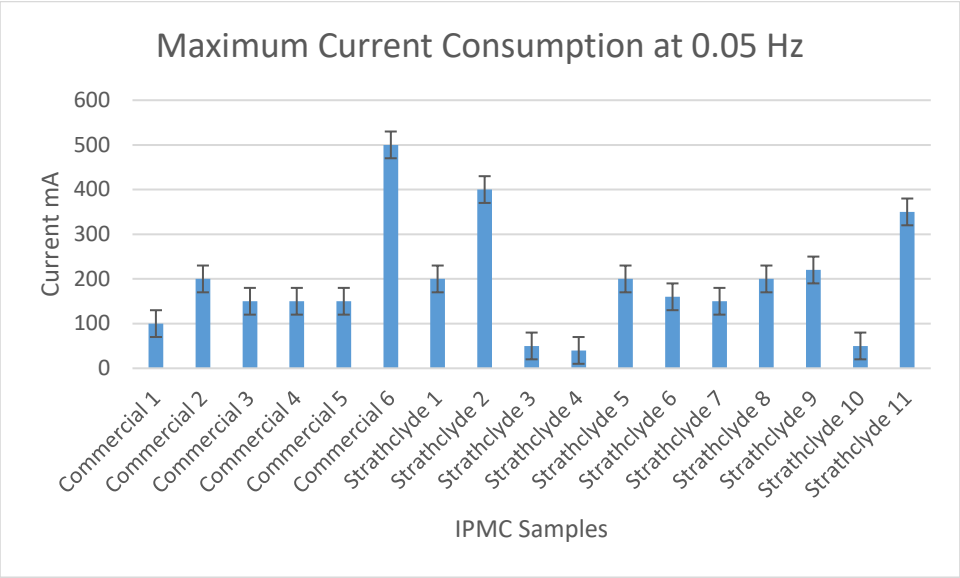

Figure 4.30 Maximum current consumption at 0.05 Hz

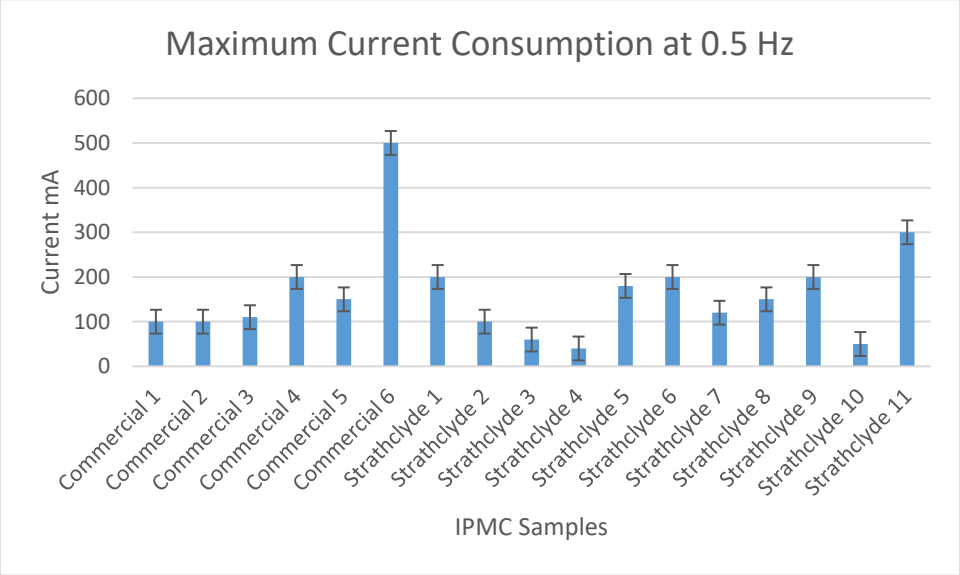

Figure 4.31 Maximum current consumption at 0.5 Hz

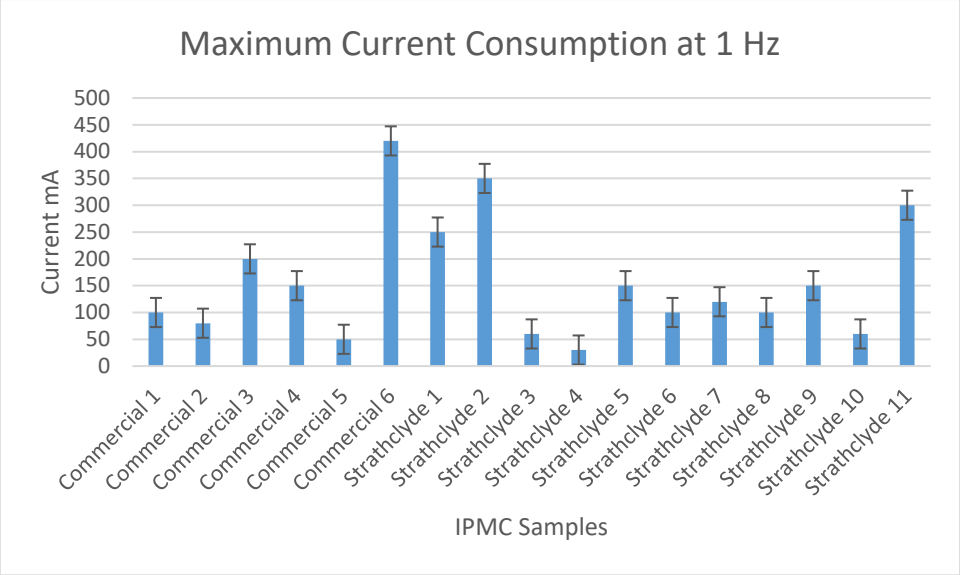

Figure 4.32 Maximum current consumption at 1 Hz

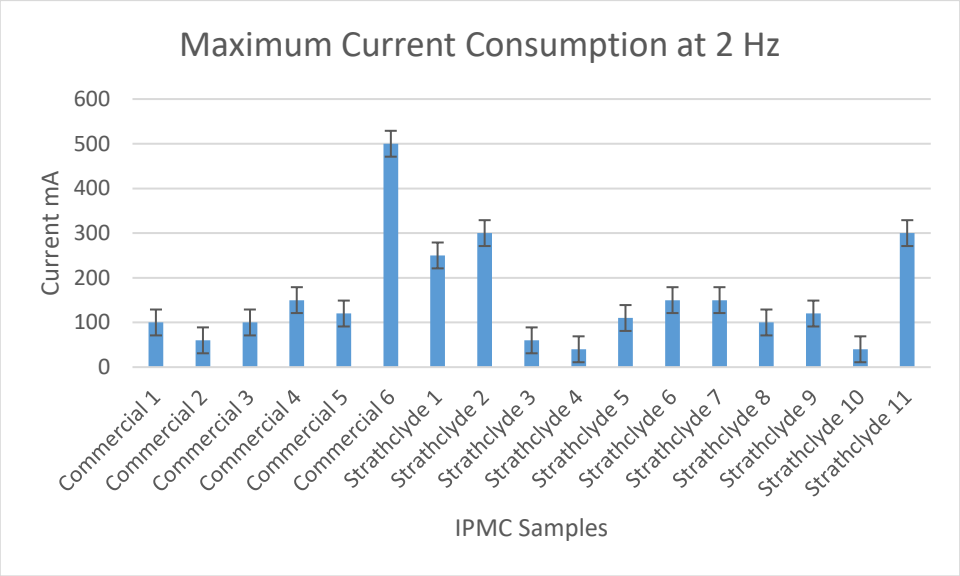

Figure 4.33 Maximum current consumption at 2 Hz

Figure 4.34, **Figure 4.35**, **Figure 4.36**, and **Figure 4.37** show the current consumption per weight in mA/mg at 0.05 Hz, 0.5 Hz, 1 Hz, and 2 Hz respectively.

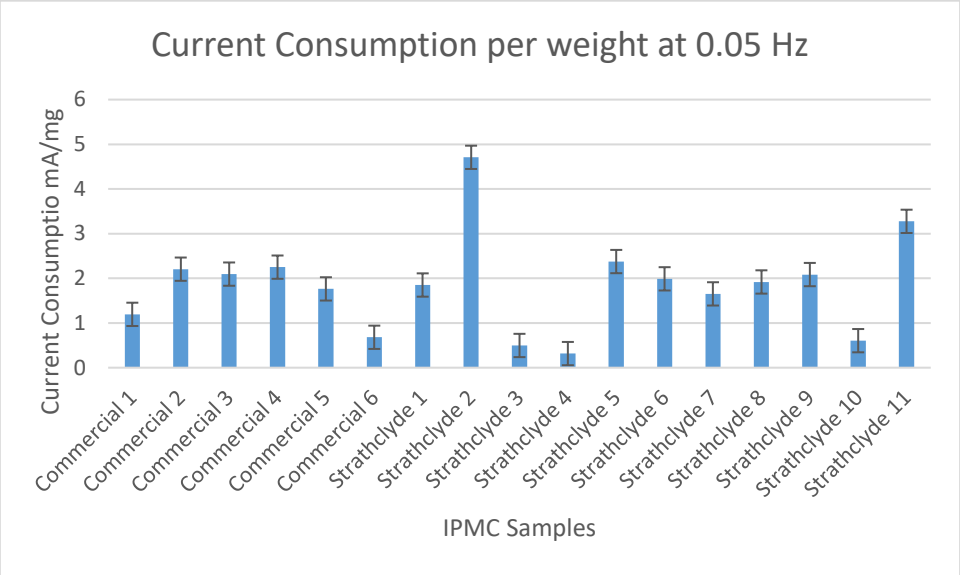

Figure 4.34 Current consumption per weight at 0.05 Hz

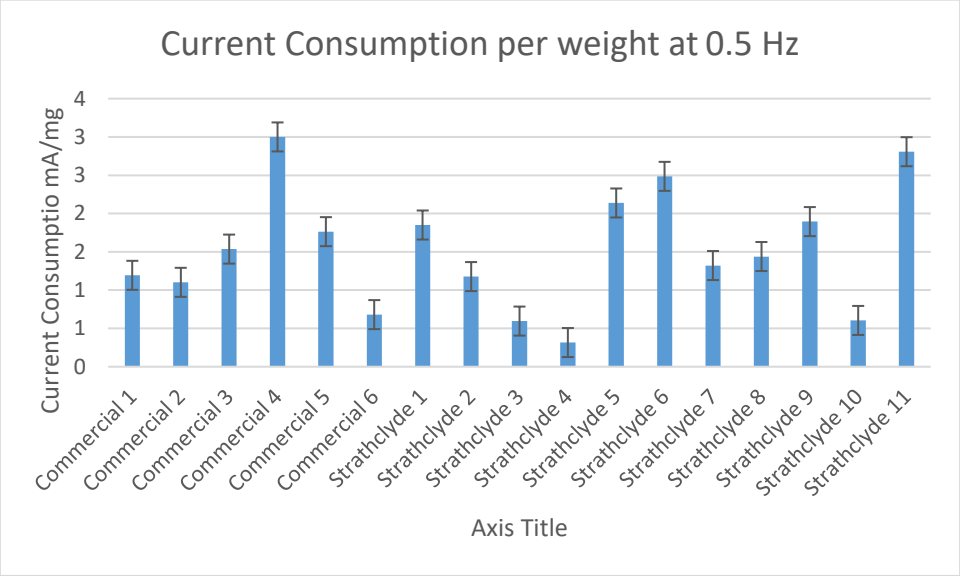

Figure 4.35 Current consumption per weight at 0.5 Hz

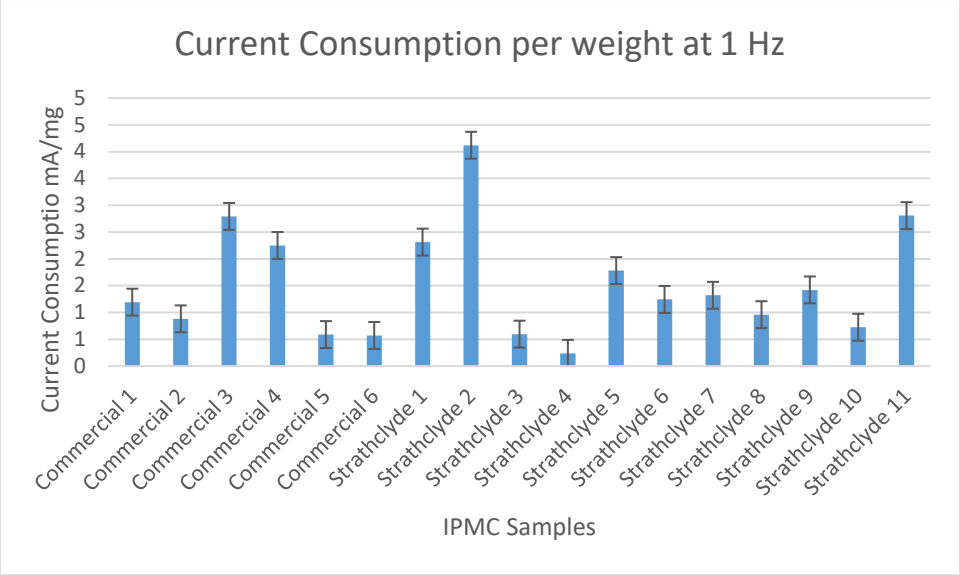

Figure 4.36 Current consumption per weight at 1 Hz

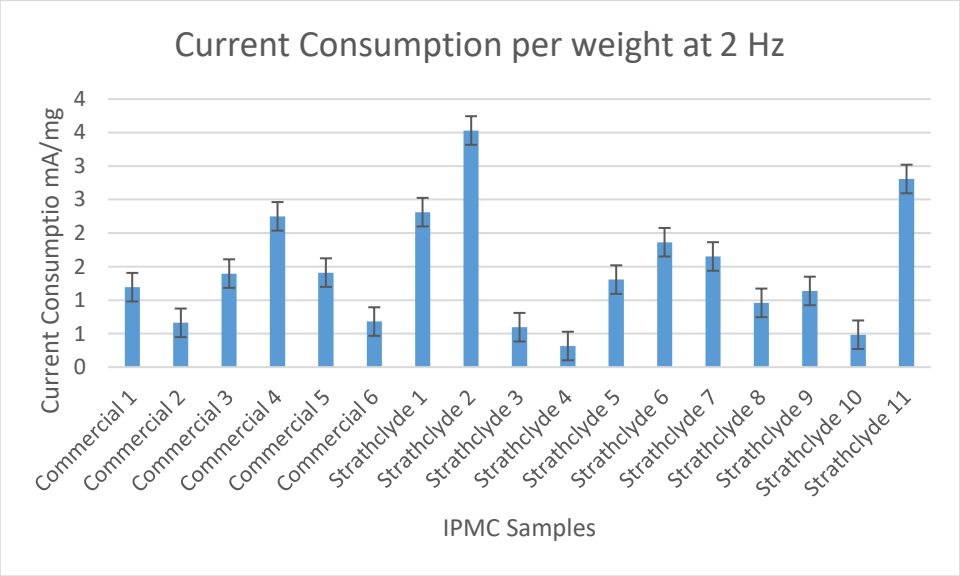

Figure 4.37 Current consumption per weight at 2 Hz

Figure 4.38, **Figure 4.39**, **Figure 4.40**, and **Figure 4.41** show the current consumption per surface area in mA/cm^2 at 0.05 Hz, 0.5 Hz, 1 Hz, and 2 Hz respectively.

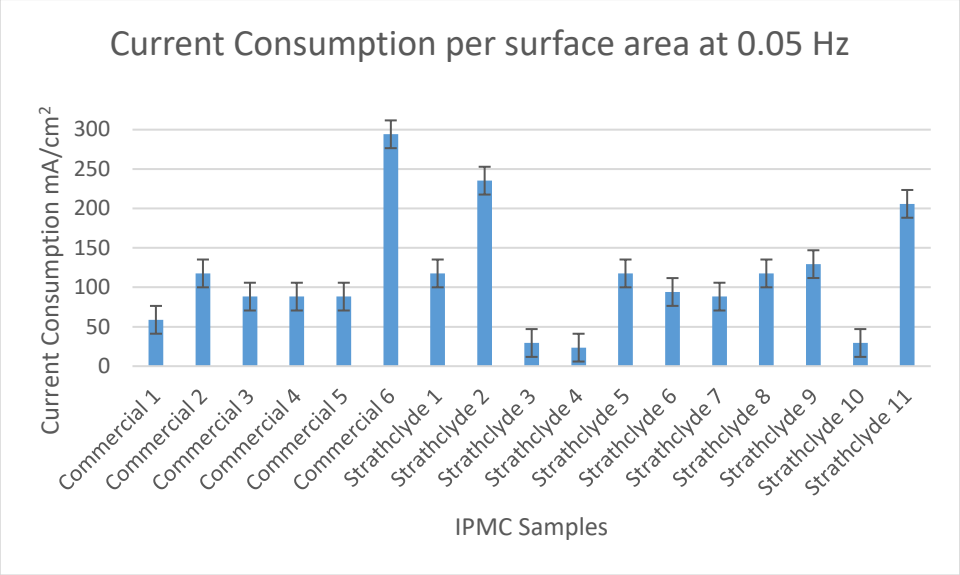

Figure 4.38 Current consumption per surface area at 0.05 Hz

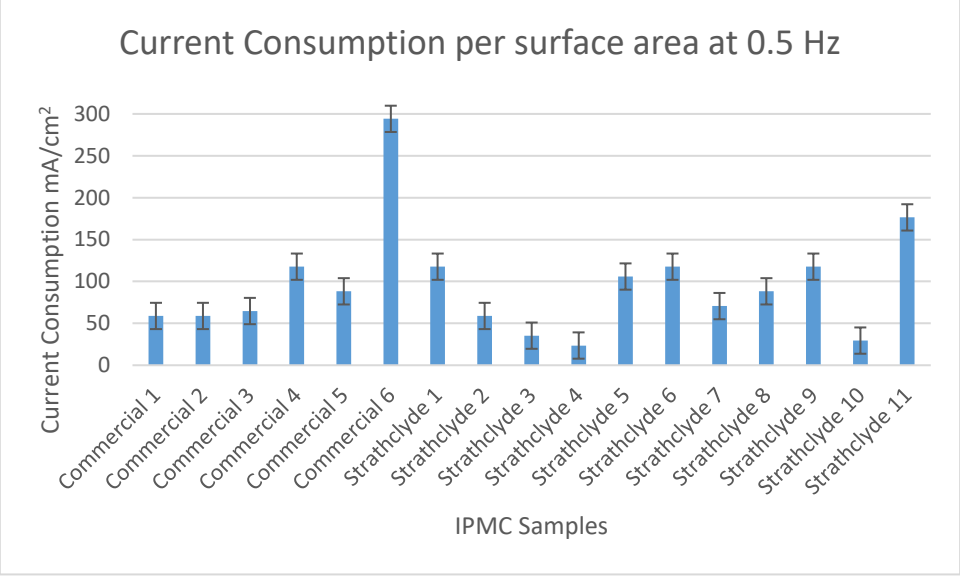

Figure 4.39 Current consumption per surface area at 0.5 Hz

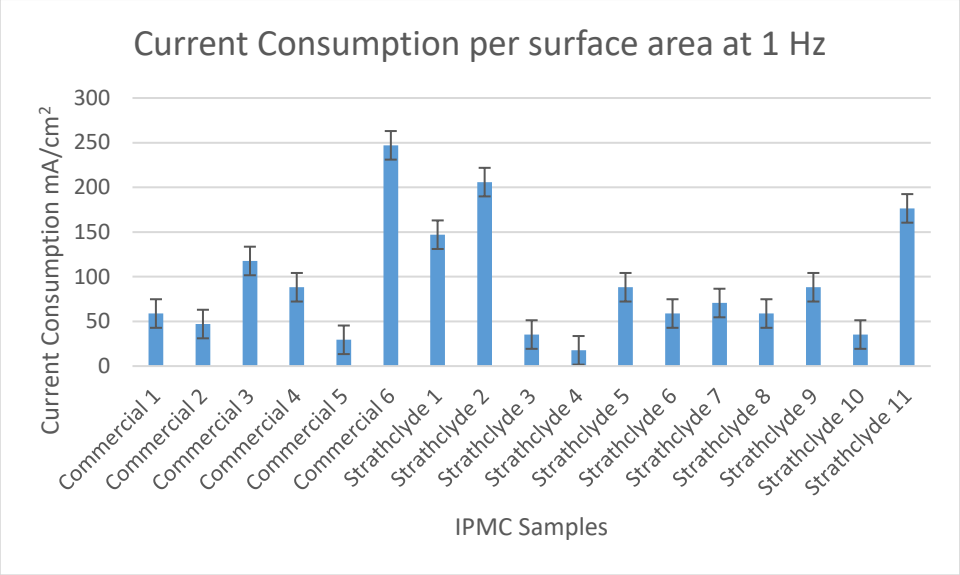

Figure 4.40 Current consumption per surface area at 1 Hz

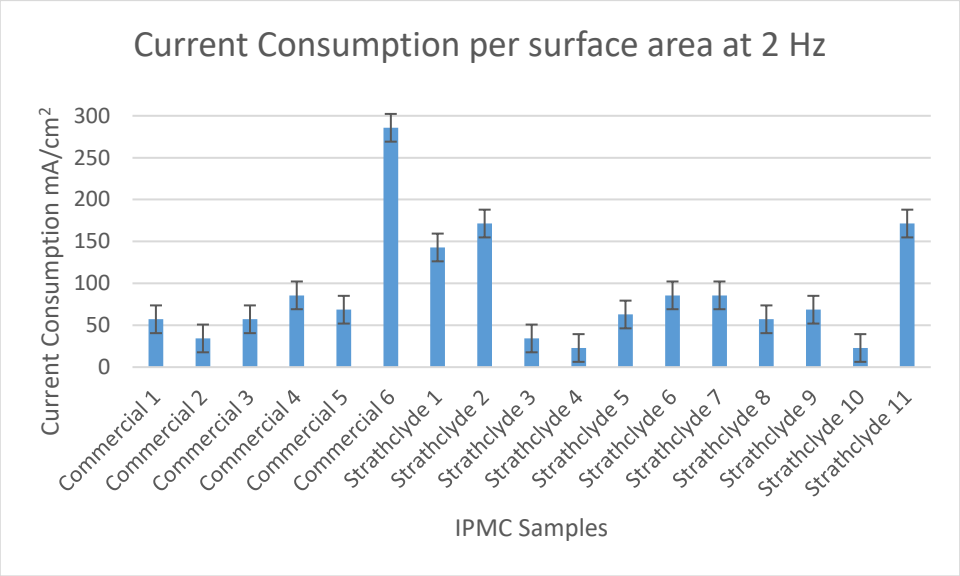

Figure 4.41 Current consumption per surface area at 2 Hz

Figure 4.42, **Figure 4.43**, **Figure 4.44**, and **Figure 4.45** show the maximum power consumption in mW at 0.05 Hz, 0.5 Hz, 1 Hz, and 2 Hz respectively.

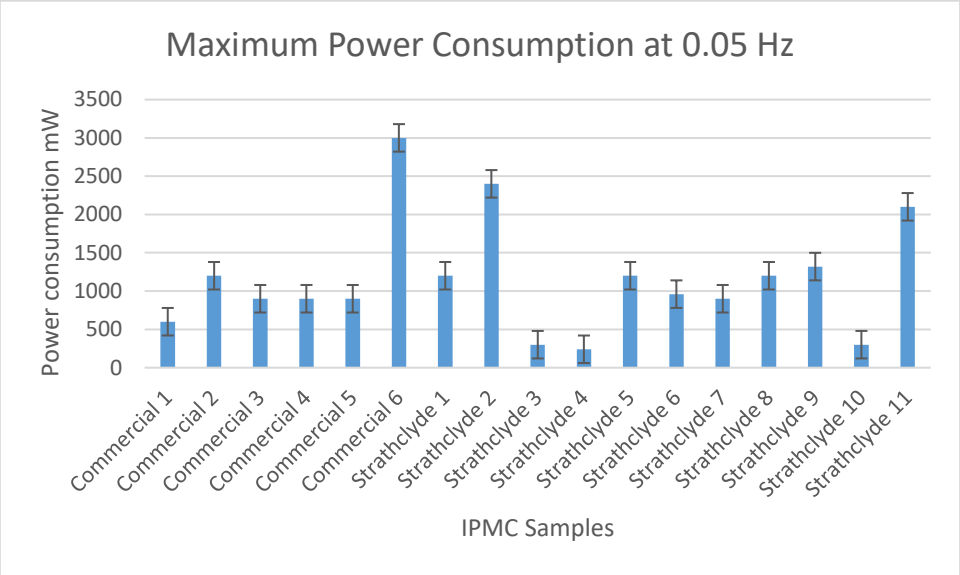

Figure 4.42 Maximum power consumption at 0.05 Hz

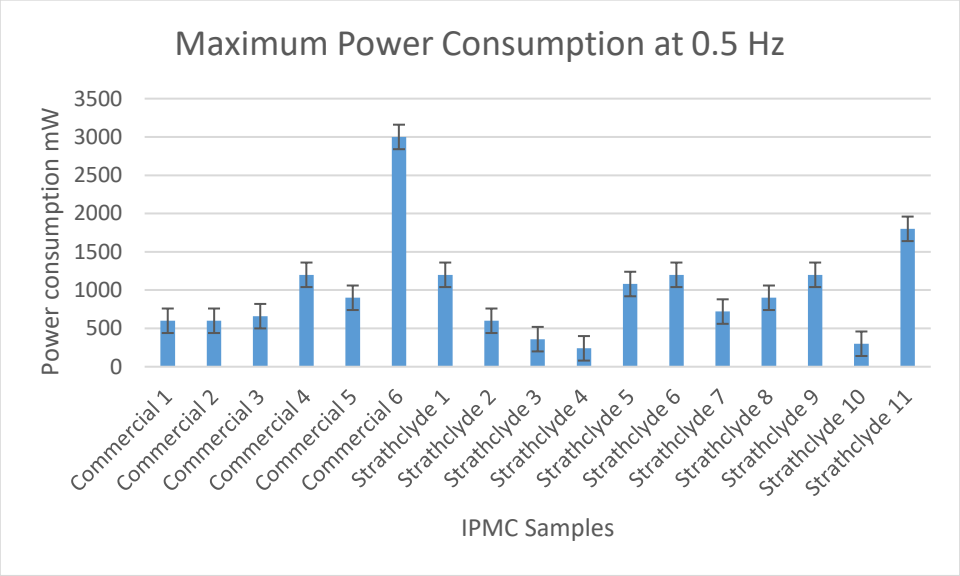

Figure 4.43 Maximum power consumption at 0.5 Hz

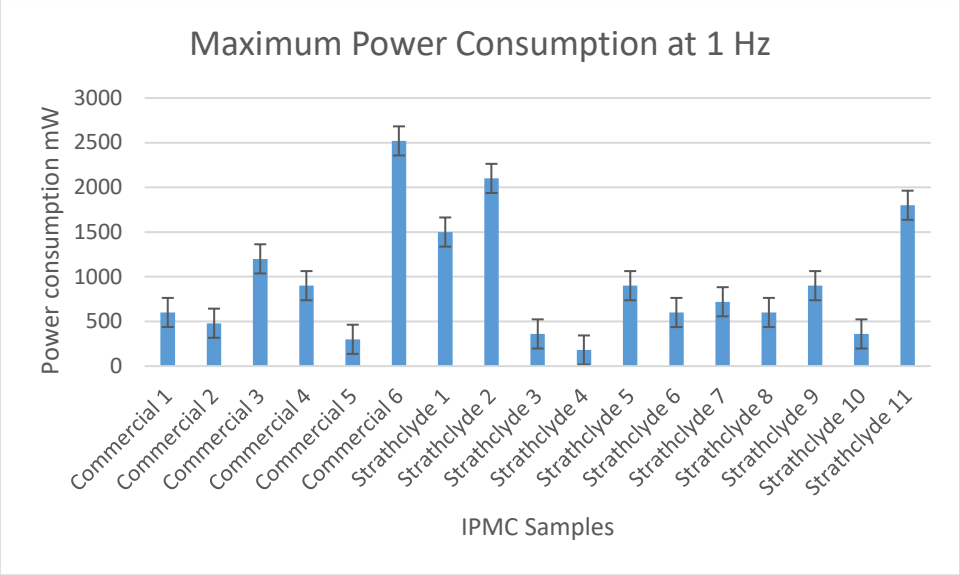

Figure 4.44 Maximum power consumption at 1 Hz

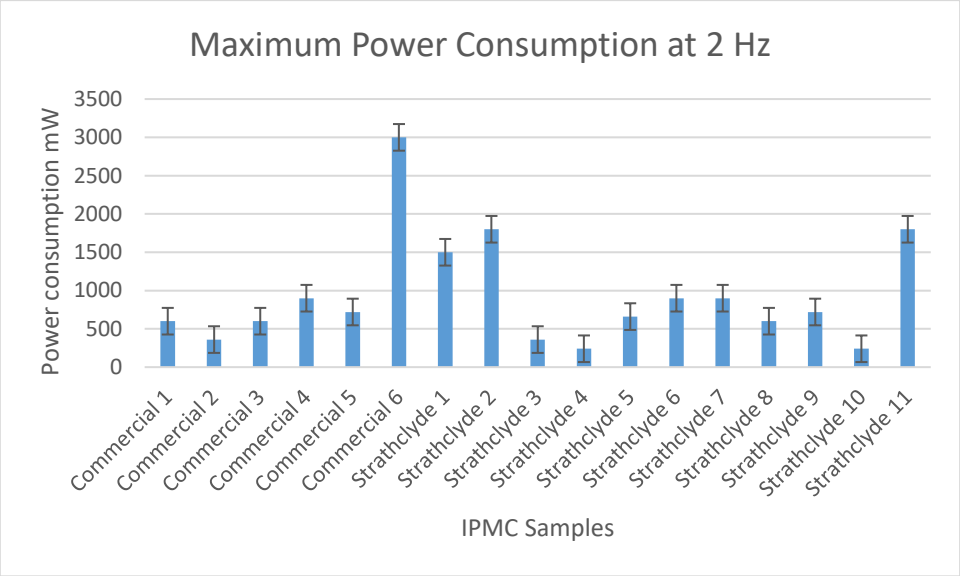

Figure 4.45 Maximum power consumption at 2 Hz

Figure 4.46, **Figure 4.47**, **Figure 4.48**, and **Figure 4.49** show the power consumption per weight in mW/mg at 0.05 Hz, 0.5 Hz, 1 Hz, and 2 Hz respectively.

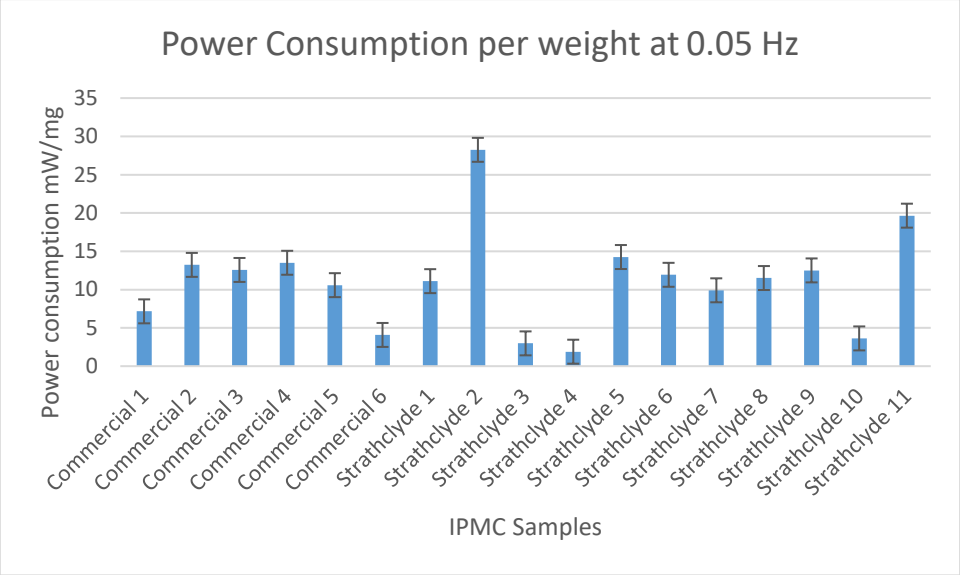

Figure 4.46 Power consumption per weight at 0.05 Hz

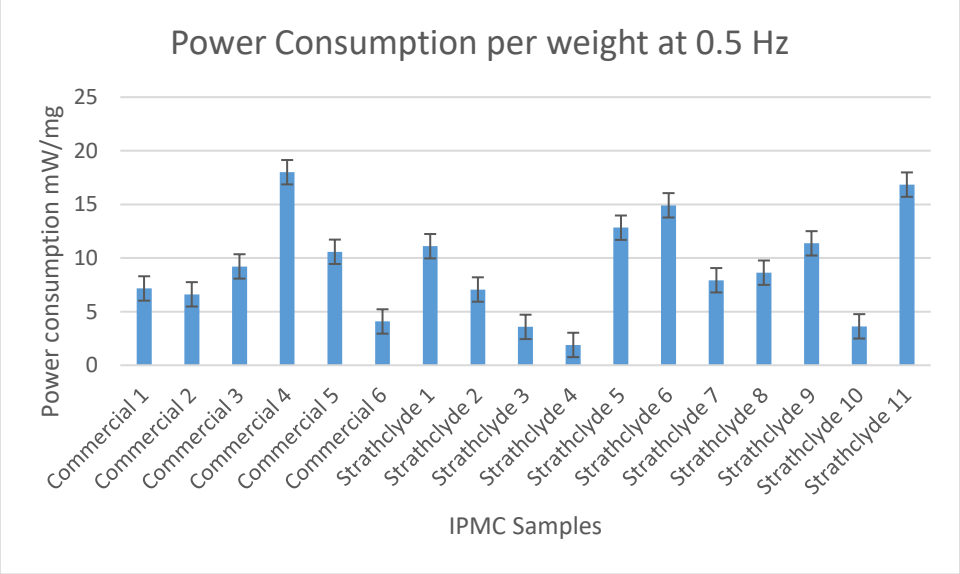

Figure 4.47 Power consumption per weight at 0.5 Hz

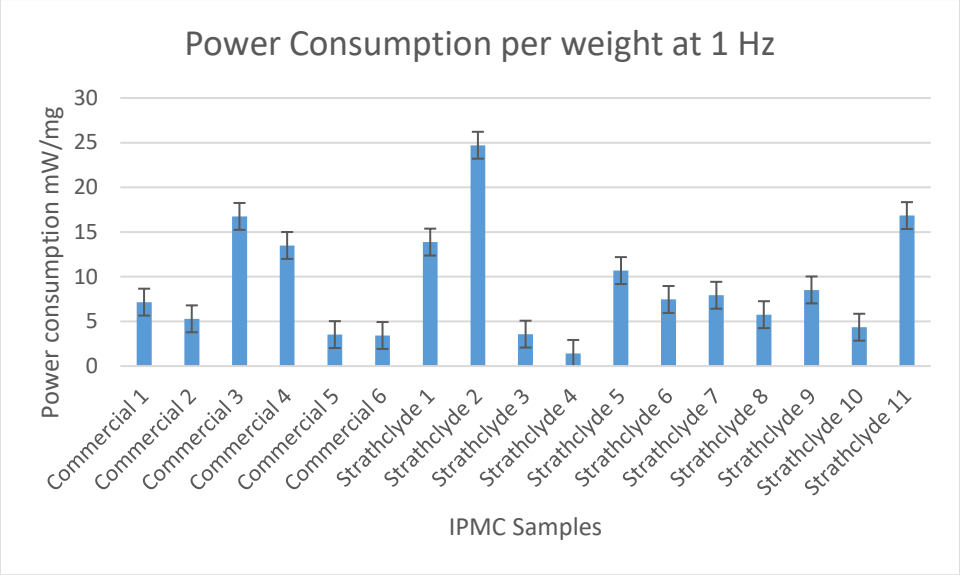

Figure 4.48 Power consumption per weight at 1 Hz

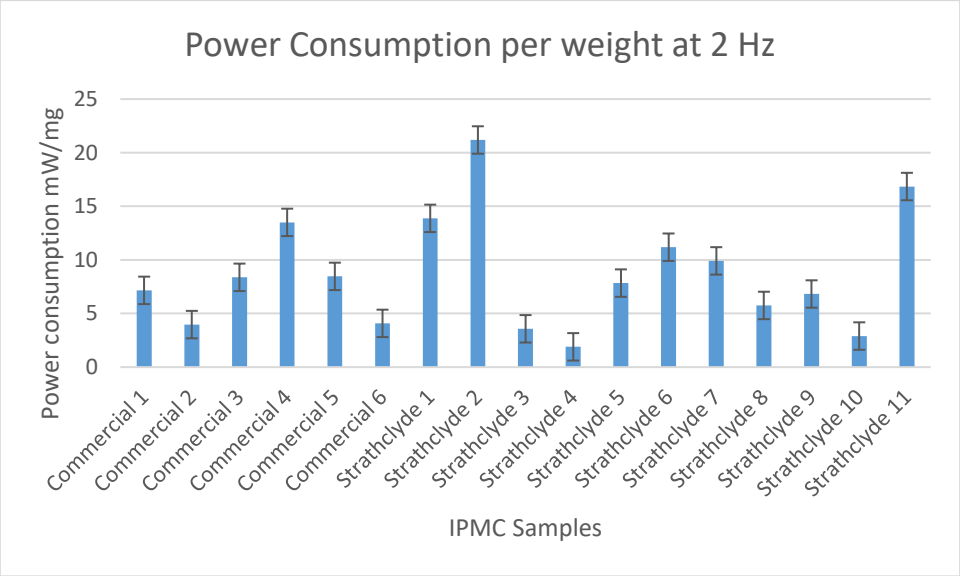

Figure 4.49 Power consumption per weight at 2 Hz

Figure 4.50, **Figure 4.51**, **Figure 4.52**, and **Figure 4.53** show the power consumption per surface area in mW/cm^2 at 0.05 Hz, 0.5 Hz, 1 Hz, and 2 Hz respectively.

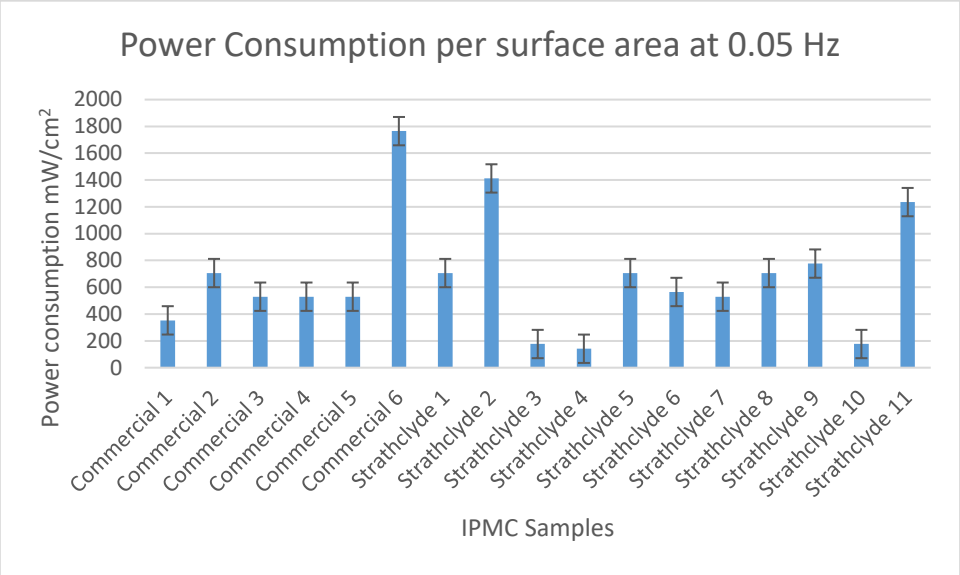

Figure 4.50 Power consumption per surface area at 0.05 Hz

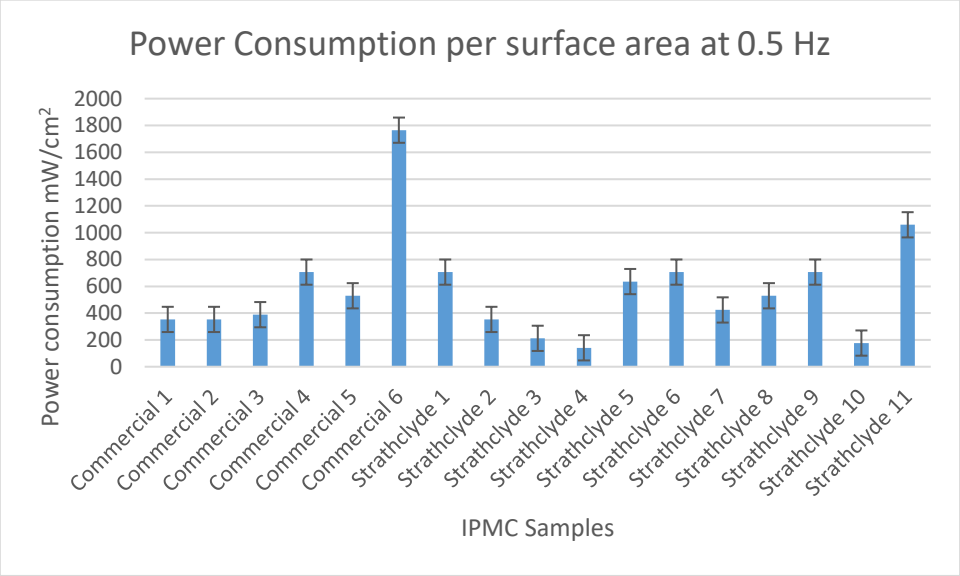

Figure 4.51 Power consumption per surface area at 0.5 Hz

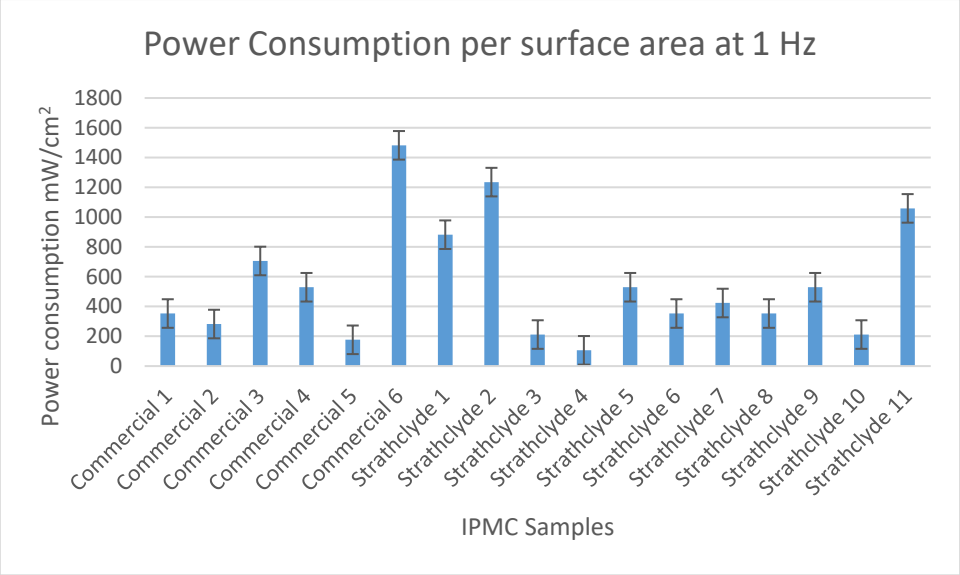

Figure 4.52 Power consumption per surface area at 1 Hz

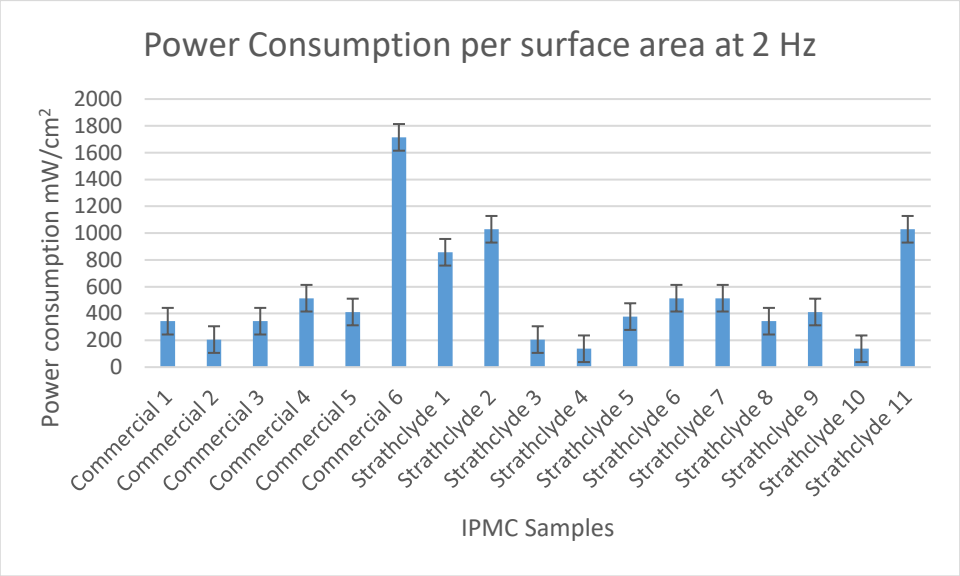

Figure 4.53 Power consumption per surface area at 2 Hz

2.3 Summary

This test showed the electrical power needed for each IPMC sample to actuate under the same conditions. This information will be used to determine which is the best power source for the proposed device.

4.7 Displacement Test

The primary mechanism of bending motion of IPMC relies on the imbalance of water density inside the membrane (Yu, Shen et al. 2007). When applying an AC voltage, IPMC undergoes a swinging motion, and the displacement level is strongly influenced by the voltage amplitude, the frequency, and the hydration level. The higher its water content, the larger the displacement it undergoes under the same externally applied voltage (Bonomo, Fortuna et al. 2005). It is also reported that lower frequencies (0.1 to 0.01 Hz) lead to a higher displacement (Shahinpoor, Bar-Cohen et al. 1998).

During displacement tests, It is observed that IPMC reached its maximum tip displacement after 20 seconds and then a fast relaxation occurs (Nguyen, Lee et al. 2007). Back relaxation is the movement of the IPMC actuator towards the natural state when activated by a low-frequency signal; it disappears on frequencies higher than 0.5 Hz.

There are two methods to record the displacement of IPMCs; the first uses a laser position sensor such as (BANNER, LG10A65PU) (Chung, Fung et al. 2006, Vunder, Itik et al. 2014). The other uses a video camera to record and measure the changes of the tip of the IPMC (Vunder, Itik et al. 2014)

Table 4.2 lists the displacement results of different studies at different testing conditions.

Study	Displacement	Size of the sample	Testing conditions
(Chung, Fung et al. 2006)	2.1 mm 4.4 mm 6.87 mm		1V 2V 3V
(Yu, Shen et al. 2007)	4 mm	30x3x0.2 mm	square wave, 2.5 V and 0.1 Hz
(Lee, Jung et al. 2006)	3 mm		2V DC
(Jain, Datta et al. 2010)	14 mm	30x6x0.2 mm	4V
(Jung, Nam et al. 2003)	0.85 mm 2 mm	10x2x0.2 mm 20x5x0.2 mm	1.5 V DC 3V square wave
(Liu, McDaid et al. 2011)	10.27 mm	30x10x0.6 mm	4V

Table 4.2 Displacement results from previous studies

2.1 Experiment Setup

This test used the video camera method to record the tip displacement of the IPMC. The samples were placed in a cantilever position, with one end was connected to the IPMC driver using the alligator clip, and the other end was left free to move. The driving signal was 6 V, and the frequency range was 0.05, 0.5, 1, 2, DC. This signal was generated by Lab View 2015 and connected to the IPMC driver through NI 6225 DAQ module. A graph paper was placed behind the IPMC sample, and a Nikon D5300 camera was used to record the displacement. **Figure 4.54** shows the graph paper and the IPMC holder, **Figure 4.55** shows the full experiment setup.

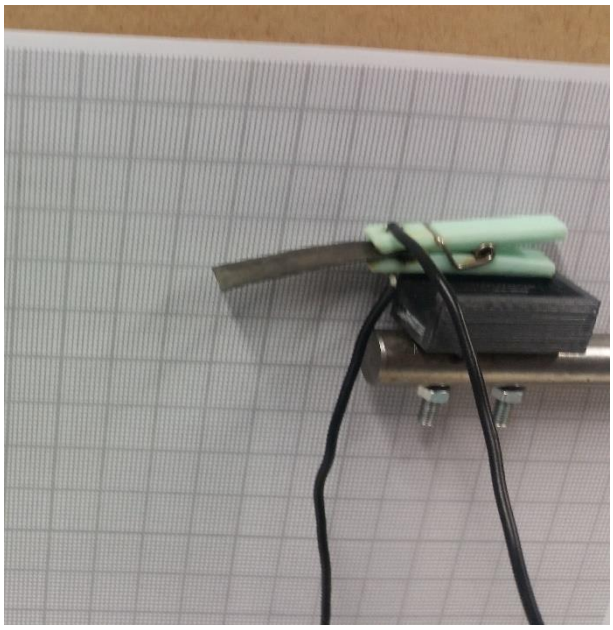

Figure 4.54 Graph paper behind the IPMC holder

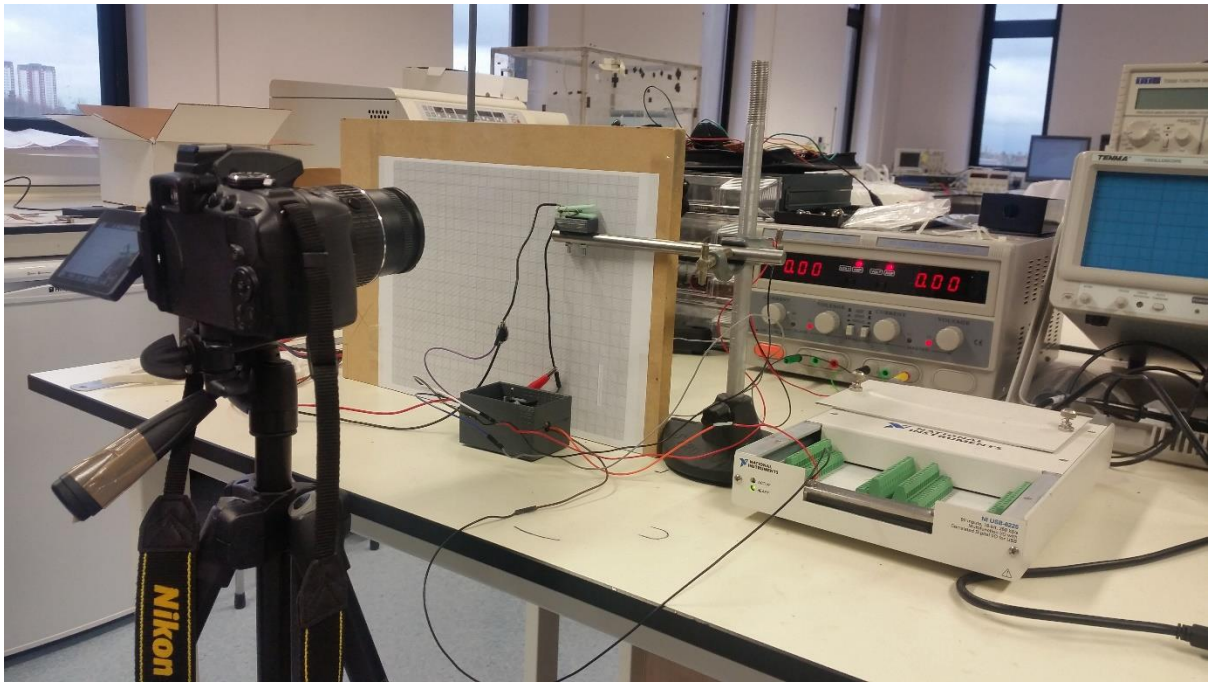

Figure 4.55 The complete experiment setup for displacement test

Figure 4.56 shows the block diagram of the displacement test.

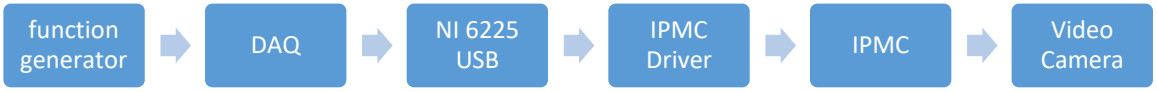

Figure 4.56 Block Diagram of the displacement test

All videos were analysed later, and the maximum tip displacement was recorded.

2.2 Result

Figure 4.57, **Figure 4.58**, **Figure 4.59**, **Figure 4.60**, and **Figure 4.61** show the maximum tip displacement in mm of the IPMC actuators at DC, 0.05 Hz, 0.5 Hz, 1 Hz, and 2 Hz respectively.

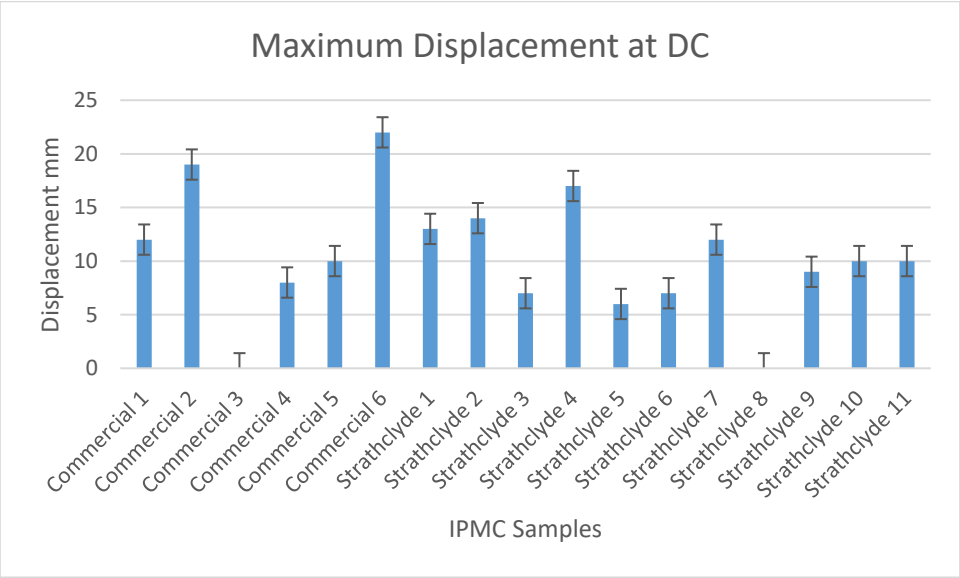

Figure 4.57 Maximum tip displacement at DC

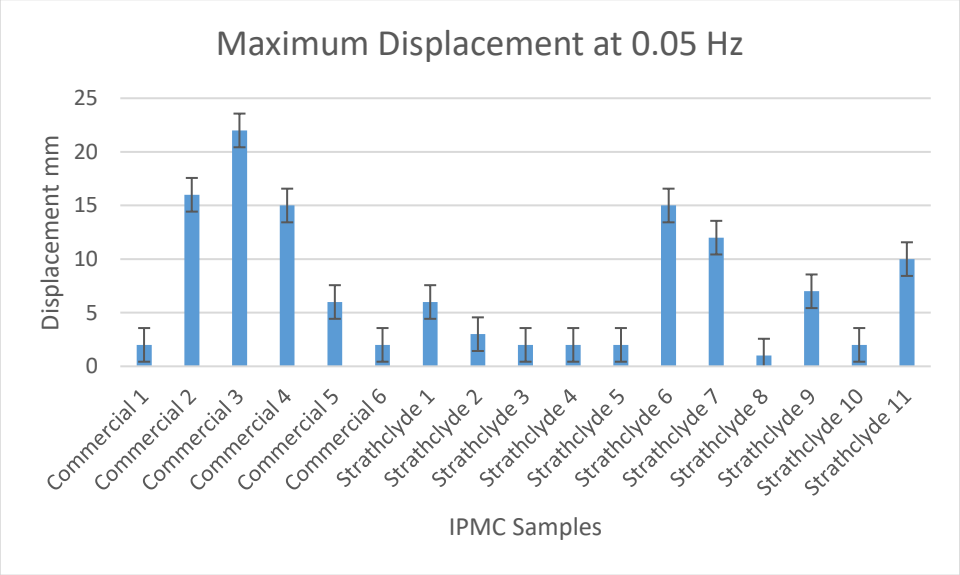

Figure 4.58 Maximum tip displacement at 0.05 Hz

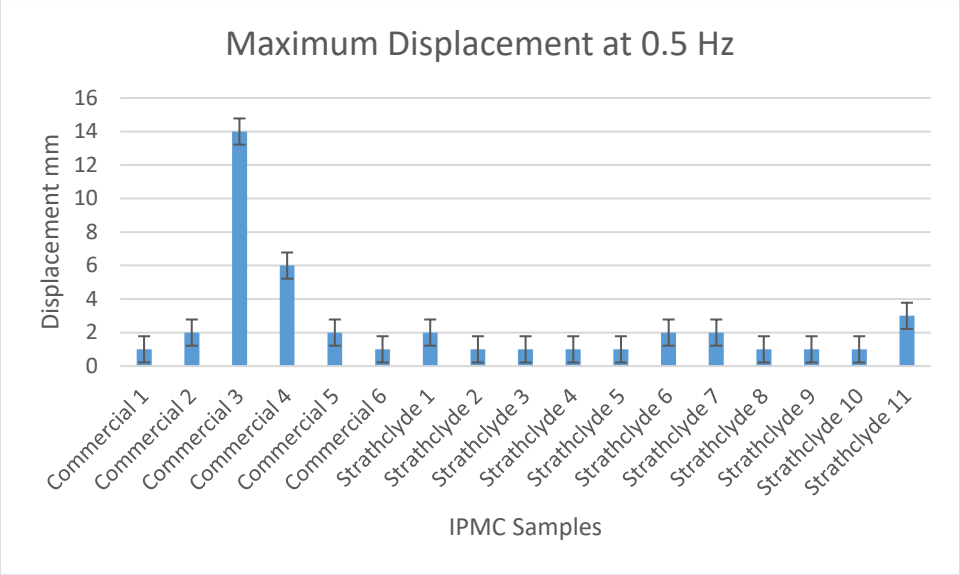

Figure 4.59 Maximum tip displacement at 0.5 Hz

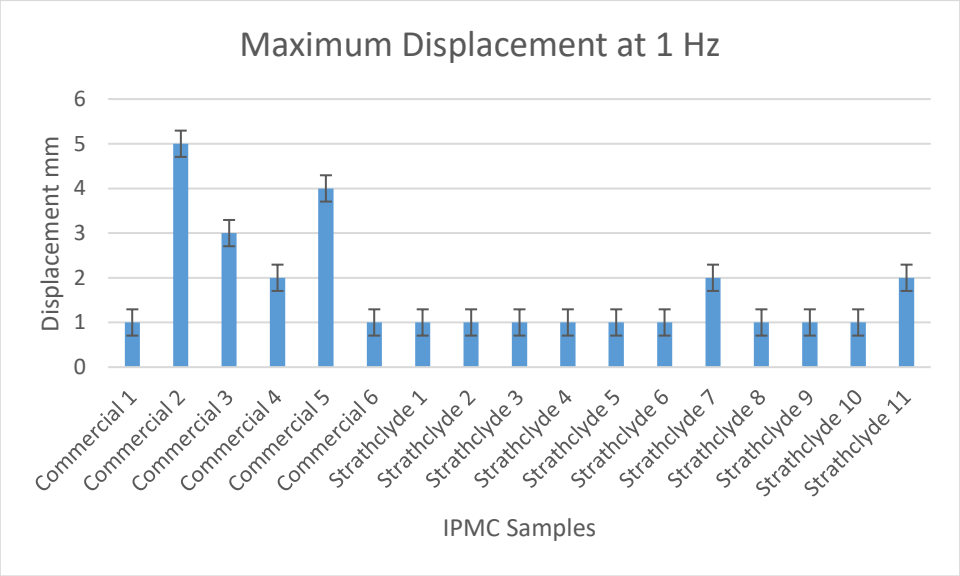

Figure 4.60 Maximum tip displacement at 1 Hz

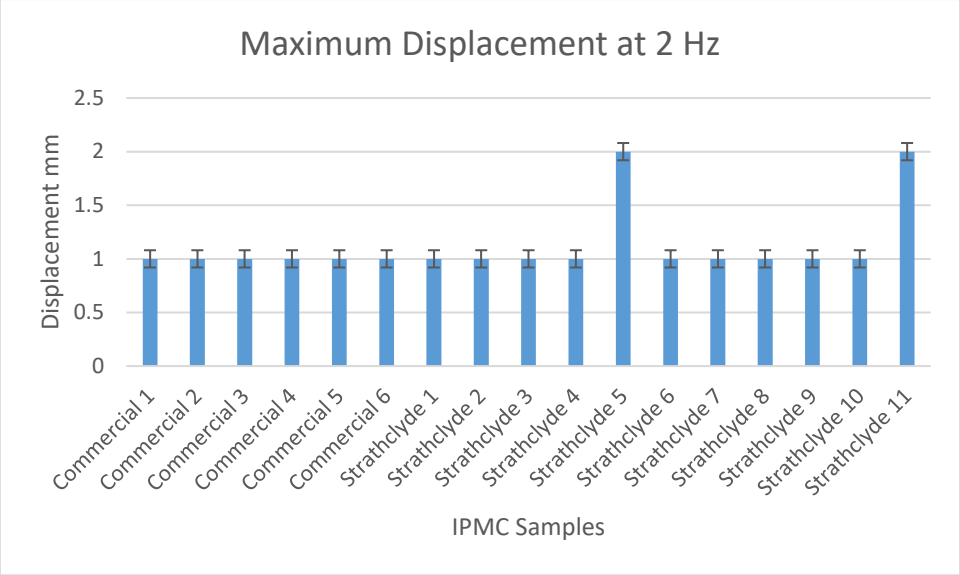

Figure 4.61 Maximum tip displacement at 2 Hz

Figure 4.62, **Figure 4.63**, **Figure 4.64**, **Figure 4.65**, and **Figure 4.66** show the maximum tip displacement as a percentage of the original length of the IPMC actuators at DC, 0.05 Hz, 0.5 Hz, 1 Hz, and 2 Hz respectively.

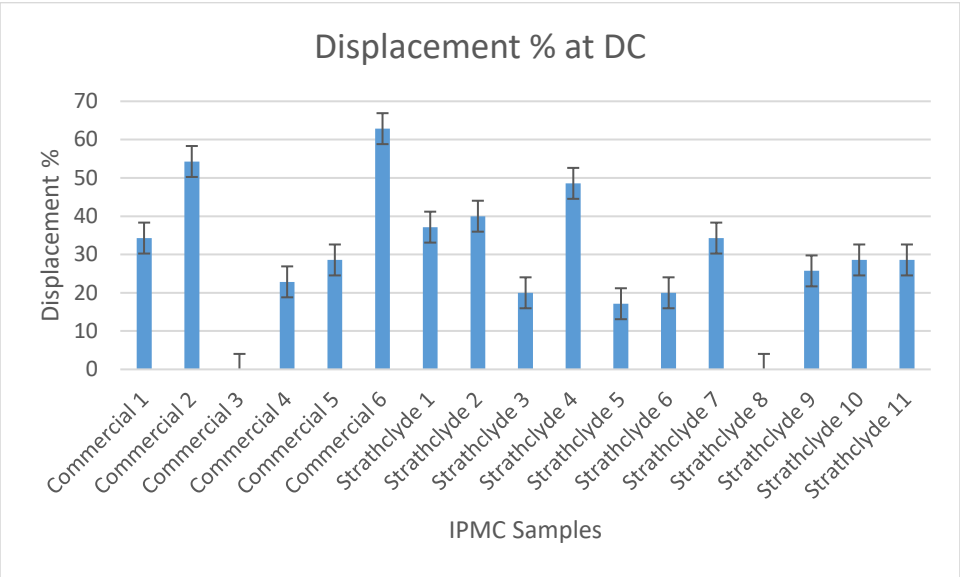

Figure 4.62 Tip displacement % at DC

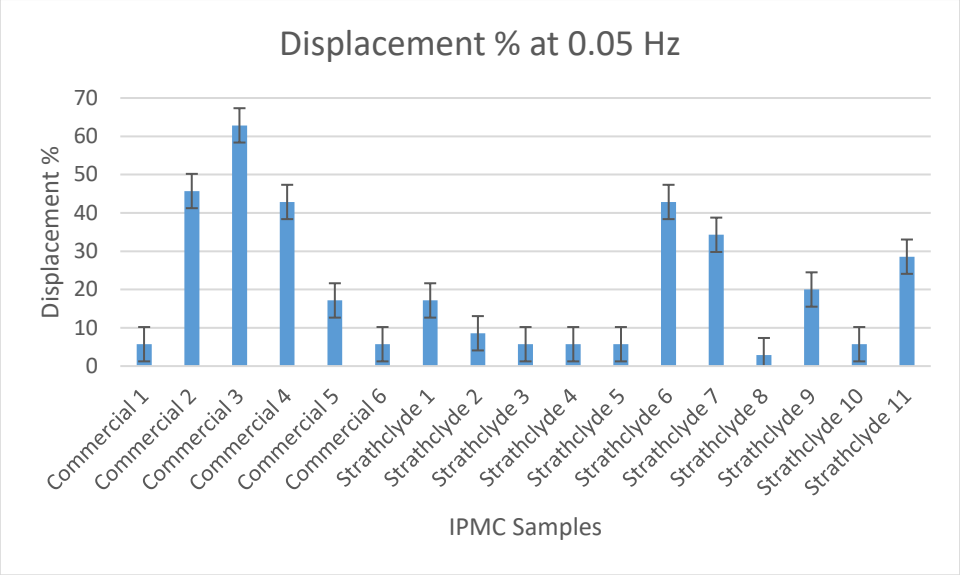

Figure 4.63 Tip displacement % at 0.05 Hz

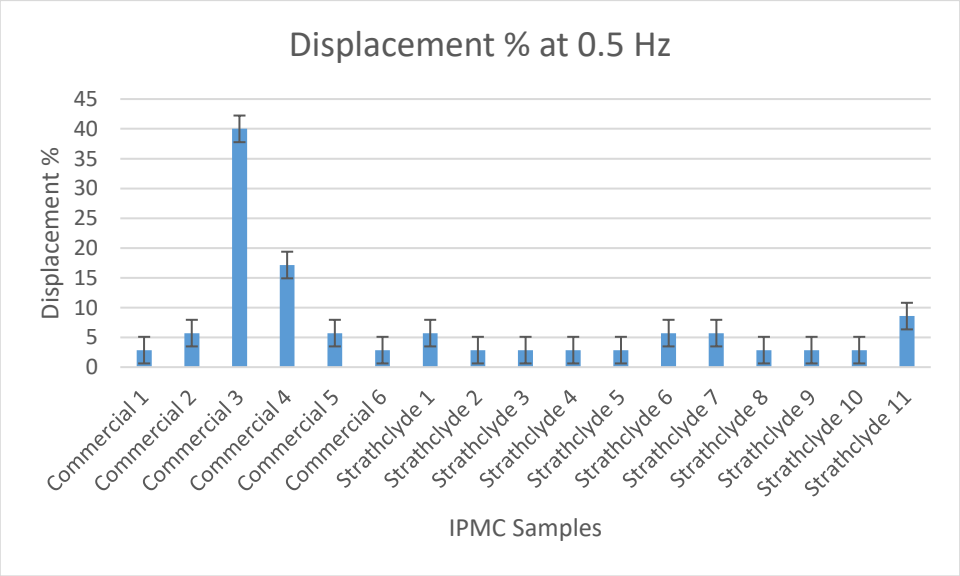

Figure 4.64 Tip displacement % at 0.5 Hz

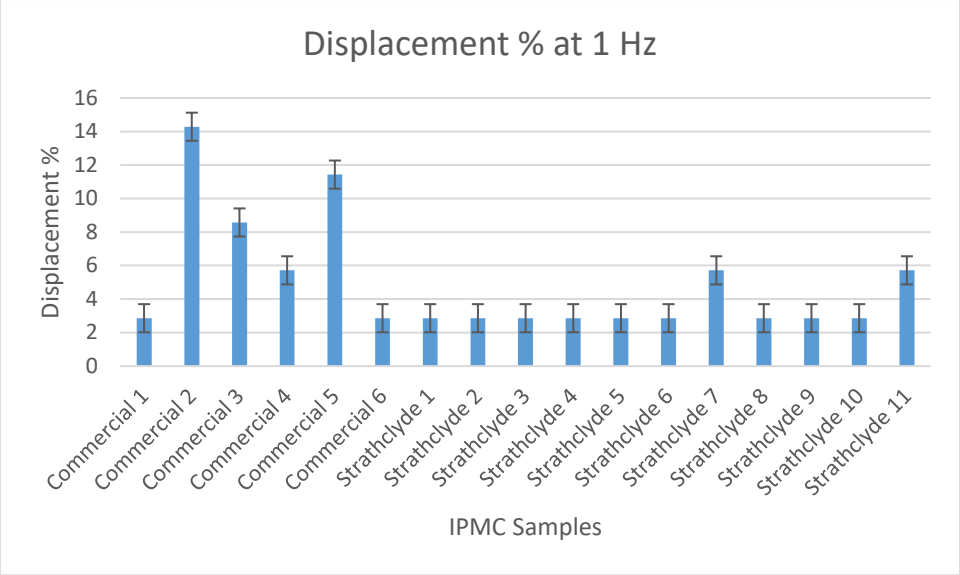

Figure 4.65 Tip displacement % at 1 Hz

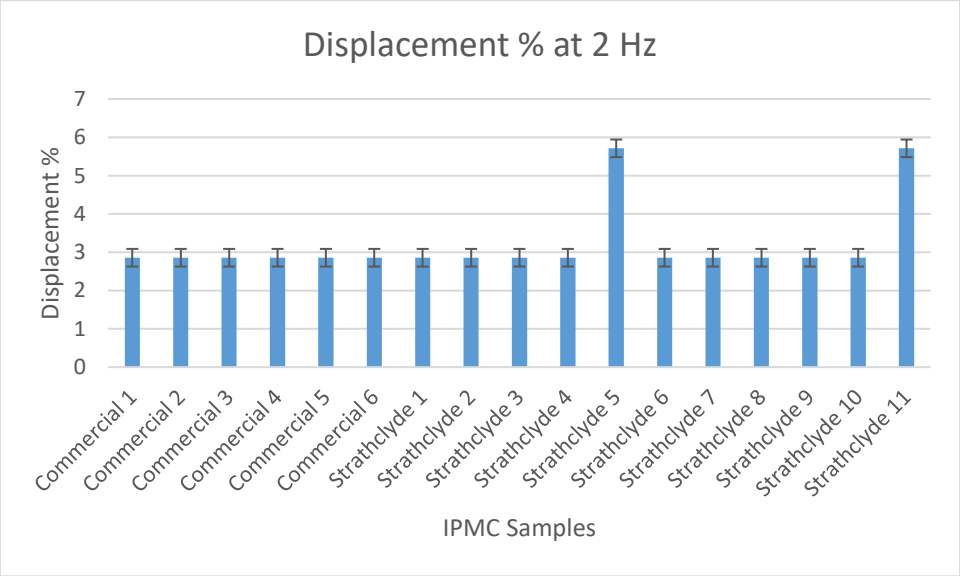

Figure 4.66 Tip displacement % at 2 Hz

2.3 Summary

The tip displacement test presented that the IPMC samples showed a larger response when stimulated with a DC signal, and the response decreased by increasing the frequency. These results from the Commercials and our own Strathclyde materials match what was found in the literature previously, and confirm the conformity with other investigators and our own materials.

4.8 Blocking Force Test

Blocking force is the force measured at the tip of the IPMC actuator when an electric field is applied (Anton, Aabloo et al. 2008).

To measure the blocking force, the IPMC sample is placed between two electrodes from one side, and the other end is positioned opposite to the load cell. Upon activation, the IPMC actuator free end will bend towards the load cell, which will generate a voltage output proportional to the applied force. By measuring the output voltage of the load cell, the blocking force can be calculated using the provided information in the load cell's datasheet. **Figure 4.67** shows the experiment setup to measure the blocking force.

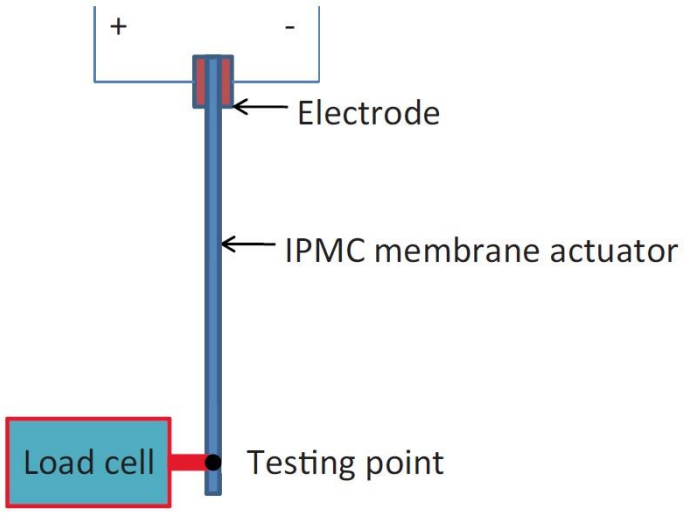

Figure 4.67 Blocking force experiment setup (Chen, Um et al. 2011)

Different sensors and load cells were used to measure this force in the literature, **Table 4.3** lists some of the force sensors used to measure the blocking force.

Study	Sensor
(Chung, Fung et al. 2006)	KYOWA, LVS-10GA (Japan)
(Lee and Yoo 2011)	CB-G150,Dacell (Korea)
(Chen, Um et al. 2011)	GS0-10, Transducer Techniques (USA)
(Vunder, Itik et al. 2014)	Millinewton,IPR EPFL (Switzerland)
(He, Yu et al. 2011)	CETR-UMT (USA)
(Liu, McDaid et al. 2011)	SS-2 Precision, Sherborne Sensors Limited (UK)

Table 4.3 Blocking Force Sensors

Figure 4.68 shows a typical blocking force signal generated from 42x9.9x0.5 mm IPMC.

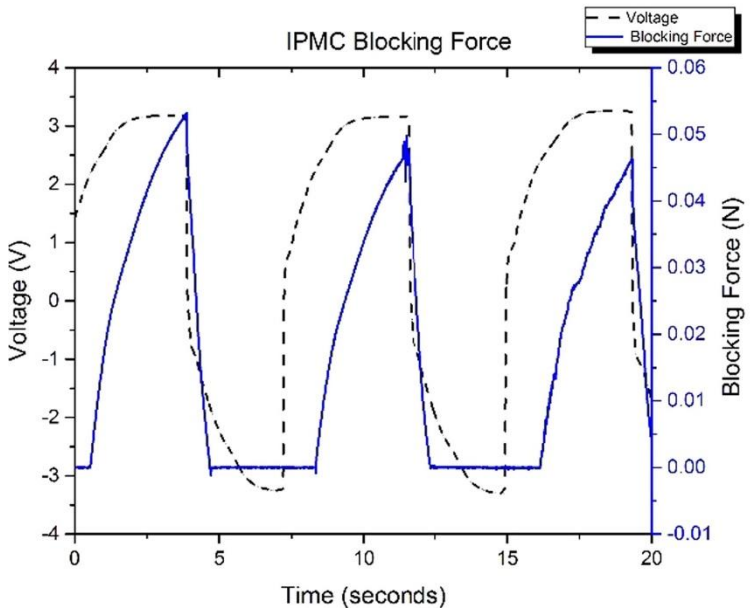

Figure 4.68 IPMC Blocking Force (Trabia, Hwang et al. 2016)

IPMC can generate a few mN of blocking force. Most of the researchers focused on improving the blocking force of IPMC by optimisation and additional treatment of the electrode layer during the fabrication process, increasing the thickness of IPMC, or using specific inner solution systems based on ionic liquid (Nguyen and Yoo 2007).

Table 4.4 lists the blocking force results of different studies at different testing conditions.

Study	Force	Size of the sample	Testing conditions
(Malone and Lipson 2006)	Max force 0.678 mN Average force 0.15 mN	10x30x0.25 mm	
(Hwang, Palmre et al. 2015)	13.5 mN		3V DC
(Yu, Shen et al. 2007)	1 mN	30x3x0.2 mm	square wave, 0.1 Hz and 2.5 V
(Jain, Datta et al. 2010)	10 mN	30x6x0.2 mm	4V
(Vunder, Itik et al. 2014)	1.2 mN	20x5 mm	2V
(Han, Park et al. 2006)	1.12 gf (10.9 mN)	40x5x0.58 mm	2V DC
(Chung, Fung et al. 2006)	0.114 gf (1.11 mN) 0.168 gf (1.64 mN) 0.222 gf (2.17 mN)		1V 2V 3V
(Panwar, Kang et al. 2011)	2.29 gf (22.44 mN) 3.59 gf (35.18 mN)		2.5V 3 V
(Shahinpoor and Kim 2002)	1 gf (9.8 mN) 1.2 gf (11.76 mN)	20x5x0.2 mm	1V at 0.5 Hz 1.5V at 0.5 Hz
(Chen, Um et al. 2011)	0.15 gf (1.47 mN)		
(Lee, Jung et al. 2006)	0.9 gf (8.82 mN) 0.95 gf (9.31 mN) 1 gf (9.8 mN)	178 µm	2 V 2.5 V 3 V
(Nguyen, Lee et al. 2007)	0.6 gf (5.88 mN)	5x20x0.3 mm	3V
(Liu, McDaid et al. 2011)	5.21 gf (51.05 mN)	30x10x0.6 mm	4V

Table 4.4 Blocking Force results from previous studies

2.1 Experiment Setup

Blocking force was measured using a small force sensor Millinewton-B-1000 (Pewatron sensors, Zurich, Switzerland). The force is measured through bending of a cantilever beam, which carries a piezoresistive bridge. The electronics on the base carry out the signal amplification and deliver a voltage output, which is a linear function of the force. This force sensor has three terminals, input 5V DC, output, and ground, as shown in **Figure 4.69**.

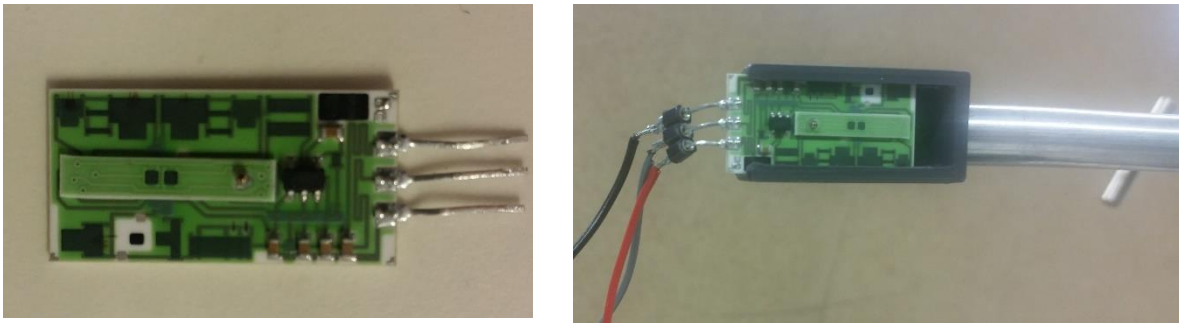

Figure 4.69 Force Sensor

The force sensor has a linear output voltage, based on the datasheet. The output equation (4.6) was:

$$Y = 0.003X + 0.5 \quad (4.6)$$

Where **Y** is the output voltage in mV, and **X** is the applied force in mN.

However, upon trying some certified weights and recording the results, some changes were found between the measured voltage of the sensor and the results using Equation (11). Therefore, a full calibration of the sensor was required, using the certified weights, and the new linear equation (4.7) was formed:

$$Y = 0.0026X + 0.5031 \quad (4.7)$$

Figure 4.70 shows both set of results, the calculated values using equation (4.7), and the actual measured values.

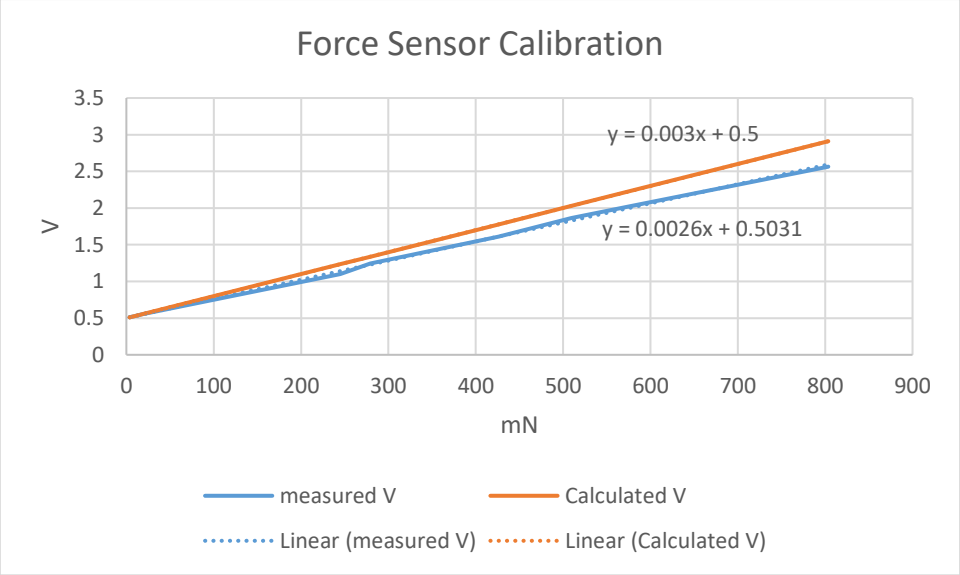

Figure 4.70 Calibration graph of the force sensor

NI 6225 DAQ module was used as an interface between the electronic parts (force sensor, and IPMC driver) from one side, and the software (Lab View 2015) from the other side, as shown in **Figure 4.71**. Two analogue output channels and one analogue input were used. The output channels were used one for the generated signal for the IPMC driver, and the other to power the force sensor, while the input channel was connected to the force sensor's output.

Figure 4.71 NI 6225 USB DAQ system

Lab View 2015 was used to generate the driving signal and record the data. **Figure 4.72** shows the front panel of the code. The testing signal was a 6V square wave, as it has been proven before to get the best response to other waves. All samples were tested using different frequencies (0.05, 0.5, 1, 2) Hz to match the requirements of the proposed device, see **Table**

3.1. Lab View sent the generated signal to NI 6225 USB DAQ, which was used as a Digital to Analogue Converter (DAC), and then connected with the IPMC driver. The other function of Lab View was to record the measured data from the sensor. First, the sensor's output was connected to the NI 6225 USB DAQ, which was used as an Analogue to Digital Converter (ADC). Then, the digital signal was filtered using a low pass filter to remove any noise. After that, equation (4.7) was used to calculate the measured force in mN. Finally, both the generated square wave and the measured force signal were saved in an Excel file. **Figure 4.73**, and **Figure 4.74** show the block diagram of the Lab View code.

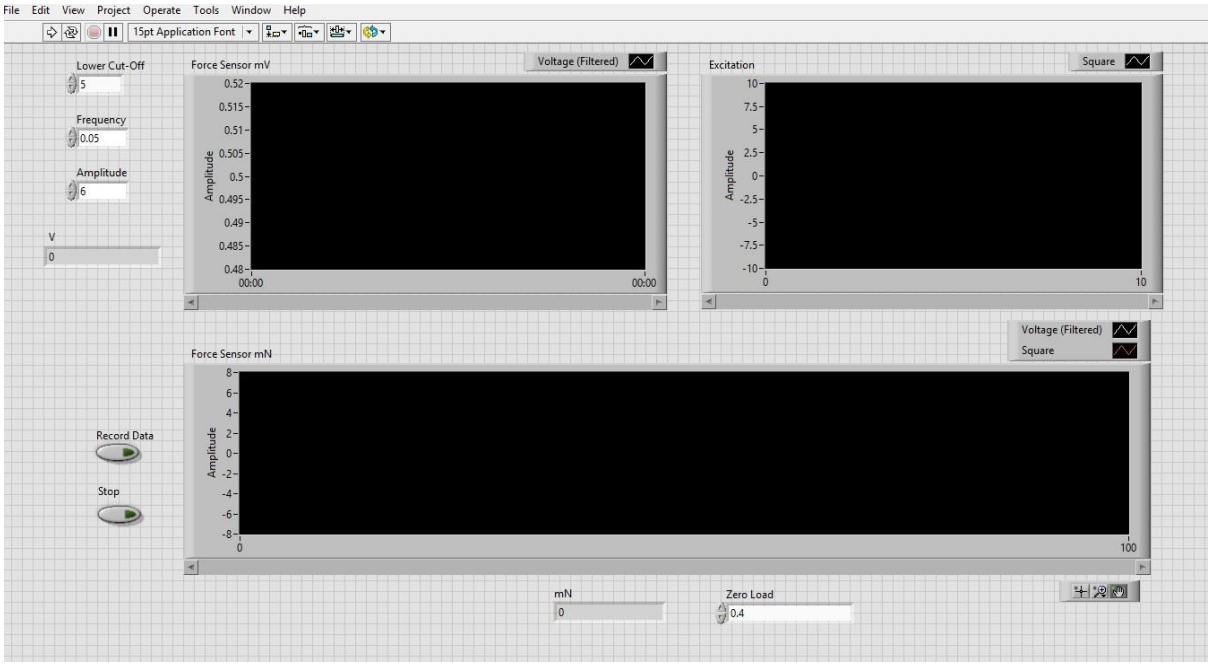

Figure 4.72 Front Panel of Lab View

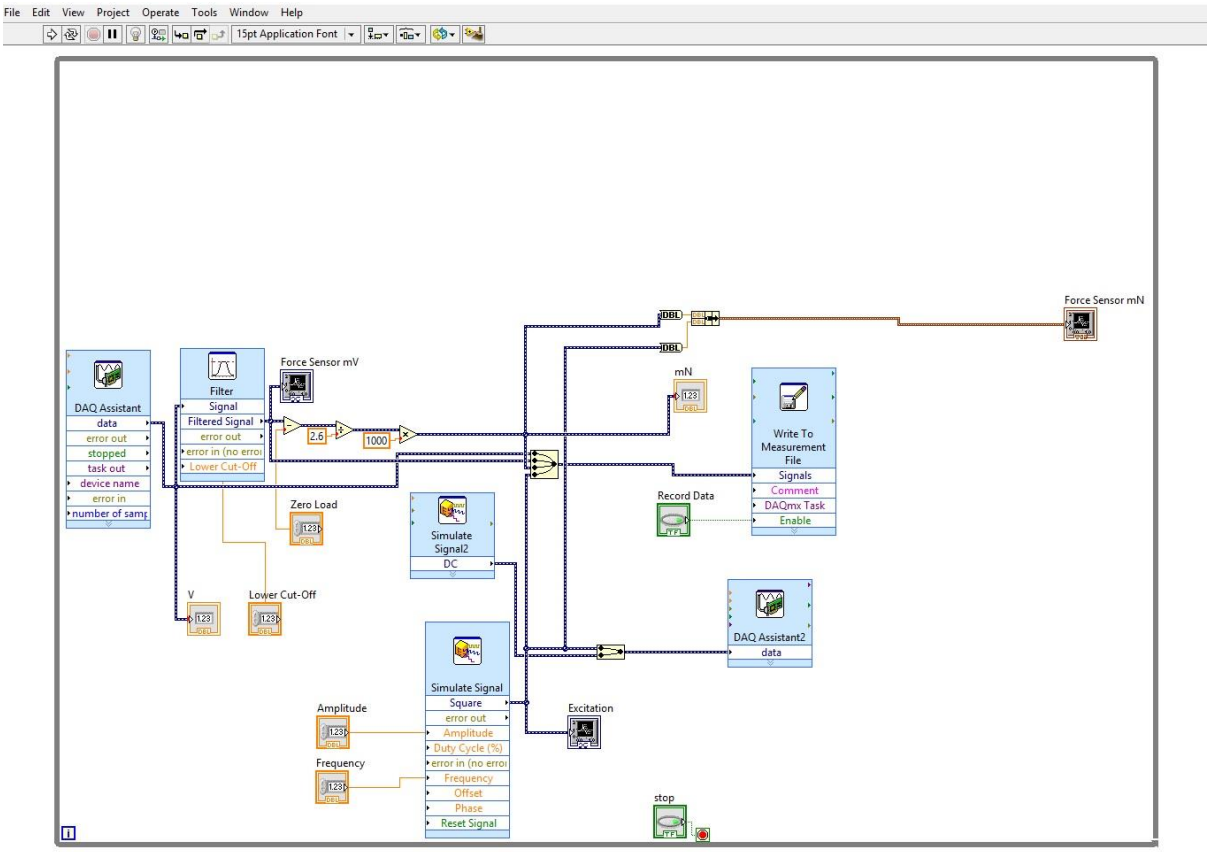

Figure 4.73 Block diagram of Lab View

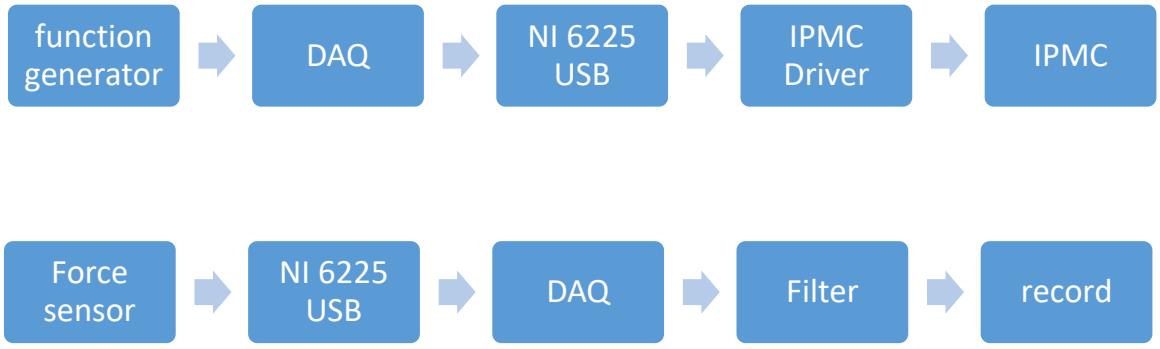

Figure 4.74 Block diagram of the blocking force test

The complete setup is shown in **Figure 4.75**.① is the NI 6225 USB DAQ, ②is the IPMC driver, ③is the power supply, ④is the Force Sensor, ⑤is the IPMC sample, and ⑥is the IPMC alligator holder.

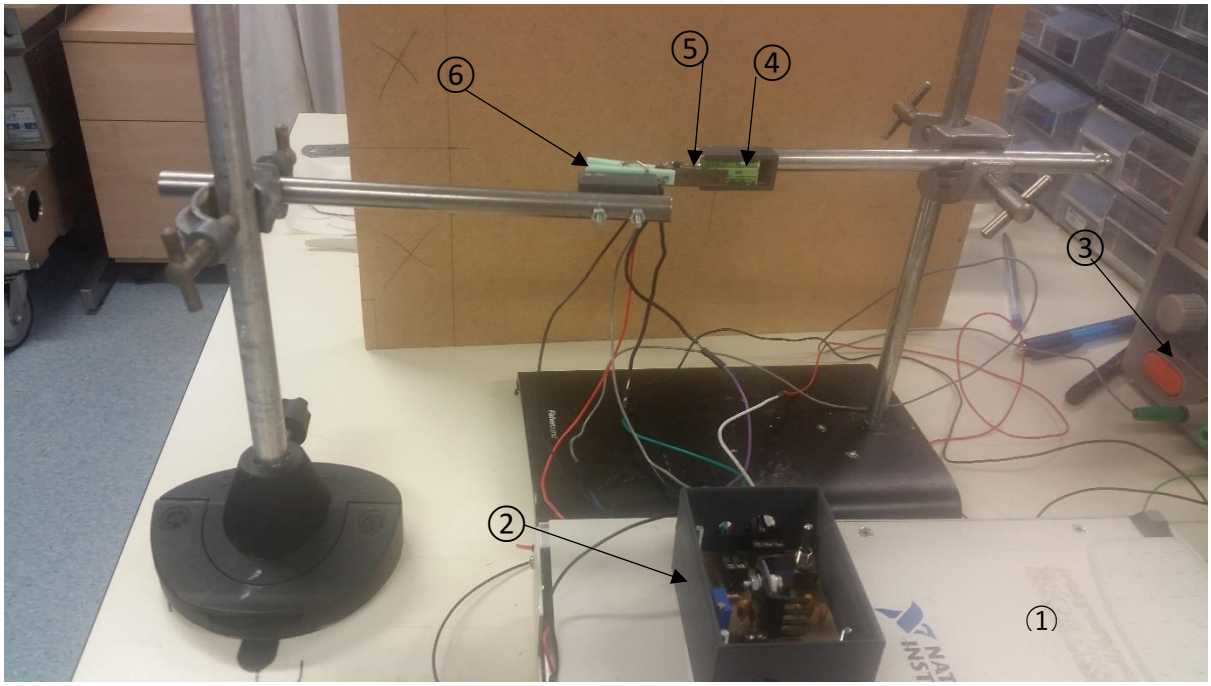

Figure 4.75 The complete setup of the experiment

2.2 Results

In this section, a few examples of the blocking force are shown. The rest of the graphs can be found in the Appendices section (11.5).

Figure 4.76, **Figure 4.77**, **Figure 4.78**, and **Figure 4.79** show the blocking force of the Commercial 6 IPMC sample at different frequencies.

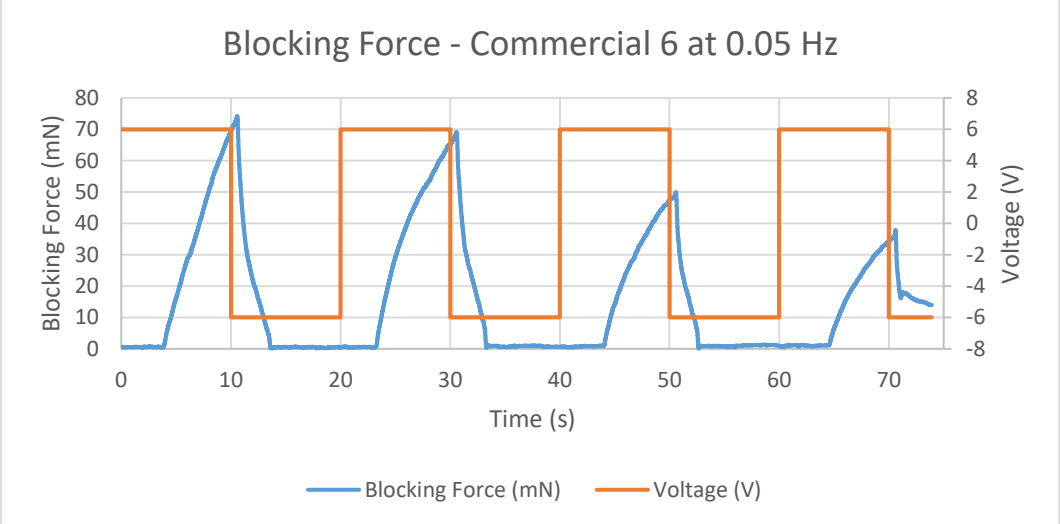

Figure 4.76 Blocking Force of Commercial 6 sample at 0.05 Hz

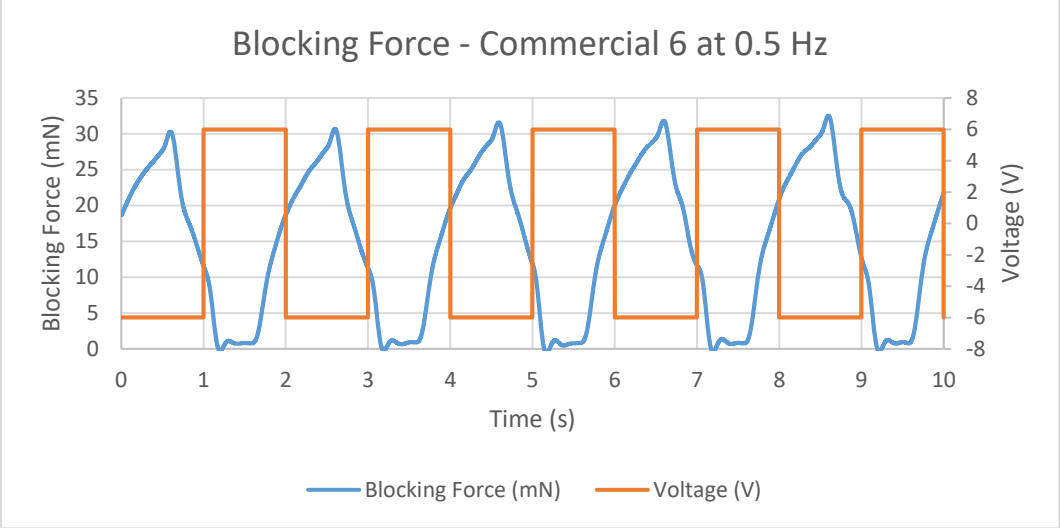

Figure 4.77 Blocking Force of Commercial 6 Sample at 0.5 Hz

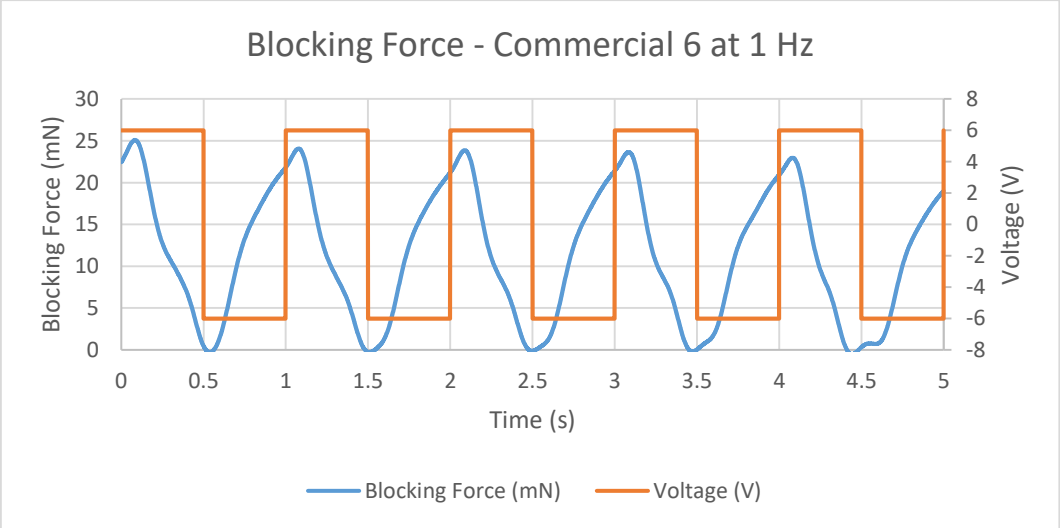

Figure 4.78 Blocking Force of Commercial 6 Sample at 1 Hz

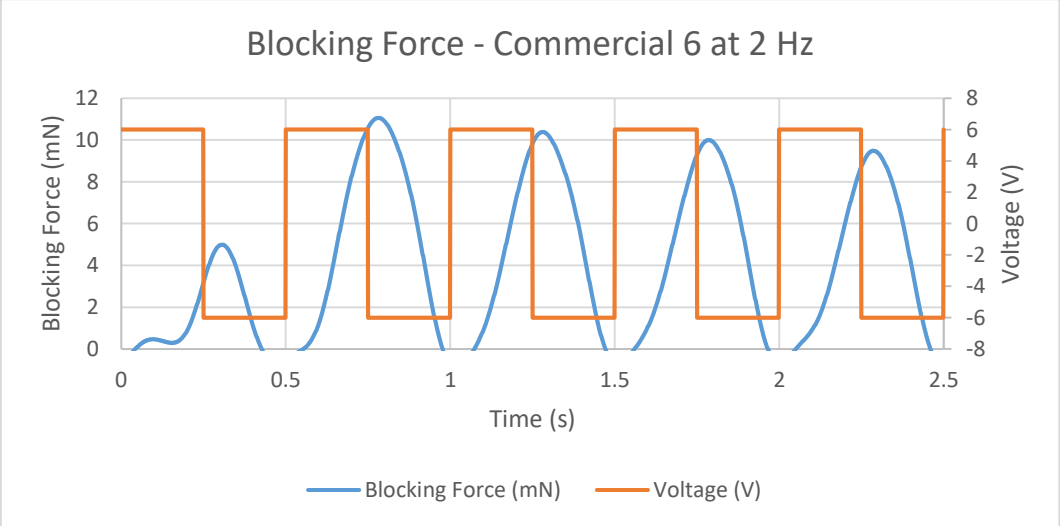

Figure 4.79 Blocking Force of Commercial 6 Sample at 2 Hz

Figure 4.80, **Figure 4.81**, **Figure 4.82**, and **Figure 4.83** show the blocking force of the Strathclyde 2 IPMC sample at different frequencies.

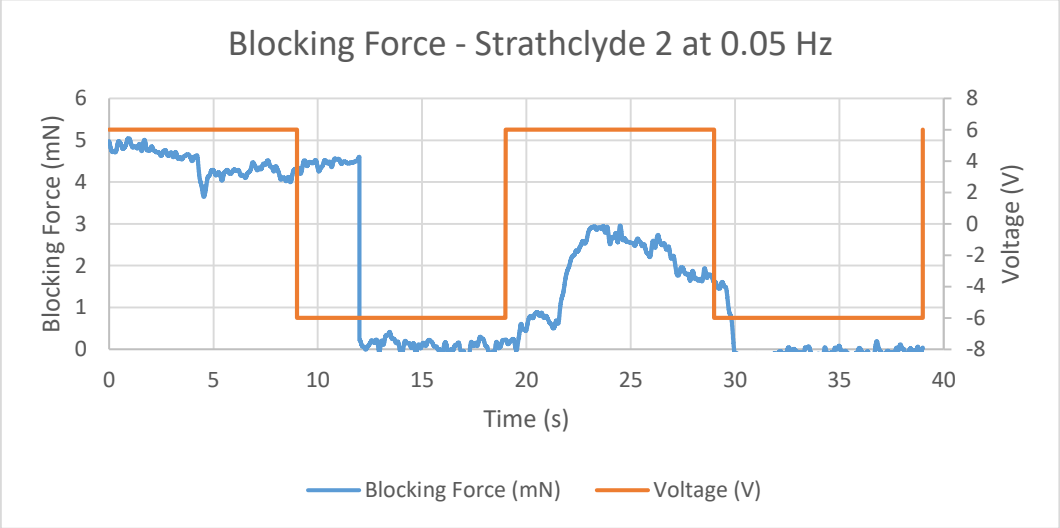

Figure 4.80 Blocking Force of Strathclyde 2 Sample at 0.05 Hz

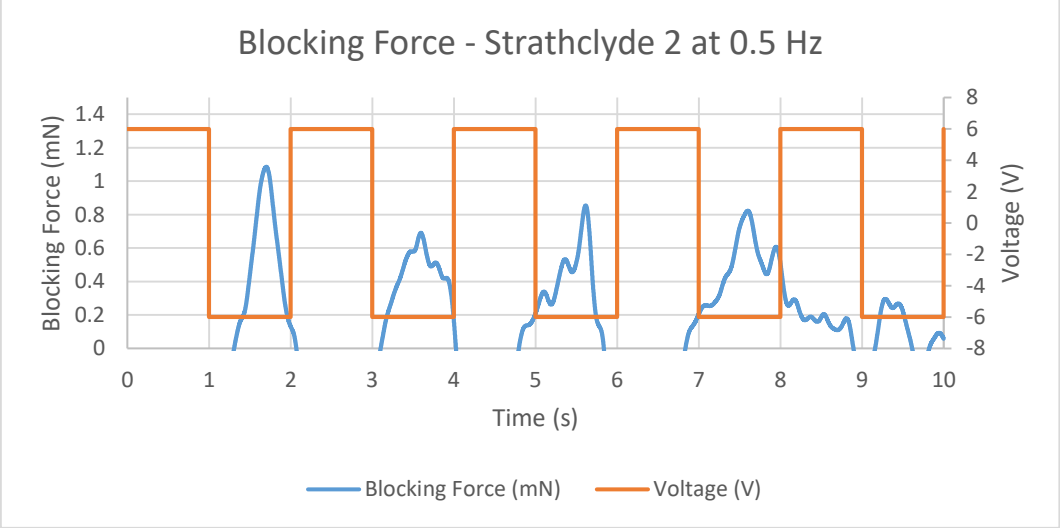

Figure 4.81 Blocking Force of Strathclyde 2 Sample at 0.5 Hz

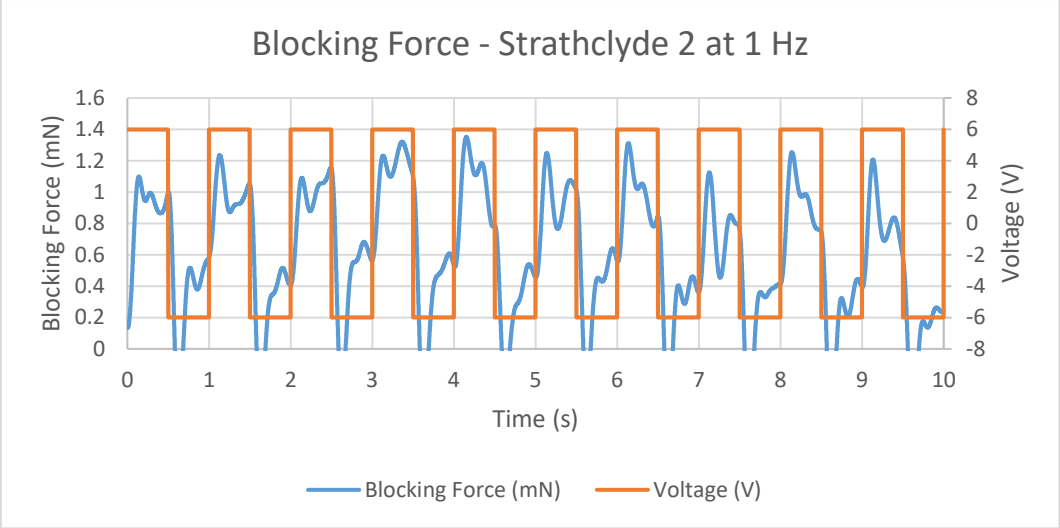

Figure 4.82 Blocking Force of Strathclyde 2 Sample at 1 Hz

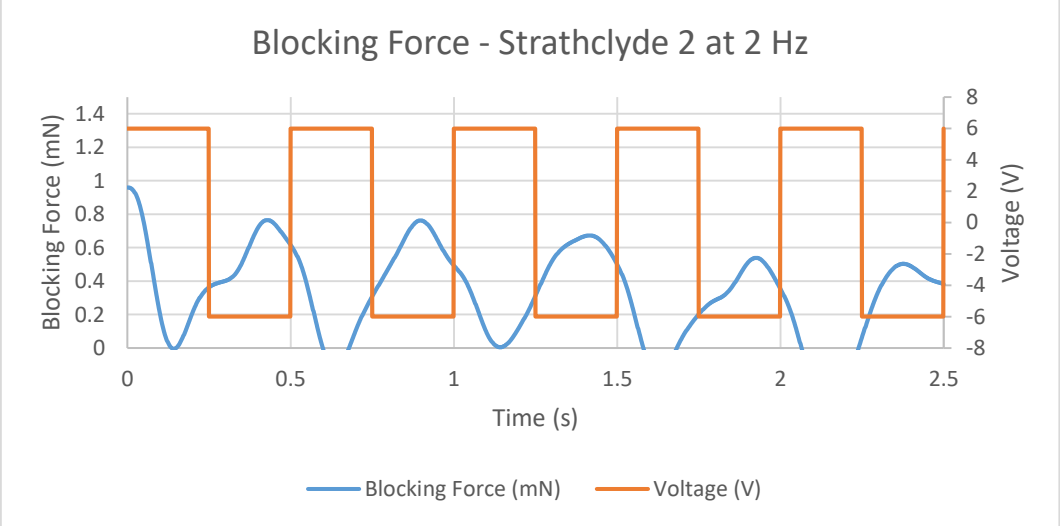

Figure 4.83 Blocking Force of Strathclyde 2 Sample at 2 Hz

Figure 4.84, **Figure 4.85**, **Figure 4.86**, and **Figure 4.87** show the maximum blocking force of all IPMC samples in mN at 0.05 Hz, 0.5 Hz, 1 Hz, and 2 Hz respectively. Commercial 6 produced 74 mN at 0.05 Hz, 32 mN at 0.5 Hz, 25 mN at 1 Hz, and 11 mN at 2 Hz.

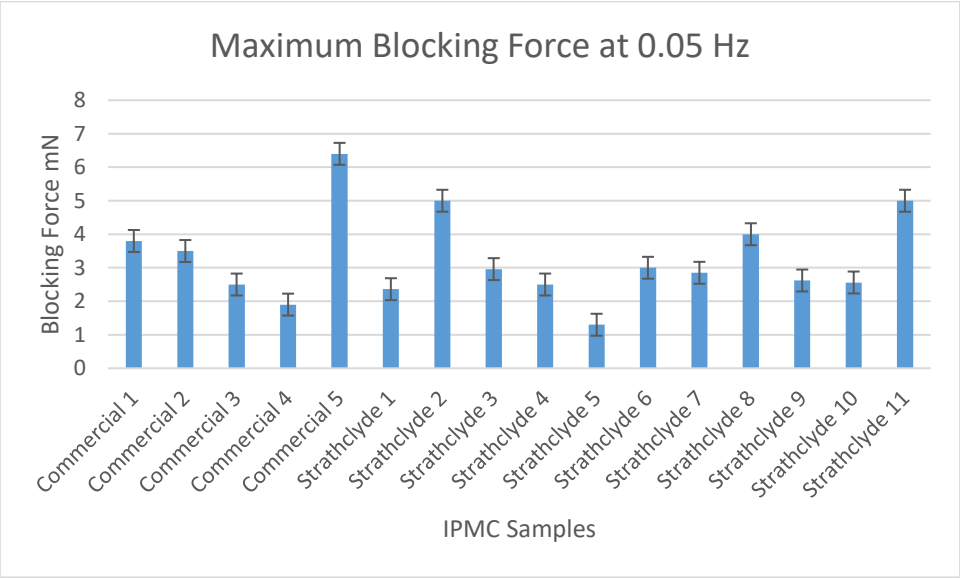

Figure 4.84 Maximum blocking force at 0.05 Hz

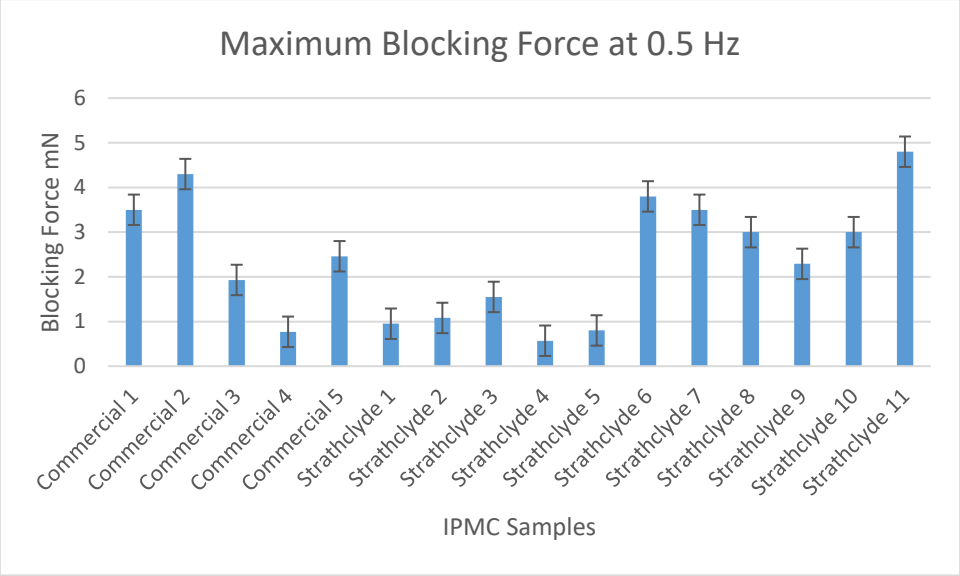

Figure 4.85 Maximum blocking force at 0.5 Hz

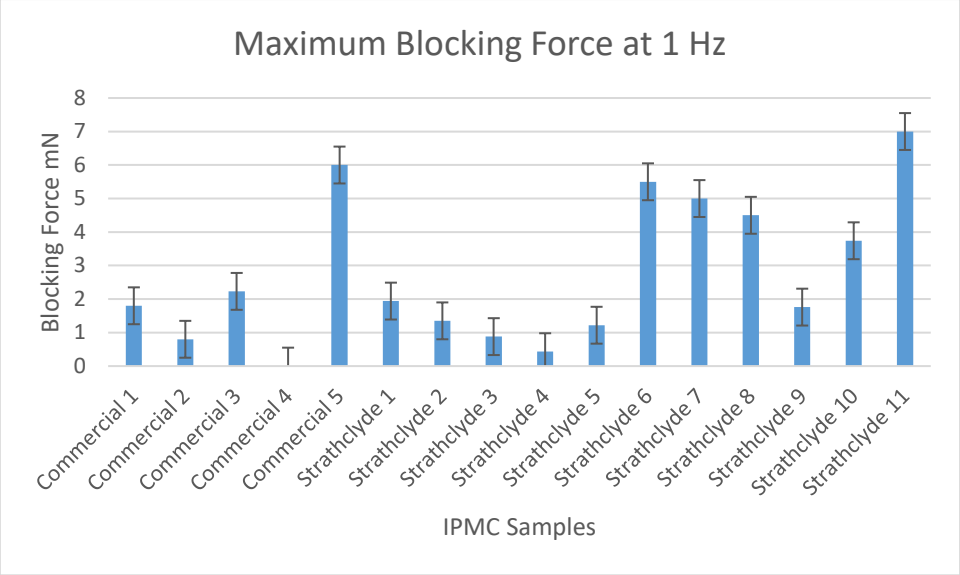

Figure 4.86 Maximum blocking force at 1 Hz

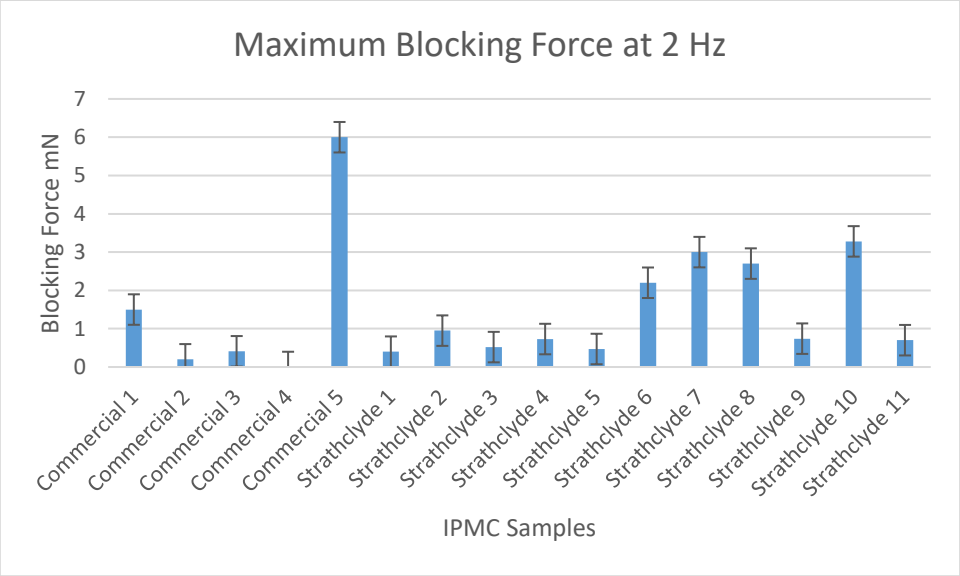

Figure 4.87 Maximum blocking force at 2 Hz

Figure 4.88, **Figure 4.89**, **Figure 4.90**, and **Figure 4.91** show the maximum blocking force per weight of all IPMC samples in mN/mg at 0.05 Hz, 0.5 Hz, 1 Hz, and 2 Hz respectively.

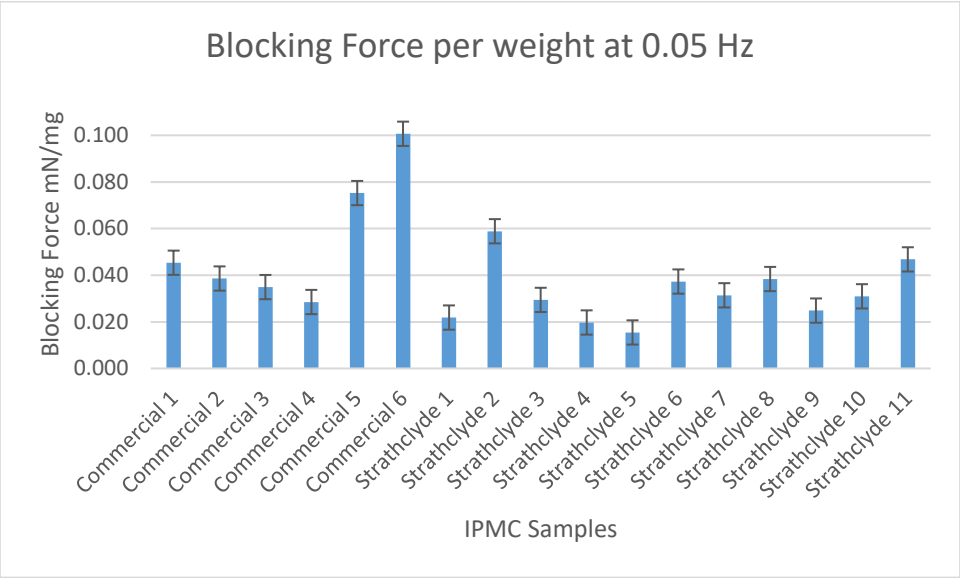

Figure 4.88 Maximum blocking force per weight at 0.05 Hz

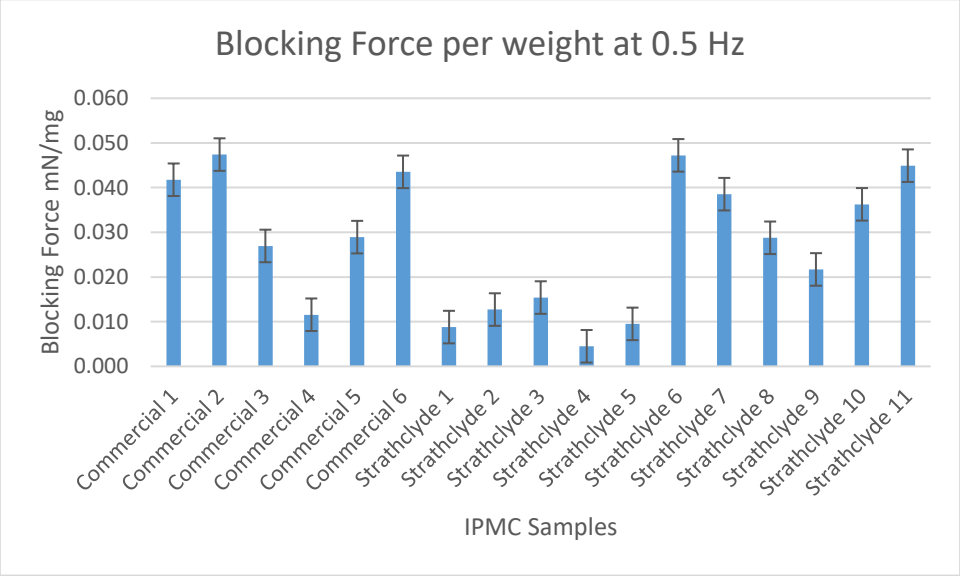

Figure 4.89 Maximum blocking force per weight at 0.5 Hz

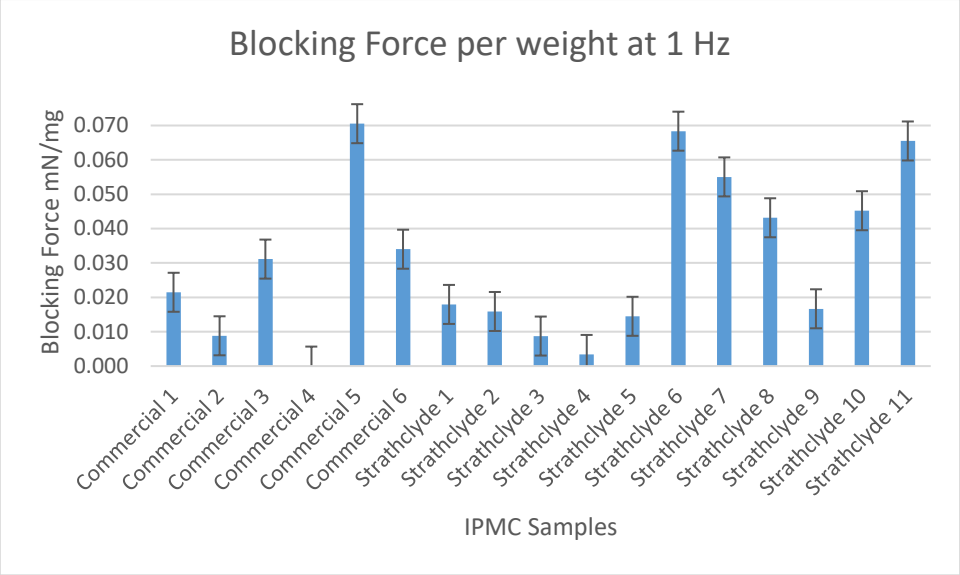

Figure 4.90 Maximum blocking force per weight at 1 Hz

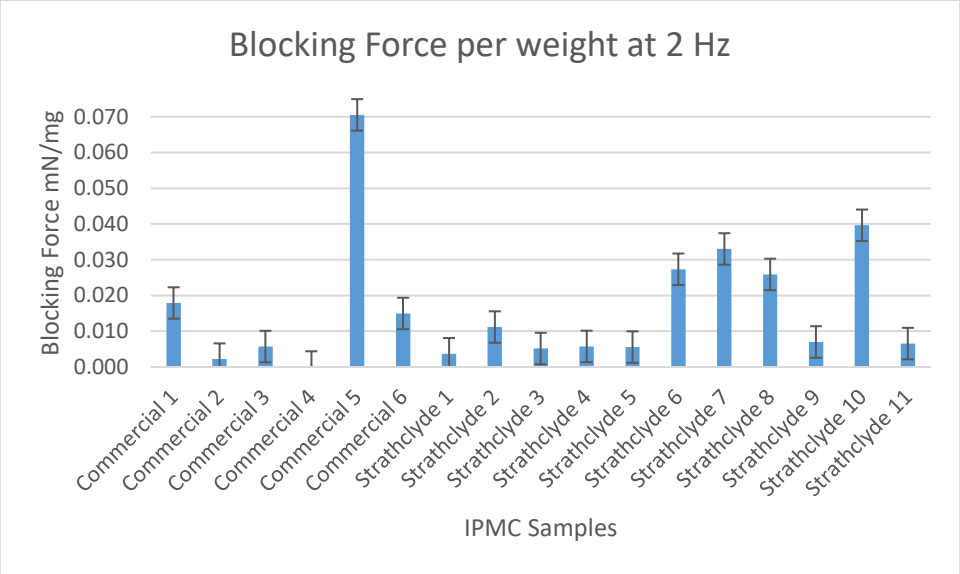

Figure 4.91 Maximum blocking force per weight at 2 Hz

Figure 4.92, **Figure 4.93**, **Figure 4.94**, and **Figure 4.95** show the maximum blocking force per surface area of all IPMC samples in mN/mm^2 at 0.05 Hz, 0.5 Hz, 1 Hz, and 2 Hz respectively. Commercial 6 showed 43.52 mN/cm^2 at 0.05 Hz, 18.82 mN/cm^2 at 0.5 Hz, 14.7 mN/cm^2 at 1 Hz, and 6.74 mN/cm^2 at 2 Hz.

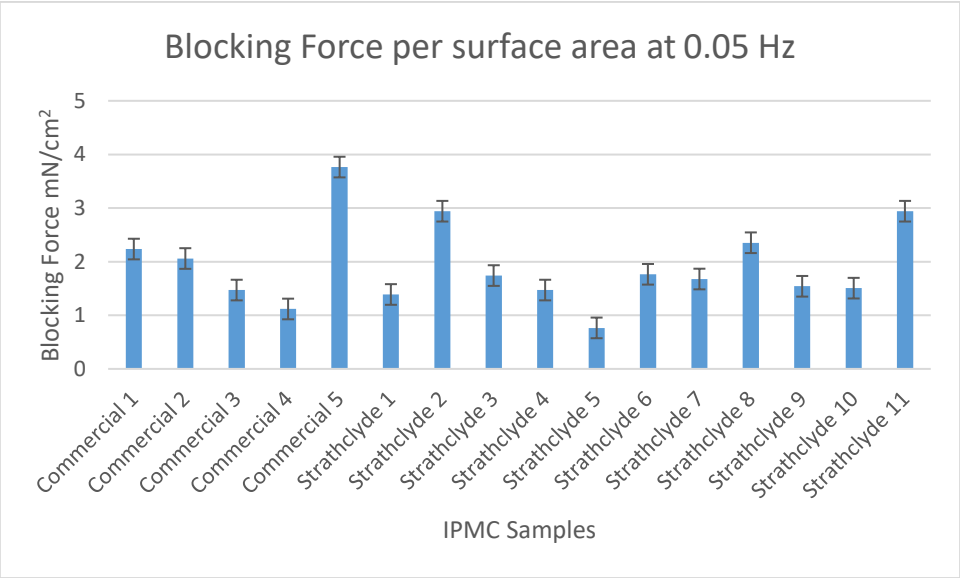

Figure 4.92 Maximum blocking force per surface area at 0.05 Hz

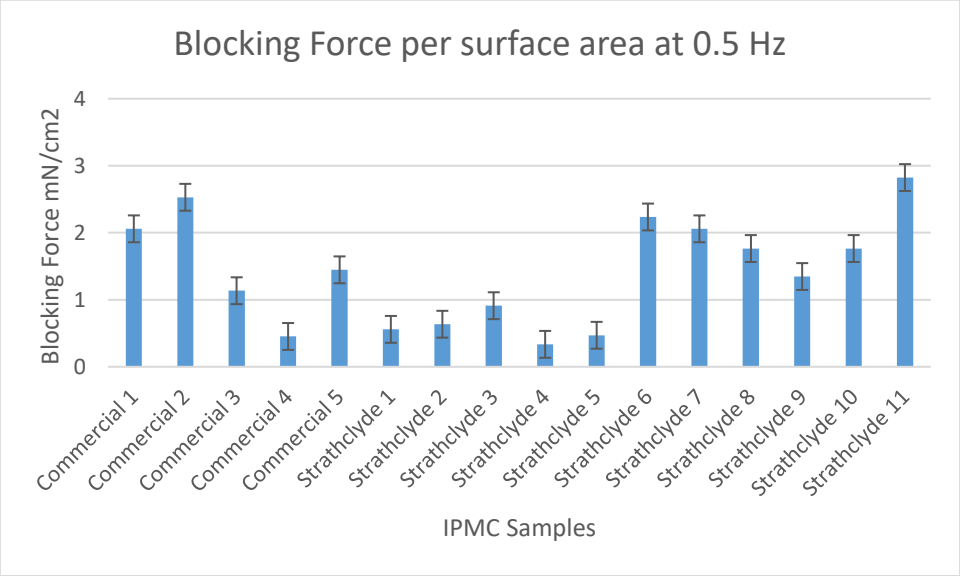

Figure 4.93 Maximum blocking force per surface area at 0.5 Hz

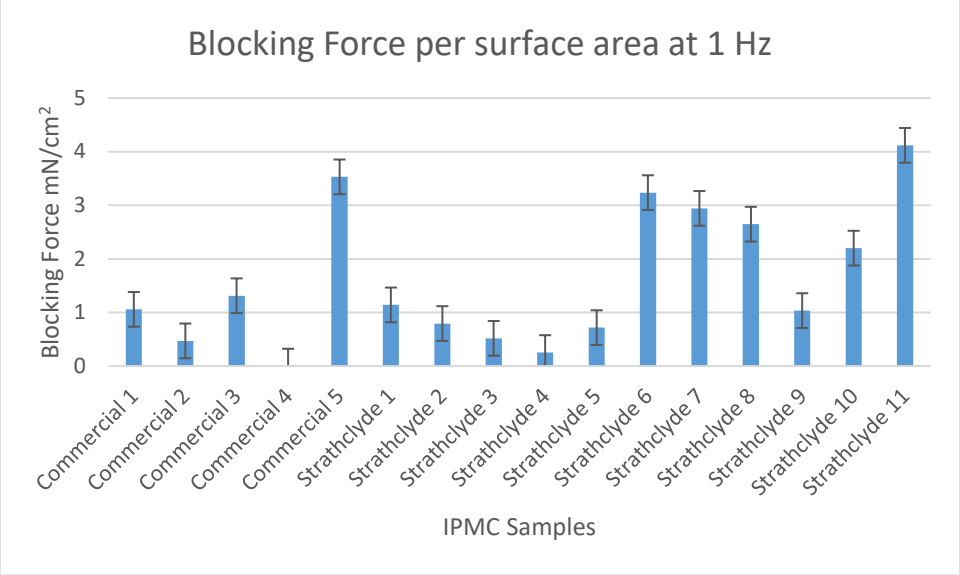

Figure 4.94 Maximum blocking force per surface area at 1 Hz

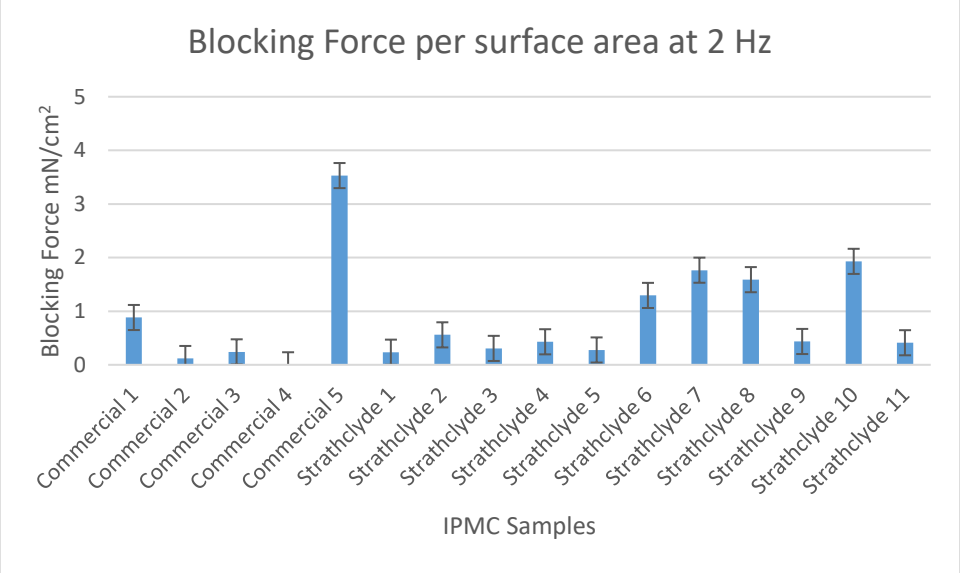

Figure 4.95 Maximum blocking force per surface area at 2 Hz

2.3 Summary

Table 3.1, the required force for the proposed device was between 13.6 N and 47N. The maximum blocking force recorded out of all IPMC was 74 mN from Commercial 6 at 0.05 Hz. This means to generate the required force it needs 183 actuators of Commercial 6 to generate 13.6 N, and 635 actuators to generate 47 N. In the Strathclyde group, the maximum force recorded was from Strathclyde 11 at 1 Hz, measuring only 7 mN. This means, it needs 1943, and 6715 actuators, to generate 13.6 N, and 47 N respectively.

4.9 Summary

This chapter illustrated the characterisation of the Commercial and Strathclyde IPMC actuators. These findings will be discussed in more detail in chapter 6 to compare them with the requirements of the proposed device. The next chapter will demonstrate the possibility of using IPMC to power the proposed device.

Chapter 5
Power Harvesting and Sensing

5. *Power Harvesting and Sensing*

5.1 Introduction

Power harvesting is the ability of the device to efficiently collect energy from the environment. Harvesting systems are defined as systems that can transform dusty environmental energy into electrical energy. These systems have aroused considerable interest in the last two decades. Researchers focused on transforming mechanical environmental vibration into electrical energy (Brufau-Penella, Puig-Vidal et al. 2007). Electroactive Polymer (EAP) is a material that exhibits a measurable response to a given stimuli, most commonly a change in shape or voltage potential (Biddiss and Chau 2006). When the IPMC sheet mechanically deforms (bending, stretching, or mechanically pressing), the electrode surface deforms, and the IPMC produces a voltage in the range of millivolts, as shown in **Figure 5.1**.

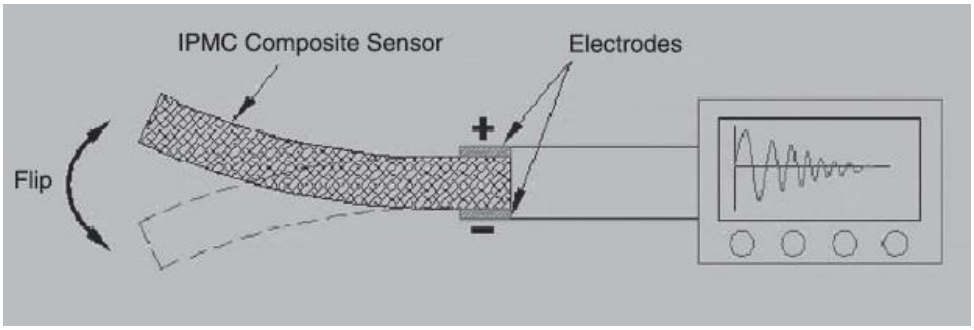

Figure 5.1 IPMC as a sensor (Shahinpoor 2009)

Currently, there are a few reasons for this generated voltage; one is based on the movement of the electrical charges, and the other is based on the electrical properties of the electrode. The first; It is believed that this voltage potential is generated by a shift of mobile charges caused by material stresses induced by deformation, resulting in charge imbalance (Biddiss and Chau 2006). The second; it is believed the deformations in the electrode surface cause proportional changes in the surface resistance. This is most probably caused by the nature of the cracked surfaces of metal electrodes to extend cracks when being extended, comparing to normal state (Hunt, Punning et al. 2008). **Figure 5.2** shows the typical electrical response of IPMC under an oscillating excitation.

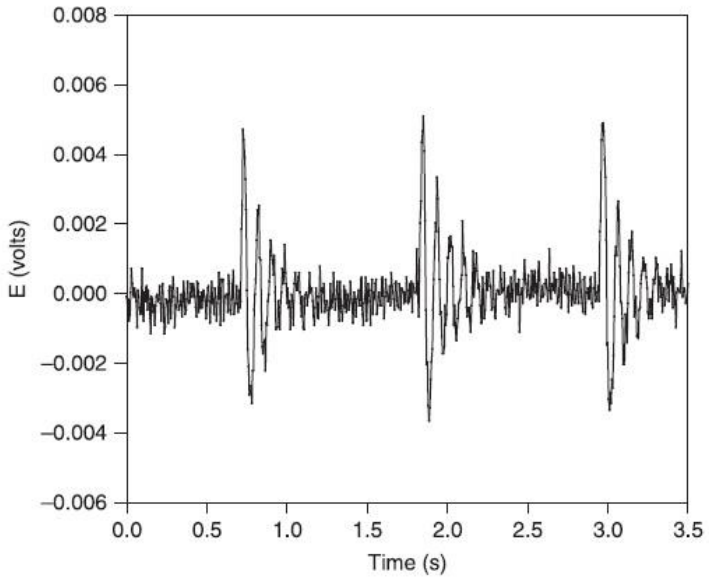

Figure 5.2 Typical voltage response of an IPMC strip (10x40x0.2 mm) under oscillating mechanical excitation (Shahinpoor 2009)

(Kim and Shahinpoor 2003, Shahinpoor 2009) Designed Material Testing System (MTS) that was used to apply a consistent pure compressive loads of 200 N and 350 N across the surface of an IPMC sheet (2x2 cm). The output pressure response for the 200 N load was 80 mV in amplitude, and for the 350 N it was 108 mV. This type of power generation may be useful in heels of boots and shoes or places where there is a lot of foot or car traffic.

During bending, IPMCs exhibit as both capacitors and resistors. They are represented as distributed RC line model (Punning, Johanson et al. 2009, Moeinkhah, Akbarzadeh et al. 2014). The cumulated charge depends on the testing conditions, such as temperature and humidity (Kruusamäe, Punning et al. 2015). This advantage is very useful in many application, such as measuring changes in angles, position sensing, and vibration detection (Punning, Kruusmaa et al. 2007). For example, IPMC size 12x6.2 cm generated a 3 nW at an oscillation frequency of 7.09 $rads^{-1}$ (1.12 Hz) (Brufau-Penella, Puig-Vidal et al. 2007). **Figure 5.3** shows the electrical response of IPMC under different testing conditions.

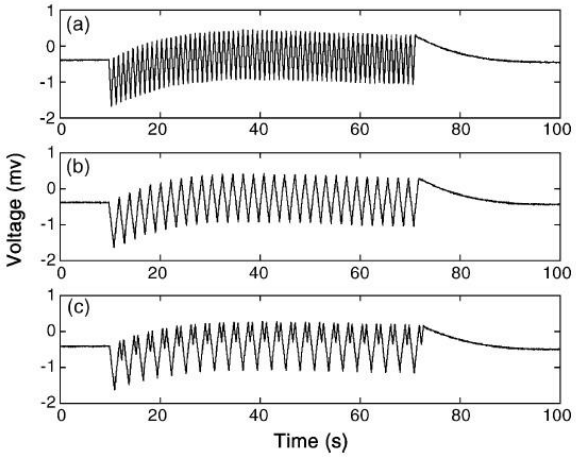

Figure 5.3 IPMC response to (a) 1 Hz, 90° bending stimuli; (b) 0.5 Hz, 90° bending stimuli and (c) an alternating 90° and 30° stimuli (Biddiss and Chau 2006)

A Self-sensing piezoelectric actuator was also reported, where an electric charge is used to estimate the position and the velocity (Kruusamäe, Punning et al. 2015), a Nafion based accelerometer was also reported (Shahinpoor and Kim 2004), and an Ionic actuator used as a humidity sensor was demonstrated (Tailoka, Fray et al. 2003, Must, Johanson et al. 2013). IPMC are multifunctional materials, can be used as actuators and sensors in the same time, where they required working in some environments without a power supply, such as wireless sensors. The transduction capabilities of IPMC can be reversible so that they can sense external stimuli and react to them (De Luca, Digiamberardino et al. 2013).

(Kruusamäe, Brunetto et al. 2010) Created self-sensing IPMC actuators by patterning its surface and creating separate actuator and sensor. This new IPMC could be used as an actuator with sensor providing a feedback for a better control. **Figure 5.4** shows the self-sensing IPMC.

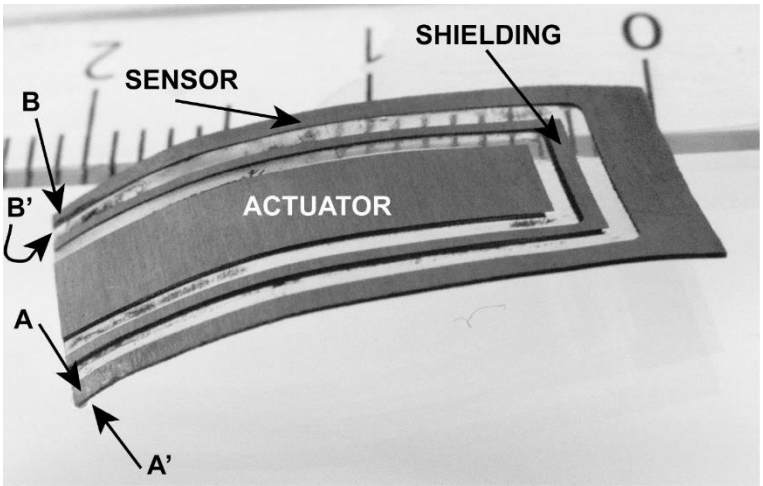

Figure 5.4 Self-sensing IPMC actuator (Kruusamäe, Brunetto et al. 2010)

5.2 Experiment Setup

This test was divided into two experiments; the first one was to measure the voltage generated under an oscillating excitation, and the other one was to measure the generated electrical current under the same excitation.

To measure the generated voltage, the IPMC samples were placed in a cantilever configuration, where the sample was fixed at one end using the alligator clip, while the other end was left free to move. Both ends of the alligator clip were connected to NI 6225 DAQ module, which was used as an Analogue to Digital Converter (ADC), and then linked to Lab View 2015. The software was used to display, record, and save generated voltage. Later, the data were used to calculate the RMS voltage, which is the DC equivalent of the generated AC voltage. **Figure 5.5**, and **Figure 5.6** show the front panel and the block diagram of the Lab View respectively.

Figure 5.5 Front Panel of Lab View

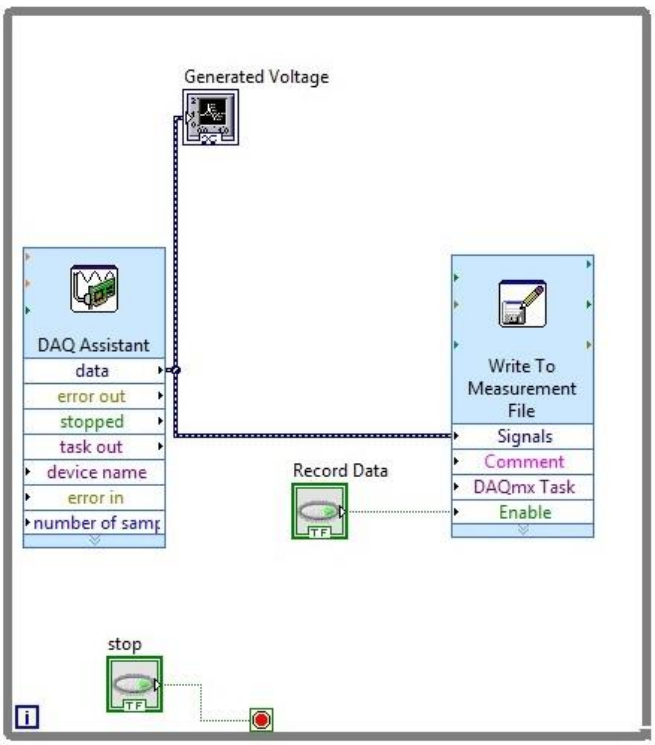

Figure 5.6 Block Diagram of Lab View

The excitation mechanism used a DC motor with a polypropylene arm to swing the IPMC sample. The motor was driven at low-frequency F=0.33 Hz, which is the same as the normal breathing frequency. **Figure 5.7** shows the DC motor with the polypropylene arm.

Figure 5.7 DC Motor with a polypropylene arm

Equation (5.1) was used to calculate the RMS voltage

$$V_{RMS} = \frac{V_{max}}{\sqrt{2}} \qquad (5.1)$$

Figure 5.8 shows the full experiment setup to measure the generated voltage by an oscillating excitation.

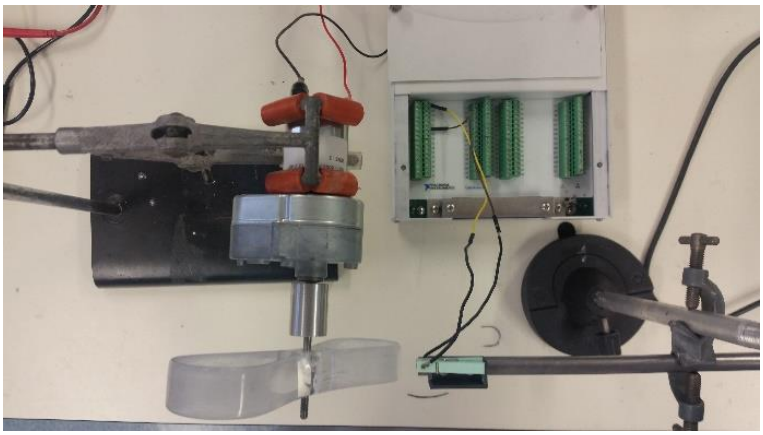

Figure 5.8 Generated voltage test setup

To measure the electrical current, a similar setup was used. Both ends of alligator clip were connected through an 8 Ω resistor, and a multimeter was used to record the flowing current. The same excitation mechanism was used to measure the electric current. **Figure 5.9** shows the full experiment setup to measure the electrical current by an oscillating excitation.

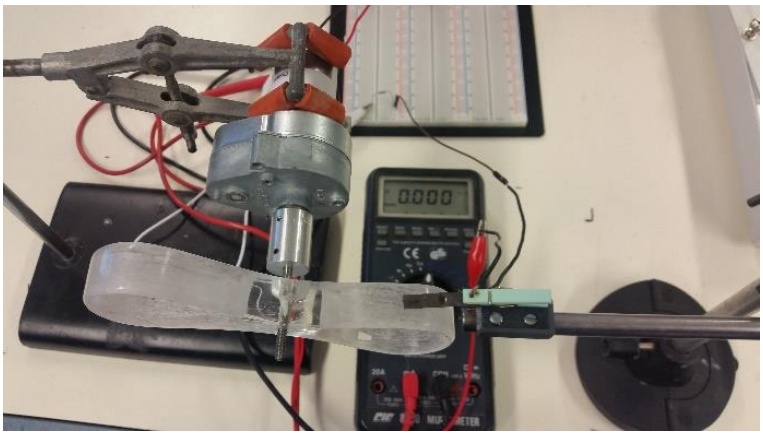

Figure 5.9 Current test setup

Finally, equation (9) was used to calculate the maximum power generated from each sample, generated power density per weight, and per surface area.

5.3 Result

Figure 5.10 shows a comparison of the voltages generated from all IPMC samples.

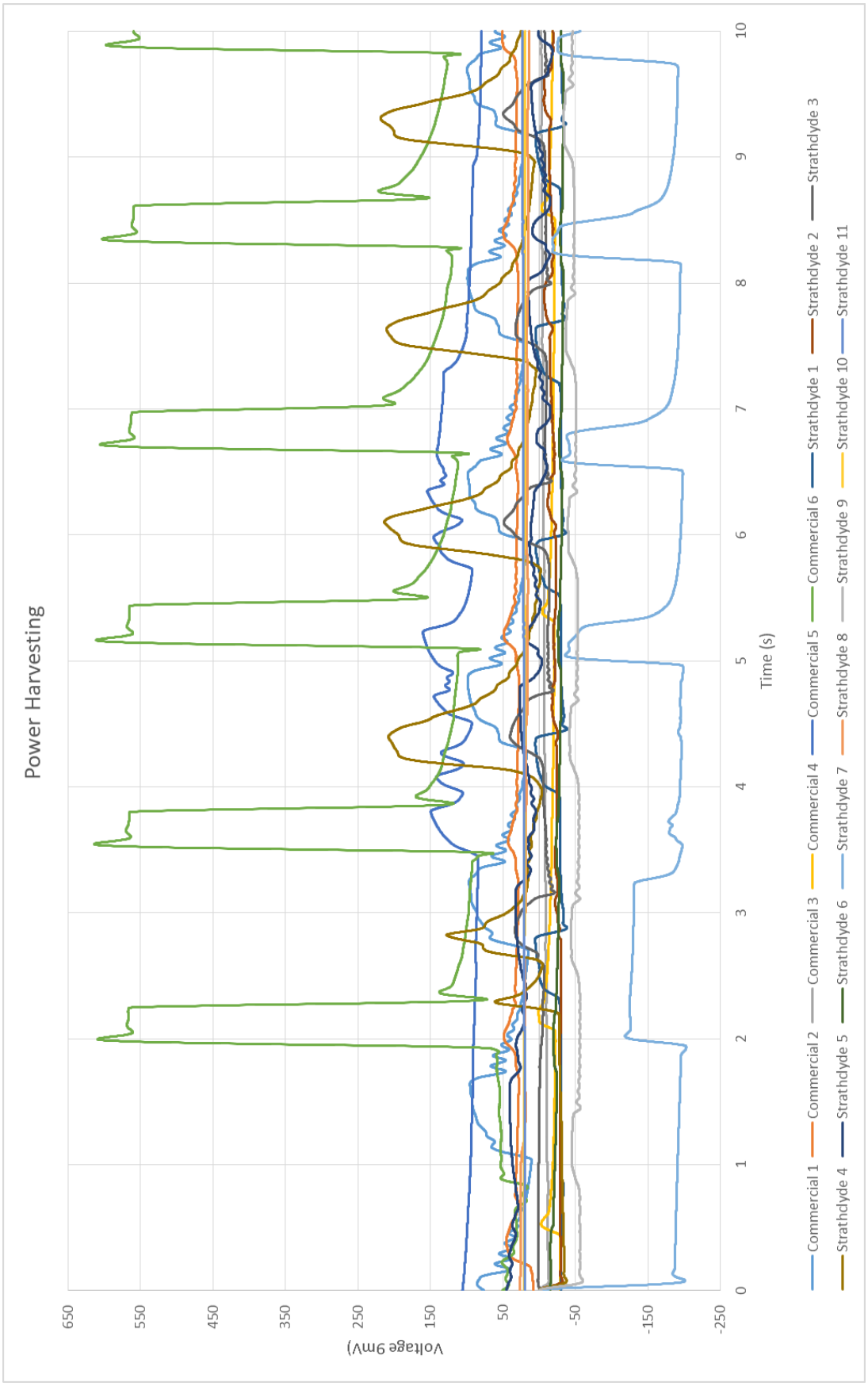

Figure 5.10 IPMC Power Harvesting

Table 5.1 shows the values of the generated voltage for all samples.

	Current (μA)	V_{p-p} (mV)	V_{rms} (mV)	Power (mW)	Power/ Weight (μW/mg)	Power/ Surface area (μW/cm^2)
Commercial 1	2	80	56.56	0.113	1.35	66.54
Commercial 2	5	20	14.14	0.070	0.78	41.59
Commercial 3	12	2	1.41	0.16	0.24	9.98
Commercial 4	14	25	17.68	0.247	3.71	145.56
Commercial 5	56	80	56.56	3.167	37.23	1863.15
Commercial 6	100	500	353.5	35.35	48.09	20794.12
Strathclyde 1	15	40	28.28	0.424	3.92	249.53
Strathclyde 2	65	60	42.42	2.757	32.45	1621.94
Strathclyde 3	65	70	49.49	3.216	31.96	1892.26
Strathclyde 4	74	200	141.40	10.46	82.52	6155.06
Strathclyde 5	72	30	21.21	1.527	18.14	898.31
Strathclyde 6	32	5	3.54	0.113	1.41	66.54
Strathclyde 7	20	180	127.26	2.545	28.02	1497.18
Strathclyde 8	4	3	2.12	0.008	0.08	4.99
Strathclyde 9	52	15	10.61	0.551	5.22	324.39
Strathclyde 10	21	2	1.41	0.029	0.36	17.47
Strathclyde 11	15	2	1.41	0.021	0.2	12.48

Table 5.1 Voltage, Current, and Power generated from IPMC

Figure 5.11 shows the maximum current generated by all IPMC.

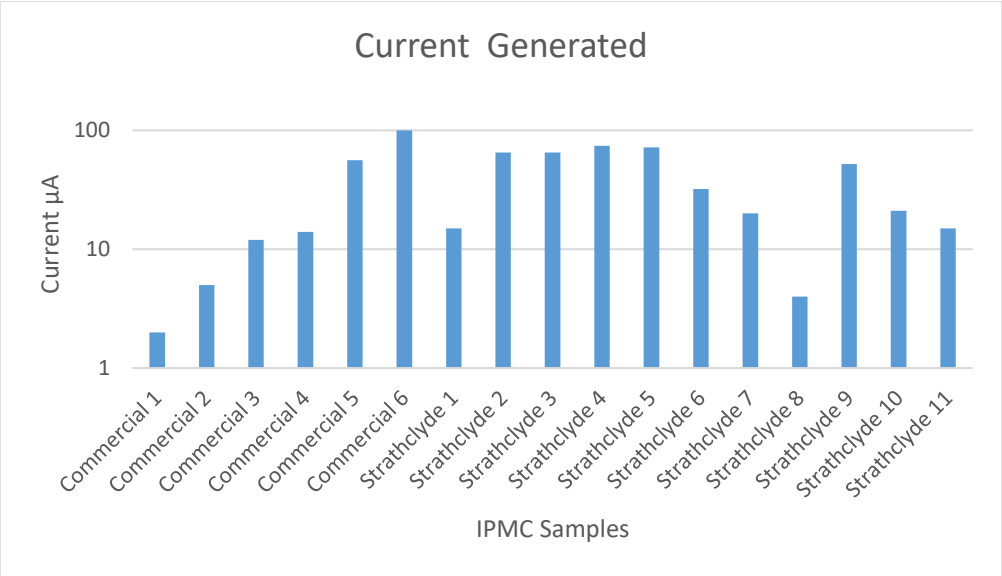

Figure 5.11 Current generated from IPMCs

Figure 5.12 shows the V_{p-p} generated by all IPMC.

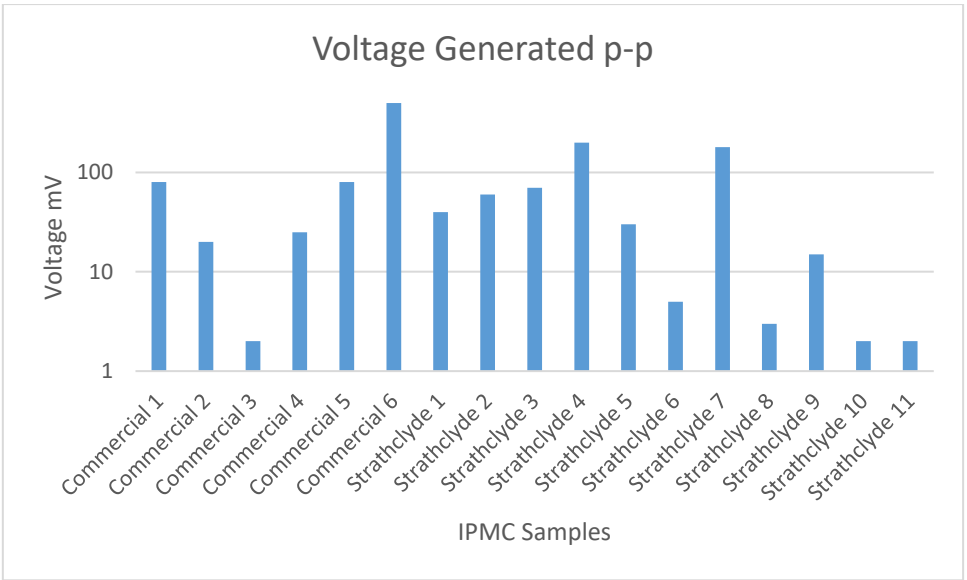

Figure 5.12 Peak to peak voltage generated from all IPMCs

Figure 5.13 shows the V_{RMS} generated by all IPMC.

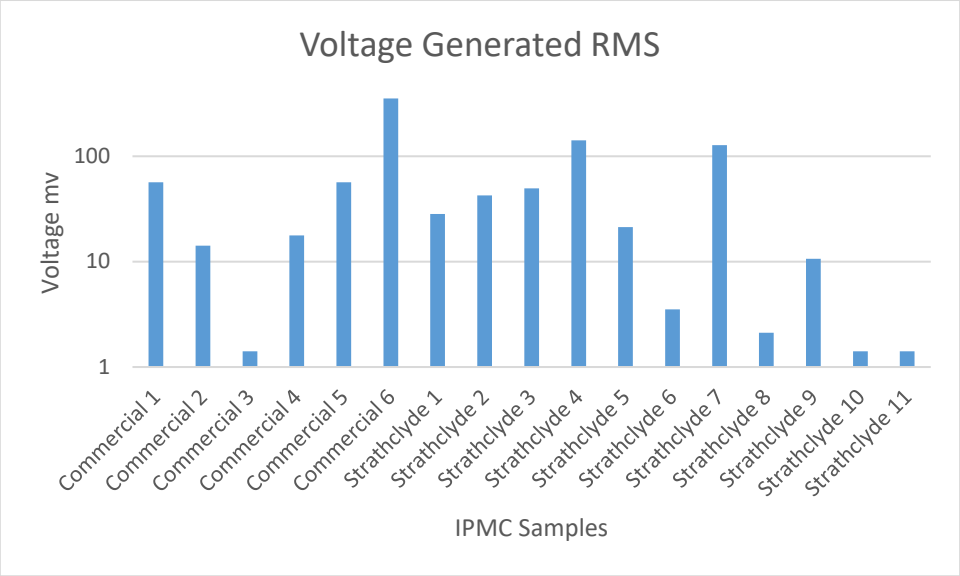

Figure 5.13 RMS voltage generated from all IPMCs

Figure 5.14 shows the maximum power generated by all IPMC.

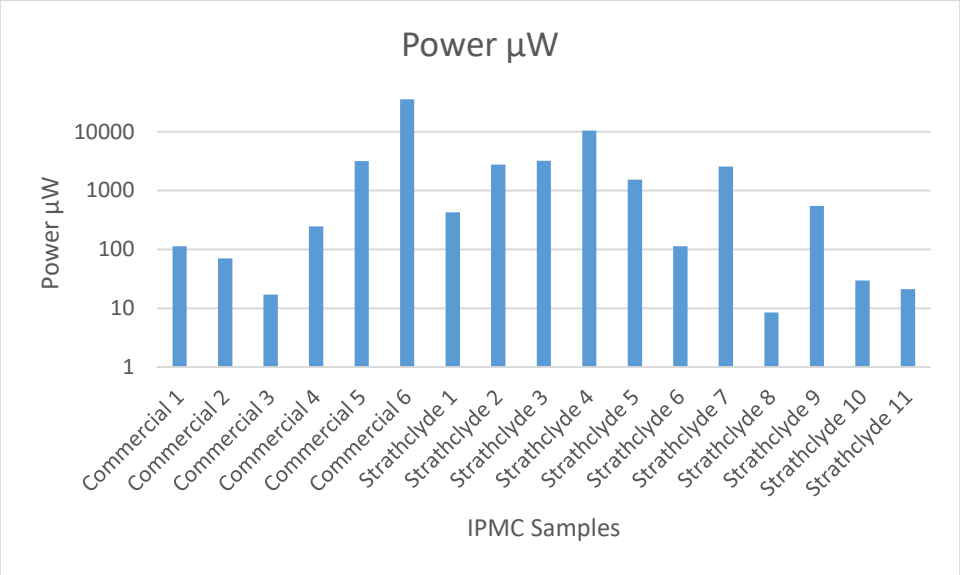

Figure 5.14 Maximum power generated from all IPMCs

Figure 5.15 shows the maximum power generated per weight by all IPMC.

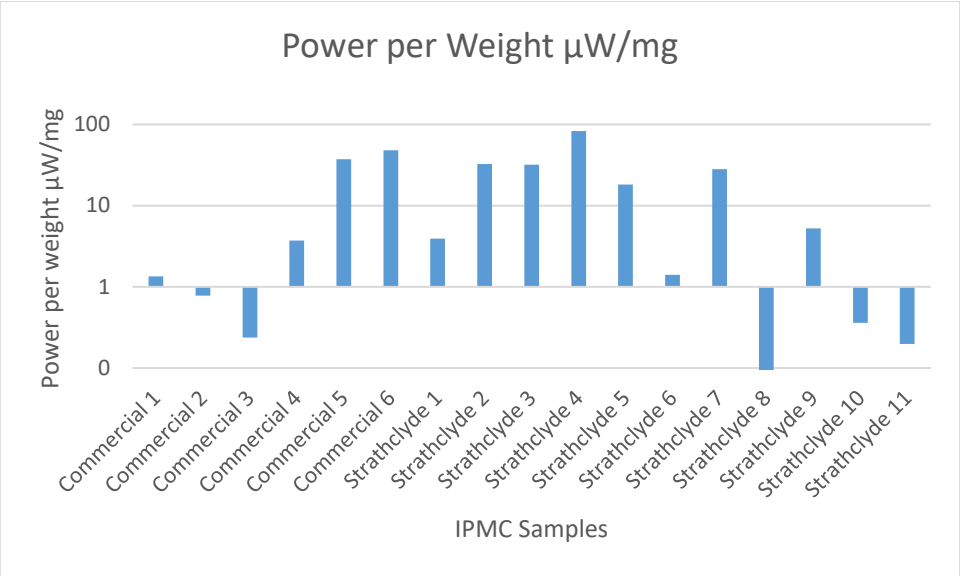

Figure 5.15 Maximum power generated per weight from all IPMCs

Figure 5.16 shows the maximum power generated per surface area by all IPMC.

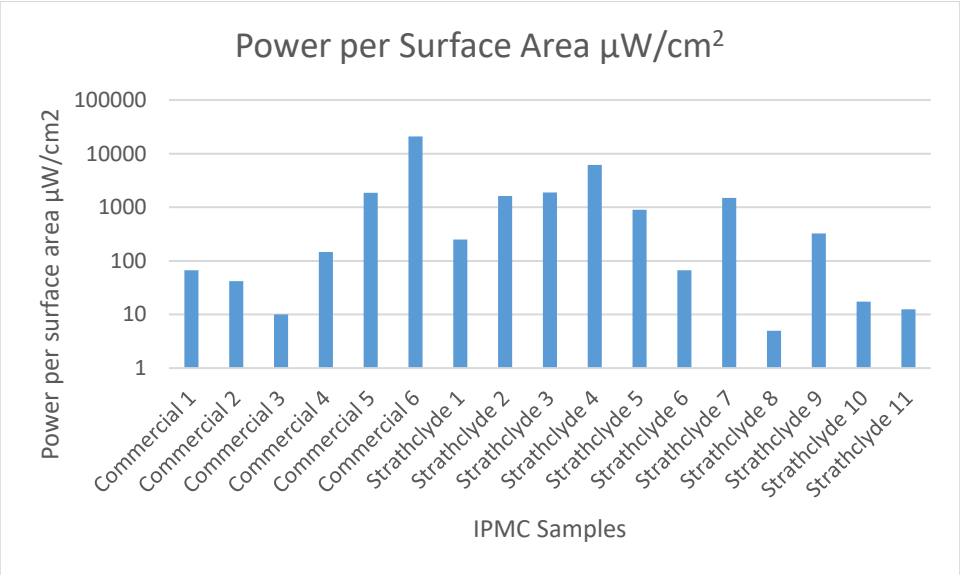

Figure 5.16 Maximum power generated per surface area from all IPMCs

5.4 Summary

This test presented the electrical power that could be generated by the IPMC if they were placed on the diaphragm as proposed earlier. The results showed that IPMC consumed power far more that it could generate, for example, sample 2 generated 65 µA, 42.42 mV while consumed 100 mA, 6V.

Chapter 6
Discussion

6. *Discussion*

6.1 Introduction

Heart failure is one of the leading causes of death worldwide; several solutions have been developed to provide support for the failing heart over the last few years. These solutions are largely suitable for adult patients, leaving paediatrics with a few options other than using heavy and bulky devices connected to their tiny bodies. In the recent years, many researchers tried to develop a VAD technology for paediatric patients, which are both miniaturised and biocompatible. Ideally, such devices should permit mobility in the paediatric patient and provide a suitable cardiac support appropriate to their age.

In this thesis, a novel method was presented to develop a new type of VAD for paediatrics. The proposed device benefits from advanced technologies in the field of Artificial Muscles developed to deliver VAD solutions for paediatrics. The solution proposed in the thesis suggested creating a thin layer of Artificial Muscles that envelop the failing heart and work as a contraction mechanism to support the circulation. The main advantage of this new approach is that it will not be in contact with the patient's blood, which will eliminate the risk of blood infection, haemolysis, and blood clotting.

6.2 Device Requirements

The development of the proposed device started with defining the mechanical demands of the new VAD. The first was to estimate the compression force needed to contract the heart. A simple analogy was used to calculate the required compression force. The left ventricle was assumed to have a conical shape, the applied force is uniform on the surface of the heart, and the pressure inside the heart is a known parameter. Then, the compression force applied to the wall of the heart can be easily estimated. The results suggested that a compression force of 1.36 N for paediatrics and 47 N for adults.

The second requirement was determining the distance the device needed to travel to match the changes in the ventricle diameter. This was measured as a percentage of the difference between the end systolic, and the end diastolic diameter of the left ventricle. It was found that the proposed device should be able to shrink its diameter by 20% to 50% from its original form.

The last factor to be determined was the working frequency of the proposed device. This was simply estimated from the average heart rate, which was found to be between 60 BPM to 130 BPM. As a result, the proposed device effective range should be between 1 and 2 Hz.

6.3 Primary Investigation Phase

The first phase of the project started by reviewing all IPMC Artificial Muscles available commercially, and choosing the most suitable one for the application. As Artificial Muscles are still under development, only a few suppliers are available to supply IPMC. An IPMC beginner kit was purchased for evaluation, containing four platinum coated IPMCs and an IPMC driver. Towards the end of the project, two more samples were bought from the same supplier; the first was platinum plated, and the second was gold.

In the initial bench test, the IPMC showed a clear mechanical response when electrically stimulated. The IPMC driver supplied a square wave with a variable frequency and amplitude. Different response times were achieved between dry and wet conditions. In the dry conditions, the samples were able to actuate for less than a minute before totally drying out and freezing, while in the wet conditions, the samples were able to move for a couple of minutes before again drying out. It was evident there was a link between the actuation time and the hydration level of the samples. Increasing the voltage also resulted in a shorter lifespan before drying out. Higher voltages more than 7 V caused the material to overheat and left some marks around the retaining interface. IPMC showed a better response at low frequencies. By increasing the frequency, the response of the materials dropped very rapidly in both wet and dry conditions.

After this investigation, it was found that IPMCs have the potential to be used in the proposed device. To quantify their mechanical and electrical properties, more samples were needed in different thicknesses, shapes, and coating metals. Therefore, the project would move to the next phase, which was manufacturing IPMC at the University of Strathclyde for characterisation and evaluation.

6.4 Fabrication of IPMC

The second phase of the project started by adapting the non-electric protocol to fabricate the IPMC Artificial Muscles. Previous researchers (Chen, Um et al. 2011, De Luca, Digiamberardino et al. 2013) have described the process extensively, with various approaches adopted,

designed for specific applications. The process of making IPMC has different steps, and the final result depends on the accuracy of following these measures. The early attempts to make IPMC were not successful, as the membrane lacked mechanical integrity, or were not structurally complete. To achieve the best results, the temperature was increased very slowly to prevent the membrane from curling and breaking. Stirring the solution was also another challenge; a rotator blade was used to stir the solution during the different stages of fabrication. If the blades were close to the membrane, they would cause some damage to the surface and leave some scraping marks which would result in a rejected IPMC. The criticality of these process steps illustrates the sensitivity of the complex fabrication process and the impact of process control on the final device function.

As the project progressed, the fabrication of IPMC was also developing. Different changes were made to the original fabrication protocol, such as repeating some steps, modifying the temperature increments, or using different metal solution. This led to the production of different samples from various protocols. Eight different protocols were used to produce 11 IPMC samples. The complexity of the manufacturing process was a key element of the device development and reflects the relative immaturity of this aspect of the material science.

At the end of this phase of the project, two groups of IPMC were ready for material tests and characterization; the first was the commercially purchased IPMC. The second group was the IPMC fabricated at the University of Strathclyde.

6.5 IPMC Driver

The actuation of IPMC depends on the electrical driving signal's parameters, such as shape, frequency, amplitude, and current. The beginner kit came with a simple driver powered by a 9V battery. This option was not able to provide sufficient current and was not able to control the signal parameters accurately. Therefore, a new IPMC driver was developed to offer the ability to adjust the shape of the signal, the frequency, and the amplitude, besides providing sufficient current to drive the IPMC actuators.

The first iteration of the driver developed used a voltage-controlled oscillator IC (XR-2209) to generate a square and triangle wave, and IC OPA548T was used as a current amplifier. The amplitude and frequency were controlled by potentiometers. This option was similar to the

driver in the beginner kit but could provide a higher current. This design suffered from low accuracy and the lack of monitoring the parameters of the generated signal.

The second iteration relied on a signal generator to generate and control the signal parameters. The output was connected to a current amplifier. This system was more accurate and was able to show the elements of the generated signal for monitoring purposes. The main disadvantage of this system was the lack of ability to record the generated signal for further comparison.

The final iteration was based on three main components; LabView software, NI USB 6225 DAQ system, and a current amplifier. This option was by far the most appropriate; LabView was used to generate, control, monitor, and record the driving signal. The DAQ system was used as a connection between LabView and the current amplifier.

From the literature (Yu, Shen et al. 2007), it was found that a square wave was the best option to get the maximum response from IPMC actuators. Therefore, other waves were eliminated, and the driver used only square wave for mechanical and electrical characterisation.

6.6 Quality of IPMC Fabrication

There are several factors that may be used to determine the quality of the fabricated IPMC. These factors include:

- Surface
- Thickness
- Water Uptake
- Surface Resistance

At this stage of the project, IPMC samples from both groups, the Commercial and Strathclyde, were tested to check the quality of the IPMC fabrication process.

2.1 Surface Tests

The surface test is one of the most common and easy methods used to assess the quality of the IPMC. Two main approaches were used in this test; the first was to scan the top surface of the electrode to give an idea of the consistency of the metal deposition on the polymeric membrane. The second test was to examine the cross section of the membrane to have an idea of the depth of the metal particles penetration inside the membrane. Both aspects have a significant effect on the behaviour of the IPMC actuator.

Two issues were considered in the top surface test; the first was a uniform and smooth layer of metal particles spread on the membrane surface. The second was a surface with no cracks or isolated sections. These two most important aspects have a huge effect on the surface resistance and give a clear indication of the quality of the fabrication process.

The results of the Commercial 5 IPMC showed the top surface has a smooth, consistent layer of platinum deposited equally across the surface of the membrane. Also, there are no signs of any cracks, islands, or grooves on the electrode surface. Compared with the Strathclyde 11 IPMCs, the surface looked very rough with multiples grooves appearing under the SEM images. Strathclyde 5 IPMC after some modifications to the fabrication protocol, the surface looked smoother and more consistent but has many cracks that form isolated sections or islands. This has a huge effect on the surface resistance and the performance of the actuator. Strathclyde 3 IPMC, one of the most recently manufactured IPMC, has a clear, smooth surface, and the islands have almost disappeared. These images showed a clear indication of the improvements of the fabrication process, which suggest that the fabricated IPMCs were made successfully through the evolution of our process.

The cross section test focused on the penetration of the metallic particles inside the polymer. This penetration is critical to enhancing the performance of IMPC actuators, which can be achieved by repeating the plating process several times. Both groups, Commercial and Strathclyde, showed a clear layer of metal deposited on both sides of the membrane with different thicknesses depending on the fabrication protocol. Once again, this demonstrated adequate fabrication emerging from our development cycle.

2.2 IPMC Thickness

The thickness test was used to measure the final thickness of the IPMC actuators and the depth of particles penetrations inside the membrane. Both of these measurements were signs of the quality of the fabrication process.

All Strathclyde samples have a total thickness between 180 µm and 195 µm, which is very close to the results of the Commercial samples. The electrode thickness results showed a range between 7 and 15 µm for the fabricated Strathclyde IPMC, which was less than the Commercial IPMC. This suggested that the Commercial samples might have been subjected to extra coating steps. On the other hand, the Strathclyde sample results match the results

found in the literature (Nguyen, Lee et al. 2007). The thickness of Pt particles deposited on the surface of the membrane is between 7 and 9 µm (see section 4.22.3), which again gave an indication of healthy fabricated Strathclyde IPMC samples. The difference in depth of the metallic particle penetration inside the membrane between Strathclyde samples and Commercial samples suggested that the Commercial samples might have a slightly different fabrication protocol that allowed the metal particles to penetrate deep in the membrane.

2.3 Water Uptake

Water molecules are the primary driving mechanism of actuation inside the IPMC membrane. That is why water uptake is a useful parameter to determine the ability of IPMC to actuate more efficiently. The test simply compared the different values of the wet and the dry IPMC, and the difference will represent the water uptake.

Both groups showed similar results. They all fall in the range between 14% and 24%, which was very close to the 16.7% value found in the literature (Inamuddin, Khan et al. 2015). This suggested that the fabricated Strathclyde samples were able to absorb water to the required limit.

2.4 Surface Resistance

Surface resistance is a significant parameter representing the quality of the electrode. Two methods were used to measure the surface resistance; Ω/□, and Ω/cm.

The results showed different values in resistance in the fabricated group; this could be as a result of the isolated sections and grooves on the electrode surface. Some samples showed larger values than the ones reported in the literature, (see section 4.5).

6.7 Electrical Power Consumption

Measuring power consumption is vital for the design of the proposed device. This will give an idea of the essential power source needed to run the proposed VAD. The measurement was simply based on recording the current consumption, the voltage applied and then calculating the electrical power consumed.

Most of the samples showed no difference in the current or power consumption under different frequencies, apart from Commercial 2, and Strathclyde 2, where they showed a decrease in the current and power consumption with increasing the frequency.

6.8 Displacement Test

This test was designed to measure the tip displacement of the IPMC samples under different frequencies. When IPMC is activated by a low-frequency signal, it will start to bend and then relax back to its neutral state. This phenomenon was reported by (Nguyen, Lee et al. 2007) and called Back Relaxation. This happened because of water leaking from the IPMC surface, and electrolysis, which results in a dry IPMC.

It is apparent from the figures that the tip displacement decreased by increasing the frequency. At DC the tip displacements for Strathclyde 1, and 2 were around 14 mm, and they dropped to less than 1 mm at 2 Hz. This happened because water molecules did not have enough time to move inside the membrane when switching the polarity between the electrodes. These results match the findings of the previous researchers (Chung, Fung et al. 2006, Liu, McDaid et al. 2011).

6.9 Mechanical Blocking Force

This test was the main core of the project to find out the mechanical power generated from the IPMCs. It was found that most IPMC produced a mechanical force in the range of mN, depending on the thickness and size of the actuator, as reported previously (Trabia, Hwang et al. 2016).

Commercial 6 produced the highest force at a low frequency, 70 mN at 0.05 Hz, and then the mechanical power decreased by increasing the frequencies to 11 mN at 2 Hz. It was also noticed that the mechanical response was fading after few cycles, this could be explained by water evaporation, and the samples were drying out. Another observation was the time difference between the driving signal activating the IPMC, and the IPMC producing the mechanical response. This happened at both high and low frequencies due to the time needed for the ions to move to the cathode side.

The mechanical outputs recorded from Strathclyde group were smaller than the Commercial samples in general. The shape of the recorded signal was not consistent due to the twisting tip of the Strathclyde samples. The delay between the application of the electrical signal and the start of the mechanical response was observed as well in all frequencies.

From the previous figures, it was found that the maximum response recorded was from Commercial 6 at 0.05 Hz, recording 74 mN. In the Strathclyde group, Strathclyde 11 produced

the highest value, recording 7 mN at 1 Hz. Comparing these findings with the required mechanical compression force (13.6 N for paediatric and 47 N for adults), it was found that it needs 183 samples of Commercial 6 (134.6 g, 0.031 m^2), or 1943 samples of Strathclyde 11 (206 g, 0.33 m^2) to match the 13.6 N required for a paediatric VAD. Also, it needs 635 samples of Commercial 6 (465.3 g, 0.108 m^2), or 6715 samples of Strathclyde 11 (712 g, 1.14 m^2) to match the 47 N required for an adult VAD. Power consumption was found to be far from practical as well; to power a VAD made from Commercial 6 IPMC it needs (91.5A, 549 W), and (317.8 A, 1906.8 W) for paediatric and adult respectively, while Strathclyde 11 needs (582.9 A, 3294 W), and (2014.5 A, 11440.8 W) for paediatric and adult respectively.

Although the project used the best commercial IPMC available, it is evident from the results that the IPMC actuators are still immature materials, mechanically weak, and consume a significant amount of electrical power to generate a tiny mechanical response. It needs to combine thousands of IPMC actuators to build the proposed device, which will result in a bulky, heavy and high power consumption VAD. This device will be far from practical and, does not fit the requirements of a paediatric VAD. IPMC as a science is still developing, and step changes in IPMC technology are required to enhance the material before being able to achieve such a task. What is needed is a material that is two orders of magnitude stronger and consumes electrical power one order lower of magnitude.

Therefore, it is clear that IPMC is not suitable yet to be used in creating a paediatric VAD. However, it was considered that there might be other applications for IPMC technologies resulting from this work. In particular, they might be used as electric power generators for other implantable devices.

6.10 Power Harvesting and Sensing

The second purpose of developing IPMC was to use them for power harvesting inside the patient's body. Interestingly, by reversing the concept explained previously, IPMC could be used to generate electrical power when mechanically deformed; this principle was investigated to find out if they have the ability to produce enough electrical power to charge a battery, or run an implantable device directly.

A heart powered by the heart, or a heart powered by diaphragm concept could be achieved by placing the IPMC on the heart, the diaphragm, or any other continuous moving organ, and

then collecting the generated electrical power and use it to run a low power consumption VAD or other implantable devices, such as pacemakers, or sensors. This concept could contribute towards partially powering an existing VAD, which will offer an extra level of independence for the VAD patients. This extra time, offered by the new concept, is not to be underestimated, as it could be lifesaving.

The proposed suggestion was to place the IPMC on top of the patient's diaphragm, where they will generate electricity while the patient is breathing. To illustrate this concept, IPMC samples were mechanically deformed at low frequency 0.33 Hz to match the breathing rate, the electrical voltage and current were recorded.

It is obvious there was a huge difference between the generated voltages from the various samples. Most of the samples produced a voltage between -50 mV to 150 mV with only a few samples below or above that range. Commercial 6 produced the highest voltage and current, recording 353.5 mV, and 100 μA respectively, which means it needs 500 mA/100 μA= 5000 samples of Commercial 6 to provide enough current to drive a VAD. While Strathclyde 4 produced the highest values from the fabricated Strathclyde group recording 141.40 mV, and 74 μA for the voltage and current respectively, which meant it needs at least 540 samples of Strathclyde 4 to drive a VAD.

It is evident that the electrical energy level produced from IPMC is still minimal and it needs to deform hundreds of IPMCs to generate enough power to run one IPMC. There is a potential for developing the material to improve its efficiency in energy harvesting. The focus should be on using IPMC to power an implantable device. Therefore, it is evident that IPMC is not suitable yet to be used in generating electrical power to run a paediatric VAD, but it has the potential to achieve this goal and could produce power for lower consumption devices, such as sensors.

6.11 Results in the Context of Objectives

In the context of the present study, a number of objectives were set at the outset of the work. These objectives are listed below, with a commentary on the degree to which these were met.

1- Review the IPMC actuators and decide which one is suitable for creating a VAD- 100%
2- Make IPMC materials in the lab – 100%
3- Test the mechanical properties of the IPMC – 100%
4- Test the electrical properties of IPMC – 100%
5- Test the ability of IPMC to generate electricity – 100%
6- Design and build a VAD made from IPMC – 0%
7- Test the performance of the VAD – 0%

Chapter 7
Conclusion

7. Conclusion

The aim of this project was to explore the development of a new self-powered miniaturised VAD for paediatric implantation. The current VADs for paediatrics offer a bulky and heavy solution that is associated with a high risk of infection, due to the cables connecting the VAD with the external controller. These options immobilise the patients in hospitals, which results in an expensive treatment cost.

To achieve the aim of the project, newly developed Artificial Muscles were utilised. Amongst the various categories of Artificial Muscles, IPMC was found to be the best candidate for this project. After a successful fabrication of 11 samples of IPMC, a series of characterisation tests of the mechanical and electrical properties of the fabricated samples were conducted for performance evaluation. The work concluded that the mechanical power generated from the IPMC samples was not sufficient to compress the failing heart. Besides that, these samples demanded a large electrical current to operate, which made them unsuitable for such an implantable device. On the other hand, using IPMC for power harvesting was investigated. IPMCs showed promising results as an option to generate electricity that might power low demand implants, such as sensors.

Chapter 8
Limitations

8. *Limitation*

There were some limitations, which have impacts on the scope and the quality of the presented work including:

1- Slow production of IPMC: IPMC fabrication is a very long and time-consuming chemical coating process; it needs more than a week to produce one sample. It includes various precise steps; any small mistake will result in a rejected sample.

2- Control of IPMC bending motion: the bending motion was not uniform; membranes were twisting at different angles. These twisting motions were limiting the ability to measure the blocking force.

3- Bending Feedback: the system lacks a feedback to measure the IPMC movement when electrically stimulated.

4- Low mechanical power output: Most of the samples produced mechanical responses in the range of mN, which is very difficult to detect, and requires a very accurate force sensor. It requires considerable attention to the surrounding environment, as any change in the testing conditions might affect the results.

5- High electrical power consumption: connecting few IPMC samples together required a high current power source; each sample needs a few hundreds of mA.

6- Automated testing system: developing an automated system for IPMC characterisation would make the testing faster and more efficient.

Chapter 9
Future Work

9. *Future work*

This project represented a proof of concept of developing IPMC Artificial Muscles for a VAD. Although the results did not support the proposed idea, there are still areas of improvement in the future to achieve that concept. These improvements include:

1- Trying different metals for plating and coatings.
2- Improving the force density per weight and surface area.
3- Reducing electrical power consumption to make it suitable as an implantable device.
4- Increasing sensing and power harvesting capabilities.
5- Creating thin threads of IPMC and then weave them together to create a powerful structure.

Chapter 10
References

10. *References*

Adachi, I. and C. D. Fraser (2011). Mechanical circulatory support for infants and small children. Seminars in Thoracic and Cardiovascular Surgery: Pediatric Cardiac Surgery Annual, Elsevier.

Alici, G. and N. N. Huynh (2006). A robotic gripper based on conducting polymer actuators. Advanced Motion Control, 2006. 9th IEEE International Workshop on, IEEE.

Amaral, F., S. Gross-Hardt, D. Timms, C. Egger, U. Steinseifer and T. Schmitz-Rode (2013). "The Spiral Groove Bearing as a Mechanism for Enhancing the Secondary Flow in a Centrifugal Rotary Blood Pump." Artif Organs 37(10): 866-874.

Amodeo, A., G. Brancaccio, G. Michielon, S. Filippelli, Z. Ricci, S. Morelli, M. G. Gagliardi, R. Iacobelli, G. Pongiglione and R. M. Di Donato (2010). "Pneumatic Pulsatile Ventricular Assist Device as a Bridge to Heart Transplantation in Pediatric Patients." Artif Organs 34(11): 1017-1022.

Anton, M., A. Aabloo, A. Punning and M. Kruusmaa (2008). "A mechanical model of a non-uniform ionomeric polymer metal composite actuator." Smart Materials & Structures 17(2): 025004.

Aviram, A. (1978). "Mechanophotochemistry." Macromolecules 11(6): 1275-1280.
Bahramzadeh, Y. and M. Shahinpoor (2014). "A review of ionic polymeric soft actuators and sensors." Soft Robotics 1(1): 38-52.

Baldwin, J. T. and B. W. Duncan (2006). "Ventricular assist devices for children." Progress in Pediatric Cardiology 21(2): 173-184.

Bar-Cohen, Y. (2004). Electroactive polymer (EAP) actuators as artificial muscles: reality, potential, and challenges, SPIE press.

Bar-Cohen, Y., X. Bao, S. Sherrit and S.-S. Lih (2002). Characterization of the electromechanical properties of Ionomeric Polymer-Metal Composite (IPMC). SPIE's 9th Annual International Symposium on Smart Structures and Materials, International Society for Optics and Photonics.

Bar-Cohen, Y. and Q. Zhang (2008). "Electroactive polymer actuators and sensors." MRS bulletin 33(03): 173-181.

Bauer, F., E. Fousson, Q. Zhang and L. Lee (2002). Ferroelectric copolymers and terpolymers for electrostrictors: synthesis and properties. Electrets, 2002. ISE 11. Proceedings. 11th International Symposium on, IEEE.

Baughman, R. H., C. Cui, A. A. Zakhidov, Z. Iqbal, J. N. Barisci, G. M. Spinks, G. G. Wallace, A. Mazzoldi, D. De Rossi, A. G. Rinzler, O. Jaschinski, S. Roth and M. Kertesz (1999). "Carbon nanotube actuators." Science 284(5418): 1340-1344.

Biddiss, E. and T. Chau (2006). "Electroactive polymeric sensors in hand prostheses: bending response of an ionic polymer metal composite." Med Eng Phys 28(6): 568-578.

Boehning, F., D. Timms, P. L. Hsu, T. Schmitz-Rode and U. Steinseifer (2013). "Experimental and Analytical Performance Evaluation of Short Circular Hydrodynamic Journal Bearings Used in Rotary Blood Pumps." Artif Organs 37(10): 913-920.

Bonomo, C., P. Brunetto, L. Fortuna, P. Giannone, S. Graziani and S. Strazzeri (2008). "A tactile sensor for biomedical applications based on IPMCs." Sensors Journal, IEEE 8(8): 1486-1493.

Bonomo, C., L. Fortuna, P. Giannone and S. Graziani (2005). "A method to characterize the deformation of an IPMC sensing membrane." Sensors and Actuators A: Physical 123: 146-154.

Brochu, P. and Q. Pei (2010). "Advances in dielectric elastomers for actuators and artificial muscles." Macromol Rapid Commun 31(1): 10-36.

Brufau-Penella, J., M. Puig-Vidal, P. Giannone, S. Graziani and S. Strazzeri (2007). "Characterization of the harvesting capabilities of an ionic polymer metal composite device." Smart Materials and Structures 17(1).

Capoccia, M., C. T. Bowles, A. Sabashnikov and A. Simon (2013). "Recurrent Early Thrombus Formation in HeartMate II Left Ventricular Assist Device." J Investig Med High Impact Case Rep 1(2).

Carpi, F., I. Anderson, S. Bauer, G. Frediani, G. Gallone, M. Gei, C. Graaf, C. Jean-Mistral, W. Kaal, G. Kofod, M. Kollosche, R. Kornbluh, B. Lassen, M. Matysek, S. Michel, S. Nowak, B. O'Brien, Q. B. Pei, R. Pelrine, B. Rechenbach, S. Rosset and H. Shea (2015). "Standards for dielectric elastomer transducers." Smart Materials and Structures 24(10).

Carpi, F., G. Frediani and D. De Rossi (2012). Electroactive elastomeric actuators for biomedical and bioinspired systems. Biomedical Robotics and Biomechatronics (BioRob), 2012 4th IEEE RAS & EMBS International Conference on, IEEE.

Carpi, F., G. Frediani, S. Turco and D. De Rossi (2011). "Bioinspired Tunable Lens with Muscle-Like Electroactive Elastomers." Advanced Functional Materials 21(21): 4152-4158.

Carpi, F., R. Kornbluh, P. Sommer-Larsen and G. Alici (2011). "Electroactive polymer actuators as artificial muscles: are they ready for bioinspired applications?" Bioinspiration & biomimetics 6(4).

Chan, C. H., A. Hilton, G. Foster, K. M. Hawkins, N. Badiei and C. A. Thornton (2013). "The evaluation of leukocytes in response to the in vitro testing of ventricular assist devices." Artif Organs 37(9): 793-801.

Chang, A. C. and E. D. McKenzie (2005). "Mechanical cardiopulmonary support in children and young adults: extracorporeal membrane oxygenation, ventricular assist devices, and long-term support devices." Pediatr Cardiol 26(1): 2-28.

Chen, Z. and X. B. Tan (2010). "Monolithic fabrication of ionic polymer-metal composite actuators capable of complex deformation." Sensors and Actuators a-Physical 157(2): 246-257.

Chen, Z., T. I. Um and H. Bart-Smith (2011). "A novel fabrication of ionic polymer-metal composite membrane actuator capable of 3-dimensional kinematic motions." Sensors and Actuators a-Physical 168(1): 131-139.

Cheng, Z., T.-B. Xu, Q. Zhang, S. R. Meyer Jr, D. Van Tol and J. Hughes (2002). "Design, fabrication, and performance of a flextensional transducer based on electrostrictive polyvinylidene fluoride-trifluoroethylene copolymer." Ultrasonics, Ferroelectrics, and Frequency Control, IEEE Transactions on 49(9): 1312-1320.

Choe, K., K. J. Kim, D. Kim, C. Manford, S. Heo and M. Shahinpoor (2006). "Performance characteristics of electro-chemically driven polyacrylonitrile fiber bundle actuators." Journal of Intelligent Material Systems and Structures 17(7): 563-576.

Chung, C. K., P. K. Fung, Y. Z. Hong, M. S. Ju, C. C. K. Lin and T. C. Wu (2006). "A novel fabrication of ionic polymer-metal composites (IPMC) actuator with silver nano-powders." Sensors and Actuators B-Chemical 117(2): 367-375.

De Luca, V., P. Digiamberardino, G. Di Pasquale, S. Graziani, A. Pollicino, E. Umana and M. G. Xibilia (2013). "Ionic electroactive polymer metal composites: Fabricating, modeling, and applications of postsilicon smart devices." Journal of Polymer Science Part B: Polymer Physics 51(9): 699-734.

De Rossi, D., F. Carpi, N. Carbonaro, A. Tognetti and E. P. Scilingo (2011). Electroactive polymer patches for wearable haptic interfaces. Engineering in Medicine and Biology Society, EMBC, 2011 Annual International Conference of the IEEE, IEEE.

Del Nido, P. J., B. W. Duncan, J. E. Mayer, D. L. Wassel, R. A. LaPierre and R. A. Jonas (1999). "Left Ventricular Assist Device Improves Survival in Children with Left Ventricular Dysfunction after Repair of Anomalous Origion of the Left Coronary Artery from the Pulmonary Artery." The Annals of Thoratic Surgery 67: 169-172.

Deole, U., R. Lumia, M. Shahinpoor and M. Bermudez (2008). "Design and test of IPMC artificial muscle microgripper." Journal of Micro-Nano Mechatronics 4(3): 95-102.

DuPont, D. F. C. (2009). DuPont Nafion PFSA Membranes, data sheet.

Egger, C., J. Maas, T. Hufen, T. Schmitz-Rode and U. Steinseifer (2013). "Establishing a method for in vitro investigation of mechanical parameters causing acquired von Willebrand syndrome in ventricular assist devices." Artif Organs 37(9): 833-839.

Fang, B. K., M. S. Ju and C. C. K. Lin (2007). "A new approach to develop ionic polymer-metal composites (IPMC) actuator: Fabrication and control for active catheter systems." Sensors and Actuators a-Physical 137(2): 321-329.

Fang, Y., X. Tan and G. Alici (2008). "Robust adaptive control of conjugated polymer actuators." Control Systems Technology, IEEE Transactions on 16(4): 600-612.

Feng, G. H. and K. M. Liu (2014). "Fabrication and characterization of a micromachined swirl-shaped ionic polymer metal composite actuator with electrodes exhibiting asymmetric resistance." Sensors (Basel) 14(5): 8380-8397.

Finkelmann, H., H. J. Kock and G. Rehage (1981). "Investigations on liquid crystalline polysiloxanes 3. Liquid crystalline elastomers—a new type of liquid crystalline material." Die Makromolekulare Chemie, Rapid Communications 2(4): 317-322.

Frazier, O. H., J. T. Bricker, M. P. Macris and D. A. Cooley (1989). "Use of a Left-Ventricular Assist Device as a Bridge to Transplantation in a Pediatric-Patient." Texas Heart Institute Journal 16(1): 46-50.

Fukamachi, K. and N. G. Smedira (2005). "Smaller, safer, totally implantable LVADs: fact or fantasy?" ACC Current Journal Review 14(8): 40-42.

Fumoto, H., A. Shiose, C. R. Flick, L. D. Noble, D. T. Dudzinski, F. Casas, T. Takaseya, Y. Arakawa, K. Fukamachi, W. A. Smith and B. W. Duncan (2014). "Short-term in vivo performance of the Cleveland Clinic PediPump left ventricular assist device." Artif Organs 38(5): 374-382.

Fynn-Thompson, F. and C. Almond (2007). "Pediatric ventricular assist devices." Pediatr Cardiol 28(2): 149-155.

Gandhi, S. K. (2009). "Ventricular assist devices in children." Progress in Pediatric Cardiology 26(1): 11-19.

Garbade, J., H. B. Bittner, M. J. Barten and F. W. Mohr (2011). "Current trends in implantable left ventricular assist devices." Cardiol Res Pract 2011.

Gibson, P. H., H. Becher and J. B. Choy (2014). "Classification of left ventricular size: diameter or volume with contrast echocardiography?" Open heart 1(1).

Glaser, R., V. Caccese and M. Shahinpoor (2011). "Development of magneto-rheological fluid composites with rigidification characteristics." Smart Materials & Structures 20(4).

Gong, Y. Q., C. Y. Tang, C. P. Tsui and J. P. Fan (2009). "Modelling of ionic polymer-metal composites by a multi-field finite element method." International Journal of Mechanical Sciences 51(11-12): 741-751.

Han, M. J., J. H. Park, J. Y. Lee and J. Y. Jho (2006). "Ionic polymer-metal composite actuators employing radiation-grafted fluoropolymers as ion-exchange membranes." Macromolecular rapid communications 27(3): 219-222.

Hanley, C. A., Y. K. Gun'ko, G. Frediani and F. Carpi (2014). "Stretchable optical device with electrically tunable absorbance and fluorescence." Smart Materials and Structures 23(1).

He, Q. S., M. Yu, L. L. Song, H. T. Ding, X. Q. Zhang and Z. D. Dai (2011). "Experimental Study and Model Analysis of the Performance of IPMC Membranes with Various Thickness." Journal of Bionic Engineering 8(1): 77-85.

HEGDE, A., W. BUCH and H. KARABEY (2004). CARDIAC APPARATUS INCLUDING ELECTROACTIVE POLYMER ACTUATORS AND METHODS OF USING THE SAME. USA, WO Patent 2,004,086,946. US 7,198,595 B2.

Hines, M. H. (2013). Neonatal cardiovascular physiology. Seminars in pediatric surgery, Elsevier.
Hirokawa, Y., T. Tanaka, D. Johnson and P. Sen (1984). Volume phase transition in a non-ionic gel. AIP Conference Proceedings, AIP.

Hu, Y. and W. Chen (2011). "Externally Induced Thermal Actuation of Polymer Nanocomposites." Macromolecular Chemistry and Physics 212(10): 992-998.

Hu, Y., W. Chen, L. Lu, J. Liu and C. Chang (2010). "Electromechanical actuation with controllable motion based on a single-walled carbon nanotube and natural biopolymer composite." ACS nano 4(6): 3498-3502.

Huang, H., M. Yang, C. Lu, L. Xu, X. Zhuang and F. Meng (2013). "A numerical method to enhance the performance of a cam-type electric motor-driven left ventricular assist device." Artif Organs 37(10): 875-883.

HUB, K. (2017). "Ventricles of the Heart." from https://www.kenhub.com/en/library/anatomy/the-ventricles-of-the-heart.

Hunt, A., A. Punning, M. Anton, A. Aabloo and M. Kruusmaa (2008). A multilink manipulator with IPMC joints. The 15th International Symposium on: Smart Structures and Materials & Nondestructive Evaluation and Health Monitoring, International Society for Optics and Photonics.

Hwang, T., V. Palmre, J. Nam, D. C. Lee and K. J. Kim (2015). "A new ionic polymer-metal composite based on Nafion/ poly(vinyl alcohol-co-ethylene) blends." Smart Materials and Structures 24(10).

Inamuddin, A. Khan, R. K. Jain and M. Naushad (2015). "Development of sulfonated poly(vinyl alcohol)/polpyrrole based ionic polymer metal composite (IPMC) actuator and its characterization." Smart Materials and Structures 24(9).

Inoue, T., T. Nishimura, A. Murakami, K. Itatani, T. Takaoka, K. Kitahori, A. Umeki, T. Takezoe, K. Kashiwa, S. Kyo and M. Ono (2011). "Left Ventricular Assist Device Support with a Centrifugal Pump for 2 Months in a 5 kg Child." The Japanese Society for Artificial Organs 14: 253-256.

Instruments, K. (2001). "Volume and surface resistivity measurements of insulating materials using the model 6517A electrometer/high resistance meter." Application Note Series(314).

Jager, E. W. (2013). Conducting polymer actuators for medical devices and cell mechanotransduction. Advanced Intelligent Mechatronics (AIM), 2013 IEEE/ASME International Conference on, IEEE.

Jain, R., S. Datta and S. Majumder (2010). IPMC based micro gripper for miniature part handling. Mechatronics and Automation (ICMA), 2010 International Conference on, IEEE.

Jain, R., S. Datta, S. Majumder, S. Mukherjee, D. Sadhu, S. Samanta and K. Banerjee (2010). Bio-mimetic behaviour of IPMC artificial muscle using EMG signal. Advances in Recent Technologies in Communication and Computing (ARTCom), 2010 International Conference on, IEEE.

Jain, R. K., S. Datta and S. Majumder (2014). "Biomimetic Behavior of Ipmc Using Emg Signal for Micro Robot." Mechanics Based Design of Structures and Machines 42(3): 398-417.

Jain, R. K., S. Datta, S. Majumder and A. Dutta (2011). "Two IPMC Fingers Based Micro Gripper For Handling." International Journal of Advanced Robotic Systems 8(1): 1-9.

Jain, R. K., S. Datta, S. Majumder and A. Dutta (2014). "Development of Multi Micro Manipulation System Using IPMC Micro Grippers." Journal of Intelligent & Robotic Systems 74(3-4): 547-569.

Jain, R. K., S. Majumder and A. Dutta (2013). "SCARA based peg-in-hole assembly using compliant IPMC micro gripper." Robotics and Autonomous Systems 61(3): 297-311.

Jaquiss, R. and M. Imamura (2011). Implantation of a Berlin Heart ventricular assist device. Seminars in Thoracic and Cardiovascular Surgery: Pediatric Cardiac Surgery Annual, Elsevier.

Jeewa, A., C. Manlhiot, B. W. McCrindle, G. Van Arsdell, T. Humpl and A. I. Dipchand (2010). "Outcomes With Ventricular Assist Device Versus Extracorporeal Membrane Oxygenation as a Bridge to Pediatric Heart Transplantation." Artif Organs 34(12): 1087-1091.

Jefferies, J. L. and J. A. Towbin (2010). "Dilated cardiomyopathy." Lancet 375(9716): 752-762.

Jeon, J. H., S. W. Yeorn and I. K. Oh (2008). "Fabrication and actuation of ionic polymer metal composites patterned by combining electroplating with electroless plating." Composites Part a-Applied Science and Manufacturing 39(4): 588-596.

Johanson, U., A. Punning, M. Kruusmaa and A. Aabloo (2008). Self healing properties of Cu-Pt coated ionic polymer actuators. The 15th International Symposium on: Smart Structures and Materials & Nondestructive Evaluation and Health Monitoring, International Society for Optics and Photonics.

John, R. (2008). Current axial-flow devices—the HeartMate II and Jarvik 2000 left ventricular assist devices. Semin Thorac Cardiovasc Surg, Elsevier.

Jung, K., J. Nam and H. Choi (2003). "Investigations on actuation characteristics of IPMC artificial muscle actuator." Sensors and Actuators a-Physical 107(2): 183-192.

Katchalsky, A. (1949). "Rapid swelling and deswelling of reversible gels of polymeric acids by ionization." Cellular and Molecular Life Sciences 5(8): 319-320.

Kenny, D. and A. G. Stuart (2009). "Long-term outcome of the child with congenital heart disease." Paediatrics and child health 19(1): 37-42.

Kikuchi, K., T. Sakamoto, S. Tsuchitani and K. Asaka (2011). "Comparative study of bending characteristics of ionic polymer actuators containing ionic liquids for modeling actuation." Journal of Applied Physics 109(7).

Kim, J. and Y. B. Seo (2002). "Electro-active paper actuators." Smart Materials & Structures 11(3): 355-360.

Kim, K. J. and M. Shahinpoor (2002). "A novel method of manufacturing three-dimensional ionic polymer-metal composites (IPMCs) biomimetic sensors, actuators and artificial muscles." Polymer 43(3): 797-802.

Kim, K. J. and M. Shahinpoor (2003). "Effective diffusivity of nanoscale ion-water clusters within ion-exchange membranes determined by a novel mechano-electrical technique." International journal of hydrogen energy 28(1): 99-104.

Kim, K. J. and M. Shahinpoor (2003). "Ionic polymer-metal composites: II. Manufacturing techniques." Smart Materials & Structures 12(1): 65-79.

Kim, S. H., K. Ishiyama, S. Hashi, Y. Shiraishi, Y. Hayatsu, M. Akiyama, Y. Saiki and T. Yambe (2013). "Preliminary validation of a new magnetic wireless blood pump." Artif Organs 37(10): 920-926.

Kim, S. M. and K. J. Kim (2008). "Palladium buffer-layered high performance ionic polymer-metal composites." Smart Materials & Structures 17(3).
Kobayashi, K., K. Ohuchi, H. Hoshi, N. Morimoto, Y. Iwasaki and S. Takatani (2005). "Segmented polyurethane modified by photopolymerization and cross-linking with 2-methacryloyloxyethyl phosphorylcholine polymer for blood-contacting surfaces of ventricular assist devices." J Artif Organs 8(4): 237-244.

Kosaka, R., T. Yada, M. Nishida, O. Maruyama and T. Yamane (2013). "Geometric optimization of a step bearing for a hydrodynamically levitated centrifugal blood pump for the reduction of hemolysis." Artif Organs 37(9): 778-785.

Kosidlo, U., M. Omastova, M. Micusik, G. Ciric-Marjanovic, H. Randriamahazaka, T. Wallmersperger, A. Aabloo, I. Kolaric and T. Bauernhansl (2013). "Nanocarbon based ionic actuators-a review." Smart Materials and Structures 22(10).

Kruusamäe, K., P. Brunetto, S. Graziani, L. Fortuna, M. Kodu, R. Jaaniso, A. Punning and A. Aabloo (2010). Experiments with self-sensing IPMC actuating device. SPIE Smart Structures and Materials+ Nondestructive Evaluation and Health Monitoring, International Society for Optics and Photonics.

Kruusamäe, K., P. Brunetto, S. Graziani, A. Punning, G. Di Pasquale and A. Aabloo (2010). "Self-sensing ionic polymer–metal composite actuating device with patterned surface electrodes." Polymer international 59(3): 300-304.

Kruusamäe, K., P. Brunetto, A. Punning, M. Kodu, R. Jaaniso, S. Graziani, L. Fortuna and A. Aabloo (2011). "Electromechanical model for a self-sensing ionic polymer–metal composite actuating device with patterned surface electrodes." Smart Materials and Structures 20(12).

Kruusamäe, K., A. Punning, A. Aabloo and K. Asaka (2015). Self-Sensing Ionic Polymer Actuators: A Review. Actuators, Multidisciplinary Digital Publishing Institute.

Lee, J. H., J. H. Lee, J.-D. Nam, H. Choi, K. Jung, J. W. Jeon, Y. K. Lee, K. J. Kim and Y. Tak (2005). "Water uptake and migration effects of electroactive ion-exchange polymer metal composite (IPMC) actuator." Sensors and Actuators A: Physical 118(1): 98-106.

Lee, J. W. and Y. T. Yoo (2011). "Preparation and performance of IPMC actuators with electrospun Nafion (R)-MWNT composite electrodes." Sensors and Actuators B-Chemical 159(1): 103-111.

Lee, J. W., Y. T. Yoo and J. Y. Lee (2014). "Ionic polymer-metal composite actuators based on triple-layered polyelectrolytes composed of individually functionalized layers." ACS Appl Mater Interfaces 6(2): 1266-1271.

Lee, M.-J., S.-H. Jung, S. Lee, M.-S. Mun and I. Moon (2006). Control of IPMC-based artificial muscle for myoelectric hand prosthesis. Biomedical Robotics and Biomechatronics, 2006. BioRob 2006. The First IEEE/RAS-EMBS International Conference on, IEEE.

Lee, S. J., M. J. Han, S. J. Kim, J. Y. Jho, H. Y. Lee and Y. H. Kim (2006). "A new fabrication method for IPMC actuators and application to artificial fingers." Smart Materials & Structures 15(5): 1217-1224.

Lewandowski, B. E., K. L. Kilgore and K. J. Gustafson (2009). "In vivo demonstration of a self-sustaining, implantable, stimulated-muscle-powered piezoelectric generator prototype." Ann Biomed Eng 37(11): 2390-2401.

Li, S. L., W. Y. Kim, T. H. Cheng and I. K. Oh (2011). "A helical ionic polymer-metal composite actuator for radius control of biomedical active stents." Smart Materials & Structures 20(3).

Liu, D., A. McDaid, K. Aw and S. Xie (2011). "Position control of an ionic polymer metal composite actuated rotary joint using iterative feedback tuning." Mechatronics 21(1): 315-328.

Liu, J., Y. Wang, D. Zhao, C. Zhang, H. Chen and D. Li (2014). Design and fabrication of an IPMC-embedded tube for minimally invasive surgery applications. SPIE Smart Structures and Materials+ Nondestructive Evaluation and Health Monitoring, International Society for Optics and Photonics.

Liu, Y., M. Ghaffari, R. Zhao, J. H. Lin, M. R. Lin and Q. M. Zhang (2012). "Enhanced Electromechanical Response of Ionic Polymer Actuators by Improving Mechanical Coupling between Ions and Polymer Matrix." Macromolecules 45(12): 5128-5133.

Lodge, A. J., A. G. Antunez and R. D. Jaquiss (2012). "Pediatric ventricular assist devices." Progress in Pediatric Cardiology 33(2): 169-176.

Lowe, J. E., G. C. Hughes and S. S. Biswas (1999). "Non–Blood-Contacting Biventricular Support: Direct Mechanical Ventricular Actuation." Operative Techniques in Thoracic and Cardiovascular Surgery 4(4): 345-351.

Lumia, R. and M. Shahinpoor (2008). IPMC microgripper research and development. Journal of Physics: Conference Series, IOP Publishing.

Macfarlane, F. (2006). PAEDIATRIC ANATOMY AND PHYSIOLOGY AND THE BASICS OF PAEDIATRIC ANAESTHESIA, London: Anaesthesia UK.

Madden, J. D. (2006). "Artificial muscle begins to breathe." Science 311(5767): 1559-1560.

Madden, J. D. W., N. A. Vandesteeg, P. A. Anquetil, P. G. A. Madden, A. Takshi, R. Z. Pytel, S. R. Lafontaine, P. A. Wieringa and I. W. Hunter (2004). "Artificial muscle technology: Physical principles and naval prospects." Ieee Journal of Oceanic Engineering 29(3): 706-728.

Malone, E. and H. Lipson (2006). "Freeform fabrication of ionomeric polymer-metal composite actuators." Rapid Prototyping Journal 12(5): 244-253.

Marchese, A. D., R. K. Katzschmann and D. Rus (2015). "A recipe for soft fluidic elastomer robots." Soft Robotics 2(1): 7-25.

Martini F. , J. L. N., Edwin F. Bartholomew (2011). Fundamentals of Anatomy & Physiology, Pearson.

Masuoka, A., T. Katogi, M. Iwazaki, T. Kobayashi, T. Nishimura and S. Kyo (2008). "Bridge to transplantation with a Toyobo-NCVC left ventricular assist device in a 3-year-old girl." Gen Thorac Cardiovasc Surg 56(7): 357-360.

McDaid, A. J., K. C. Aw, E. Haemmerle, M. Shahinpoor and S. Q. Xie (2011). "Adaptive tuning of a 2DOF controller for robust cell manipulation using IPMC actuators." Journal of Micromechanics and Microengineering 21(12).

McKay, T., B. O'Brien, E. Calius and I. Anderson (2010). "Self-priming dielectric elastomer generators." Smart Materials and Structures 19(5).

Miera, O., E. V. Potapov, M. Redlin, A. Stepanenko, F. Berger, R. Hetzer and M. Hubler (2011). "First experiences with the HeartWare ventricular assist system in children." Ann Thorac Surg 91(4): 1256-1260.

Ming, Y., M. L. Zhu, R. C. Richardson, M. C. Levesley, P. G. Walker and K. Watterson (2005). "Design and evaluation of linear ultrasonic motors for a cardiac compression assist device." Sensors and Actuators a-Physical 119(1): 214-220.

Mirfakhrai, T., J. D. W. Madden and R. H. Baughman (2007). "Polymer artificial muscles." Materials today 10(4): 30-38.

Mitamura, Y. (2015). "Current Status of Left Ventricular Assist Devices and Cell Sheet Engineering for Treatment of Severe Heart Disease in Japan." Artif Organs 39(7): 543-549.

Moeinkhah, H., A. Akbarzadeh and J. Rezaeepazhand (2014). "Design of a robust quantitative feedback theory position controller for an ionic polymer metal composite actuator using an analytical dynamic model." Journal of Intelligent Material Systems and Structures 25(15): 1965-1977.

Moeinkhah, H., J. Rezaeepazhand, A. Akbarzadeh and I.-K. Oh (2014). "Accurate Dynamic Modeling of Helical Ionic Polymer-Metal Composite Actuator Based on Intrinsic Equations."

Mulloy, D. P., C. M. Bhamidipati, M. L. Stone, G. Ailawadi, I. L. Kron and J. A. Kern (2013). "Orthotopic heart transplant versus left ventricular assist device: a national comparison of cost and survival." The Journal of thoracic and cardiovascular surgery 145(2): 566-574.

Must, I., U. Johanson, F. Kaasik, I. Poldsalu, A. Punning and A. Aabloo (2013). An ionic liquid-based actuator as a humidity sensor. Advanced Intelligent Mechatronics (AIM), 2013 IEEE/ASME International Conference on, IEEE.

Must, I., F. Kaasik, I. Poldsalu, L. Mihkels, U. Johanson, A. Punning and A. Aabloo (2015). "Ionic and Capacitive Artificial Muscle for Biomimetic Soft Robotics." Advanced Engineering Materials 17(1): 84-94.

Must, I., V. Vunder, F. Kaasik, I. Poldsalu, U. Johanson, A. Punning and A. Aabloo (2014). "Ionic liquid-based actuators working in air: The effect of ambient humidity." Sensors and Actuators B-Chemical 202: 114-122.

Nemat-Nasser, S. (2002). "Micromechanics of actuation of ionic polymer-metal composites." Journal of Applied Physics 92(5): 2899-2915.

Nguyen, T. T., N. S. Goo, V. K. Nguyen, Y. Yoo and S. Park (2008). "Design, fabrication, and experimental characterization of a flap valve IPMC micropump with a flexibly supported diaphragm." Sensors and Actuators a-Physical 141(2): 640-648.

Nguyen, V. K., J. W. Lee and Y. Yoo (2007). "Characteristics and performance of ionic polymer-metal composite actuators based on Nafion/layered silicate and Nafion/silica nanocomposites." Sensors and Actuators B-Chemical 120(2): 529-537.

Nguyen, V. K. and Y. T. Yoo (2007). "A novel design and fabrication of multilayered ionic polymer-metal composite actuators based on Nafion/layered silicate and Nafion/silica nanocomposites." Sensors and Actuators B-Chemical 123(1): 183-190.

Noh, M. D., J. F. Antaki, M. Ricci, J. Gardiner, D. Paden, J. Wu, E. Prem, H. Borovetz and B. E. Paden (2008). "Magnetic design for the PediaFlow ventricular assist device." Artif Organs 32(2): 127-135.

Otero, T. F., J. G. Martinez and J. Arias-Pardilla (2012). "Biomimetic electrochemistry from conducting polymers. A review Artificial muscles, smart membranes, smart drug delivery and computer/neuron interfaces." Electrochimica Acta 84: 112-128.

Ozturk, P., A. Y. Engin, S. Nalbantgil, E. Oguz, F. Ayik, C. Engin, T. Yagdi, S. Erkul, O. Balcioglu and M. Ozbaran (2013). "Comparison of continuous-flow and pulsatile-flow blood pumps on reducing pulmonary artery pressure in patients with fixed pulmonary hypertension." Artif Organs 37(9): 763-767.

Padalino, M. A., T. Bottio, V. Tarzia, G. Bortolussi, A. Cerutti, V. L. Vida, G. Gerosa and G. Stellin (2014). "HeartWare Ventricular Assist Device as Bridge to Transplant in Children and Adolescents." Artif Organs 38(5): 418-422.

Pagani, F. D. (2008). Circulatory Support for Bridging to Recovery or Transplantation. Management of Heart Failure, Springer: 111-135.

Pagani, F. D. (2008). Continuous-flow rotary left ventricular assist devices with “3rd generation” design. Semin Thorac Cardiovasc Surg, Elsevier.

Palanzo, D. A., A. El-Banayosy, E. Stephenson, C. Brehm, A. Kunselman and W. E. Pae (2013). "Comparison of Hemolysis Between CentriMag and RotaFlow Rotary Blood Pumps During Extracorporeal Membrane Oxygenation." Artif Organs 37(9): E162-E166.

Panwar, V., K. Cha, J. O. Park and S. Park (2012). "High actuation response of PVDF/PVP/PSSA based ionic polymer metal composites actuator." Sensors and Actuators B-Chemical 161(1): 460-470.

Panwar, V., B. S. Kang, J. O. Park and S. H. Park (2011). "New Ionic Polymer-Metal Composite Actuators Based on PVDF/PSSA/PVP Polymer Blend Membrane." Polymer Engineering and Science 51(9): 1730-1741.

Panwar, V., S. Y. Ko, J. O. Park and S. Park (2013). "Enhanced and fast actuation of fullerenol/PVDF/PVP/PSSA based ionic polymer metal composite actuators." Sensors and Actuators B-Chemical 183: 504-517.

Panwar, V., C. Lee, S. Y. Ko, J. O. Park and S. Park (2012). "Dynamic mechanical, electrical, and actuation properties of ionic polymer metal composites using PVDF/PVP/PSSA blend membranes." Materials Chemistry and Physics 135(2-3): 928-937.

Paquette, J. W., K. J. Kim and D. Kim (2005). "Low temperature characteristics of ionic polymer-metal composite actuators." Sensors and Actuators a-Physical 118(1): 135-143.

Park, I.-S., S.-M. Kim, D. Kim and K. J. Kim (2007). The mechanical properties of ionic polymer-metal composites. The 14th International Symposium on: Smart Structures and Materials & Nondestructive Evaluation and Health Monitoring, International Society for Optics and Photonics.

Park, I. S., K. Jung, D. Kim, S. M. Kim and K. J. Kim (2008). "Physical principles of ionic polymer-metal composites as electroactive actuators and sensors." MRS bulletin 33(3): 190-195.

Park, I. S., S. M. Kim, D. Pugal, L. M. Huang, S. W. Tam-Chang and K. J. Kim (2010). "Visualization of the cation migration in ionic polymer-metal composite under an electric field." Applied Physics Letters 96(4).

Park, J., V. Palmre, T. Hwang, K. Kim, W. Yim and C. Bae (2014). "Electromechanical performance and other characteristics of IPMCs fabricated with various commercially available ion exchange membranes." Smart Materials and Structures 23(7).

Pektok, E., Z. T. Demirozu, N. Arat, O. Yildiz, E. Oklu, D. Eker, F. Ece, C. Ciftci, N. Yazicioglu, O. Bayindir and D. S. Kucukaksu (2013). "Remote monitoring of left ventricular assist device parameters after HeartAssist-5 implantation." Artif Organs 37(9): 820-825.

Pieri, M., N. Agracheva, A. L. Di Prima, T. Nisi, M. De Bonis, F. Isella, A. Zangrillo and F. Pappalardo (2014). "Primary anticoagulation with bivalirudin for patients with implantable ventricular assist devices." Artif Organs 38(4): 342-346.

Põldsalu, I., S.-E. Mändmaa, A.-L. Peikolainen, A. Kesküla and A. Aabloo (2015). Fabrication of ion-conducting carbon polymer composite electrodes by spin coating. SPIE Smart Structures and Materials+ Nondestructive Evaluation and Health Monitoring, International Society for Optics and Photonics.

Potapov, E. V., B. Stiller and R. Hetzer (2007). "Ventricular assist devices in children: current achievements and future perspectives." Pediatr Transplant 11(3): 241-255.

Punning, A., M. Anton, M. Kruusmaa and A. Aabloo (2005). An engineering approach to reduced power consumption of IPMC (Ion-Polymer Metal Composite) actuators. Advanced Robotics, 2005. ICAR'05. Proceedings., 12th International Conference on, IEEE.

Punning, A., U. Johanson, M. Anton, A. Aabloo and M. Kruusmaa (2009). "A Distributed Model of Ionomeric Polymer Metal Composite." Journal of Intelligent Material Systems and Structures 20(14): 1711-1724.

Punning, A., A. Kruusmaa and A. Aabloo (2007). "Surface resistance experiments with IPMC sensors and actuators." Sensors and Actuators a-Physical 133(1): 200-209.

Punning, A., M. Kruusmaa and A. Aabloo (2007). "A self-sensing ion conducting polymer metal composite (IPMC) actuator." Sensors and Actuators a-Physical 136(2): 656-664.

Punning, A., I. Must, I. Põldsalu, V. Vunder, F. Kaasik, R. Temmer and A. Aabloo (2015). Long-term degradation of the ionic electroactive polymer actuators. SPIE Smart Structures and Materials+ Nondestructive Evaluation and Health Monitoring, International Society for Optics and Photonics.

Ramnarine, I. R., M. Capoccia, Z. Ashley, H. Sutherland, M. Russold, N. Summerfield, S. Salmons and J. C. Jarvis (2006). "Counterpulsation from the skeletal muscle ventricle and the intraaortic balloon pump in the normal and failing circulations." Circulation 114(1 Suppl): I10-15.

Ren, K., S. Liu, M. Lin, Y. Wang and Q. Zhang (2008). "A compact electroactive polymer actuator suitable for refreshable Braille display." Sensors and Actuators A: Physical 143(2): 335-342.

Richardson, R. C., M. C. Levesley, M. D. Brown, J. A. Hawkes, K. Watterson and P. G. Walker (2003). "Control of ionic polymer metal composites." Ieee-Asme Transactions on Mechatronics 8(2): 245-253.

Riddle, R. O., Y. Jung, S.-M. Kim, S. Song, B. Stolpman, K. J. Kim and K. K. Leang (2010). Sectored-electrode IPMC actuator for bending and twisting motion. SPIE Smart Structures and Materials+ Nondestructive Evaluation and Health Monitoring, International Society for Optics and Photonics.

Roche, E. T., M. A. Horvath, I. Wamala, A. Alazmani, S.-E. Song, W. Whyte, Z. Machaidze, C. J. Payne, J. C. Weaver, G. Fishbein, J. Kuebler, N. V. Vasilyev, D. J. Mooney, F. A. Pigula and C. J. Walsh (2017). "Soft robotic sleeve supports heart function." Science Translational Medicine 9(373).

Roentgen, W. (1880). "About the changes in shape and volume of dielectrics caused by electricity." Section III in G. Wiedemann (Ed.), Annual Physics and Chemistry Series 11: 771-786.

Rojas, S. V., M. Avsar, J. S. Hanke, Z. Khalpey, S. Maltais, A. Haverich and J. D. Schmitto (2015). "Minimally invasive ventricular assist device surgery." Artif Organs 39(6): 473-479.

Rossiter, J., K. Takashima and T. Mukai (2012). "Shape memory properties of ionic polymer-metal composites." Smart Materials and Structures 21(11).

Sabashnikov, A., P. Mohite, B. Zych, A.-F. Popov, J. Fatullayev, M. Zeriouh, R. Hards, D. G. Sáez, M. Capoccia and Y.-H. Choi (2014). Outcomes in Patients Receiving HeartMate II Versus HVAD Left Ventricular Assist Device as a Bridge to Transplantation. Transplant Proc, Elsevier.

Santos, J., B. Lopes and P. J. C. Branco (2010). "Ionic polymer-metal composite material as a diaphragm for micropump devices." Sensors and Actuators a-Physical 161(1-2): 225-233.

Sareh, S. and J. Rossiter (2013). "Kirigami artificial muscles with complex biologically inspired morphologies." Smart Materials and Structures 22(1).

Sareh, S. and J. Rossiter (2013). "Kirigami artificial muscles with complex biologically inspired morphologies." Smart Materials and Structures 22(1): 1-13.

Sareh, S., J. Rossiter, A. Conn, K. Drescher and R. E. Goldstein (2012). "Swimming like algae: biomimetic soft artificial cilia." Journal of The Royal Society Interface.

Schima, H., M. Stoiber, T. Schlöglhofer, Z. Hartner, T. Haberl and D. Zimpfer (2013). "Repair of Left Ventricular Assist Device Driveline Damage Directly at the Transcutaneous Exit Site." Artif Organs.

Schreyer, H. B., N. Gebhart, K. J. Kim and M. Shahinpoor (2000). "Electrical activation of artificial muscles containing polyacrylonitrile gel fibers." Biomacromolecules 1(4): 642-647.

Shahinpoor, M. (2003). "Ionic polymer-conductor composites as biomimetic sensors, robotic actuators and artificial muscles - a review." Electrochimica Acta 48(14-16): 2343-2353.

Shahinpoor, M. (2003). "Mechanoelectrical phenomena in ionic polymers." Mathematics and Mechanics of Solids 8(3): 281-288.

Shahinpoor, M. (2005). "Soft plastic robots and artificial muscles." Int. J. Adv. Robotic Systems 2(2): 161-174.

Shahinpoor, M. (2009). "Implantable Heart-Assist and Compression Devices Employing an ActiveNetwork of Ellectrically-Controllable Ionic Polymer-Metal Nanocomposites." Biomedical Applications of Electroactive Polymer Actuators, F. Capri and E. Smela, eds., Wiley, Chichester, United Kingdom.

Shahinpoor, M. (2010). "A Review of Patents on Implantable Heart-Compression/Assist Devices and Systems." Recent Patents on Biomedical Engineering 3(1): 54-71.

Shahinpoor, M., Y. Bar-Cohen, J. O. Simpson and J. Smith (1998). "Ionic polymer-metal composites (IPMCs) as biomimetic sensors, actuators and artificial muscles - a review." Smart Materials & Structures 7(6): R15-R30.

Shahinpoor, M. and K. J. Kim (2000). "The effect of surface-electrode resistance on the performance of ionic polymer-metal composite (IPMC) artificial muscles." Smart Materials and Structures 9(4): 543.

Shahinpoor, M. and K. J. Kim (2001). "Ionic polymer-metal composites: I. Fundamentals." Smart Materials & Structures 10(4): 819-833.

Shahinpoor, M. and K. J. Kim (2002). "Mass transfer induced hydraulic actuation in ionic polymer-metal composites." Journal of Intelligent Material Systems and Structures 13(6): 369-376.

Shahinpoor, M. and K. J. Kim (2002). "Novel ionic polymer-metal composites equipped with physically loaded particulate electrodes as biomimetic sensors, actuators and artificial muscles." Sensors and Actuators a-Physical 96(2-3): 125-132.

Shahinpoor, M. and K. J. Kim (2004). "Ionic polymer-metal composites: III. Modeling and simulation as biomimetic sensors, actuators, transducers, and artificial muscles." Smart Materials & Structures 13(6): 1362-1388.

Shahinpoor, M. and K. J. Kim (2005). "Ionic polymer-metal composites: IV. Industrial and medical applications." Smart Materials & Structures 14(1): 197-214.

Shahinpoor, M. and M. Mojarrad (2002). Ionic polymer sensors and actuators, Google Patents.

Sharland, G. and L. Allan (1992). "Normal fetal cardiac measurements derived by cross-sectional echocardiography." Ultrasound in Obstetrics and Gynecology 2(3): 175-181.

Simon, D. T., E. W. Jager, K. Tybrandt, K. C. Larsson, S. Kurup, A. Richter-Dahlfors and M. Berggren (2009). An organic electronic ion pump to regulate intracellular signaling at high spatiotemporal resolution. Solid-State Sensors, Actuators and Microsystems Conference, 2009. TRANSDUCERS 2009. International, IEEE.

Stanfield, J. R. and C. H. Selzman (2013). "In vitro hydrodynamic analysis of pin and cone bearing designs of the Jarvik 2000 adult ventricular assist device." Artif Organs 37(9): 825-833.
Støylen, A., H. E. Mølmen and H. Dalen (2016). "Importance of length and external diameter in left ventricular geometry. Normal values from the HUNT Study." Open heart 3(2).

Tailoka, F., D. J. Fray and R. V. Kumar (2003). "Application of Nafion electrolytes for the detection of humidity in a corrosive atmosphere." Solid State Ionics 161(3-4): 267-277.

Talley, N. J. and S. O'Connor (2009). Examination Medicine, Churchill Livingstone Elsevier.
Thunberg, C. A., B. D. Gaitan, F. A. Arabia, D. J. Cole and A. M. Grigore (2010). "Ventricular assist devices today and tomorrow." J Cardiothorac Vasc Anesth 24(4): 656-680.

Timms, D. (2011). "A review of clinical ventricular assist devices." Med Eng Phys 33(9): 1041-1047.
Trabia, S., T. Hwang and K. J. Kim (2016). "A fabrication method of unique Nafion® shapes by painting for ionic polymer–metal composites." Smart Materials and Structures 25(8): 085006.

Trumble, D. R. (2011). "Potential mechanisms for muscle-powered cardiac support." Artif Organs 35(7): 715-720.

Trumble, D. R., D. B. Melvin, D. A. Dean and J. A. Magovern (2008). "In vivo performance of a muscle-powered drive system for implantable blood pumps." ASAIO J 54(3): 227-232.
Vertechy, R., A. Frisoli, M. Bergamasco, F. Carpi, G. Frediani and D. De Rossi (2012). "Modeling and experimental validation of buckling dielectric elastomer actuators." Smart Materials and Structures 21(9): 094005.

Vunder, V., M. Itik, I. Poldsalu, A. Punning and A. Aabloo (2014). "Inversion-based control of ionic polymer-metal composite actuators with nanoporous carbon-based electrodes." Smart Materials and Structures 23(2).

Vunder, V., M. Itik, A. Punning and A. Aabloo (2014). Force control of ionic polymer-metal composite actuators with carbon-based electrodes. SPIE Smart Structures and Materials+ Nondestructive Evaluation and Health Monitoring, International Society for Optics and Photonics.

Wang, H., S. Cai, F. Carpi and Z. Suo (2012). "Computational model of hydrostatically coupled dielectric elastomer actuators." Journal of Applied Mechanics 79(3).

Winslow, W. M. (1949). "Induced fibrillain of suspemsions." Journal of applied physics 20: 1137.

Woodward, C. S. (2011). "Keeping children with congenital heart disease healthy." J Pediatr Health Care 25(6): 373-378.

Yambe, T., S. Amae, S. Maruyama, Y. Luo, H. Takagi, S.-s. Nanka, A. Tanaka, N. Kamiyama, R. Ohi and K. Tabayashi (2001). "Application of a shape memory alloy for internal artificial organs." Journal of Artificial Organs 4(2): 88-91.

Yasui, K., R. Kosaka, M. Nishida, O. Maruyama, Y. Kawaguchi and T. Yamane (2013). "Optimal design of the hydrodynamic multi-arc bearing in a centrifugal blood pump for the improvement of bearing stiffness and hemolysis level." Artif Organs 37(9): 768-777.

Yeom, S. W. and I. K. Oh (2009). "A biomimetic jellyfish robot based on ionic polymer metal composite actuators." Smart Materials & Structures 18(8).

Yeung, F. (2007). "Heart Embryology." 2017, from http://pie.med.utoronto.ca/htbg/HTBG_content/HTBG_heartEmbryologyApp.html.

Yoon, W. J., P. G. Reinhall and E. J. Seibel (2007). "Analysis of electro-active polymer bending: A component in a low cost ultrathin scanning endoscope." Sensors and Actuators a-Physical 133(2): 506-517.

Yu, M., H. Shen and Z. D. Dai (2007). "Manufacture and Performance of Ionic Polymer-Metal Composites." Journal of Bionic Engineering 4(3): 143-149.

Zadin, V., A. V. Krasheninnikov, F. Djurabekova and K. Nordlund (2015). "Simulations of electromechanical shape transformations of Au nanoparticles." Physica Status Solidi B-Basic Solid State Physics 252(1): 144-148.

Zhao, D., Y. Wang, J. Liu, M. Luo, D. Li and H. Chen (2015). A multi-segment soft actuator for biomedical applications based on IPMCs. SPIE Smart Structures and Materials+ Nondestructive Evaluation and Health Monitoring, International Society for Optics and Photonics.

Chapter 11
Appendices

11. *Appendices*

11.1 IPMC Fabrication Protocols:

2.1 Protocol A

1. Use sandpaper to rough both sides of the membrane, very gently (such as Norton 600A) (2sec/cm^2).

2. Clean the membrane in an ultrasonic water bath cleaner for about 10 minutes.

3. Rinse the membrane with pure (deionised) water and boil at 80^oC in a 2.4N aqueous solution of HCl for about 30 minutes. **(Gloves must be used; HCl is a highly corrosive acid)**

4. Rinse the membrane again with pure water and boil in pure water for about 30 minutes to completely swell the membrane. **(Hotplate is used to boil the membrane; carefully deal with the boiling water, do not move the plate with hot water, let it cool first and then move it)**

5. platinum-amine complex

- Prepare 0.2% platinum-amine complex ($Pt(NH_3)_4\ Cl_2$) (tetra-amine platinum chloride hydrate, 98%) add 1 ml of NH_4OH 30% to equalise the PH. Leave the solution for 3 hours, preferably for the next day.
- Immerse the membrane in the solution for 8 hours at room temperature slowly stirring the solution. The final amount of platinum deposited on the membrane must be about 3.75 mg/cm^2 for each face of the membrane surface. This produces a pair of porous electrodes on the surface of the membrane. **(Gloves must be used)**

6. Rinse the membrane again with pure water and immerse in a reducing solution consisting of 180 ml H_2O, and 2 ml $NaBH_4$ 5% in a water bath at 40 degrees C while stirring at low speed (150 RPM). **(Gloves must be used; this process must be done in a fume hood)**

- Add 2 ml $NaBH_4$ 5% every 30 minutes for about 3 and a half hours while gradually increasing the temperature to 60 degrees C
- At which point add 20 ml $NaBH_4$ 5% and stir the mixture for an additional one and a half hours.
- Rinse the membrane with pure water and store in a 0.5% solution of HCl for 1 hour, and store it in deionised water for the next day.

7. Reducing agents:

- Remove the membrane from the storage.

- Immerse the membrane in 0.5% HCl for 1 hour.
- Rinse the membrane again with pure water and immerse in a solution containing 300 ml H_2O, 0.2 grams $Pt(NH_3)_4Cl_2$, 6 ml $H_2NOH.HCl$ 5% (hydroxylamine hydrochloride, 99%), 3 ml $H_2NNH_2.H_2O$ 20% (hydrazine monohydrate, 98%), and 0.5 ml NH_4OH 30% (only NH_4OH for the first time of the secondary reduction) at 40 degrees C while stirring at low speed (approximately 60 RPM). **(Gloves must be used; this process must be done in a fume hood)**
- Add reducing agents consisting of 6 ml $H_2NOH.HCl$ 5% and 3 ml $H_2NNH_2.H_2O$ 20% every 30 minutes for 4 hours while gradually increasing the temperature to 60 degrees C **(Gloves must be used, Hot plate is used to heat the solution, do not move the plate with hot solution, let it cool first and then move it)**
- After the process is over, test the solution containing the membrane for any residual Pt by boiling 2 ml of the solution with 2 ml $NaBH_4$ 5%. If the colour of the mixture turns black, the addition of reducing agents must continue for a longer time. If no colour change is visually detected, the process is complete. **(Gloves must be used; Hot plate is used to heat the solution, do not move the plate with hot solution, let it cool first and then move it)**
- Note: Step 7 is part of the developing process to deposit more platinum in the polymer matrix.

8. Rinse the membrane again with pure water and then with 0.1 N NaOH solution to replace H+ cations in the membrane with Na+ cations overnight.

9. Repeat the process:

- Repeat Steps 7, and 8
- Rinse with pure water.
- When reduction is complete, rinse the membrane with pure water and then boil with 0.1N HCl solution for 30 min to remove any other cations in the membrane. **(Gloves must be used; HCl is a highly corrosive acid)**
- Store the membrane in pure water at room temperature.
- Clean the membrane in an ultrasonic cleaner for 5 seconds and removed
- Note: Step 9 repeats the developing process to increase the amount of platinum deposited. If one starts out with a higher concentration of platinum salt in step 7, it is possible to deposit sufficient platinum on the membrane on the first pass, thereby eliminating the need for step 11. However, this will increase the risk of oxidation as well as crowding phenomena on surfaces of the membrane in a short period.

2.2 Protocol B

1. Use sandpaper to rough both sides of the membrane, very gently (such as Norton 600A) (2sec/cm^2).

2. Clean the membrane in an ultrasonic water bath cleaner for about 10 minutes.

3. Rinse the membrane with pure (deionised) water and boil at 80^oC in a 2.4N aqueous solution of HCl for about 30 minutes. **(Gloves must be used; HCl is a highly corrosive acid)**

4. Rinse the membrane again with pure water and boil in pure water for about 30 minutes to completely swell the membrane. **(Hotplate is used to boil the membrane; carefully deal with the boiling water, do not move the plate with hot water, let it cool first and then move it)**

5. platinum-amine complex

- Prepare 0.2% platinum-amine complex ($Pt(NH_3)_4\ Cl_2$) (tetra-amine platinum chloride hydrate, 98%) add 1 ml of NH_4OH 30% to equalise the PH. Leave the solution for 3 hours, preferably for the next day.
- Immerse the membrane in the solution for 8 hours at room temperature slowly stirring the solution. The final amount of platinum deposited on the membrane must be about 3.75 mg/cm^2 for each face of the membrane surface. This produces a pair of porous electrodes on the surface of the membrane. **(Gloves must be used)**

6. Rinse the membrane again with pure water and immerse in a reducing solution consisting of 180 ml H_2O, and 2 ml $NaBH_4$ 5% in a water bath at 40 degrees C while stirring at low speed (150 RPM). **(Gloves must be used; this process must be done in a fume hood)**

- Add 2 ml $NaBH_4$ 5% every 30 minutes for about 3 and a half hours while gradually raise the temperature to 60 degrees C
- At which point add 20 ml $NaBH_4$ 5% and stir the mixture for an additional one and a half hours.
- Rinse the membrane with pure water and store in a 0.5% solution of HCl for 1 hour, and store it in deionised water for the next day.

7. Reducing agents:

- Remove the membrane from the storage.
- Immerse the membrane in 0.5% HCl for 1 hour.
- Rinse the membrane again with pure water and immerse in a solution containing 300 ml H_2O, 0.2 grams $Pt(NH_3)_4Cl_2$, 6 ml $H_2NOH.HCl$ 5% (hydroxylamine hydrochloride,

99%), 3 ml $H_2NNH_2.H_2O$ 20% (hydrazine monohydrate, 98%), and 0.5 ml NH_4OH 30% (only NH_4OH for the first time of the secondary reduction) at 40 degrees C while stirring at low speed (approximately 60 RPM). **(Gloves must be used; this process must be done in a fume hood)**

- Add reducing agents consisting of 6 ml $H_2NOH.HCl$ 5% and 3 ml $H_2NNH_2.H_2O$ 20% every 30 minutes for 4 hours while gradually increasing the temperature to 60 degrees C **(Gloves must be used, Hot plate is used to heat the solution, do not move the plate with hot solution, let it cool first and then move it)**
- After the process is over, test the solution containing the membrane for any residual Pt by boiling 2 ml of the solution with 2 ml $NaBH_4$ 5%. If the colour of the mixture turns black, the addition of reducing agents must continue for a longer time. If no colour change is visually detected, the process is complete. **(Gloves must be used; Hot plate is used to heat the solution, do not move the plate with hot solution, let it cool first and then move it)**
- Note: Step 7 is part of the developing process to deposit more platinum in the polymer matrix.

8. Repeat the process 7

9. Rinse with pure water

10. When reduction is complete, rinse the membrane with pure water and then boil with 0.1N HCl solution for 30 min to remove any other cations in the membrane. **(Gloves must be used; HCl is a highly corrosive acid)**

11. Rinse the membrane again with pure water and then with 0.1 N NaOH solution to replace H+ cations in the membrane with Na+ cations overnight.

- Store the membrane in pure water at room temperature.
- Clean the membrane in an ultrasonic cleaner for 5 seconds and removed
- Note: Step 8 repeats the developing process to increase the amount of platinum deposited. If one starts out with a higher concentration of platinum salt in step 7, it is possible to deposit sufficient platinum on the membrane on the first pass, thereby eliminating the need for step 11. However, this will increase the risk of oxidation as well as crowding phenomena on surfaces of the membrane in a short period.

2.3 Protocol C

1. Use sandpaper to rough both sides of the membrane, very gently (ultrafine 600) (2sec/cm^2).

2. Clean the membrane in an ultrasonic water bath cleaner for about 10 minutes.

3. Rinse the membrane with pure (deionised) water and boil at 80^oC in a 2.4N aqueous solution of HCl for about 30 minutes. **(Gloves must be used; HCl is a highly corrosive acid)**

4. Rinse the membrane again with pure water and boil in pure water for about 30 minutes to completely swell the membrane. **(Hotplate is used to boil the membrane; carefully deal with the boiling water, do not move the plate with hot water, let it cool first and then move it)**

5. platinum-amine complex

- Prepare 0.2% platinum-amine complex ($Pt(NH_3)_4\ Cl_2$) (tetra-amine platinum chloride hydrate, 98%) add 1 ml of NH_4OH 30% to equalise the PH. Leave the solution for 3 hours, preferably for the next day.
- Immerse the membrane in the solution for 8 hours at room temperature slowly stirring the solution. The final amount of platinum deposited on the membrane must be about 3.75 mg/cm^2 for each face of the membrane surface. This produces a pair of porous electrodes on the surface of the membrane. **(Gloves must be used)**

6. Rinse the membrane again with pure water and immerse in a reducing solution consisting of 180 ml H_2O, 0.5 ml NH_4OH 30%, and 2 ml $NaBH_4$ 5% in a water bath at 40 degrees C while stirring at low speed (150 RPM). **(Gloves must be used; this process must be done in a fume hood)**

- Add 2 ml $NaBH_4$ 5% every 30 minutes for about 3 and a half hours while gradually raise the temperature to 60 degrees C
- At which point add 20 ml $NaBH_4$ 5% and stir the mixture for an additional one and a half hours.
- Rinse the membrane with pure water and store in a 0.5% solution of HCl for the next day.

7. Reducing agents:

- Remove the membrane from the storage.
- Rinse the membrane again with pure water and immerse in a solution containing 300 ml H_2O, 0.2 grams $Pt(NH_3)_4Cl_2$, 6 ml $H_2NOH.HCl$ 5% (hydroxylamine hydrochloride, 99%), 3 ml $H_2NNH_2.H_2O$ 20% (hydrazine monohydrate, 98%), and 0.5 ml NH_4OH 30%

(only NH_4OH for the first time of the secondary reduction) at 40 degrees C while stirring at low speed (approximately 60 RPM). **(Gloves must be used; this process must be done in a fume hood)**

- Add reducing agents consisting of 6 ml $H_2NOH.HCl$ 5% and 3 ml $H_2NNH_2.H_2O$ 20% every 30 minutes for 4 hours while gradually increasing the temperature to 60 degrees C **(Gloves must be used, Hot plate is used to heat the solution, do not move the plate with hot solution, let it cool first and then move it)**
- After the process is over, test the solution containing the membrane for any residual Pt by boiling 2 ml of the solution with 2 ml $NaBH_4$ 5%. If the colour of the mixture turns black, the addition of reducing agents must continue for a longer time. If no colour change is visually detected, the process is complete. **(Gloves must be used; Hot plate is used to heat the solution, do not move the plate with hot solution, let it cool first and then move it)**
- Rinse with pure water

8. First half, repeat step 7 (put the membrane in 0.5% HCl for 30 min before repeating the process)

9. Use both halves now for the following steps:

10. Boil with 0.1N HCl solution for 30 min to remove any other cations in the membrane. **(Gloves must be used; HCl is a highly corrosive acid)**

11. Rinse the membrane again with pure water and then with 0.1 N NaOH solution to replace H+ cations in the membrane with Na+ cations overnight.

12. Clean the membrane in an ultrasonic cleaner for 5 seconds and removed

13. Store the membrane in pure water at room temperature.

2.4 Protocol D

1. Use sandpaper to rough both sides of the membrane, very gently (ultrafine 600) (2sec/cm^2).

2. Clean the membrane in an ultrasonic water bath cleaner for about 10 minutes.

3. Rinse the membrane with pure (deionised) water and boil at 80^oC in a 2.4N aqueous solution of HCl for about 30 minutes. **(Gloves must be used; HCl is a highly corrosive acid)**

4. Rinse the membrane again with pure water and boil in pure water for about 30 minutes to completely swell the membrane. **(Hotplate is used to boil the membrane; carefully deal with the boiling water, do not move the plate with hot water, let it cool first and then move it)**

5. platinum-amine complex: primary coating

- Prepare 0.2% platinum-amine complex ($Pt(NH_3)_4\ Cl_2$) (tetra-amine platinum chloride hydrate, 98%) add 1 ml of NH_4OH 30% to equalise the PH. Leave the solution for 3 hours, preferably for the next day.
- Immerse the membrane in the solution for 8 hours at room temperature slowly stirring the solution. The final amount of platinum deposited on the membrane must be about 3.75 mg/cm^2 for each face of the membrane surface. This produces a pair of porous electrodes on the surface of the membrane. **(Gloves must be used)**

6. Reducing process:

Rinse the membrane again with pure water and immerse in a reducing solution consisting of 180 ml H_2O, 0.5 ml NH_4OH 30%, and 2 ml $NaBH_4$ 5% in a water bath at 40 degrees C while stirring at low speed (150 RPM). **(Gloves must be used; this process must be done in a fume hood)**

- Add 2 ml $NaBH_4$ 5% every 30 minutes for about 3 and a half hours while gradually raise the temperature to 60 degrees C
- At which point add 20 ml $NaBH_4$ 5% and stir the mixture for an additional one and a half hours.
- Rinse the membrane with pure water and store in a 0.5% solution of HCl for the next day.

7. Secondary coating:

- Remove the membrane from the storage.

- Rinse the membrane again with pure water and immerse in a solution containing 300 ml H_2O, 0.2 grams $Pt(NH_3)_4Cl_2$, 6 ml $H_2NOH.HCl$ 5% (hydroxylamine hydrochloride, 99%), 3 ml $H_2NNH_2.H_2O$ 20% (hydrazine monohydrate, 98%), and 0.5 ml NH_4OH 30% (only NH_4OH for the first time of the secondary reduction) at 40 degrees C while stirring at low speed (approximately 60 RPM). **(Gloves must be used; this process must be done in a fume hood)**
- Add reducing agents consisting of 6 ml $H_2NOH.HCl$ 5% and 3 ml $H_2NNH_2.H_2O$ 20% every 30 minutes for 4 hours while gradually increasing the temperature to 60 degrees C **(Gloves must be used, Hot plate is used to heat the solution, do not move the plate with hot solution, let it cool first and then move it)**
- After the process is over, test the solution containing the membrane for any residual Pt by boiling 2 ml of the solution with 2 ml $NaBH_4$ 5%. If the colour of the mixture turns black, the addition of reducing agents must continue for a longer time. If no colour change is visually detected, the process is complete. **(Gloves must be used; Hot plate is used to heat the solution, do not move the plate with hot solution, let it cool first and then move it)**
- Rinse with pure water

8. Repeat step 7

9. Boil with 0.1N HCl solution for 30 min to remove any other cations in the membrane. **(Gloves must be used; HCl is a highly corrosive acid)**

10. Rinse the membrane again with pure water and then with 0.1 N NaOH solution to replace H+ cations in the membrane with Na+ cations overnight.

11. Clean the membrane in an ultrasonic cleaner for 5 seconds and removed

12. Store the membrane in pure water at room temperature.

2.5 Protocol E

1. Use sandpaper to rough both sides of the membrane, very gently (ultrafine 600) (2sec/cm^2).

2. Clean the membrane in an ultrasonic water bath cleaner for about 10 minutes.

3. Rinse the membrane with pure (deionised) water and boil at 80^oC in a 2.4N aqueous solution of HCl for about 30 minutes. **(Gloves must be used; HCl is a highly corrosive acid)**

4. Rinse the membrane again with pure water and boil in pure water for about 30 minutes to completely swell the membrane. **(Hotplate is used to boil the membrane; carefully deal with the boiling water, do not move the plate with hot water, let it cool first and then move it)**

5. Prepare 0.2 g of tetraamine palladium (II) chloride in 100 ml water and leave the membrane there for 2h before immersing the membrane in Pt solution.

6. platinum-amine complex: primary coating

- Prepare 0.2% platinum amine complex ($Pt(NH_3)_4\ Cl_2$) (tetraamine platinum chloride hydrate, 98%) add 1 ml of NH_4OH 30% to equalise the PH. Leave the solution for 3 hours, preferably for the next day.
- Immerse the membrane in the solution for 8 hours at room temperature slowly stirring the solution. The final amount of platinum deposited on the membrane must be about 3.75 mg/cm^2 for each face of the membrane surface. This produces a pair of porous electrodes on the surface of the membrane. **(Gloves must be used)**

7. Reducing process:

Rinse the membrane again with pure water and immerse in a reducing solution consisting of 180 ml H_2O, 0.5 ml NH_4OH 30%, and 2 ml $NaBH_4$ 5% in a water bath at 40 degrees C while stirring at low speed (150 RPM). **(Gloves must be used; this process must be done in a fume hood)**

- Add 2 ml $NaBH_4$ 5% every 30 minutes for about 3 and a half hours while gradually raise the temperature to 60 degrees C
- At which point add 20 ml $NaBH_4$ 5% and stir the mixture for an additional one and a half hours.
- Rinse the membrane with pure water and store in a 0.5% solution of HCl for the next day.

8. Secondary coating:

- Remove the membrane from the storage.
- Rinse the membrane again with pure water and immerse in a solution containing 300 ml H_2O, 0.2 grams $Pt(NH_3)_4Cl_2$, 6 ml $H_2NOH.HCl$ 5% (hydroxylamine hydrochloride, 99%), 3 ml $H_2NNH_2.H_2O$ 20% (hydrazine monohydrate, 98%), and 0.5 ml NH_4OH 30% (only NH_4OH for the first time of the secondary reduction) at 40 degrees C while stirring at low speed (approximately 60 RPM). **(Gloves must be used; this process must be done in a fume hood)**
- Add reducing agents consisting of 6 ml $H_2NOH.HCl$ 5% and 3 ml $H_2NNH_2.H_2O$ 20% every 30 minutes for 4 hours while gradually increasing the temperature to 60 degrees C **(Gloves must be used, Hot plate is used to heat the solution, do not move the plate with hot solution, let it cool first and then move it)**
- After the process is over, test the solution containing the membrane for any residual Pt by boiling 2 ml of the solution with 2 ml $NaBH_4$ 5%. If the colour of the mixture turns black, the addition of reducing agents must continue for a longer time. If no colour change is visually detected, the process is complete. **(Gloves must be used; Hot plate is used to heat the solution, do not move the plate with hot solution, let it cool first and then move it)**
- Rinse with pure water

9. Repeat step 7 twice

10. Boil with 0.1N HCl solution for 30 min to remove any other cations in the membrane. **(Gloves must be used; HCl is a highly corrosive acid)**

11. Rinse the membrane again with pure water and then with 0.1 N NaOH solution to replace H+ cations in the membrane with Na+ cations overnight.

12. Clean the membrane in an ultrasonic cleaner for 5 seconds and removed

13. Store the membrane in pure water at room temperature.

2.6 Protocol F

1. Use sandpaper to rough both sides of the membrane, very gently (ultrafine 600) (2sec/cm^2).

2. Clean the membrane in an ultrasonic water bath cleaner for about 10 minutes.

3. Rinse the membrane with pure (deionised) water and boil at 80^oC in a 2.4N aqueous solution of HCl for about 30 minutes.

4. Rinse the membrane again with pure water and boil in pure water for about 30 minutes to completely swell the membrane.

5. platinum-amine complex: primary coating

- Prepare 0.2% platinum amine complex ($Pt(NH_3)_4\ Cl_2$) (tetraamine platinum chloride hydrate, 98%) add 5 ml of NH_4OH 30% to equalise the PH. Leave the solution for 3 hours, preferably for the next day.
- Immerse the membrane in the solution for 8 hours at room temperature slowly stirring the solution. The final amount of platinum deposited on the membrane must be about 3.75 mg/cm^2 for each face of the membrane surface. This produces a pair of porous electrodes on the surface of the membrane.

6. Reducing process:

Rinse the membrane again with pure water and immerse in a reducing solution consisting of 180 ml H_2O, 5 ml NH_4OH 30%, and 2 ml $NaBH_4$ 5% in a water bath at 40 degrees C while stirring at low speed (150 RPM). **(Gloves must be used; this process must be done in a fume hood)**

- Add 2 ml $NaBH_4$ 5% every 30 minutes for about 3 and a half hours while gradually raise the temperature to 60 degree
- At which point add 20 ml $NaBH_4$ 5% and stir the mixture for an additional one and a half hours.
- Rinse the membrane with pure water and store in a 0.5% solution of HCl overnight.

7. Repeat step 6.

8. Secondary coating:

- Remove the membrane from the storage.
- Rinse the membrane again with pure water and immerse in a solution containing 300 ml H_2O, 0.2 grams $Pt(NH_3)_4Cl_2$, 6 ml $H_2NOH.HCl$ 5% (hydroxylamine hydrochloride, 99%), 3 ml $H_2NNH_2.H_2O$ 20% (hydrazine monohydrate, 98%), and 5 ml NH_4OH 30%

(only NH_4OH for the first time of the secondary reduction) at 40 degrees C while stirring at low speed (approximately 60 RPM).

- Add reducing agents consisting of 6 ml $H_2NOH.HCl$ 5% and 3 ml $H_2NNH_2.H_2O$ 20% every 30 minutes for 4 hours while gradually increasing the temperature to 60 degree
- After the process is over, test the solution containing the membrane for any residual Pt by boiling 2 ml of the solution with 2 ml $NaBH_4$ 5%. If the colour of the mixture turns black, the addition of reducing agents must continue for a longer time. If no colour change is visually detected, the process is complete.
- Rinse with pure water

9. Repeat step 7

10. Boil with 0.1N HCl solution for 30 min to remove any other cations in the membrane.

11. Rinse the membrane again with pure water and then with 0.1 N NaOH solution to replace H+ cations in the membrane with Na+ cations overnight.

12. Clean the membrane in an ultrasonic cleaner for 5 seconds and removed

13. Store the membrane in pure water at room temperature.

2.7 Protocol G

1. Use sandpaper to rough both sides of the membrane, very gently (ultrafine 600) (2sec/cm^2).

2. Clean the membrane in an ultrasonic water bath cleaner for about 10 minutes.

3. Rinse the membrane with pure (deionised) water and boil at 80^oC in a 2.4N aqueous solution of HCl for about 30 minutes.

4. Rinse the membrane again with pure water and boil in pure water for about 30 minutes to completely swell the membrane.

5. Palladium-amine complex: primary coating

- Prepare 0.2% Tetraamminepalladium(II) chloride monohydrate add 5 ml of NH_4OH 30% to equalise the PH. Leave the solution for 3 hours, preferably for the next day.
- Immerse the membrane in the solution for 8 hours at room temperature slowly stirring the solution. The final amount of Palladium deposited on the membrane must be about 3.75 mg/cm^2 for each face of the membrane surface. This produces a pair of porous electrodes on the surface of the membrane.

6. Reducing process:

Rinse the membrane again with pure water and immerse in a reducing solution consisting of 180 ml H_2O, 5 ml NH_4OH 30%, and 2 ml $NaBH_4$ 5% in a water bath at 40 degrees C while stirring at low speed (150 RPM).

- Add 2 ml $NaBH_4$ 5% every 30 minutes for about 3 and a half hours while gradually raise the temperature to 60 degree
- At which point add 20 ml $NaBH_4$ 5% and stir the mixture for an additional one and a half hours.
- Rinse the membrane with pure water and store in a 0.5% solution of HCl for 4 hours, and store it in deionised water for the next day.

7. Repeat steps 5 and 6.

8. Secondary coating:

- Remove the membrane from the storage.
- Immerse the membrane in 0.5% HCl for 1 hour.
- Rinse the membrane again with pure water and immerse in a solution containing 300 ml H_2O, 0.2 grams Tetraamminepalladium(II) chloride monohydrate, 6 ml $H_2NOH.HCl$

5% (hydroxylamine hydrochloride, 99%), 3 ml $H_2NNH_2.H_2O$ 20% (hydrazine monohydrate, 98%), and 5 ml NH_4OH 30% (only NH_4OH for the first time of the secondary reduction) at 40 degrees C while stirring at low speed (approximately 60 RPM).

- Add reducing agents consisting of 6 ml $H_2NOH.HCl$ 5% and 3 ml $H_2NNH_2.H_2O$ 20% every 30 minutes for 4 hours while gradually increasing the temperature to 60 degree
- After the process is over, test the solution containing the membrane for any residual Pt by boiling 2 ml of the solution with 2 ml $NaBH_4$ 5%. If the colour of the mixture turns black, the addition of reducing agents must continue for a longer time. If no colour change is visually detected, the process is complete.
- Rinse with pure water

9. Repeat step 7

10. Boil with 0.1N HCl solution for 30 min to remove any other cations in the membrane.

11. Rinse the membrane again with pure water and then with 0.1 N NaOH solution to replace H+ cations in the membrane with Na+ cations overnight.

12. Clean the membrane in an ultrasonic cleaner for 5 seconds and removed

13. Store the membrane in pure water at room temperature.

2.8 Protocol H

1. Use sandpaper to rough both sides of the membrane, very gently (ultrafine 600) (2sec/cm^2).

2. Clean the membrane in an ultrasonic water bath cleaner for about 10 minutes.

3. Rinse the membrane with pure (deionised) water and boil at 80^oC in a 2.4N aqueous solution of HCl for about 30 minutes.

4. Rinse the membrane again with pure water and boil in pure water for about 30 minutes to completely swell the membrane.

5. platinum-amine complex: primary coating

- Prepare 0.2% platinum amine complex ($Pt(NH_3)_4\ Cl_2$) (tetraamine platinum chloride hydrate, 98%) add 5 ml of NH_4OH 30% to equalise the PH. Leave the solution for 3 hours, preferably for the next day.
- Immerse the membrane in the solution for 8 hours at room temperature slowly stirring the solution. The final amount of platinum deposited on the membrane must be about 3.75 mg/cm^2 for each face of the membrane surface. This produces a pair of porous electrodes on the surface of the membrane.

6. Reducing process:

Rinse the membrane again with pure water and immerse in a reducing solution consisting of 180 ml H_2O, 5 ml NH_4OH 30%, and 2 ml $NaBH_4$ 5% in a water bath at 40 degrees C while stirring at low speed (150 RPM). **(Gloves must be used; this process must be done in a fume hood)**

- Add 2 ml $NaBH_4$ 5% every 30 minutes for about 3 and a half hours while gradually raise the temperature to 60 degree
- At which point add 20 ml $NaBH_4$ 5% and stir the mixture for an additional one and a half hours.
- Rinse the membrane with pure water and store in a 0.5% solution of HCl for 4 hours, and store it in deionised water for the next day.

7. Repeat steps 5 and 6.

8. Secondary coating:

- Remove the membrane from the storage.
- Immerse the membrane in 0.5% HCl for 1 hour.

- Rinse the membrane again with pure water and immerse in a solution containing 300 ml H_2O, 0.2 grams $Pt(NH_3)_4Cl_2$, 6 ml $H_2NOH.HCl$ 5% (hydroxylamine hydrochloride, 99%), 3 ml $H_2NNH_2.H_2O$ 20% (hydrazine monohydrate, 98%), and 5 ml NH_4OH 30% (only NH_4OH for the first time of the secondary reduction) at 40 degrees C while stirring at low speed (approximately 60 RPM).
- Add reducing agents consisting of 6 ml $H_2NOH.HCl$ 5% and 3 ml $H_2NNH_2.H_2O$ 20% every 30 minutes for 4 hours while gradually increasing the temperature to 60 degree
- After the process is over, test the solution containing the membrane for any residual Pt by boiling 2 ml of the solution with 2 ml $NaBH_4$ 5%. If the colour of the mixture turns black, the addition of reducing agents must continue for a longer time. If no colour change is visually detected, the process is complete.
- Rinse with pure water

9. Repeat step 7

10. Boil with 0.1N HCl solution for 30 min to remove any other cations in the membrane.

11. Rinse the membrane again with pure water and then with 0.1 N NaOH solution to replace H+ cations in the membrane with Na+ cations overnight.

12. Clean the membrane in an ultrasonic cleaner for 5 seconds and removed

13. Store the membrane in pure water at room temperature.

11.2 Chemical Preparation

Name	Required	How to prepare
HCl (Hydrogen chloride) 36N	2.4N- 100ml	Add 20.256 mL of HCl solution to 25 mL deionised water. Adjust the final volume of solution to 100 mL with deionised water
HCl (Hydrogen chloride) 36N	0.5% - 100 ml	Add 1.38 ml of 36%HCl to 80 ml water and then continue adding water to reach 100 ml
HCl (Hydrogen chloride) 36N	0.1N -100 ml	Add 0.844 mL of HCl solution to 25 mL deionised water. Adjust the final volume of solution to 100 mL with deionised water
NaOH (Sodium hydroxide)	0.1 N -100 ml	0.4 g of NaOH per 100 ml
$Pd(NH_3)4Cl_2 \cdot H_2O$ (Tetra ammine palladium(II) chloride monohydrate) 99.99% - powder	0.2% - 100 ml	Add 0.2 g $Pd(NH_3)4Cl_2 \cdot H_2O$ to 90 ml water and then continue adding water to reach 100 ml
$(Pt(NH_3)_4\ Cl_2)$ (tetra-amine platinum chloride hydrate	0.2% - 100 ml	Add 0.2 g $Pt(NH_3)_4Cl_2$ to 90 ml water and then continue adding water to reach 100 ml
NH_4OH)Ammonium hydroxide) 30% Liquid	30% - 10 ml	ready
$NaBH_4$ (Sodium borohydride) Powder	5% - 50 ml	Add 2.5 g NaBH4 to 40 ml water and then continue adding water to reach 50 ml
$H_2NOH.HCl$ (Hydroxylamine hydrochloride) 99% - crystalline	5% - 100 ml	Add 5 g of H2NOH.HCl to 80 ml water and then continue adding water to reach 100 ml
$H_2NNH_2.H_2O$ (Hydrazine monohydrate) 65% - Liquid	20% - 50 ml	Add 15.38 ml of $H_2NNH_2.H_2O$ to 30 ml water and then continue adding water to 50 ml

Table 11.1 Chemicals preparation

11.3 Top Surface Scans

Figure 11.1 shows all top surface scanning images of Commercial 1 IPMC under 6 different magnifications.

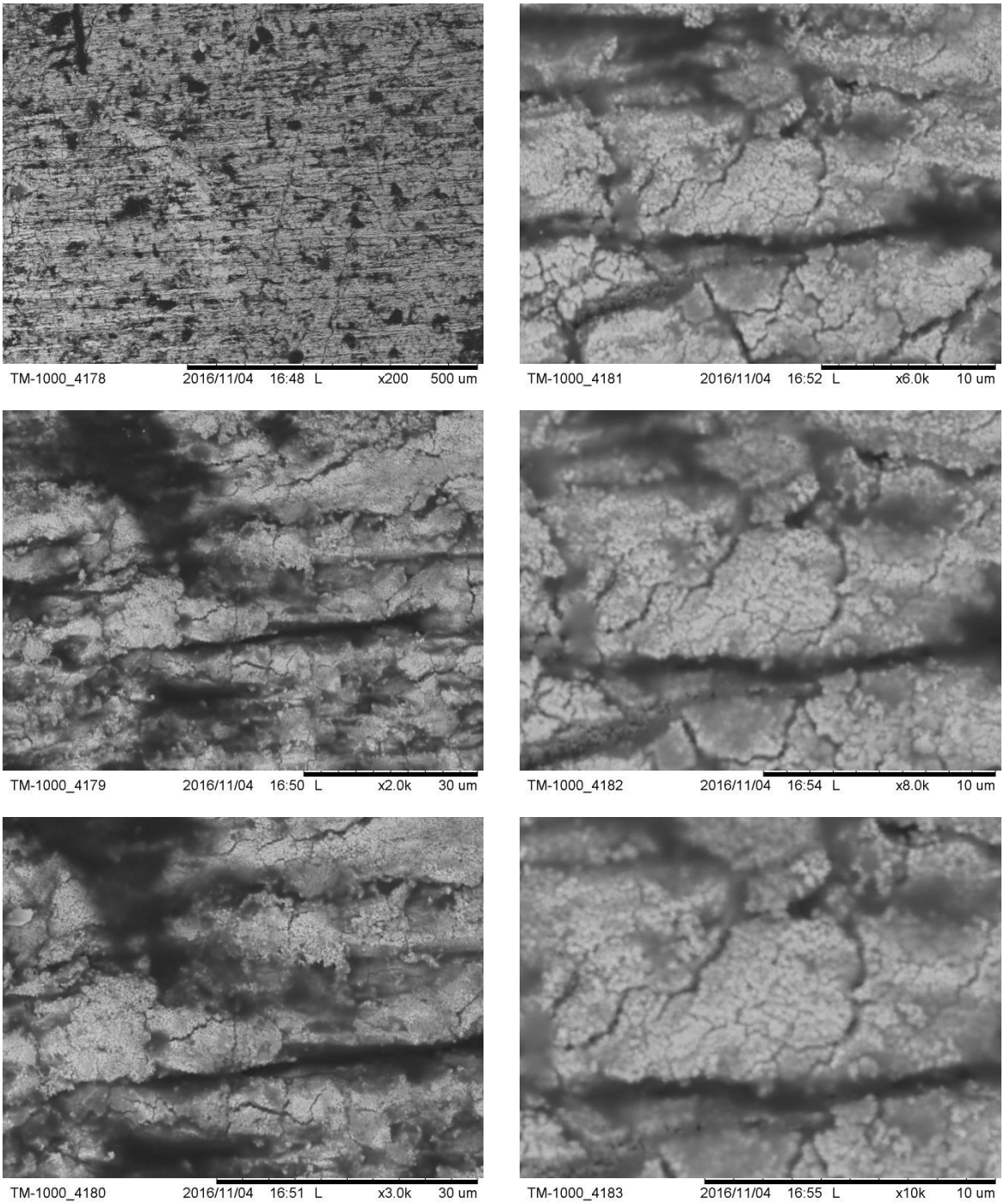

Figure 11.1 SEM images of Commercial 1

Figure 11.2 shows all top surface scanning images of Commercial 2 IPMC under 6 different magnifications.

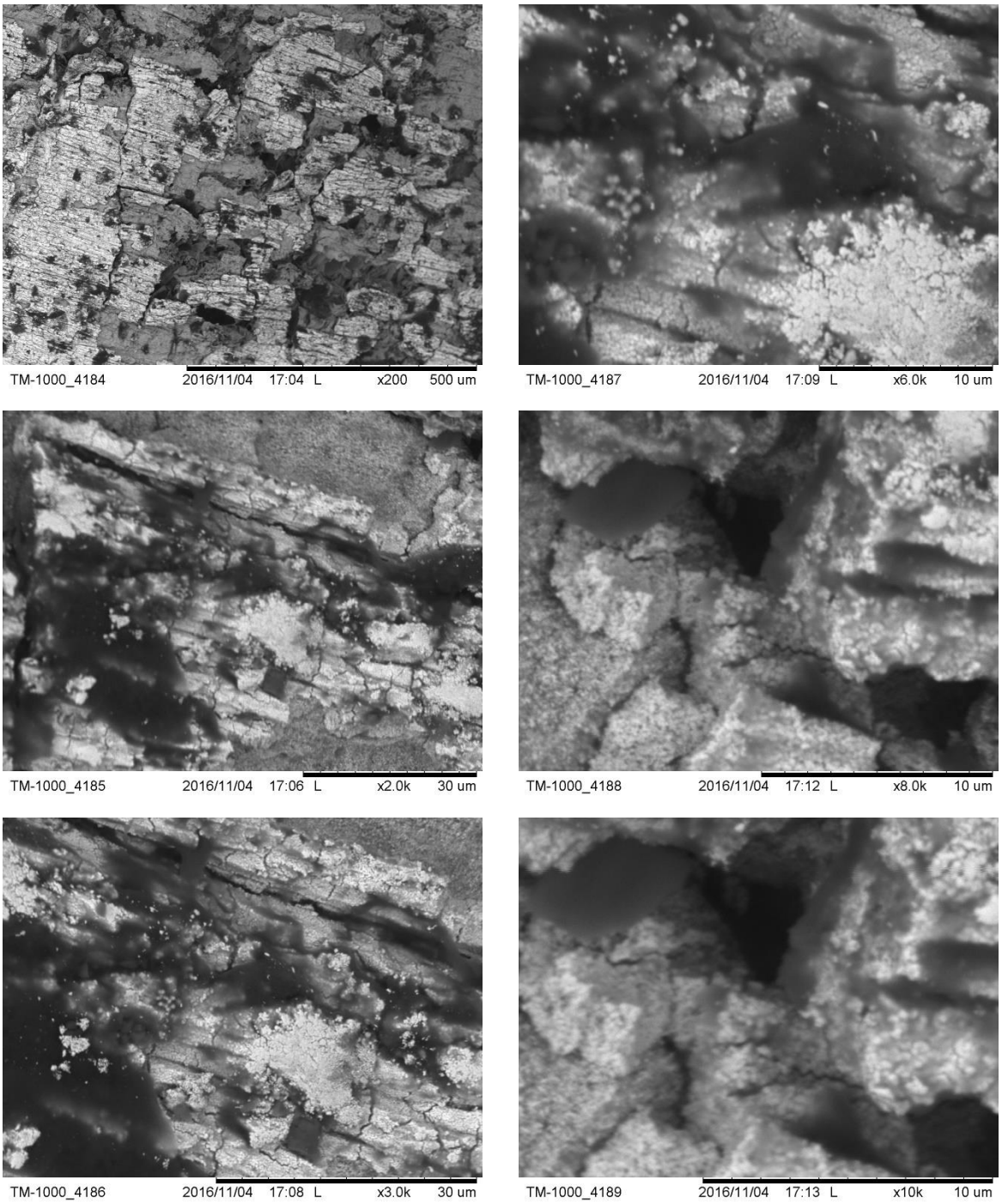

Figure 11.2 SEM images of Commercial 2

Figure 11.3 shows all top surface scanning images of Commercial 3 IPMC under 6 different magnifications.

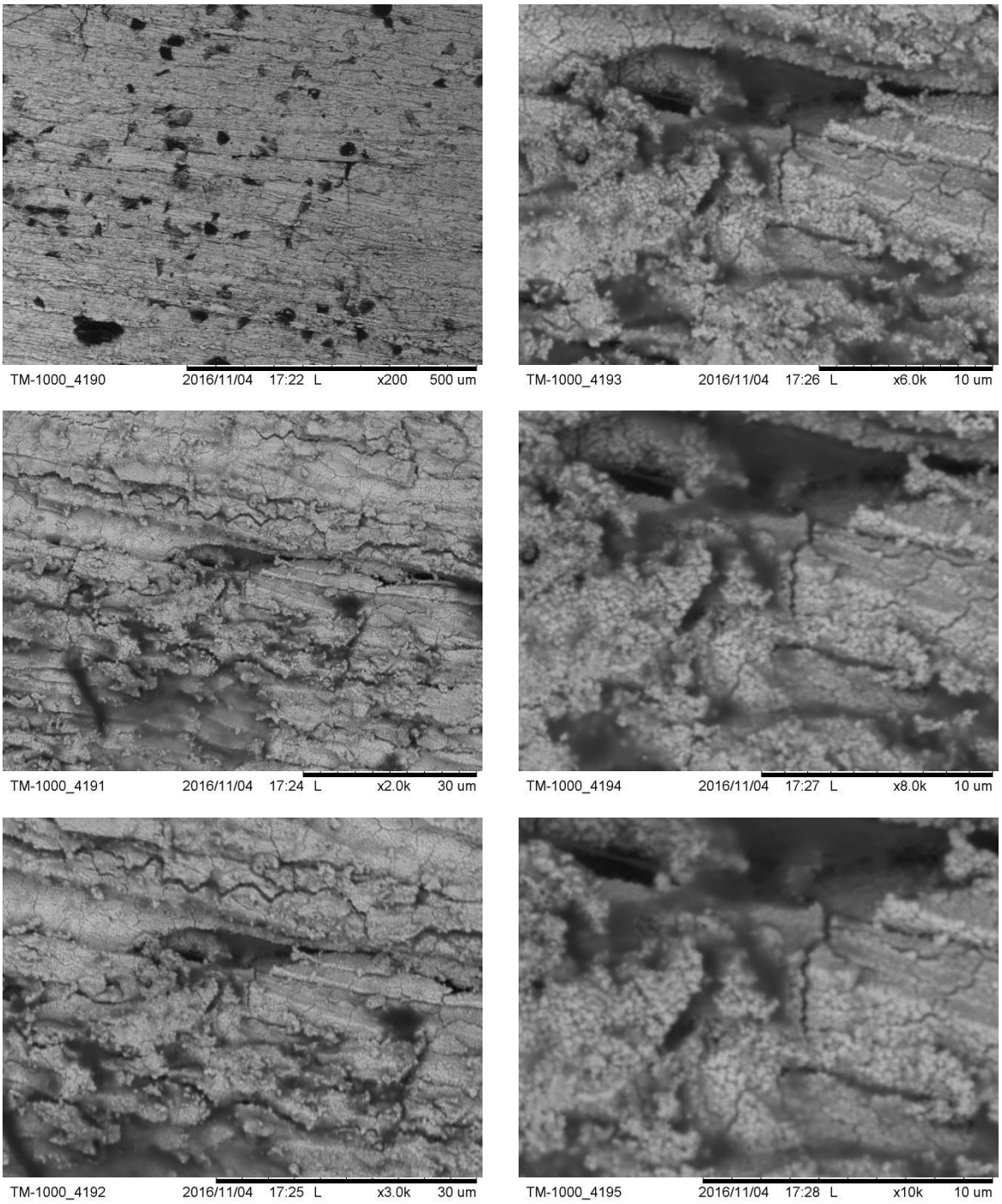

Figure 11.3 SEM images of Commercial 3

Figure 11.4 shows all top surface scanning images of Commercial 4 IPMC under 6 different magnifications.

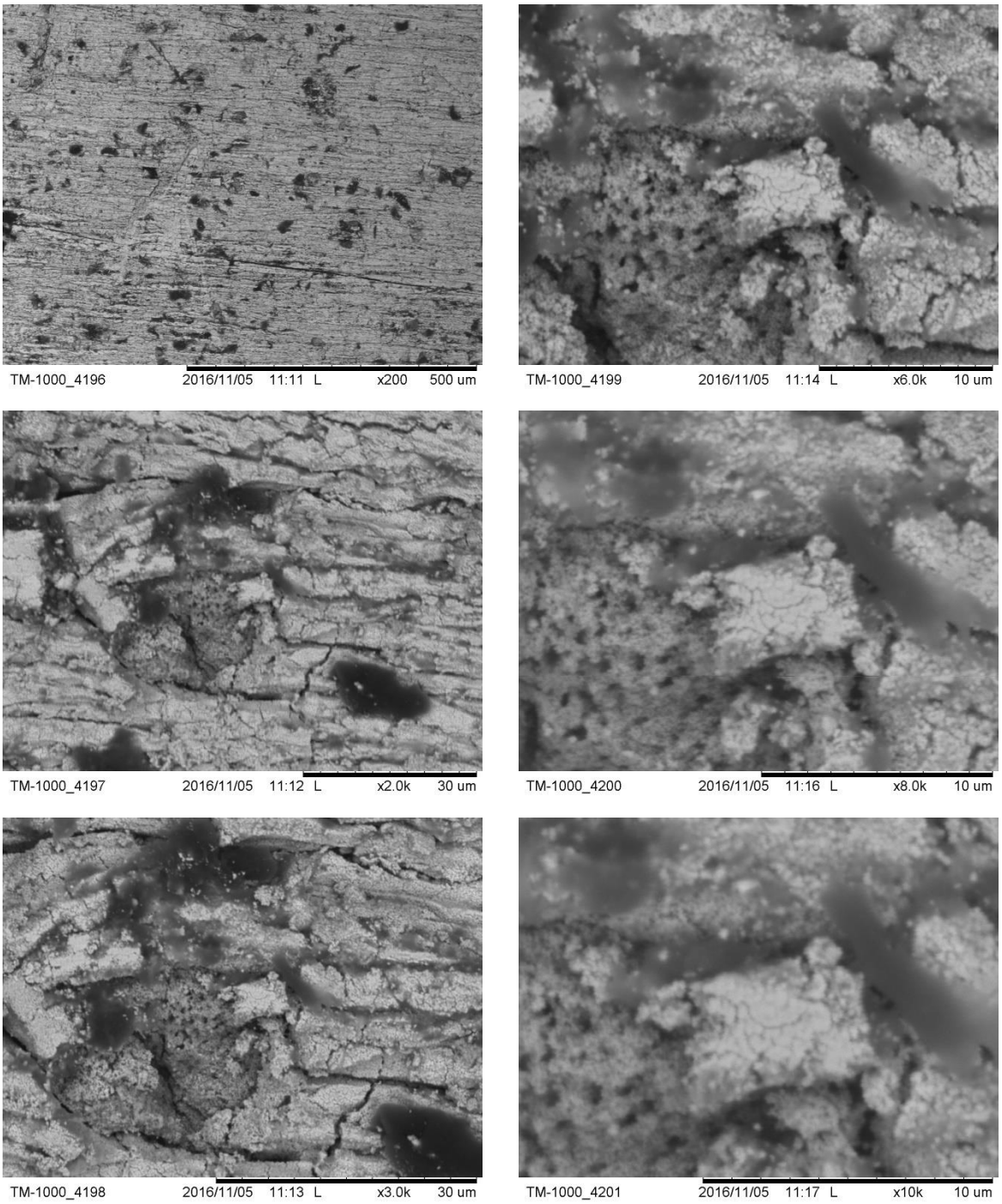

Figure 11.4 SEM images of Commercial 4

Figure 11.5 shows all top surface scanning images of Commercial 5 IPMC under 6 different magnifications.

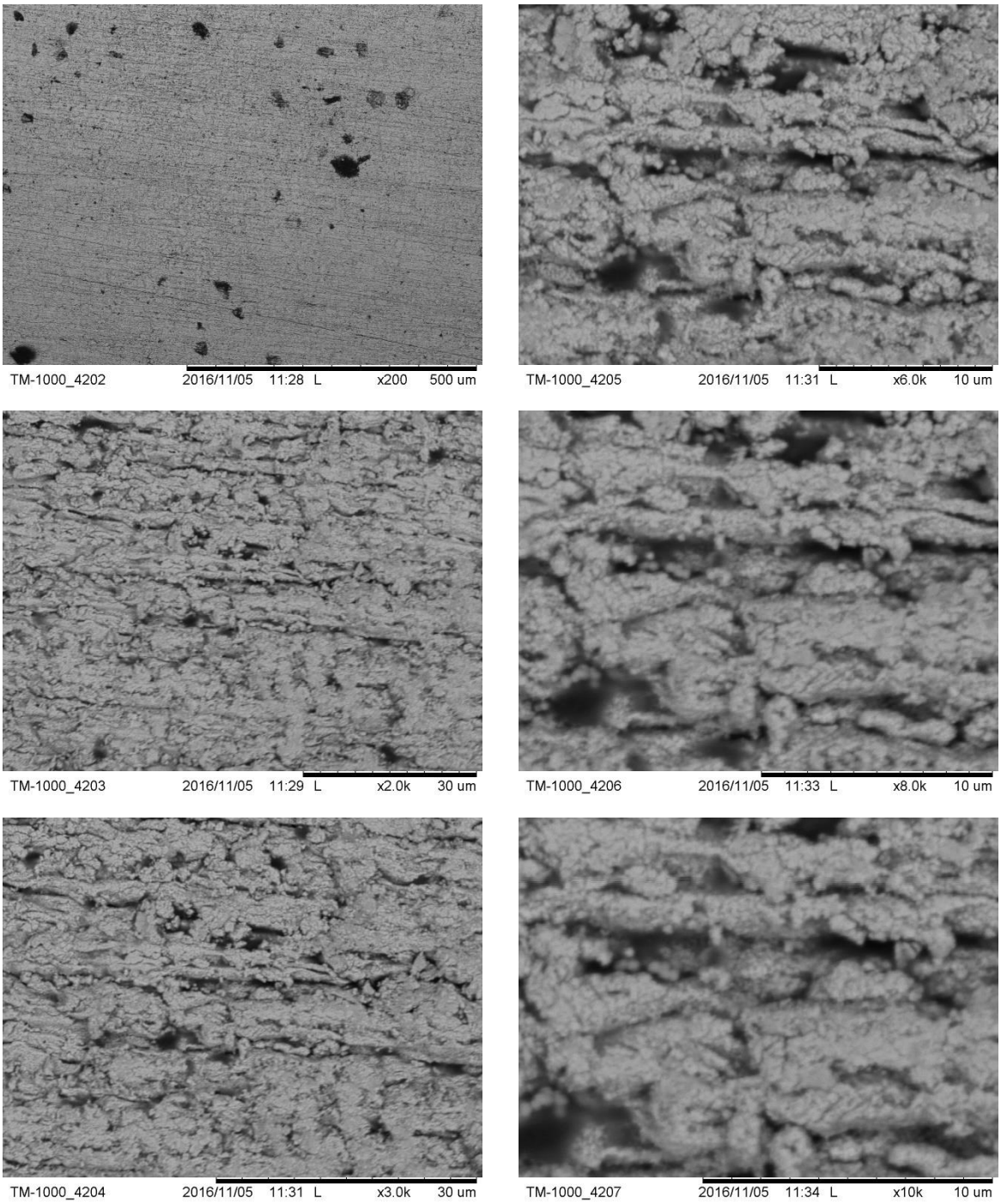

Figure 11.5 SEM images of Commercial 5

Figure 11.6 shows all top surface scanning images of Commercial 6 IPMC under 6 different magnifications.

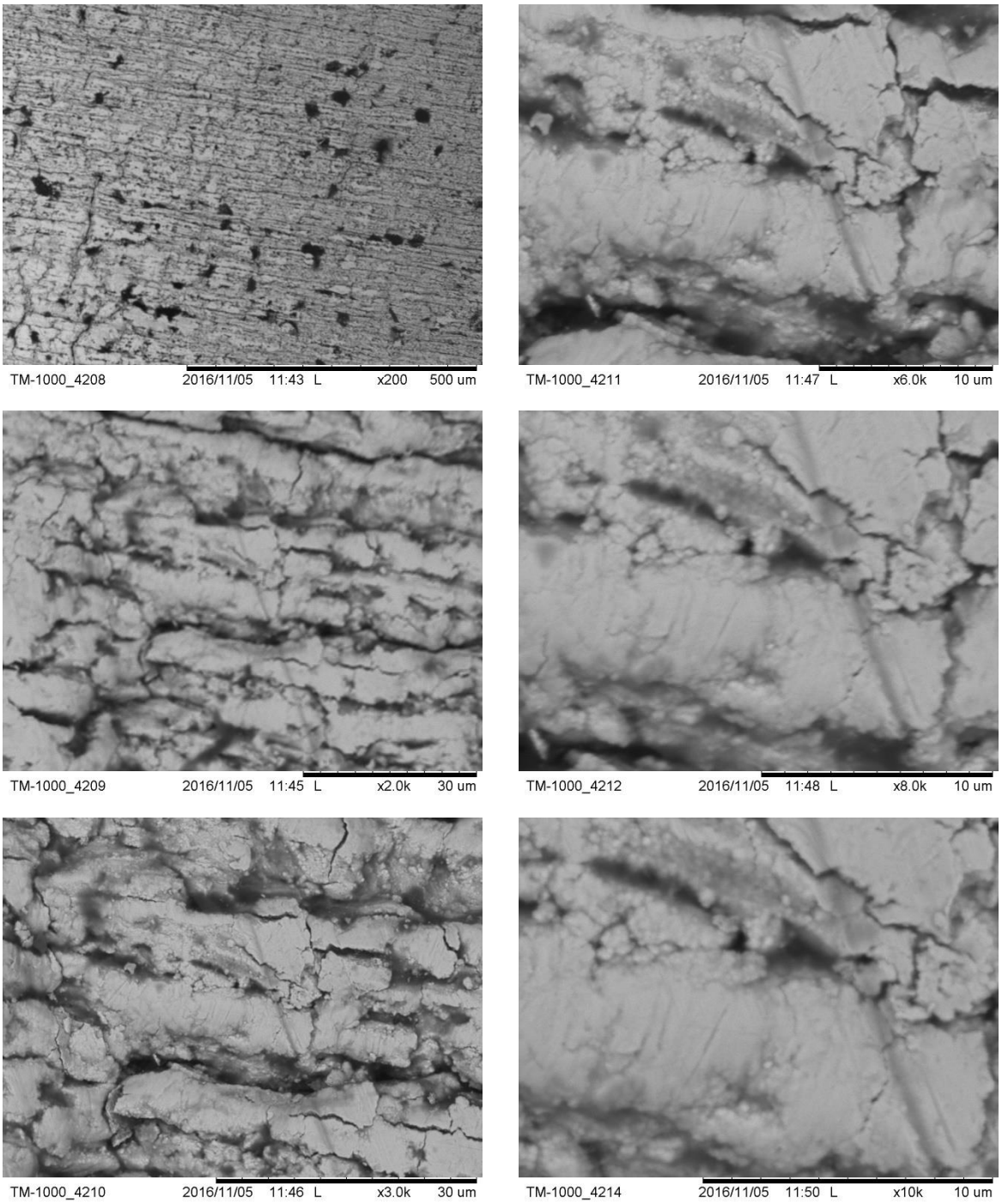

Figure 11.6 SEM images of Commercial 6

Figure 11.7 shows all top surface scanning images of Strathclyde 1 IPMC under 6 different magnifications.

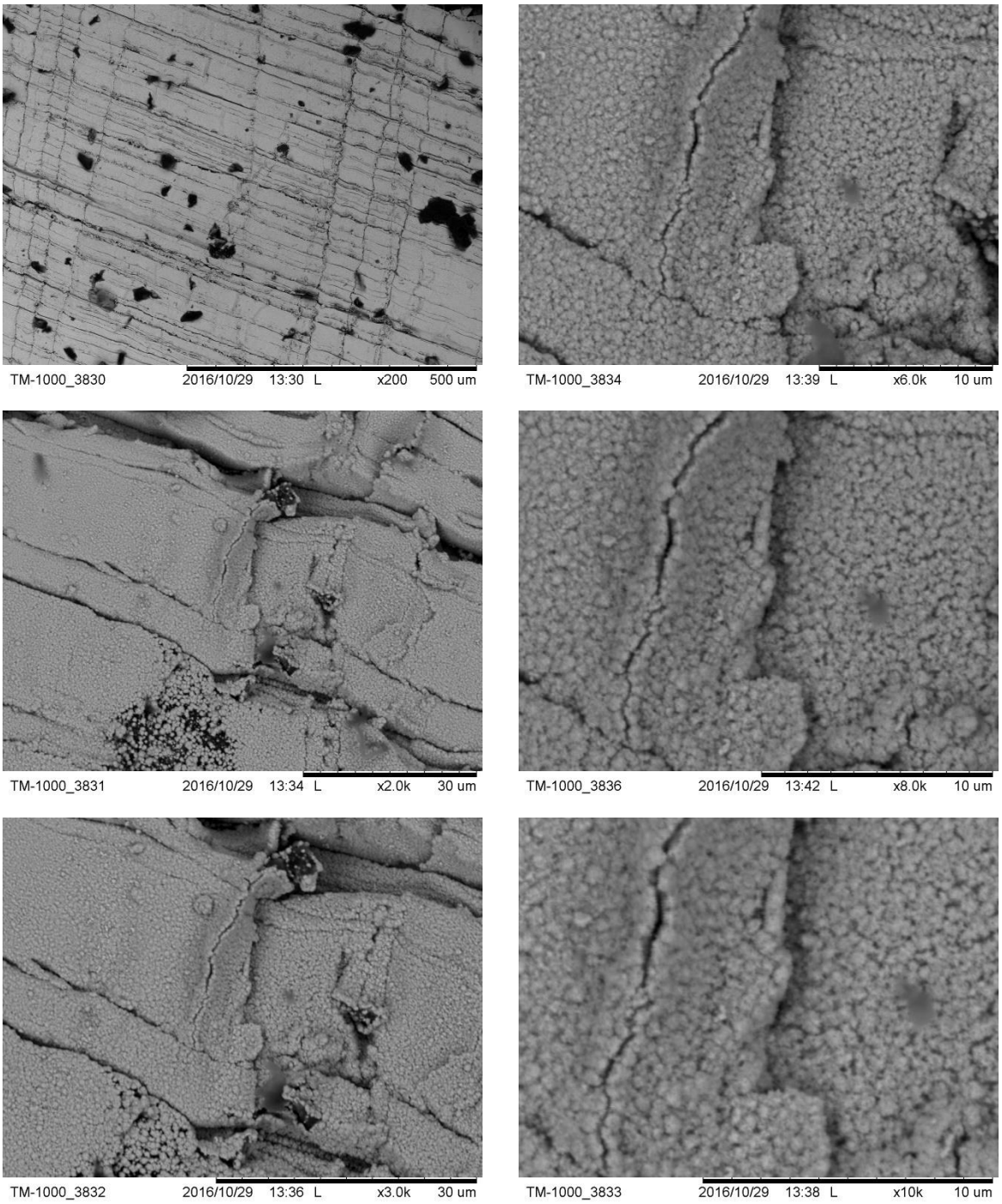

Figure 11.7 SEM images of Strathclyde 1

Figure 11.8 shows all top surface scanning images of Strathclyde 2 IPMC under 6 different magnifications.

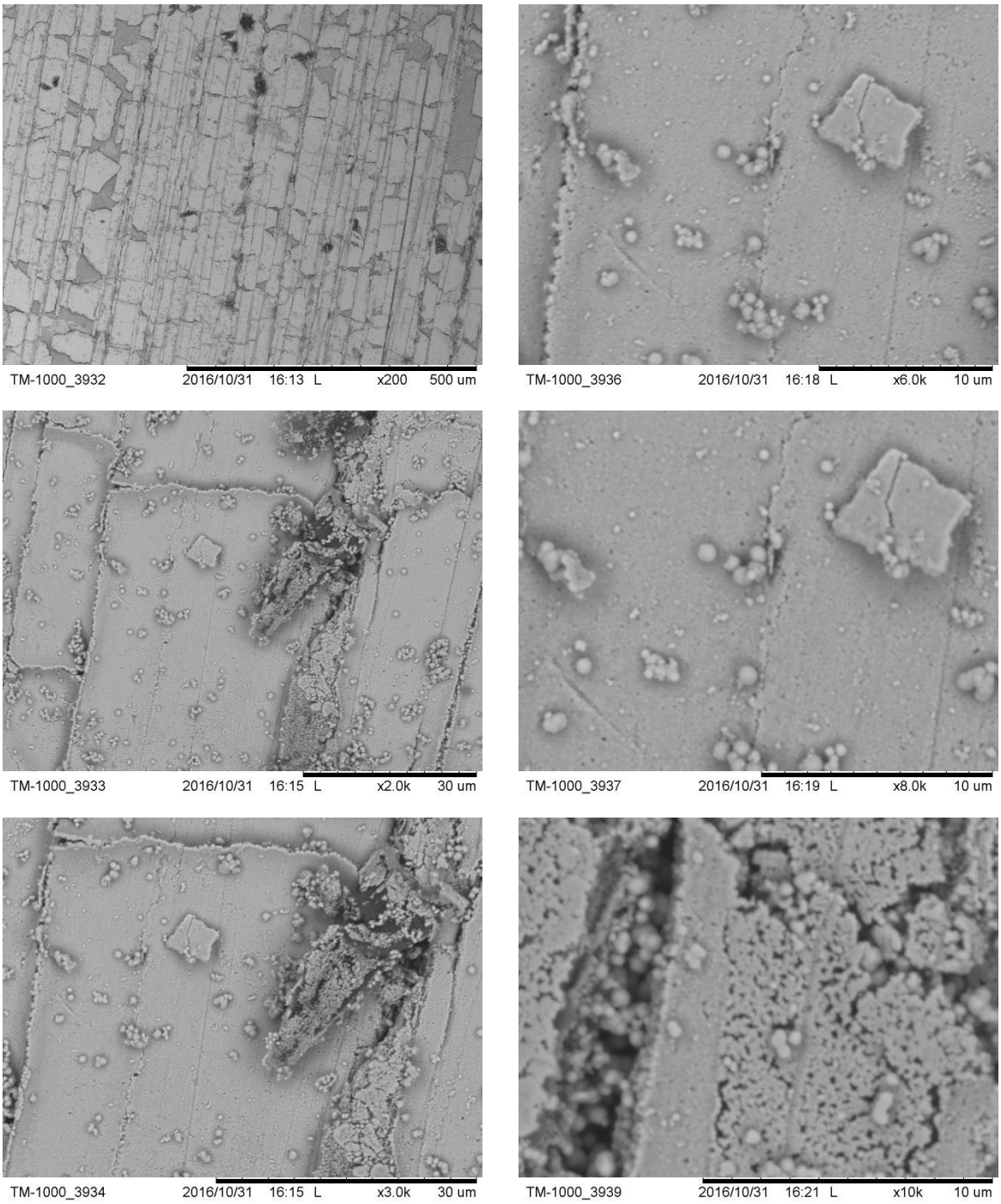

Figure 11.8 SEM images of Strathclyde 2

Figure 11.9 shows all top surface scanning images of Strathclyde 3 IPMC under 6 different magnifications.

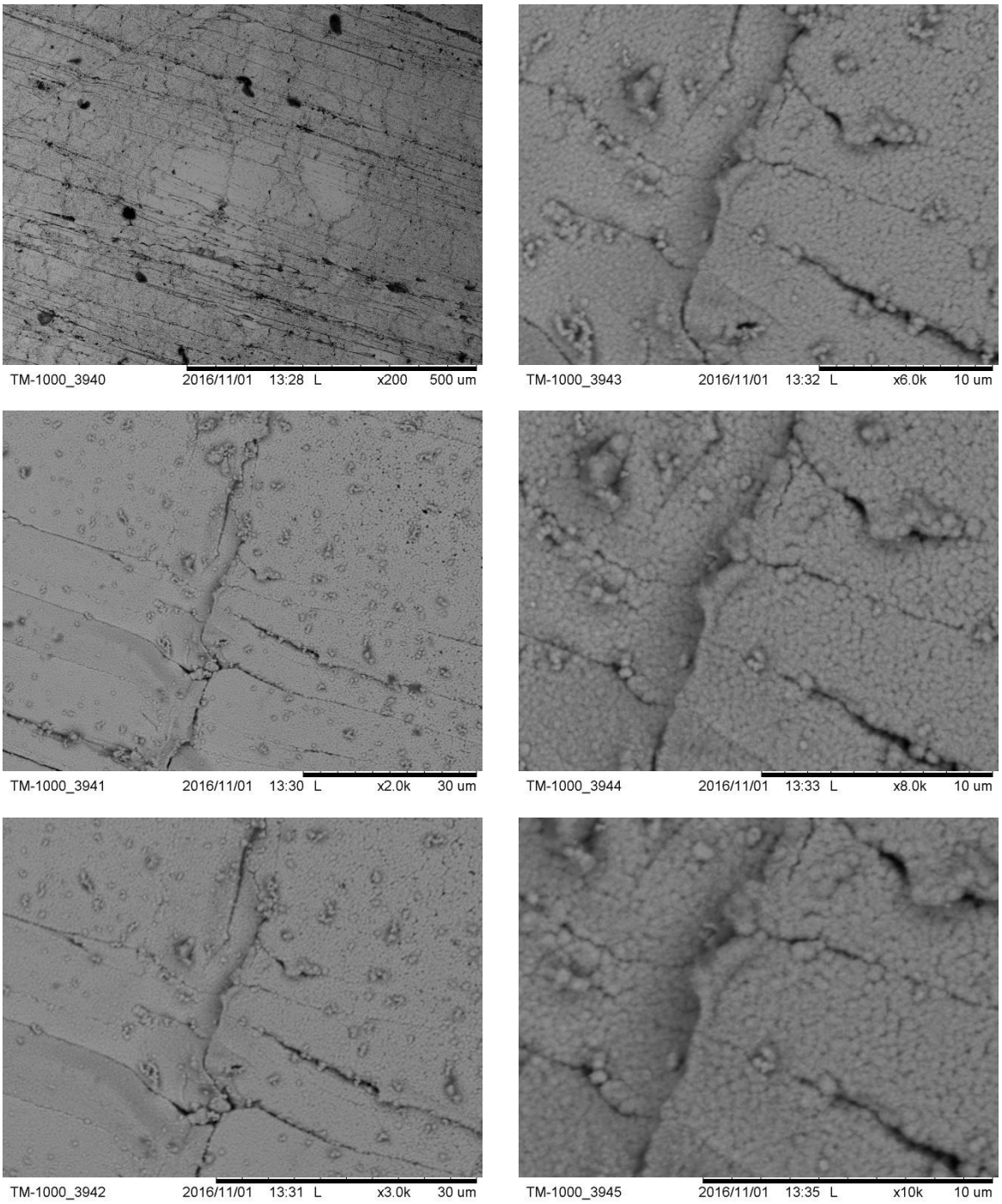

Figure 11.9 SEM images of Strathclyde 3

Figure 11.10 shows all top surface scanning images of Strathclyde 4 IPMC under 6 different magnifications.

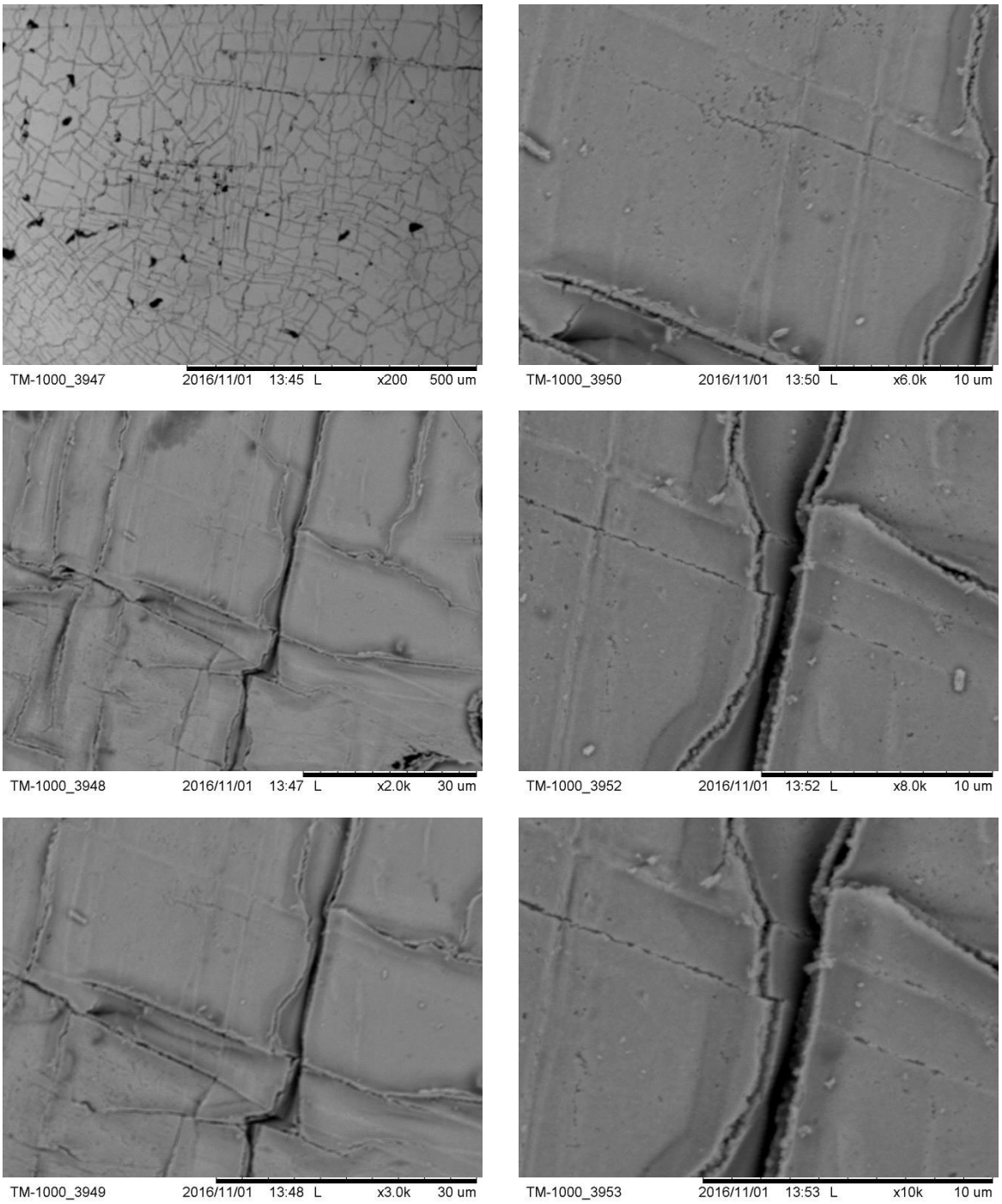

Figure 11.10 SEM images of Strathclyde 4

Figure 11.11 shows all top surface scanning images of Strathclyde 5 IPMC under 6 different magnifications.

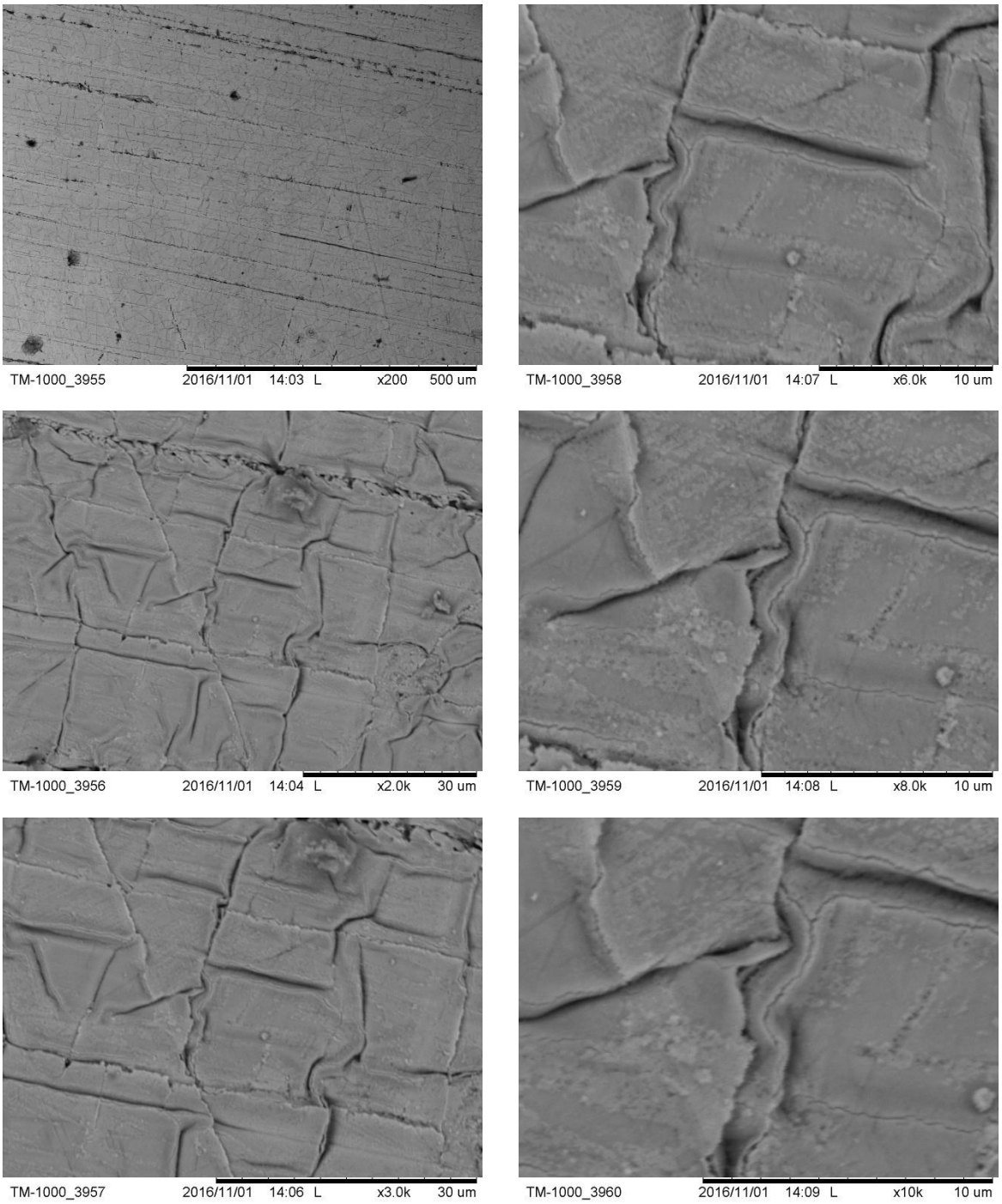

Figure 11.11 SEM images of Strathclyde 5

Figure 11.12 shows all top surface scanning images of Strathclyde 6 IPMC under 6 different magnifications.

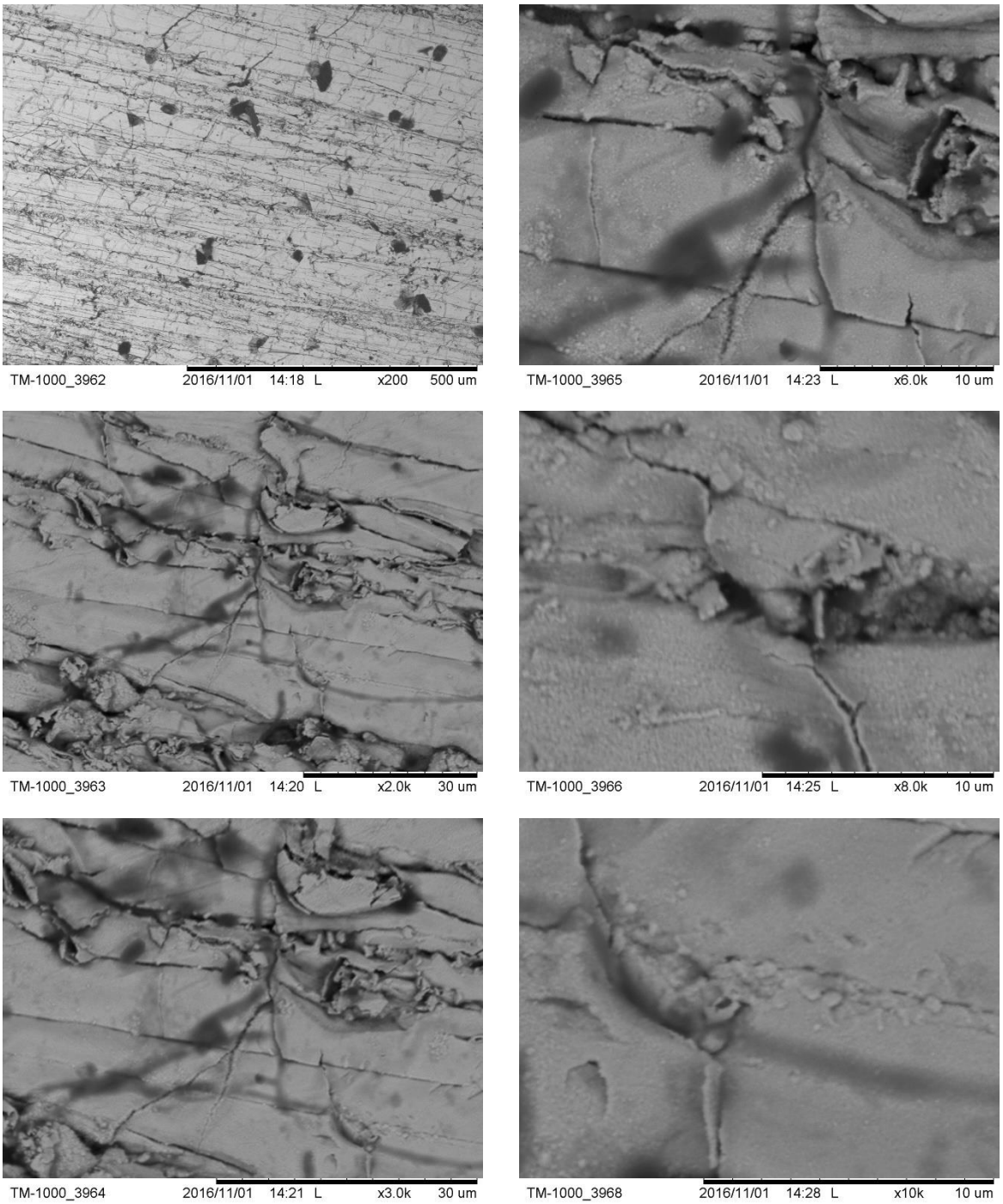

Figure 11.12 SEM images of Strathclyde 6

Figure 11.13 shows all top surface scanning images of Strathclyde 7 IPMC under 6 different magnifications.

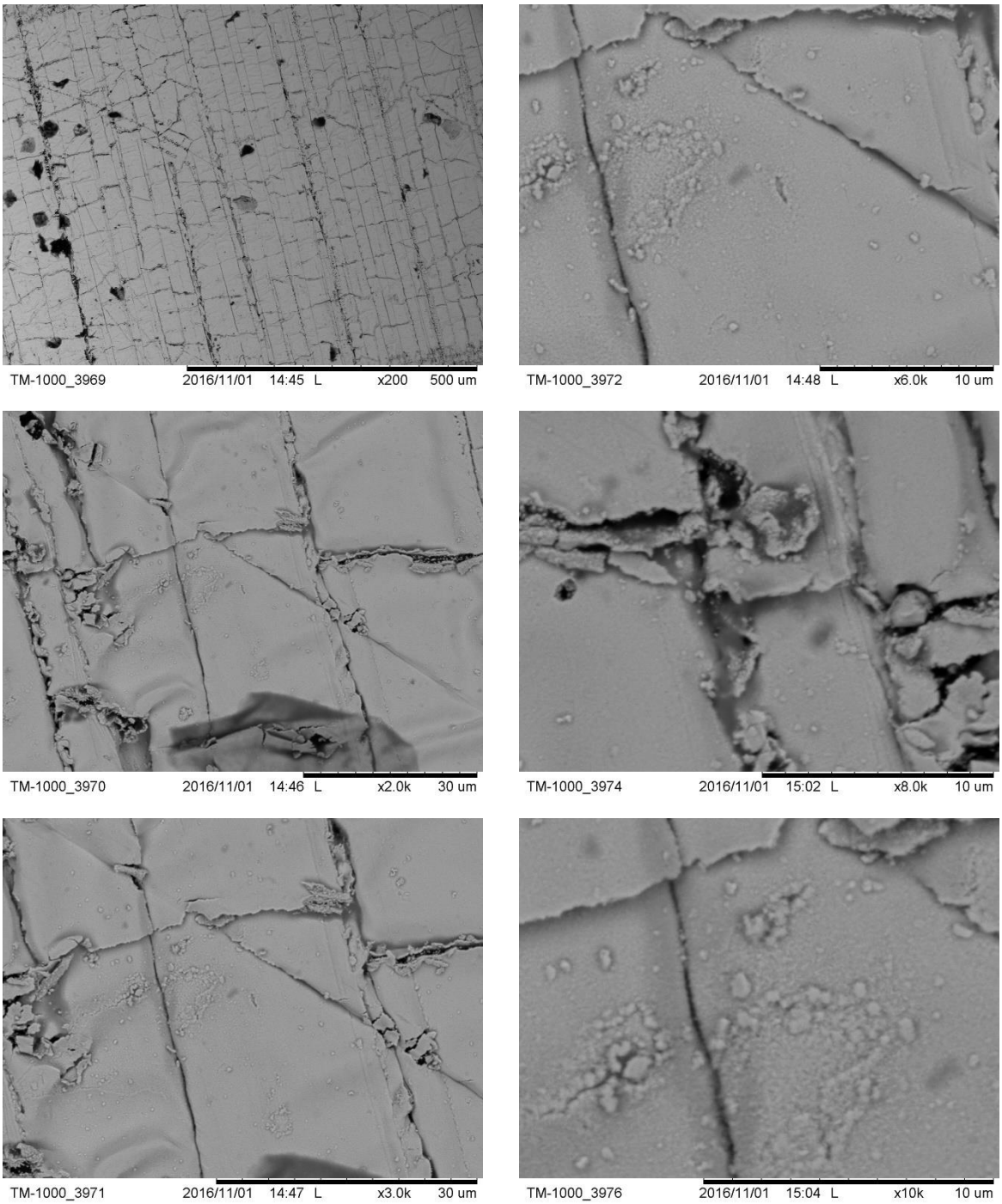

Figure 11.13 SEM images of Strathclyde 7

Figure 11.14 shows all top surface scanning images of Strathclyde 8 IPMC under 6 different magnifications.

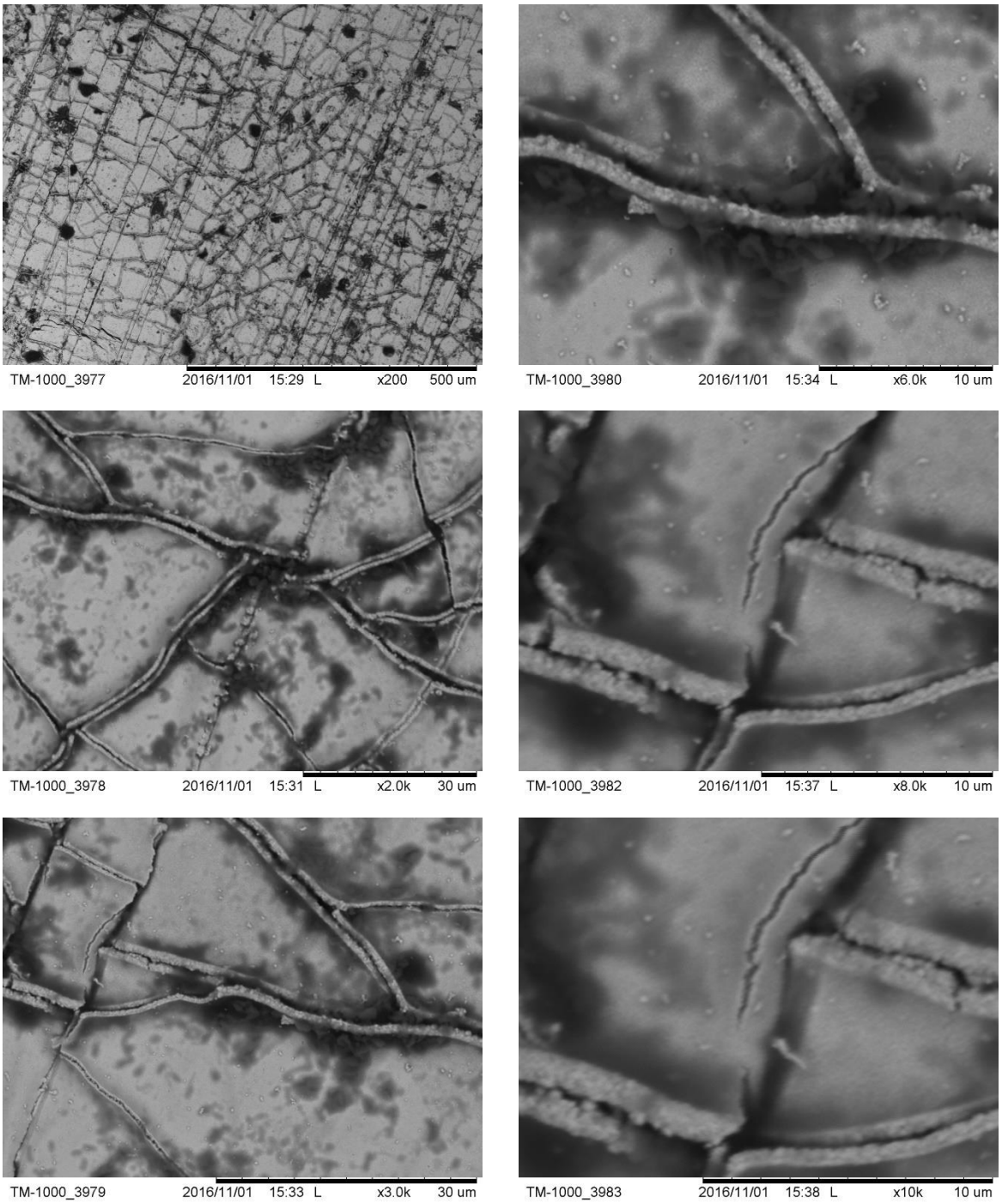

Figure 11.14 SEM images of Strathclyde 8

Figure 11.15 shows all top surface scanning images of Strathclyde 9 IPMC under 6 different magnifications.

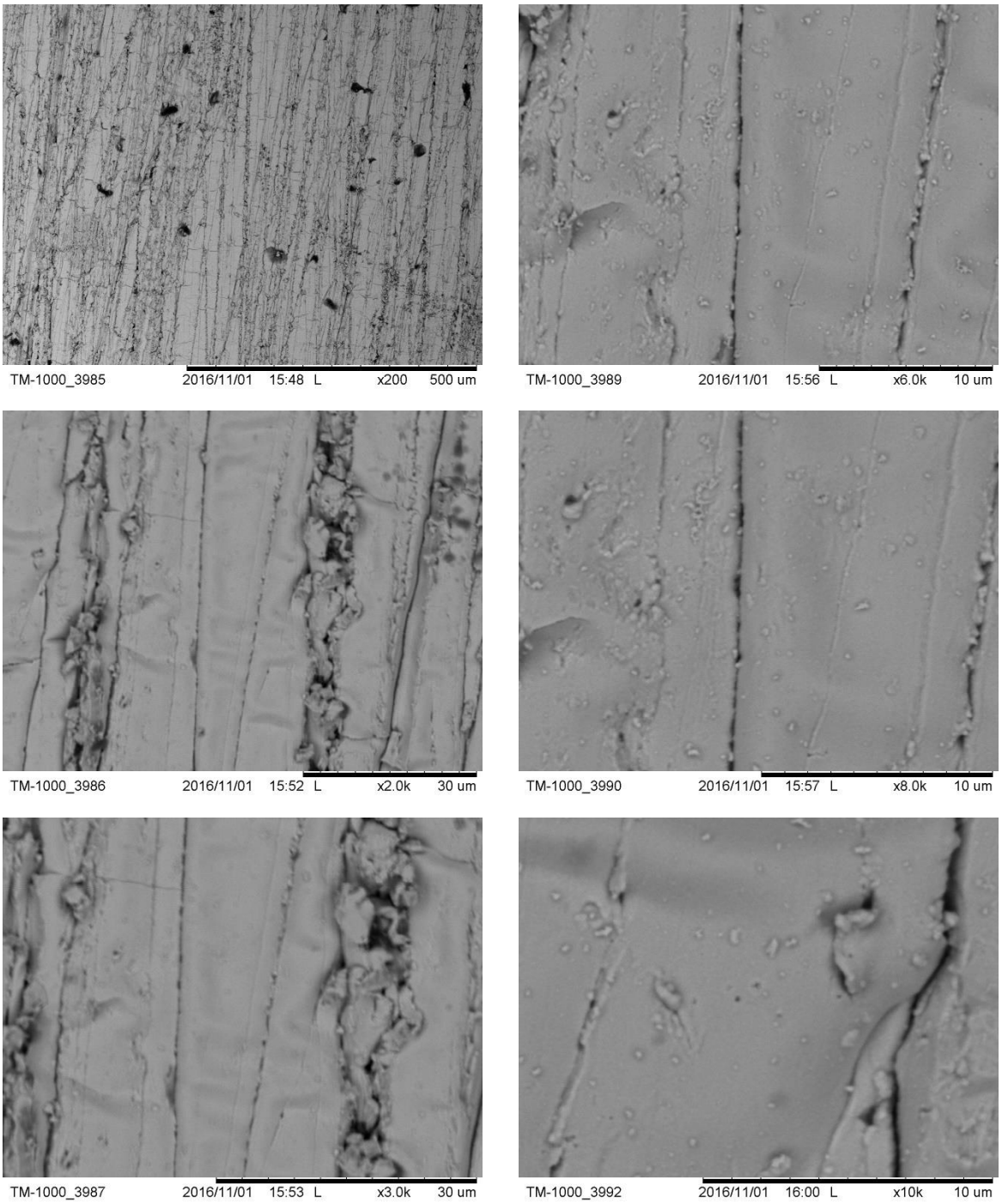

Figure 11.15 SEM images of Strathclyde 9

Figure 11.16 shows all top surface scanning images of Strathclyde 10 IPMC under 6 different magnifications.

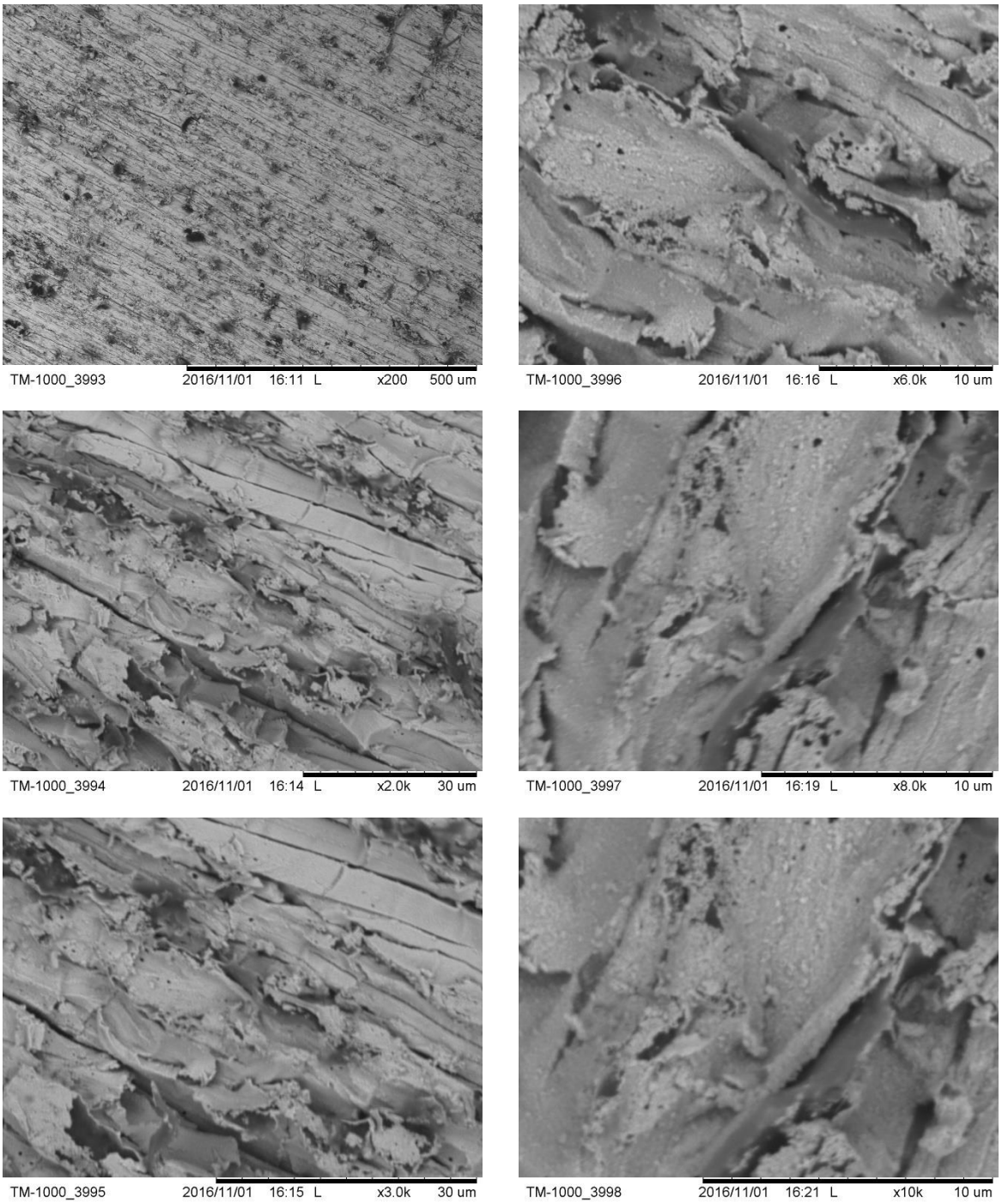

Figure 11.16 SEM images of Strathclyde 10

Figure 11.17 shows all top surface scanning images of Strathclyde 11 IPMC under 6 different magnifications.

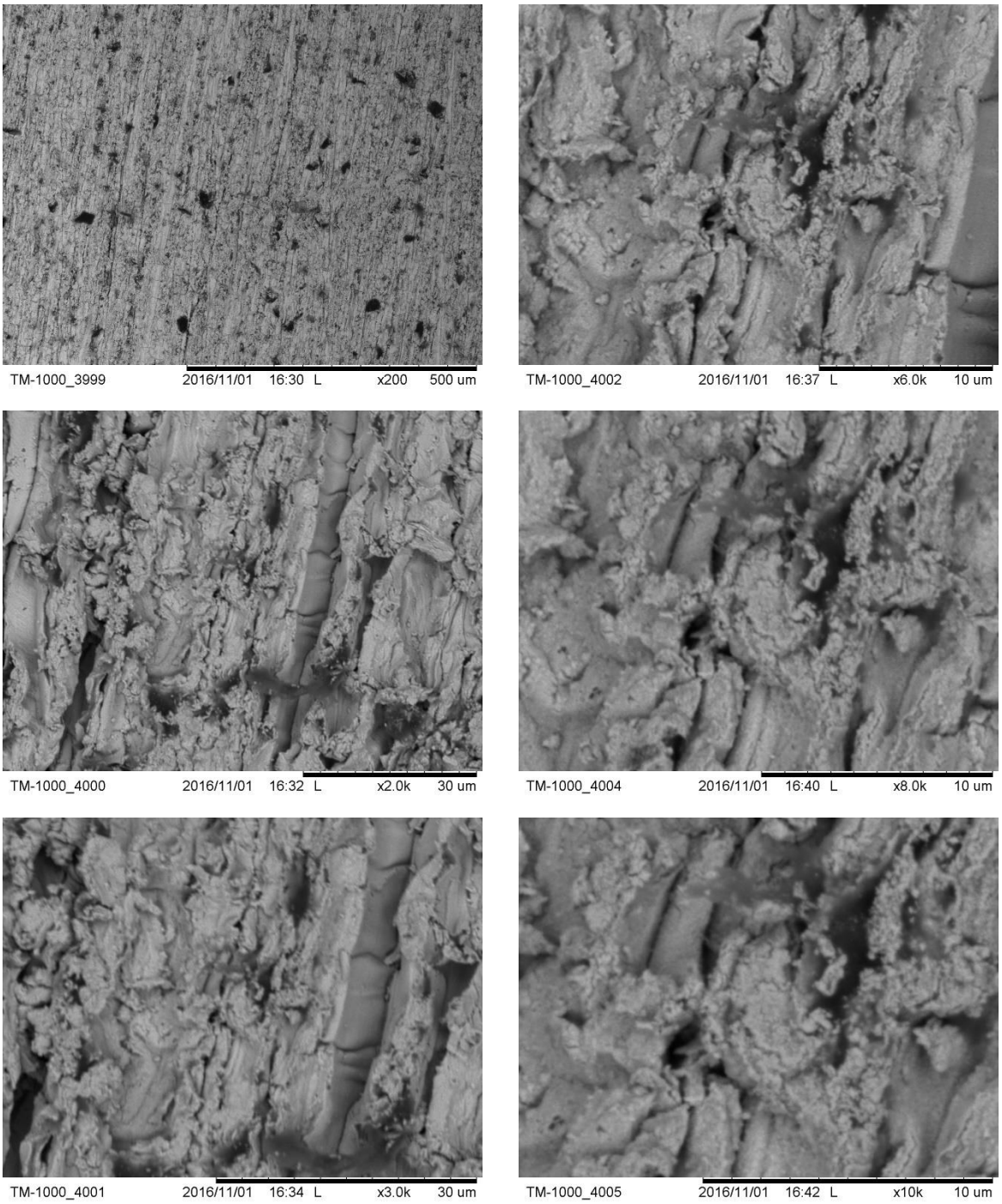

Figure 11.17 SEM images of Strathclyde 11

Figure 11.18 shows the top surface scanning images of the fragments of Strathclyde 1 at stage 4 under 6 different magnifications.

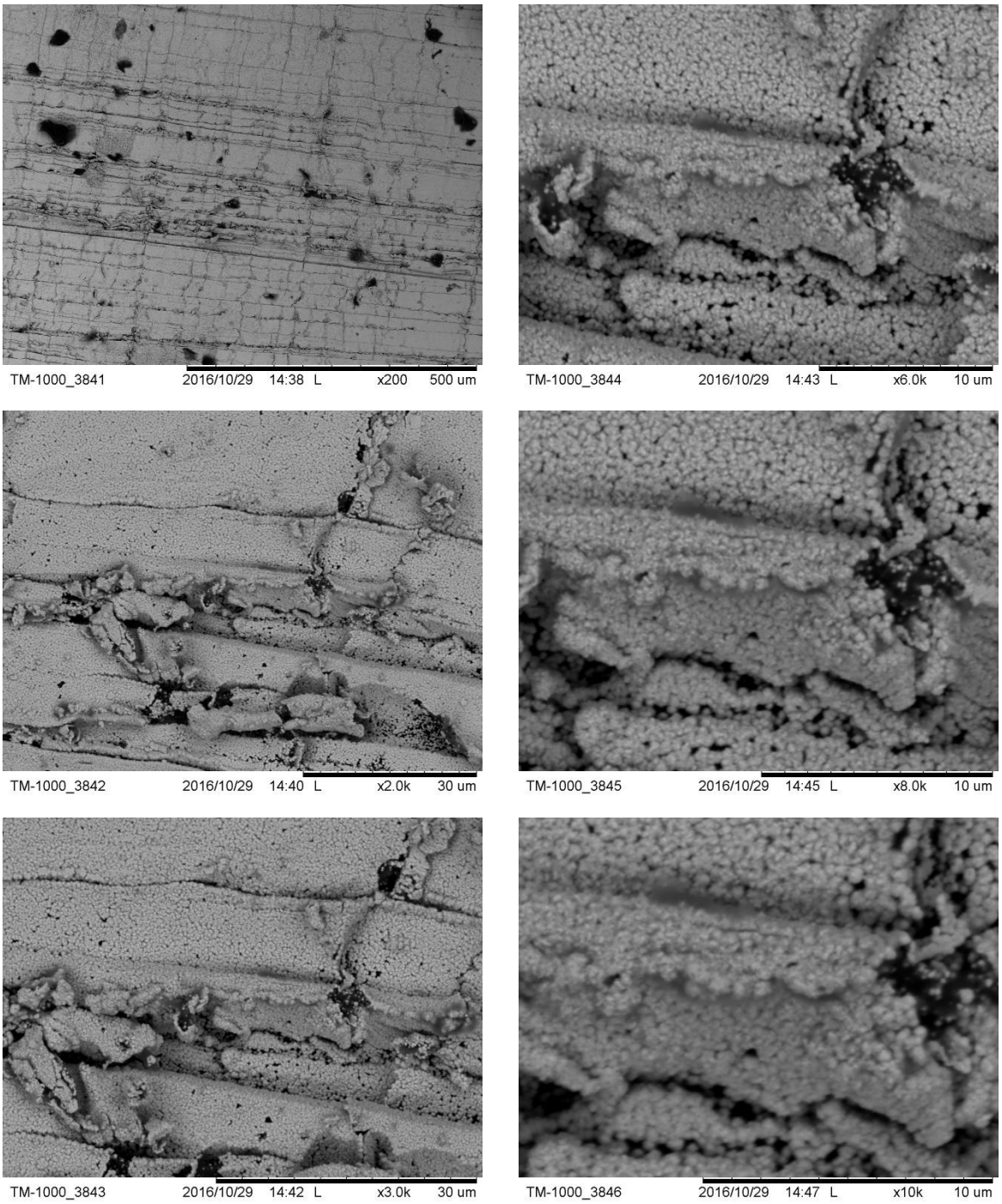

Figure 11.18 SEM images of Strathclyde 1 Stage 4

Figure 11.19 shows the top surface scanning images of the fragments of Strathclyde 1 at stage 5 under 6 different magnifications

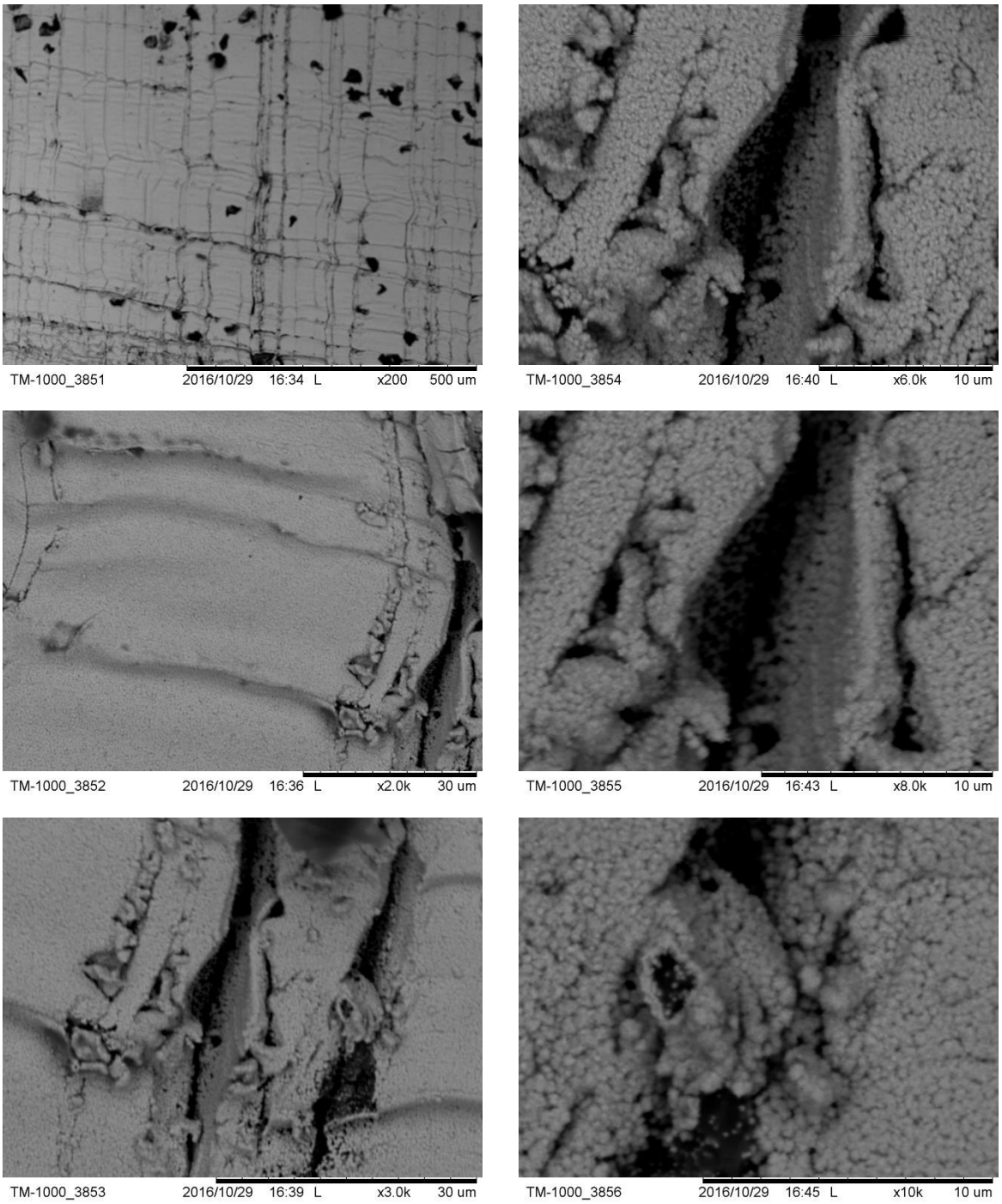

Figure 11.19 SEM images of Strathclyde 1 Stage 5

Figure 11.20 shows the top surface scanning images of the fragments of Strathclyde 1 at stage 6 under 6 different magnifications.

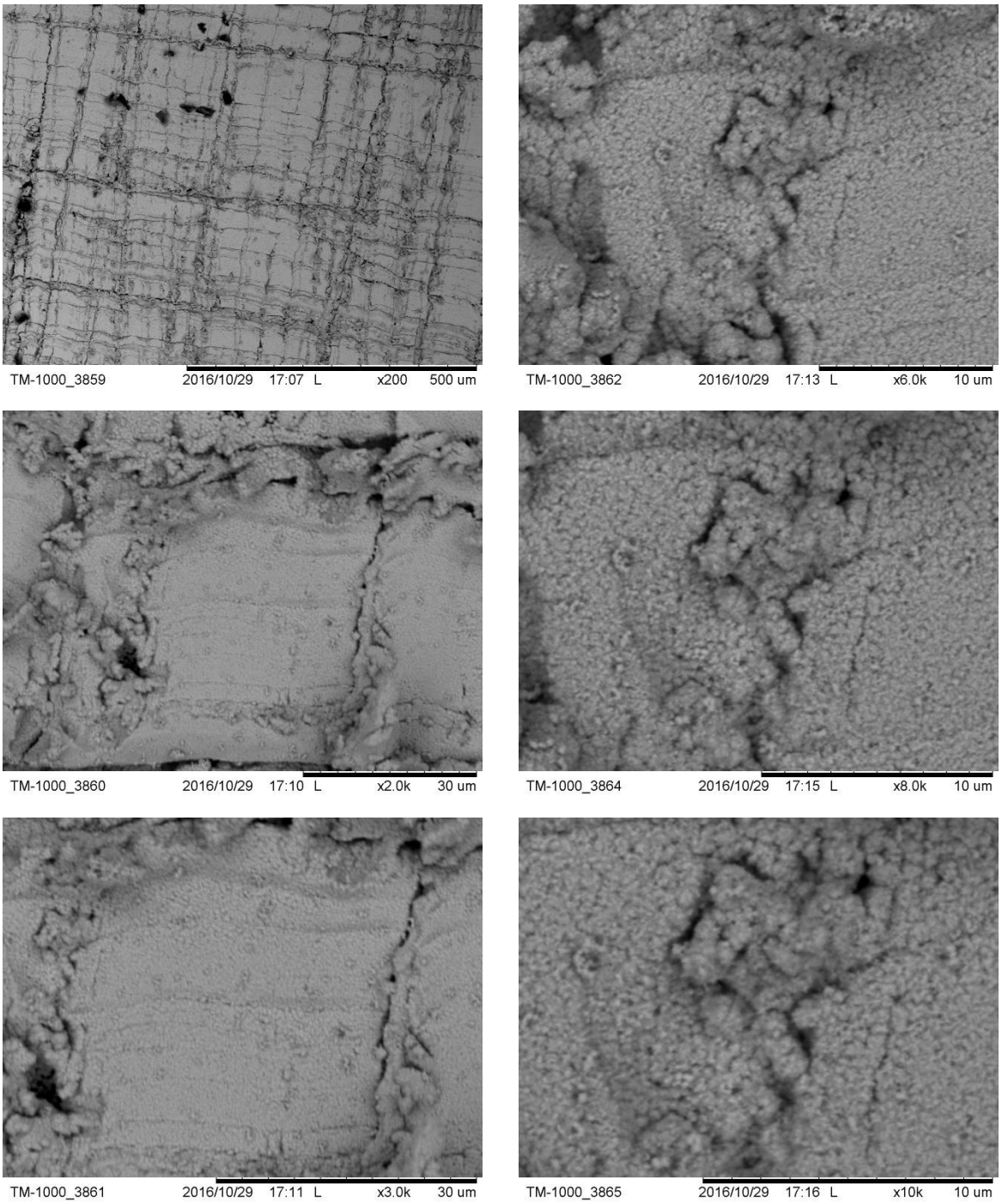

Figure 11.20 SEM images of Strathclyde 1 Stage 6

Figure 11.21 shows the top surface scanning images of the fragments of Strathclyde 1 at stage 7 under 6 different magnifications

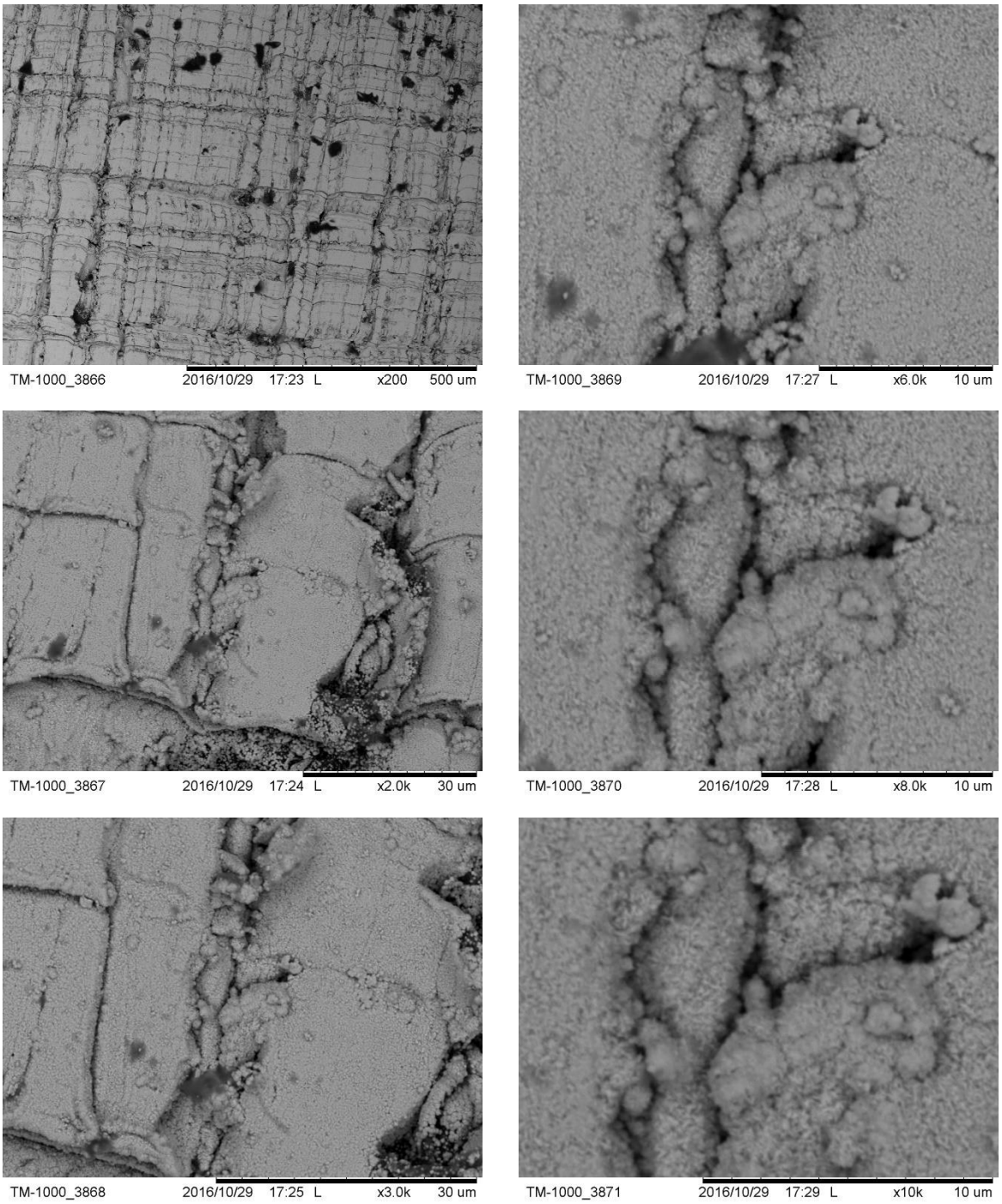

Figure 11.21 SEM images of Strathclyde 1 Stage 7

Figure 11.22 shows the top surface scanning images of the fragments of Strathclyde 1 at stage 8 under 6 different magnifications.

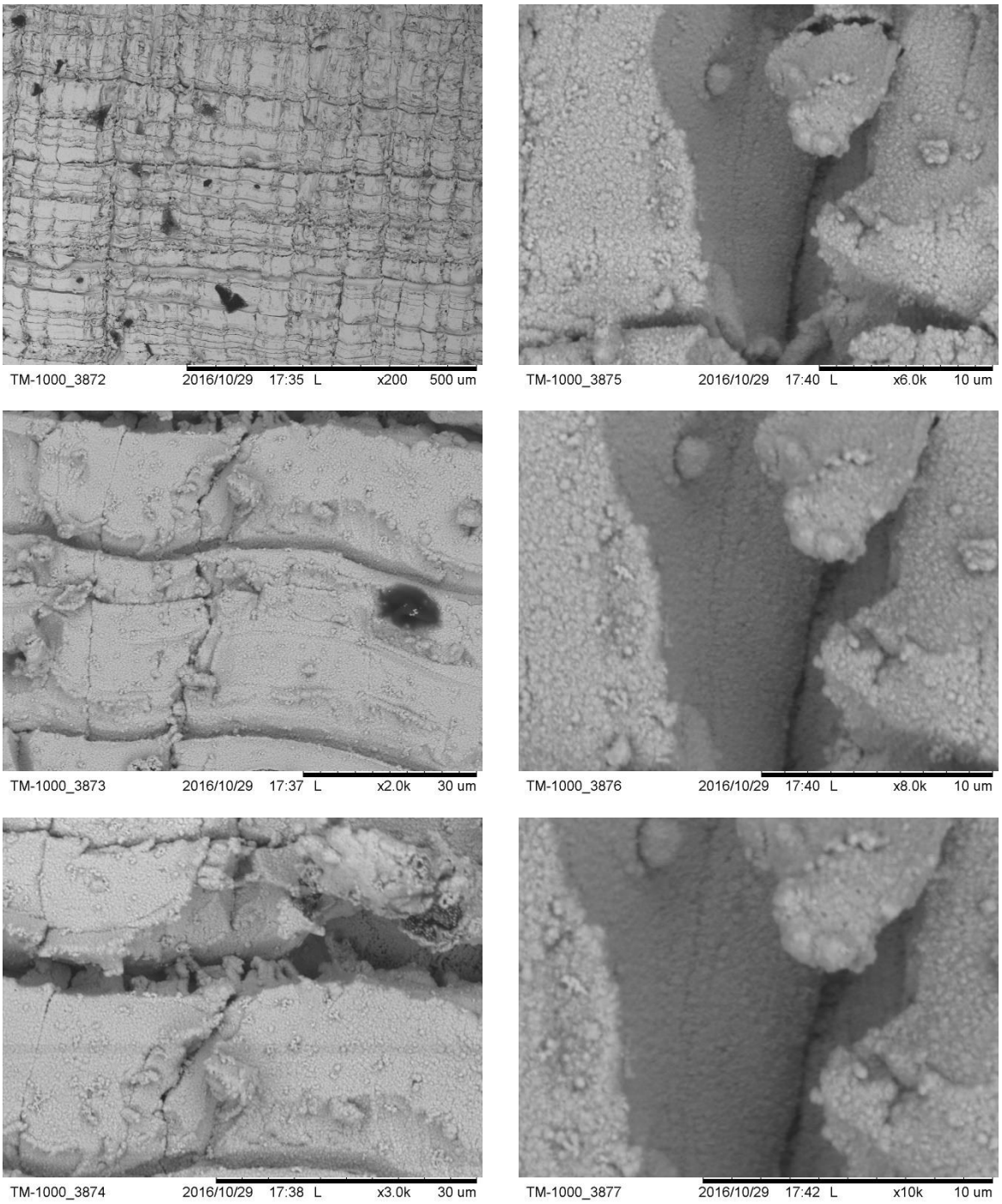

Figure 11.22 SEM images of Strathclyde 1 Stage 8

Figure 11.23 shows the top surface scanning images of the fragments of Strathclyde 2 at stage 1 under 6 different magnifications.

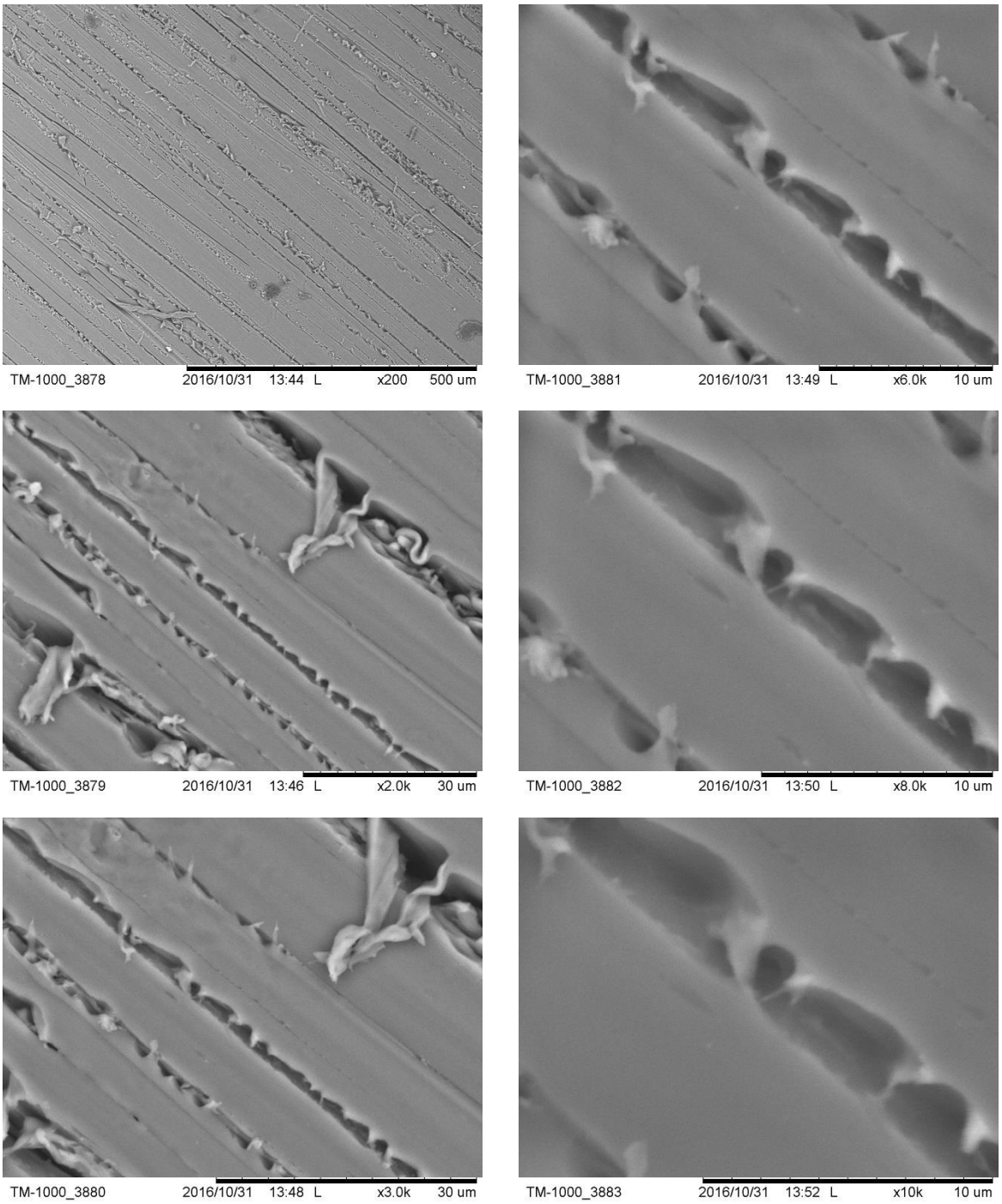

Figure 11.23 SEM images of Strathclyde 2 Stage 1

Figure 11.24 shows the top surface scanning images of the fragments of Strathclyde 2 at stage 2 under 6 different magnifications.

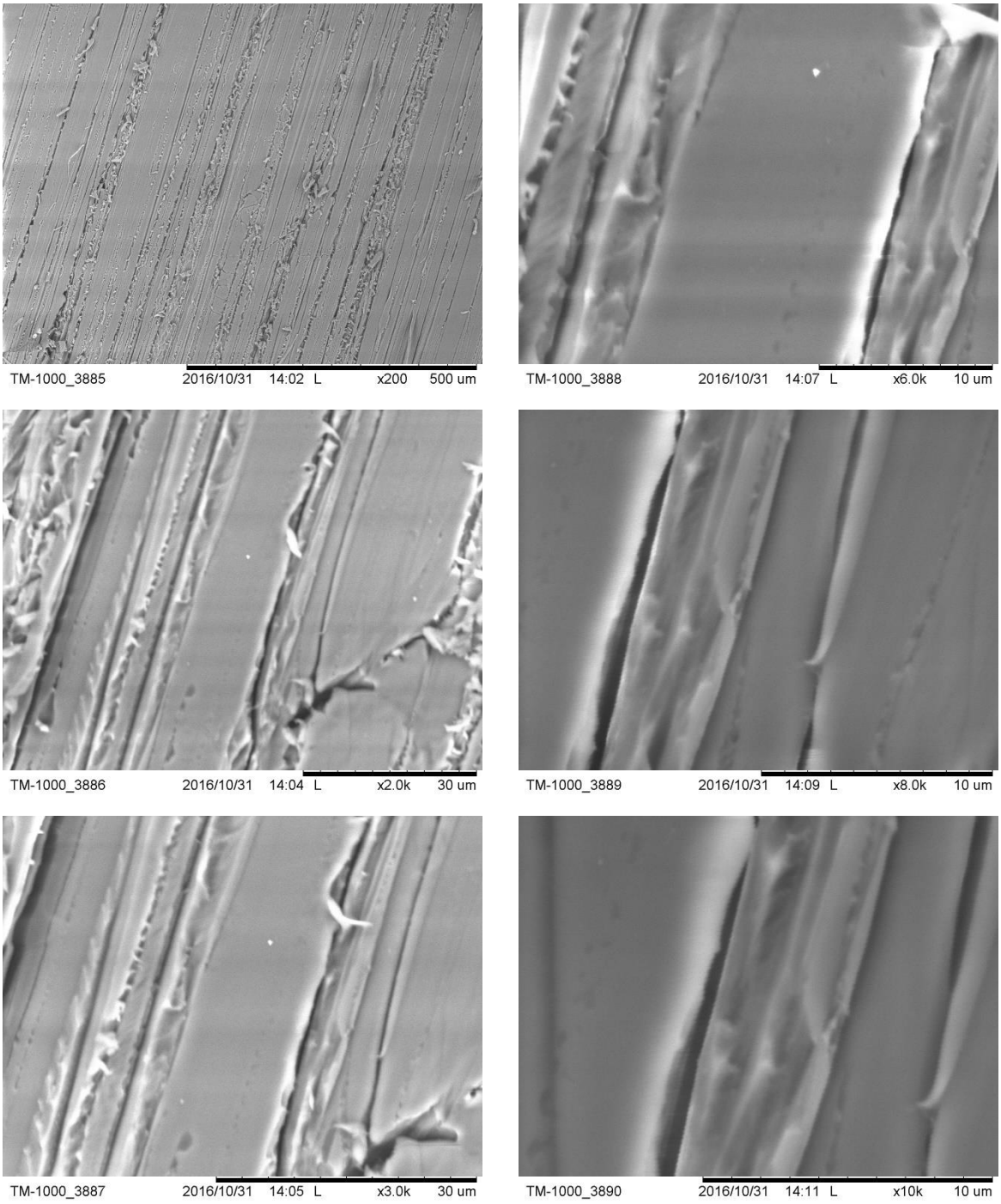

Figure 11.24 SEM images of Strathclyde 2 Stage 2

Figure 11.25 shows the top surface scanning images of the fragments of Strathclyde 2 at stage 3 under 6 different magnifications.

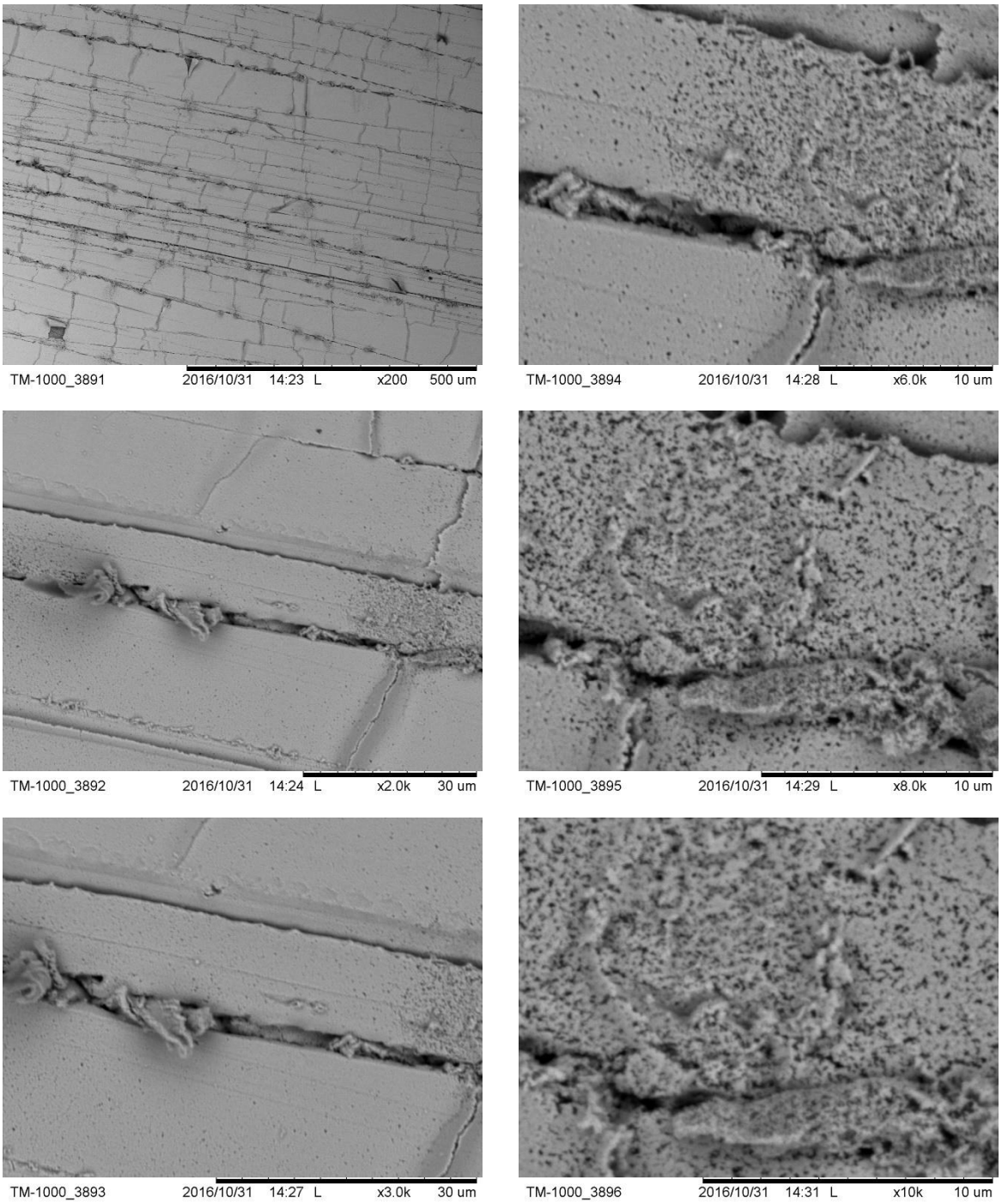

Figure 11.25 SEM images of Strathclyde 2 Stage 3

Figure 11.26 shows the top surface scanning images of the fragments of Strathclyde 2 at stage 4 under 6 different magnifications.

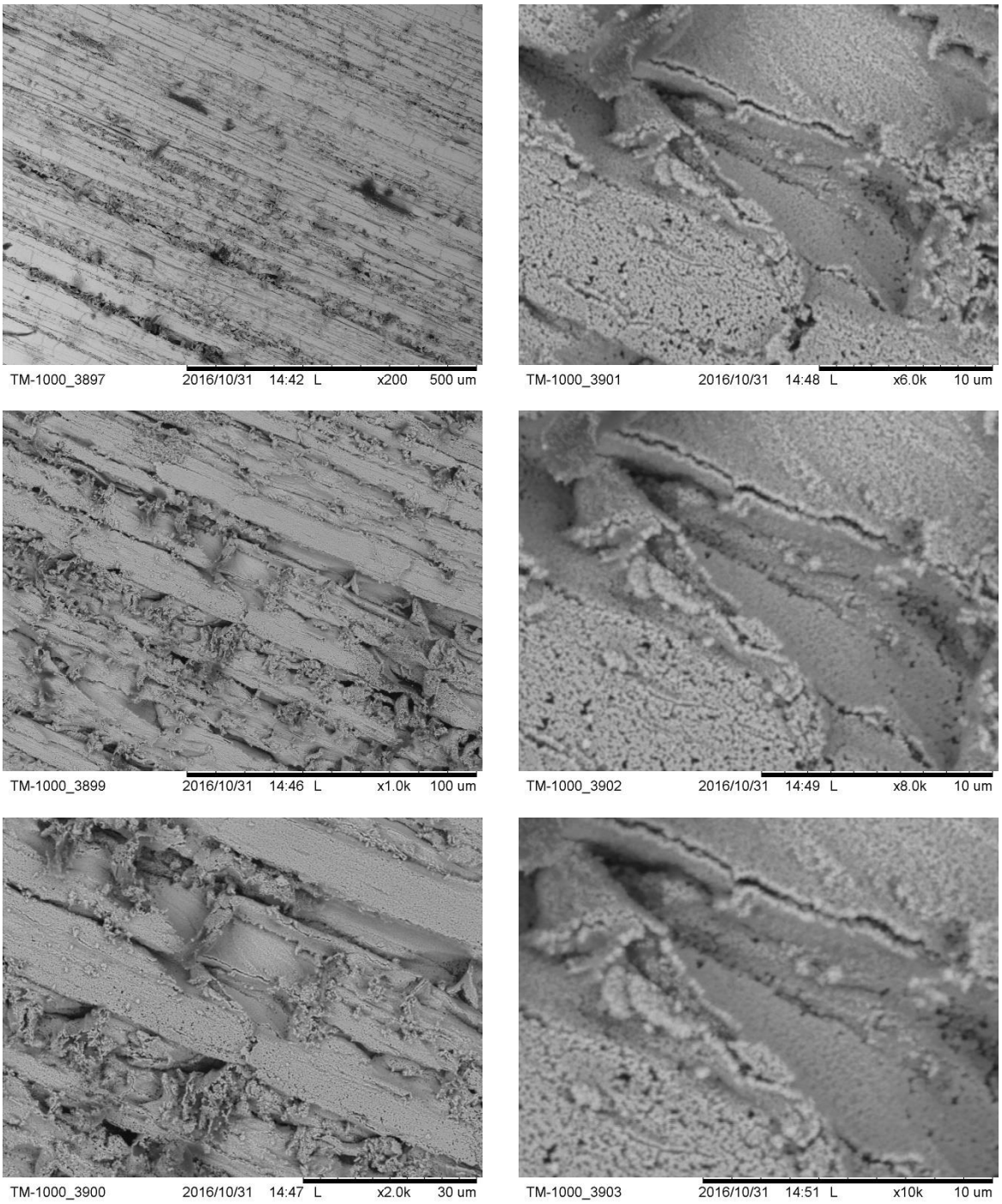

Figure 11.26 SEM images of Strathclyde 2 Stage 4

Figure 11.27 shows the top surface scanning images of the fragments of Strathclyde 2 at stage 5 under 6 different magnifications.

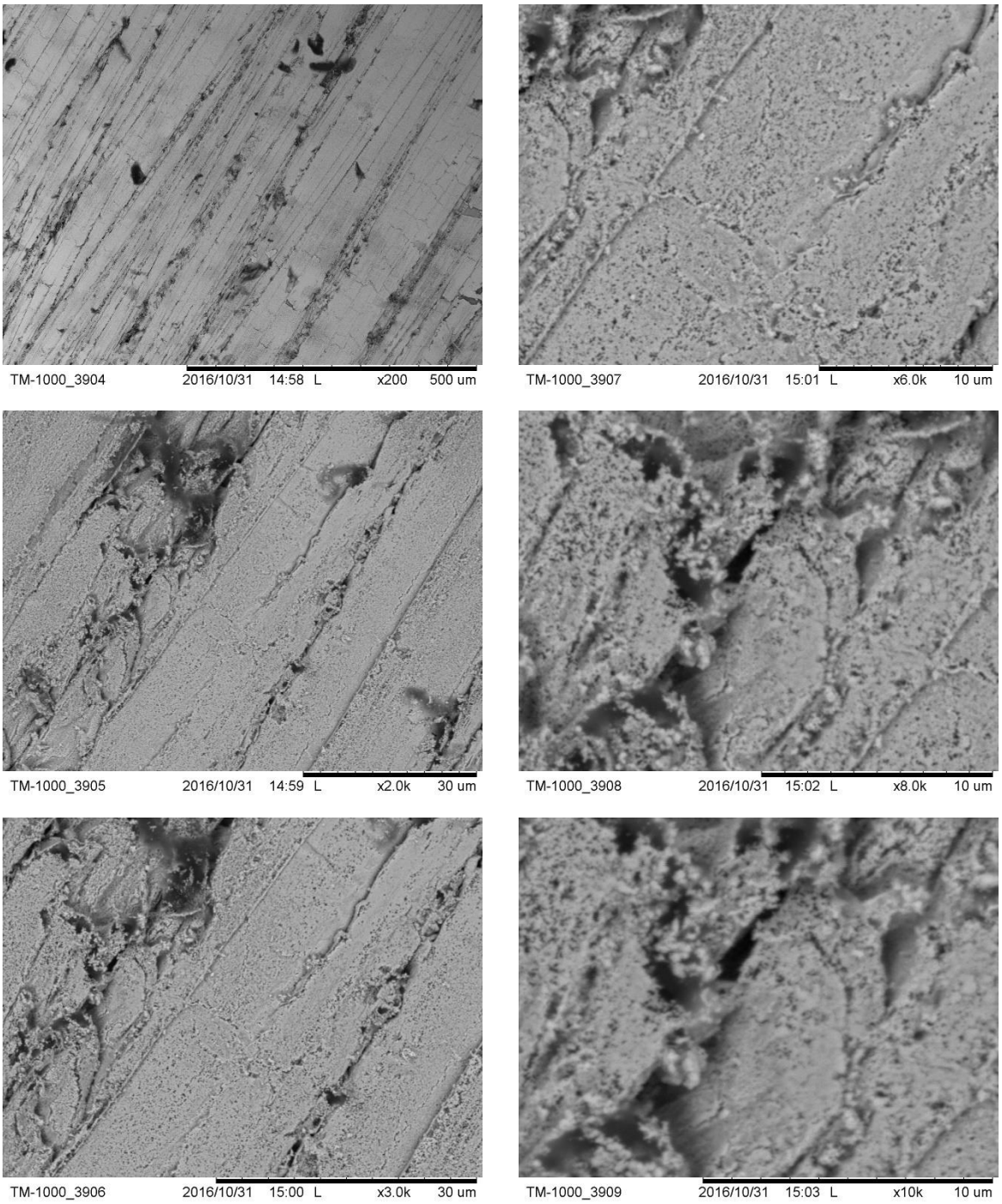

Figure 11.27 SEM images of Strathclyde 2 Stage 5

Figure 11.28 shows the top surface scanning images of the fragments of Strathclyde 2 at stage 6 under 6 different magnifications.

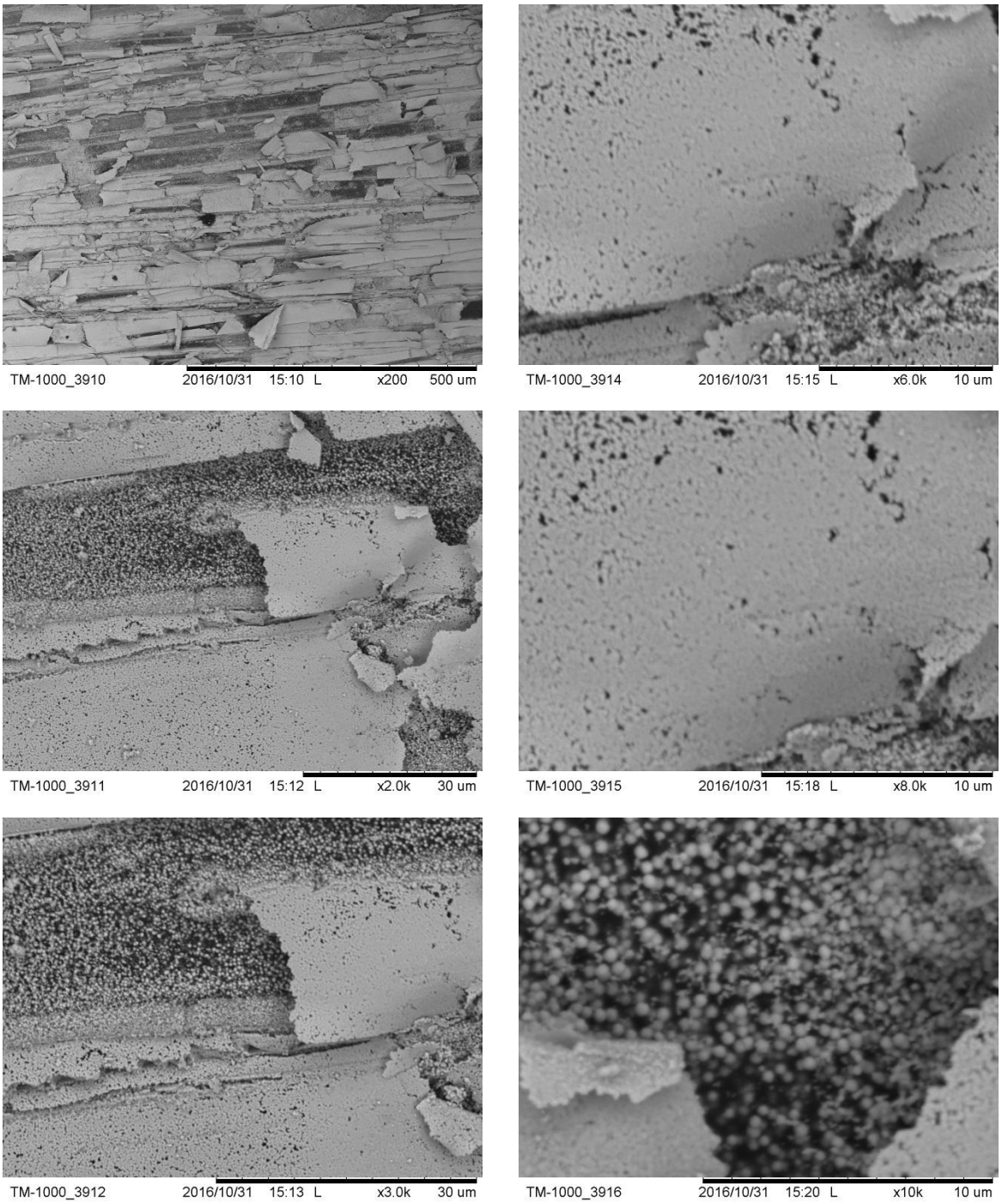

Figure 11.28 SEM images of Strathclyde 2 Stage 6

Figure 11.29 shows the top surface scanning images of the fragments of Strathclyde 2 at stage 7 under 6 different magnifications.

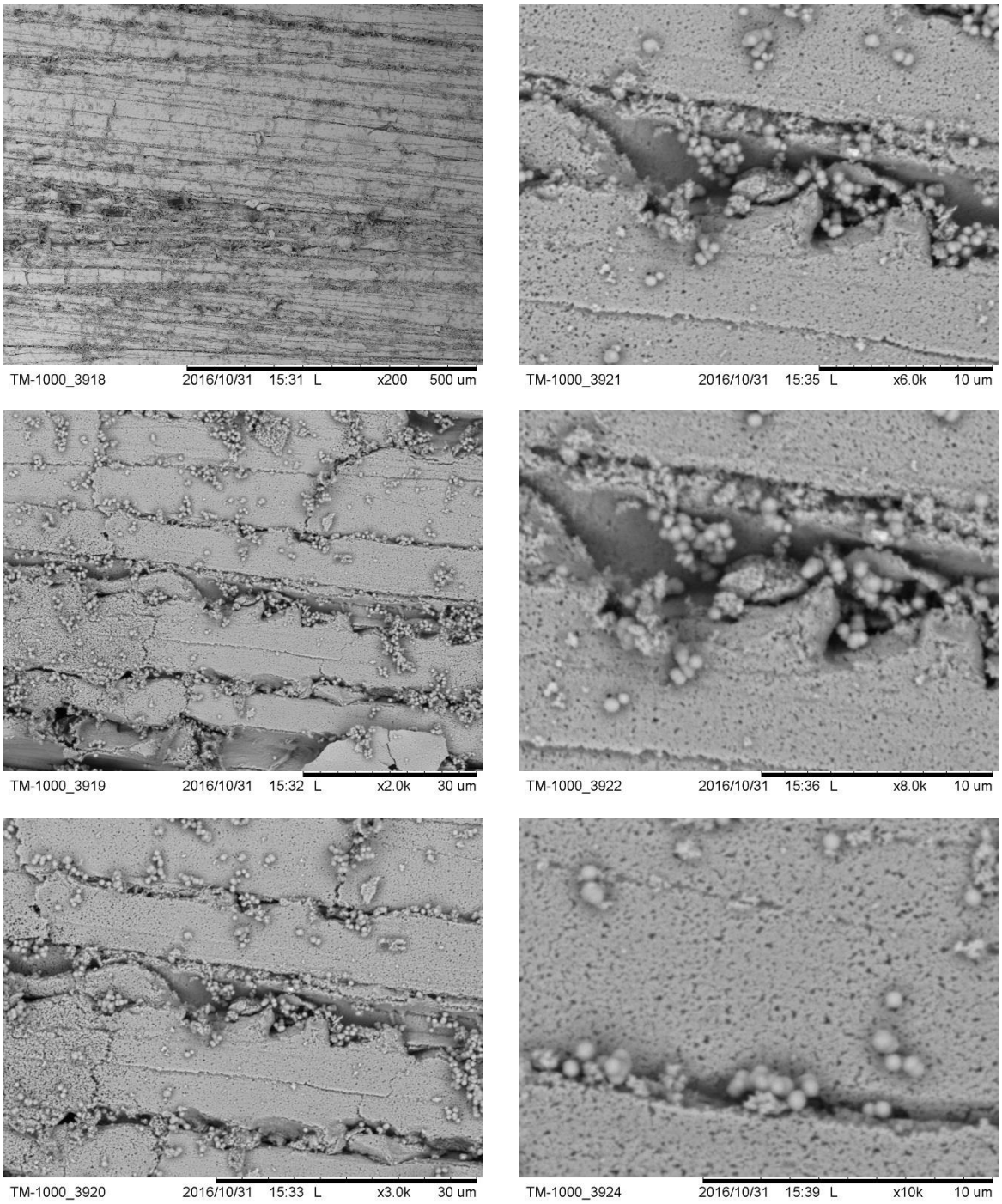

Figure 11.29 SEM images of Strathclyde 2 Stage 7

Figure 11.30 shows the top surface scanning images of the fragments of Strathclyde 2 at stage 8 under 6 different magnifications.

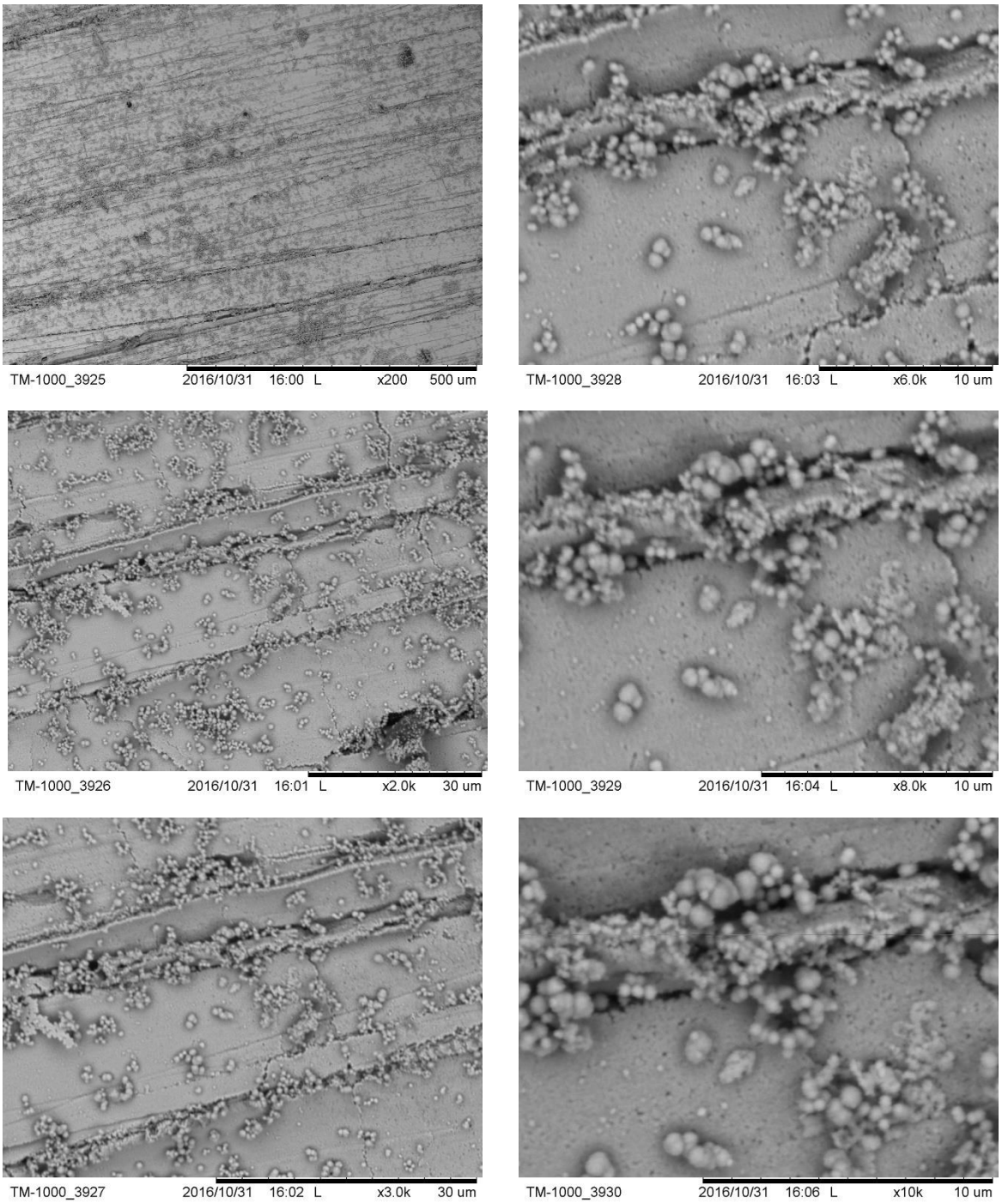

Figure 11.30 SEM images of Strathclyde 2 Stage 8

11.4 Cross Section Scans

Figure 11.31 shows cross section scanning images of the Commercial IPMC 1, 2, and 3 under 2 different magnifications.

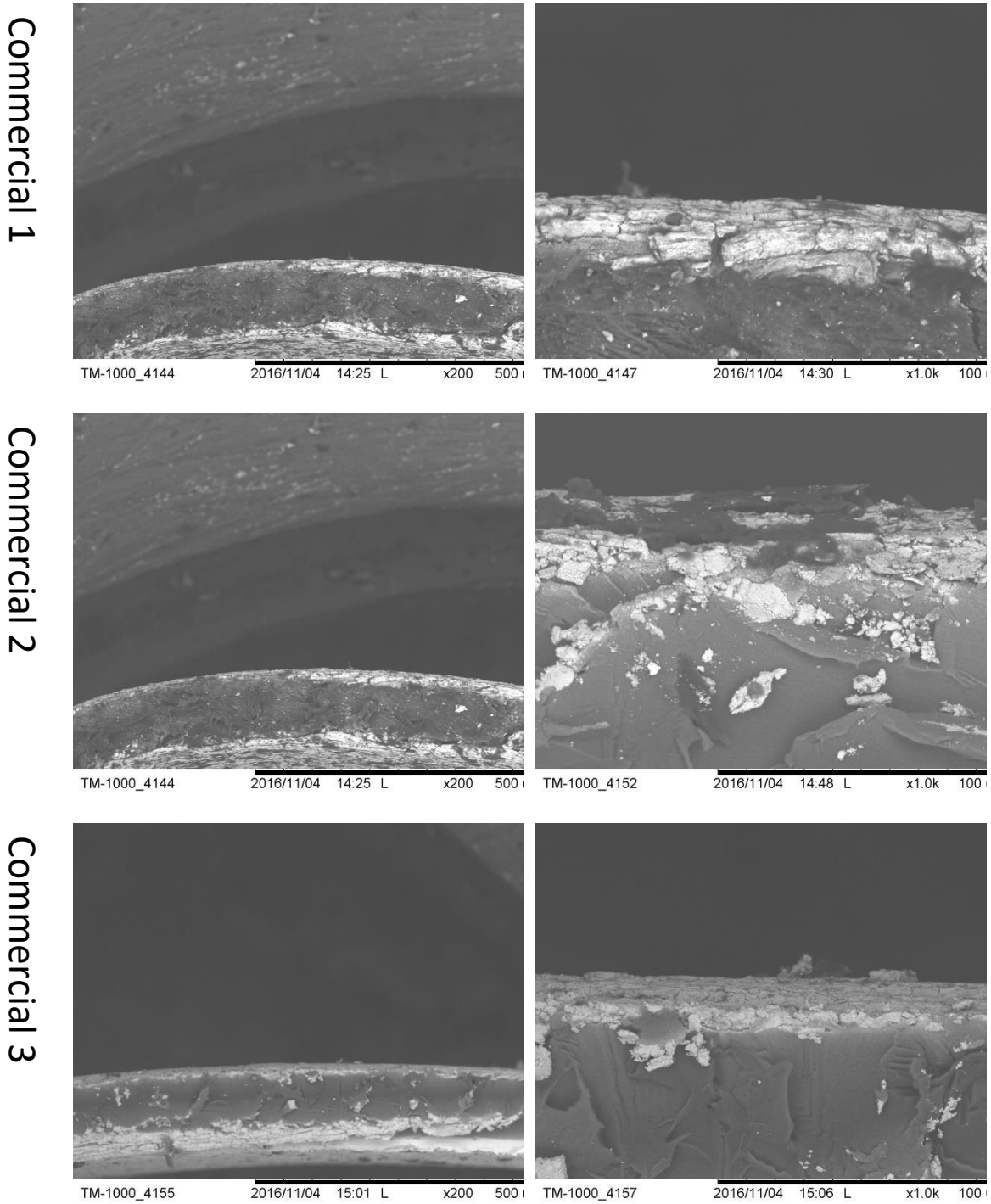

Figure 11.31 Cross Section SEM images of the Commercial IPMC

Figure 11.32 shows cross section scanning images of the Commercial IPMC 4, 5, and 6 under 2 different magnifications.

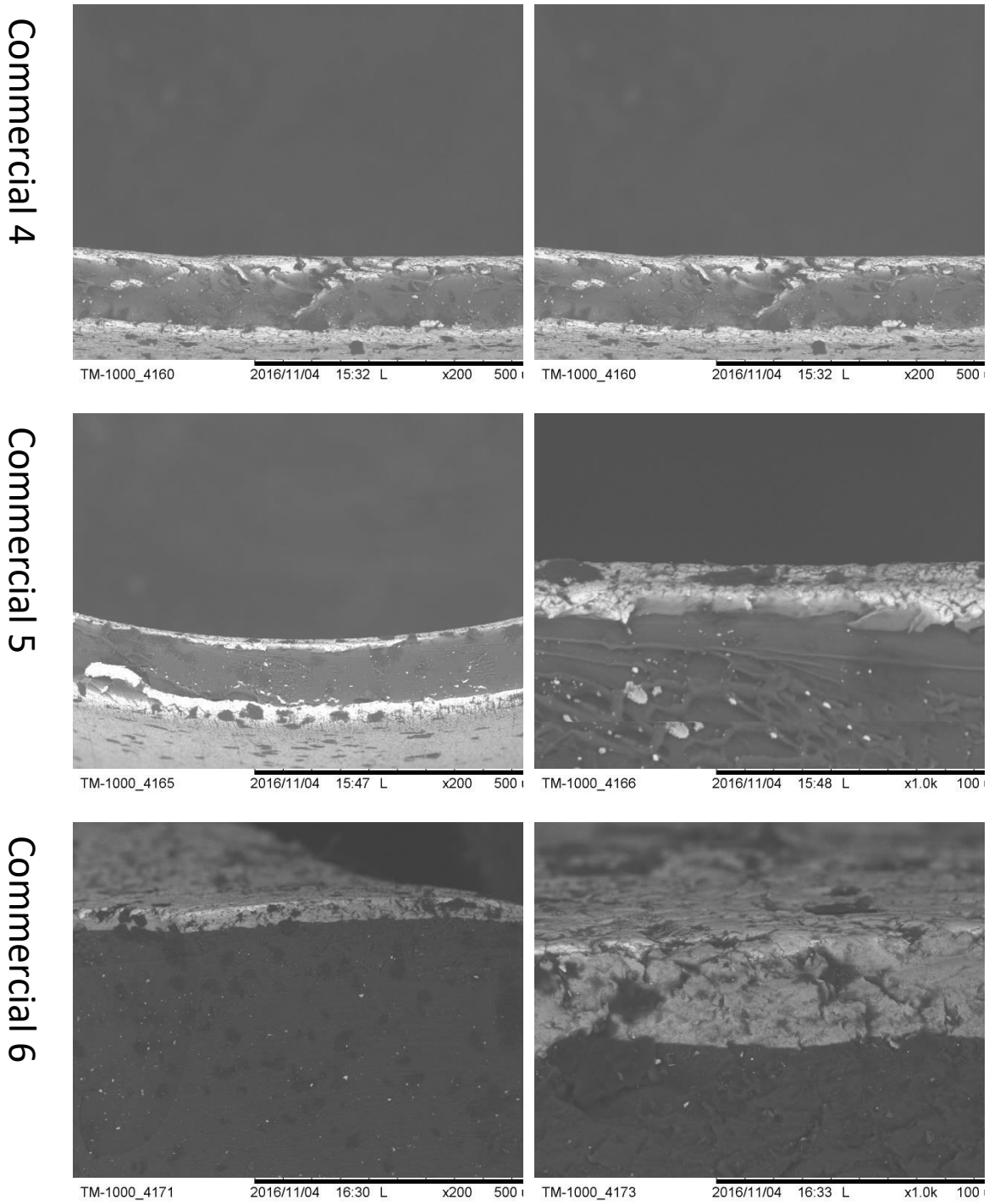

Figure 11.32 Cross Section SEM images of the Commercial IPMC

Figure 11.33 shows cross section scanning images of the Strathclyde IPMC 1, 2, and 3 under 2 different magnifications.

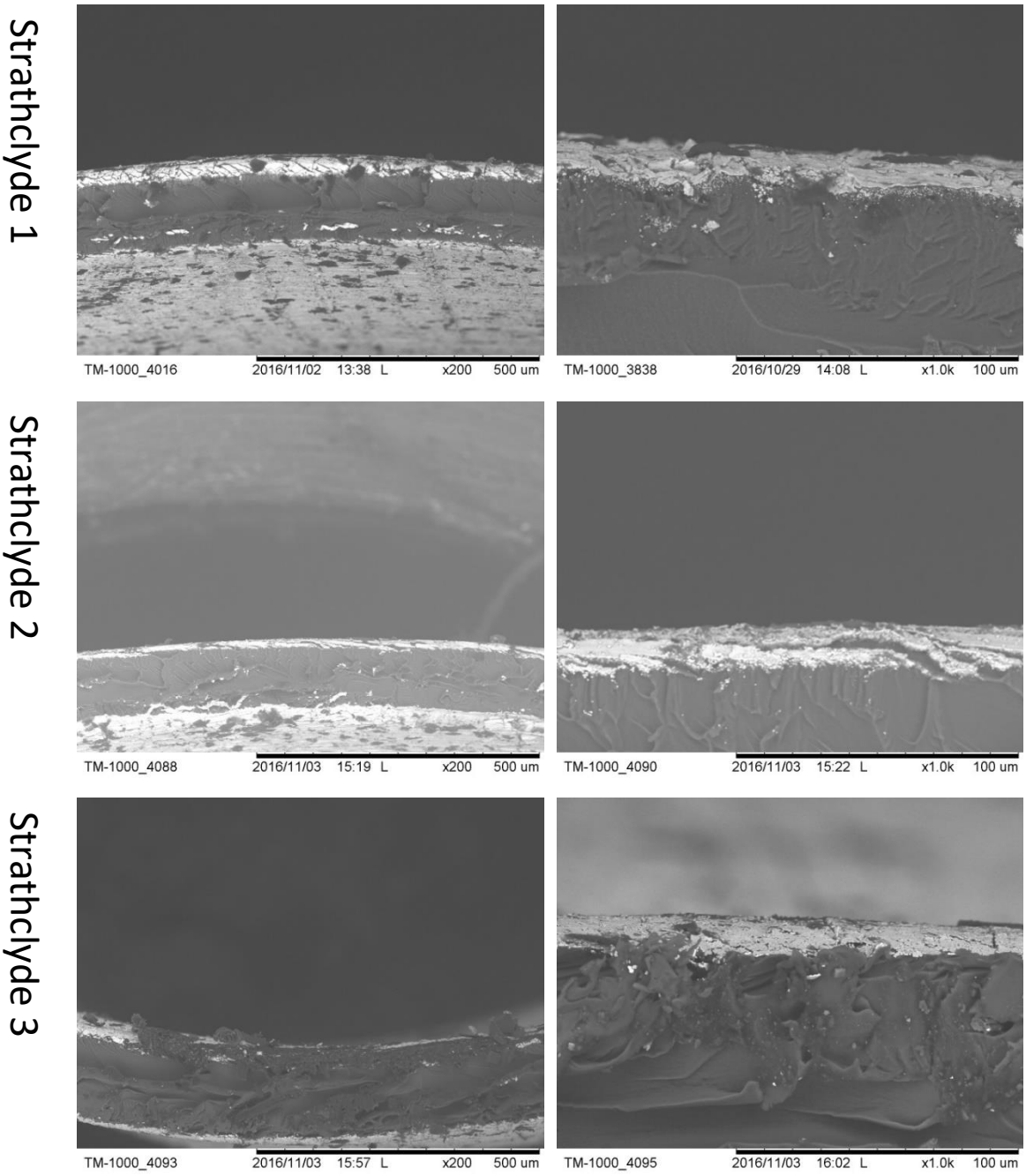

Figure 11.33 Cross Section SEM images of the Strathclyde IPMC

Figure 11.34 shows cross section scanning images of the Strathclyde IPMC 4, 5, and 6 under 2 different magnifications.

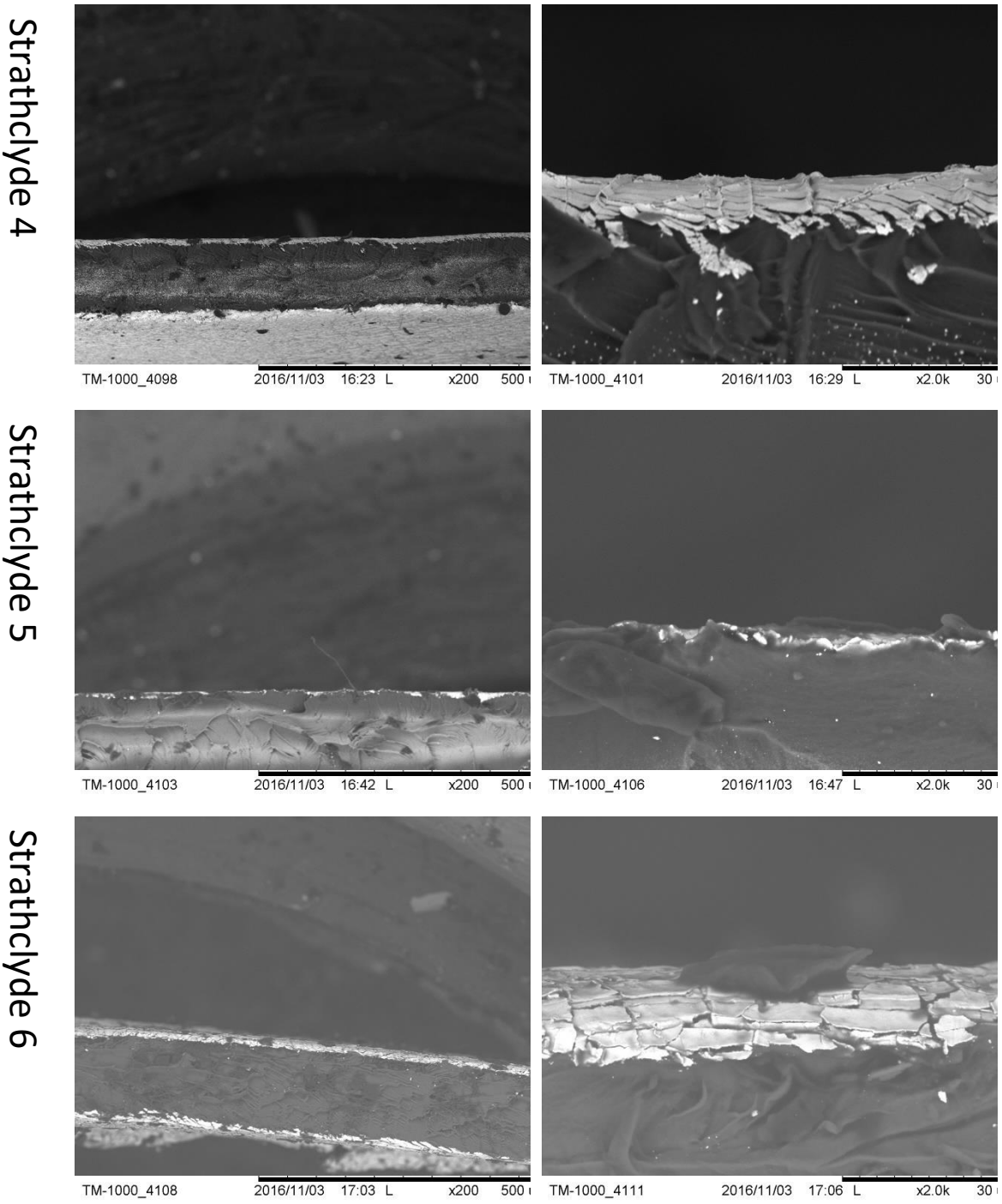

Figure 11.34 Cross Section SEM images of the Strathclyde IPMC

Figure 11.35 shows cross section scanning images of the Strathclyde IPMC 7, 8, and 9 under 2 different magnifications.

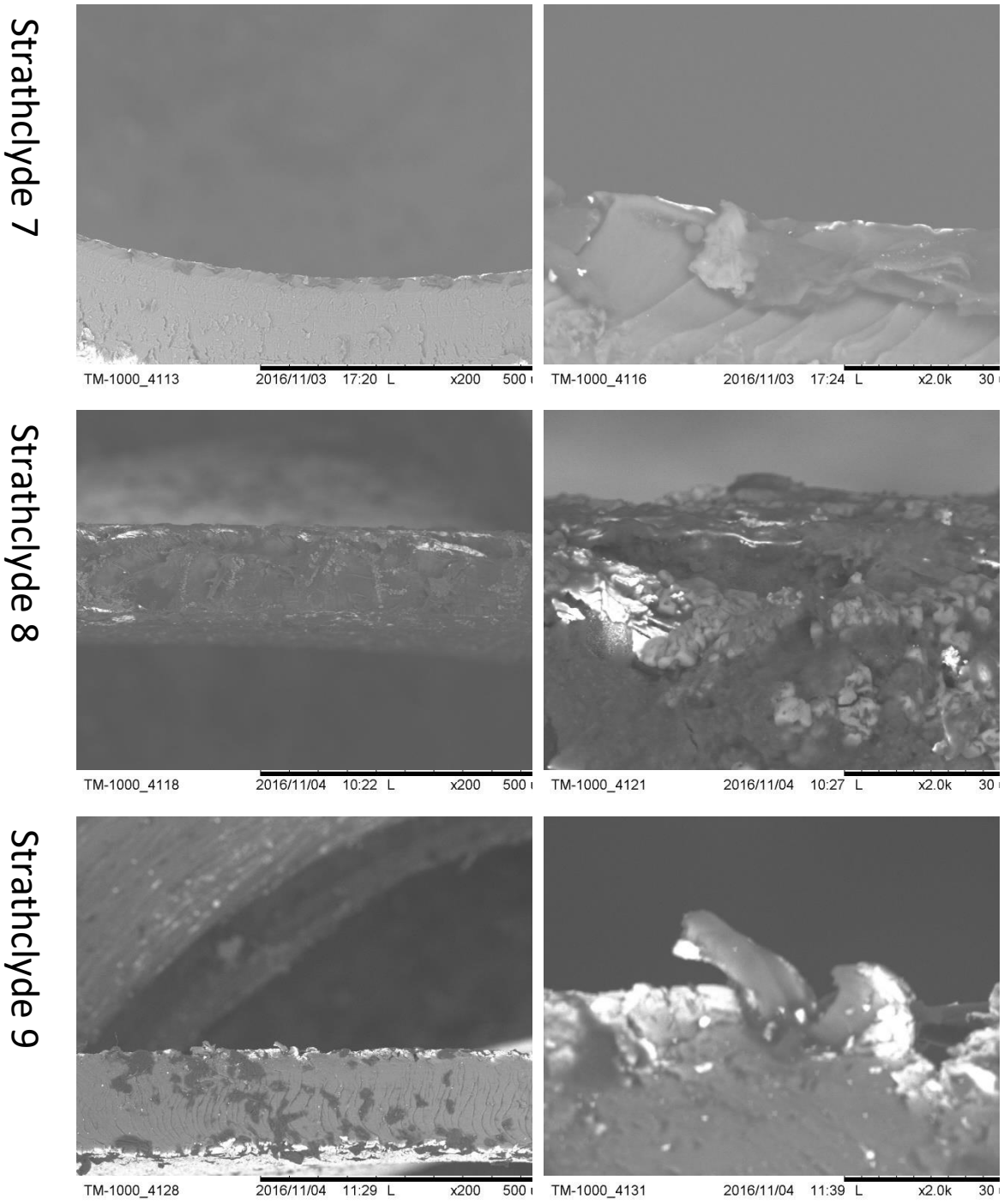

Figure 11.35 Cross Section SEM images of the Strathclyde IPMC

Figure 11.36 shows cross section scanning images of the Strathclyde IPMC 10, and 11 under 2 different magnifications

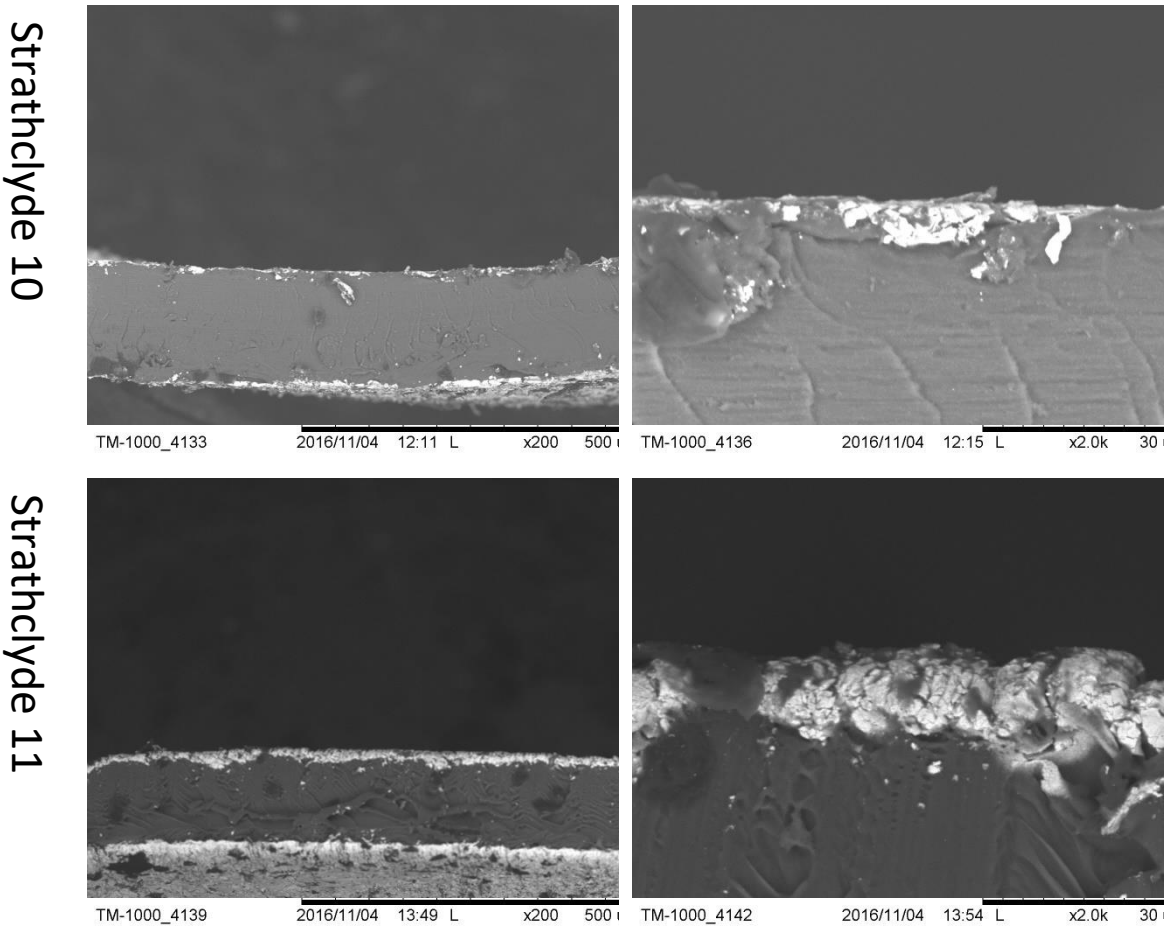

Figure 11.36 Cross Section SEM images of the Strathclyde IPMC

Figure 11.37 shows the cross section scanning images of the Strathclyde IPMC sample 1 at stage 4, 5 and 6 of fabrication under 2 different magnifications.

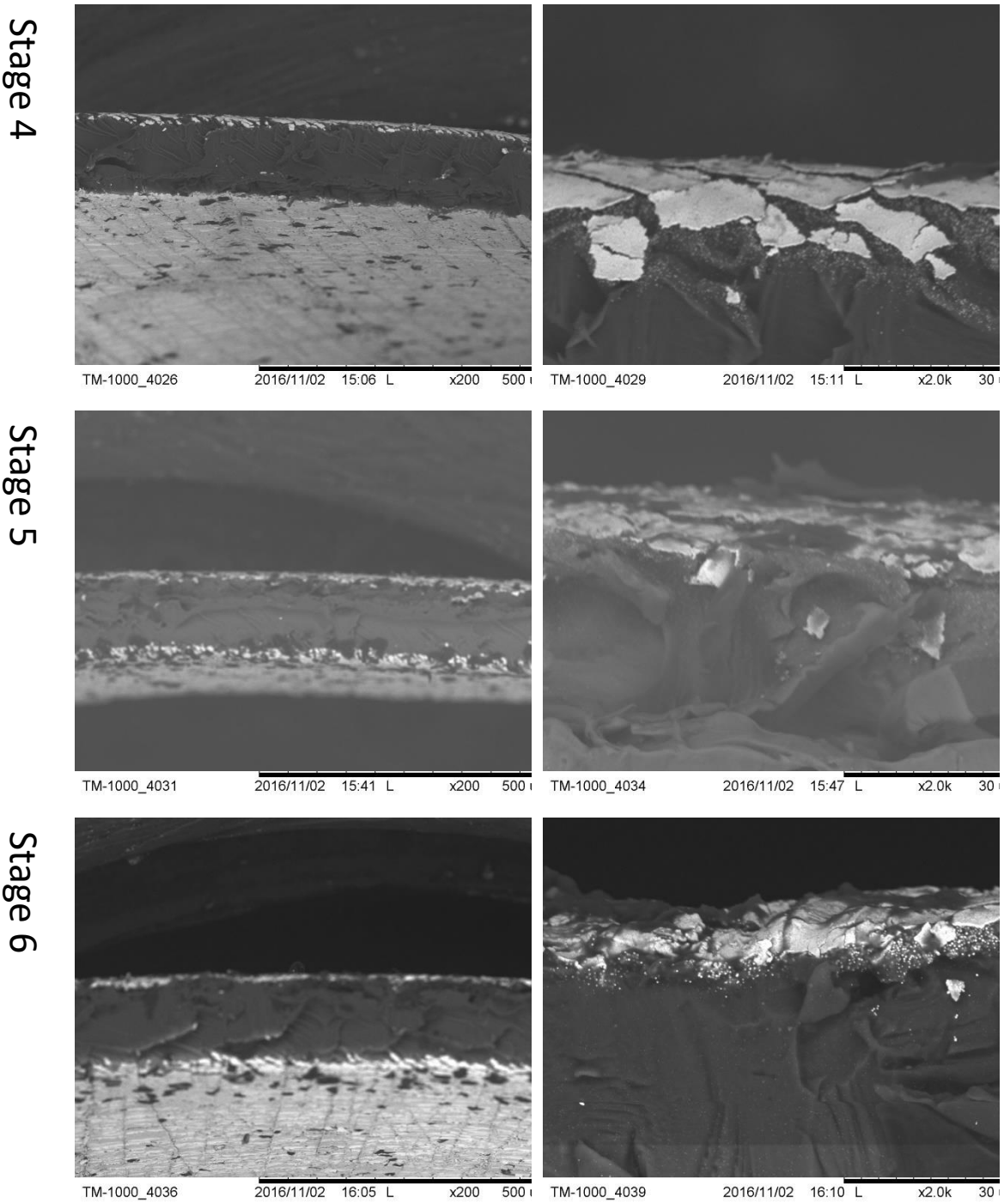

Figure 11.37 Cross Section images of Strathclyde 1

Figure 11.38 shows the cross section scanning images of the Strathclyde IPMC sample 1 at stage 7 and 8 of fabrication under 2 different magnifications.

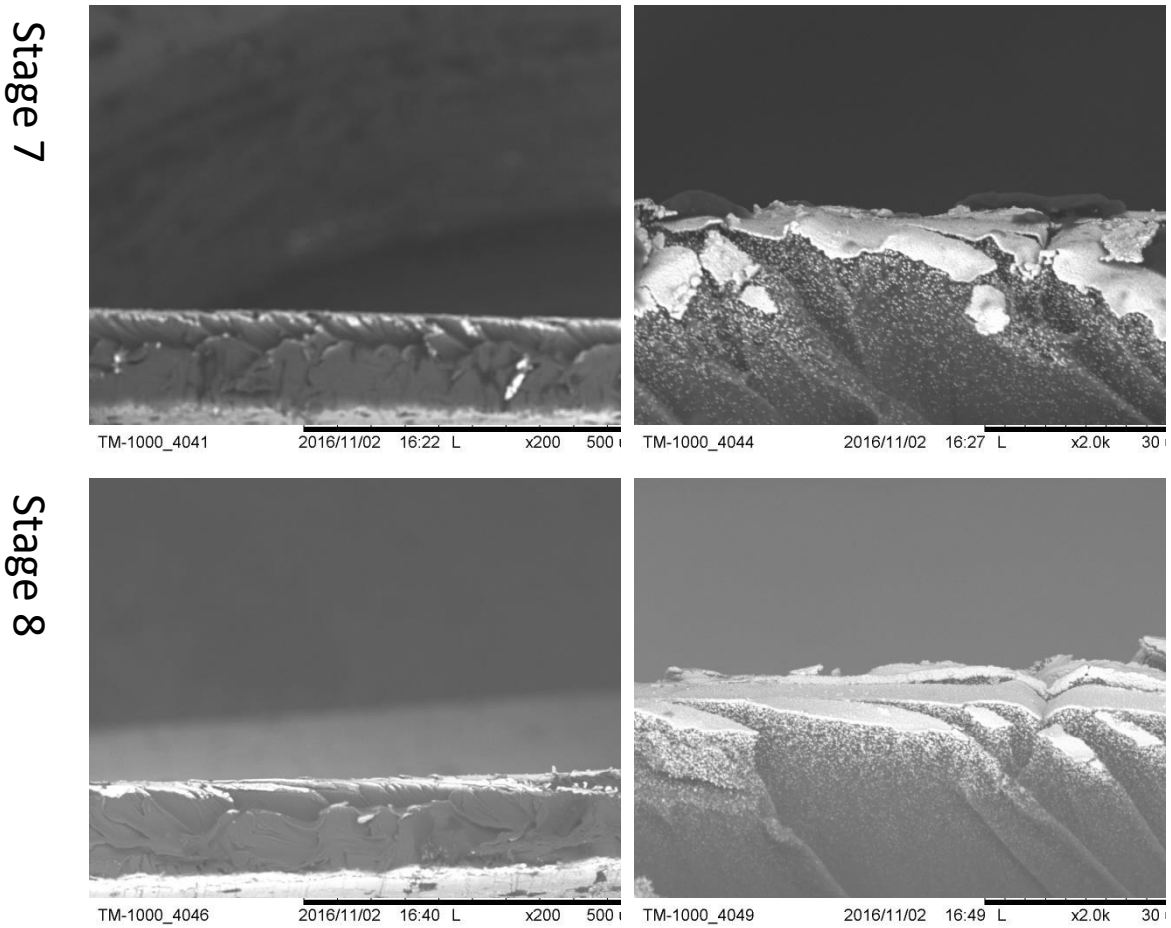

Figure 11.38 Cross Section images of Strathclyde 1

11.5 Blocking Force Diagrams

2.1 Commercial 1

Figure 11.39 to **Figure 11.42** show the blocking force diagram of Commercial 1 IPMC.

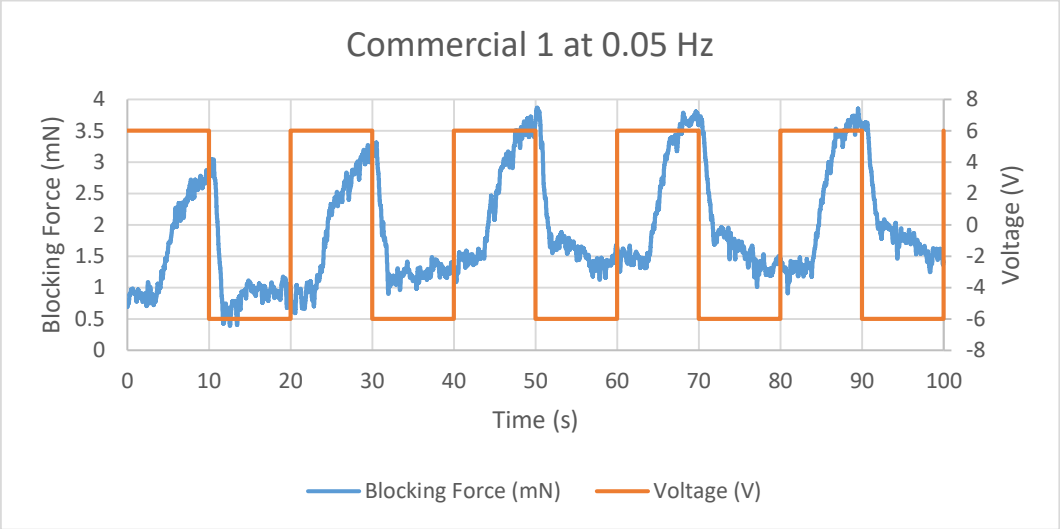

Figure 11.39 Blocking Force of Commercial 1 IPMC at 0.05 Hz

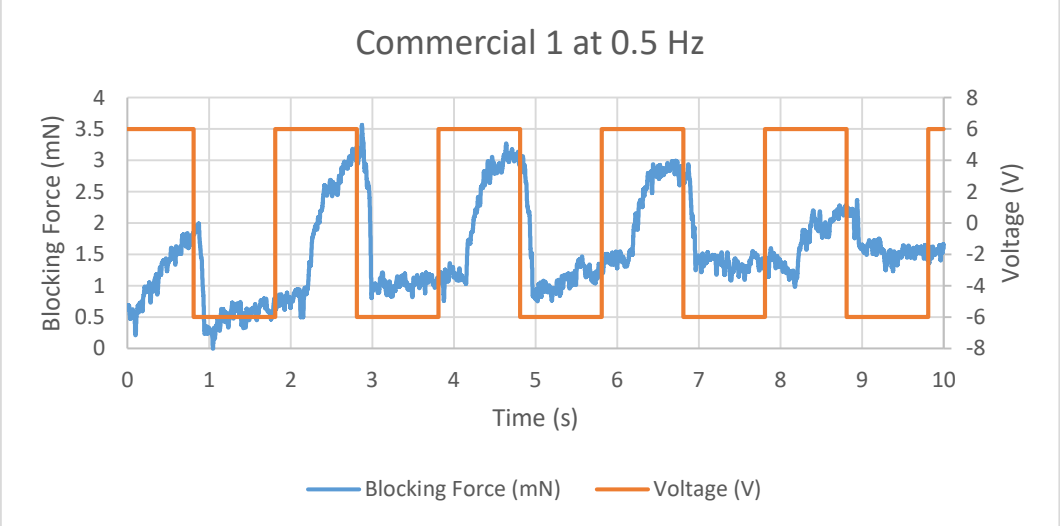

Figure 11.40 Blocking Force of Commercial 1 IPMC at 0.5 Hz

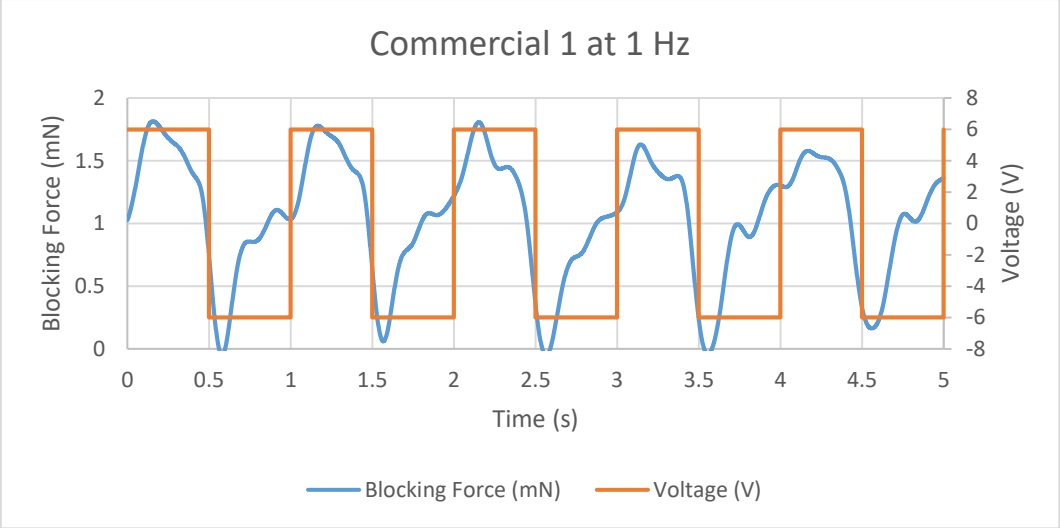

Figure 11.41 Blocking Force of Commercial 1 IPMC at 1 Hz

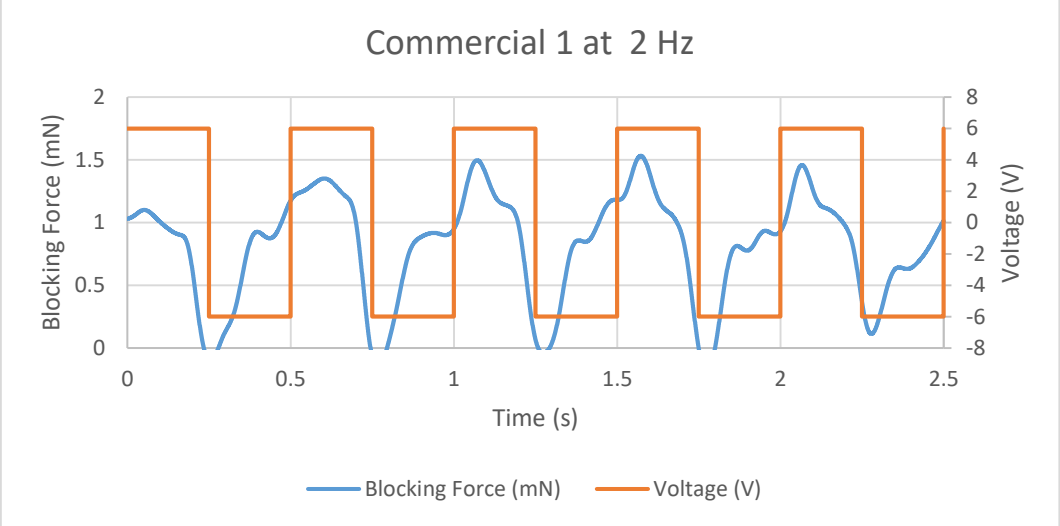

Figure 11.42 Blocking Force of Commercial 1 IPMC at 2 Hz

2.2 Commercial 2

Figure 11.43 to **Figure 11.46** show the blocking force diagram of Commercial 2 IPMC.

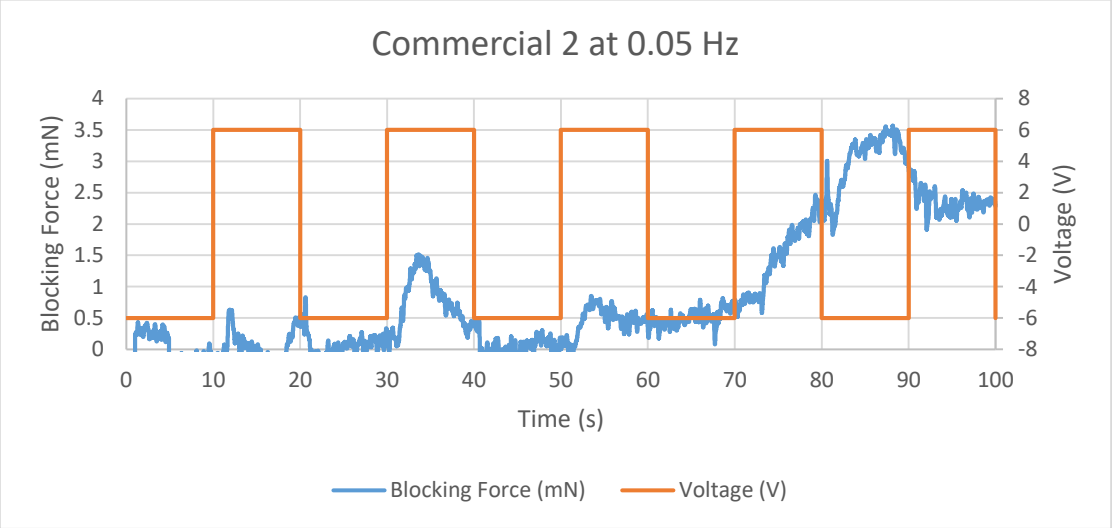

Figure 11.43 Blocking Force of Commercial 2 IPMC at 0.05 Hz

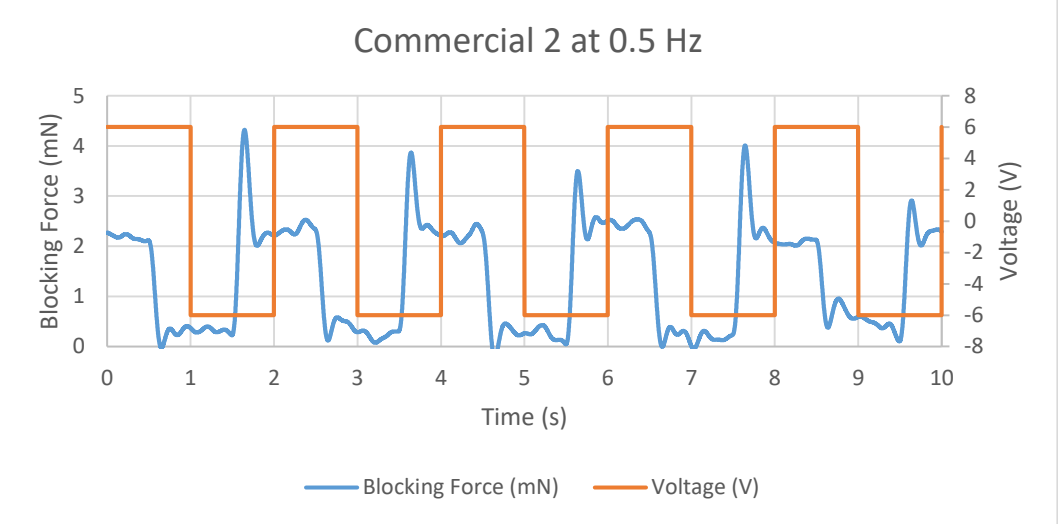

Figure 11.44 Blocking Force of Commercial 2 IPMC at 0.5 Hz

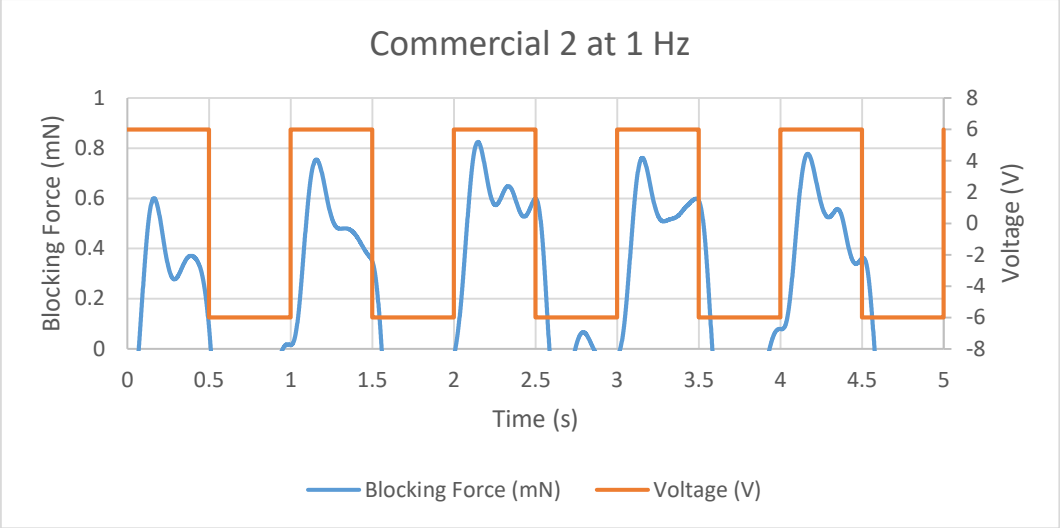

Figure 11.45 Blocking Force of Commercial 2 IPMC at 1 Hz

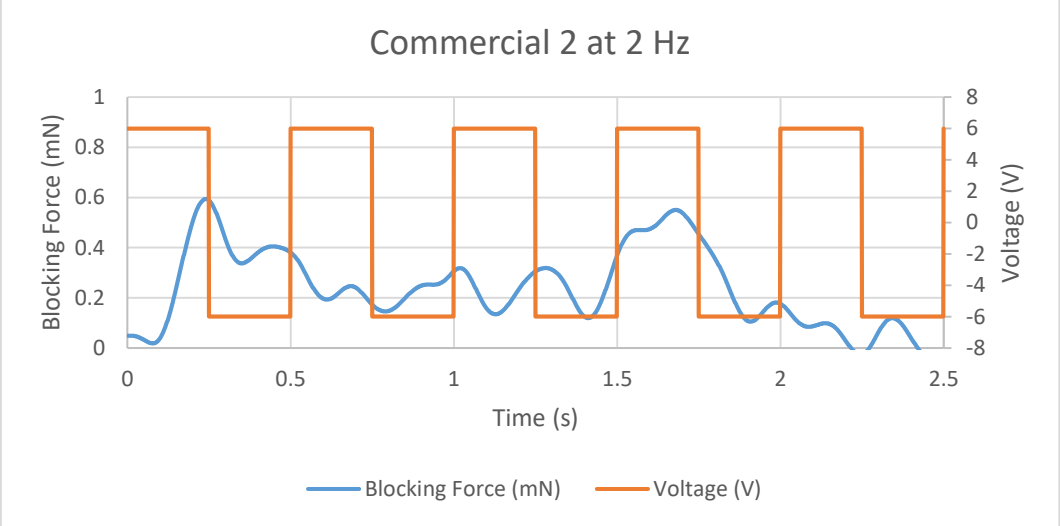

Figure 11.46 Blocking Force of Commercial 2 IPMC at 2 Hz

2.3 Commercial 3

Figure 11.47 to **Figure 11.50** show the blocking force diagram of Commercial 3 IPMC.

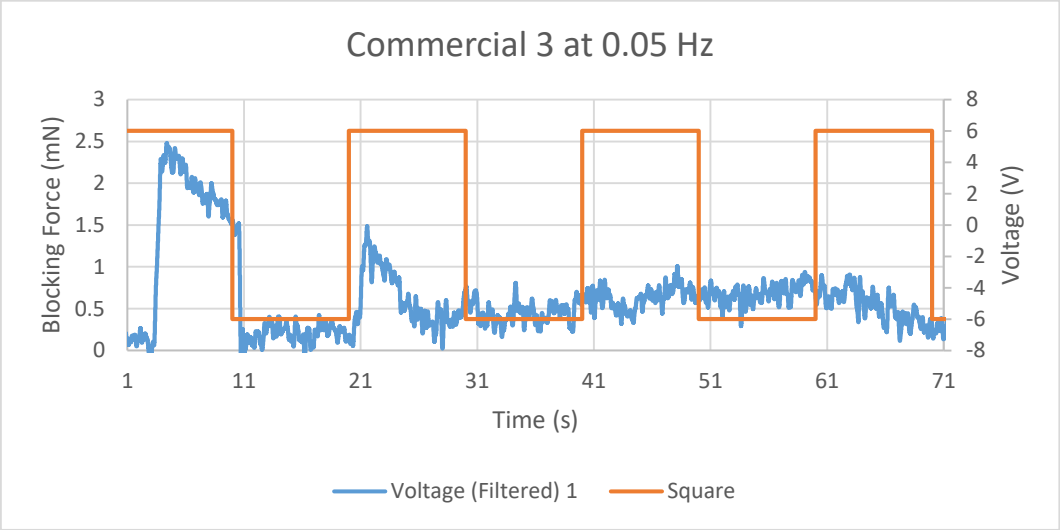

Figure 11.47 Blocking Force of Commercial 3 IPMC at 0.05 Hz

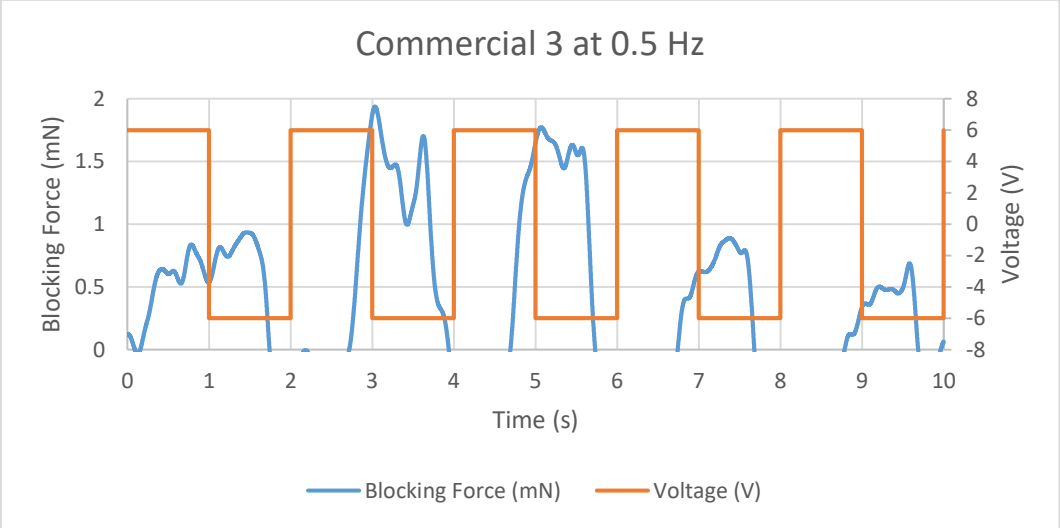

Figure 11.48 Blocking Force of Commercial 3 IPMC at 0.5 Hz

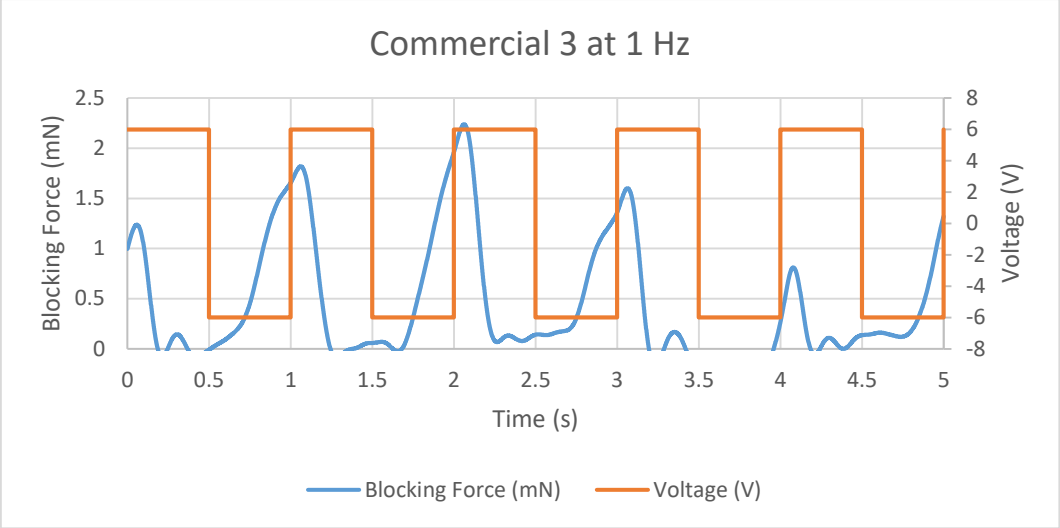

Figure 11.49 Blocking Force of Commercial 3 IPMC at 1 Hz

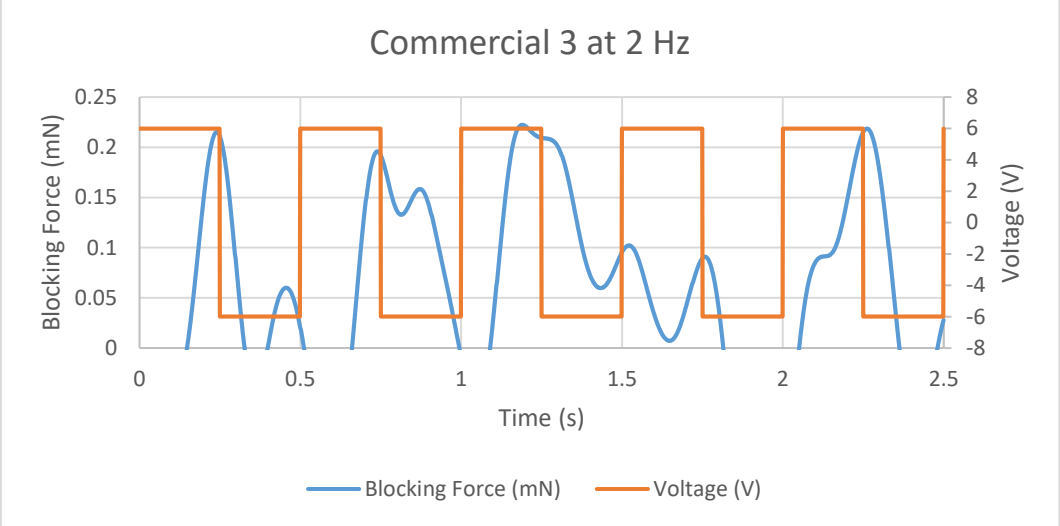

Figure 11.50 Blocking Force of Commercial 3 IPMC at 2 Hz

2.4 Commercial 4

Figure 11.51 to **Figure 11.52** show the blocking force diagram of Commercial 4 IPMC.

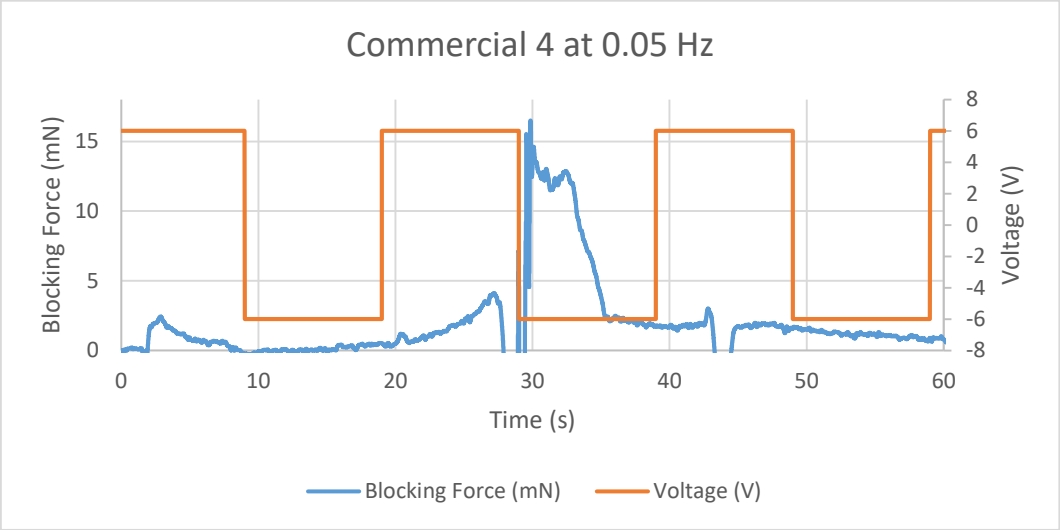

Figure 11.51 Blocking Force of Commercial 4 IPMC at 0.05 Hz

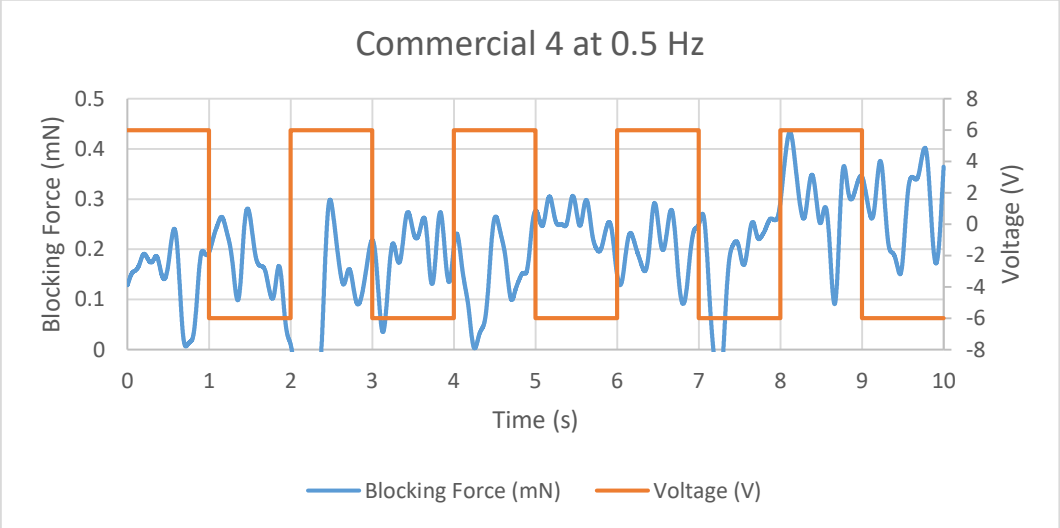

Figure 11.52 Blocking Force of Commercial 4 IPMC at 0.5 Hz

2.5 Commercial 5

Figure 11.53 to **Figure 11.56** show the blocking force diagram of Commercial 5 IPMC.

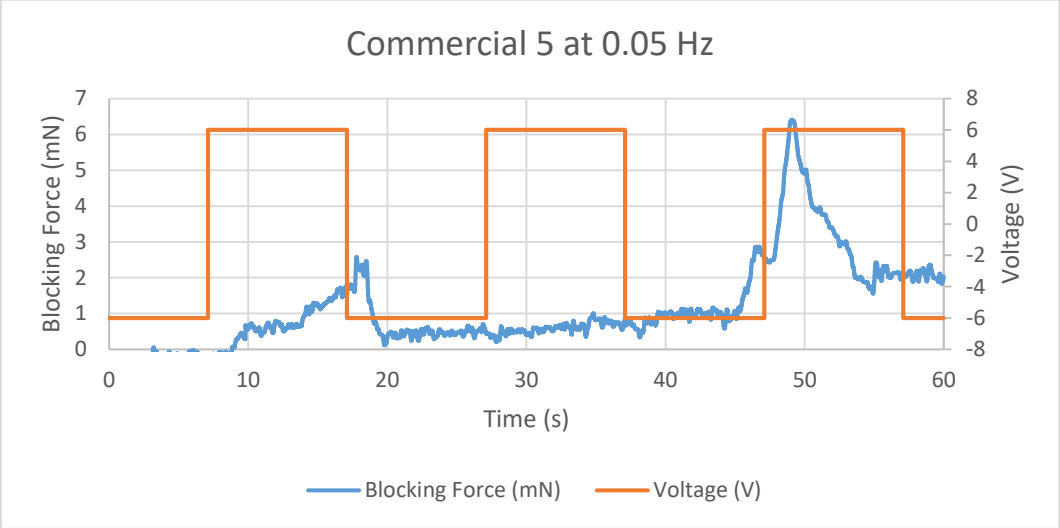

Figure 11.53 Blocking Force of Commercial 5 IPMC at 0.05 Hz

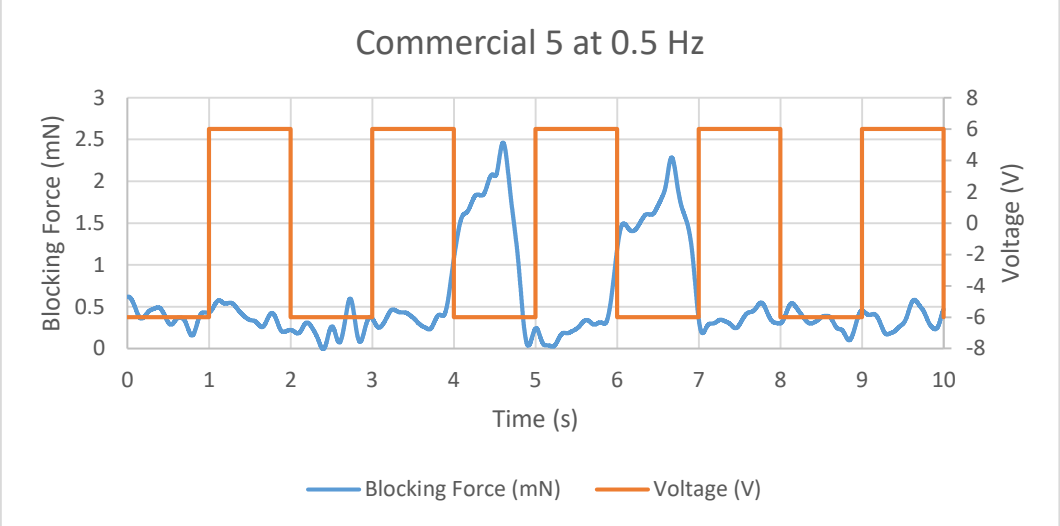

Figure 11.54 Blocking Force of Commercial 5 IPMC at 0.5 Hz

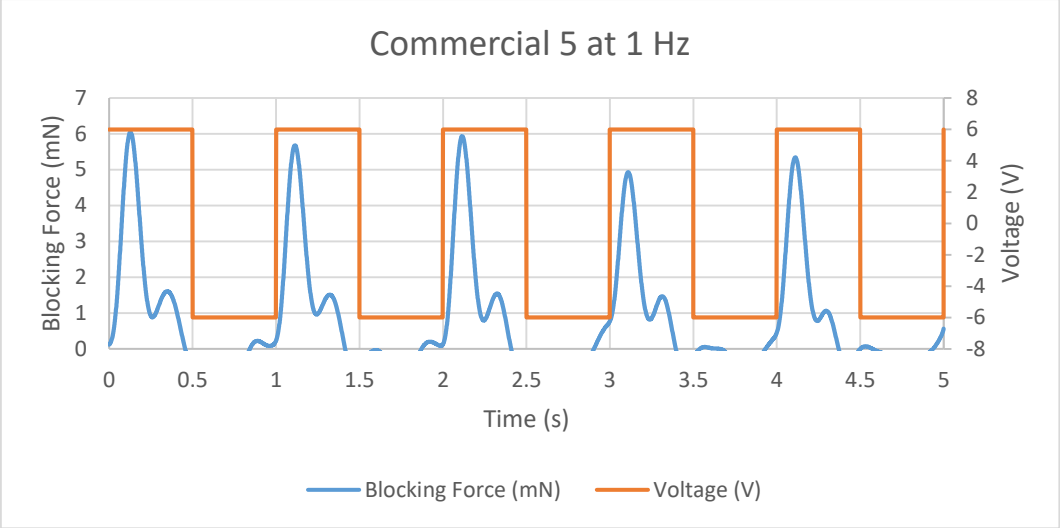

Figure 11.55 Blocking Force of Commercial 5 IPMC at 1 Hz

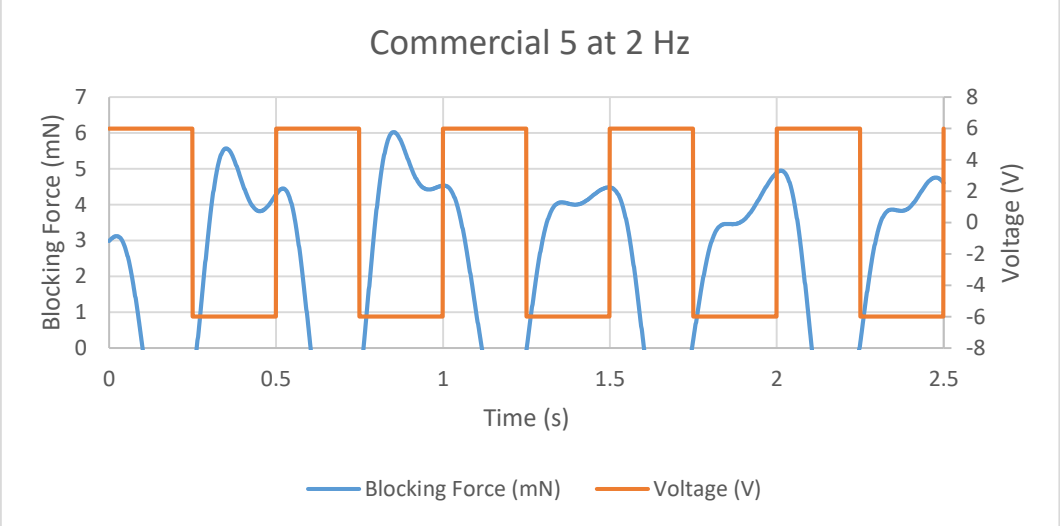

Figure 11.56 Blocking Force of Commercial 5 IPMC at 2 Hz

2.6 Commercial 6

Figure 11.57 to **Figure 11.60** show the blocking force diagram of Commercial 6 IPMC.

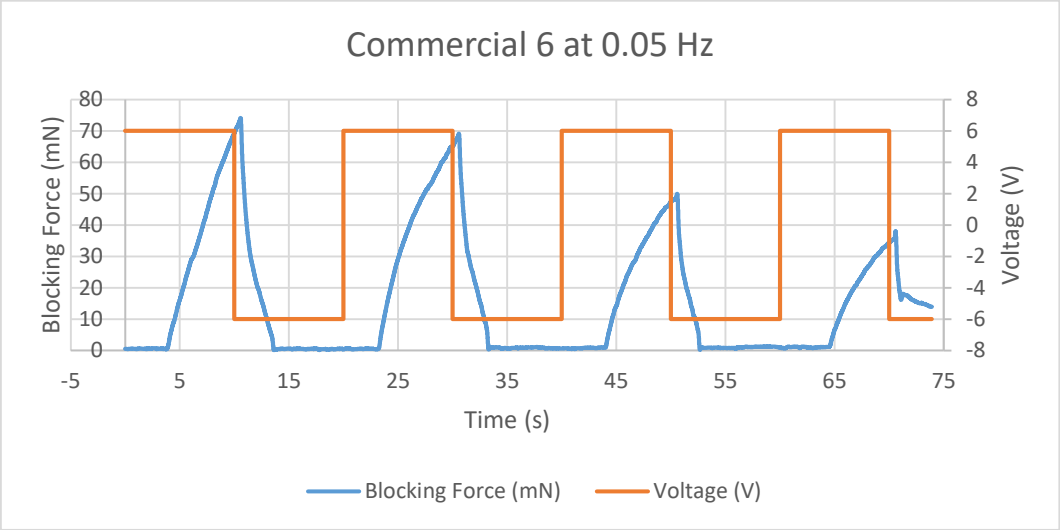

Figure 11.57 Blocking Force of Commercial 6 IPMC at 0.05 Hz

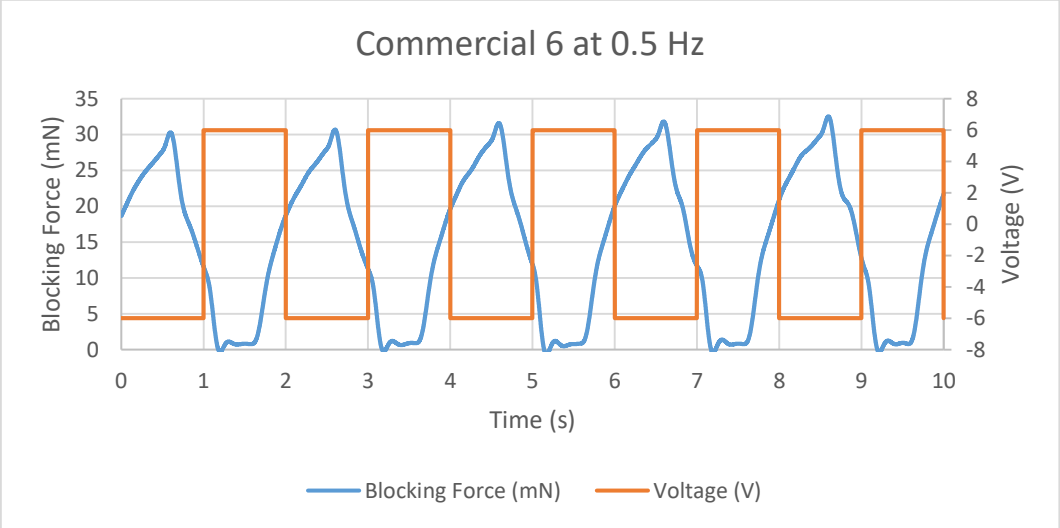

Figure 11.58 Blocking Force of Commercial 6 IPMC at 0.5 Hz

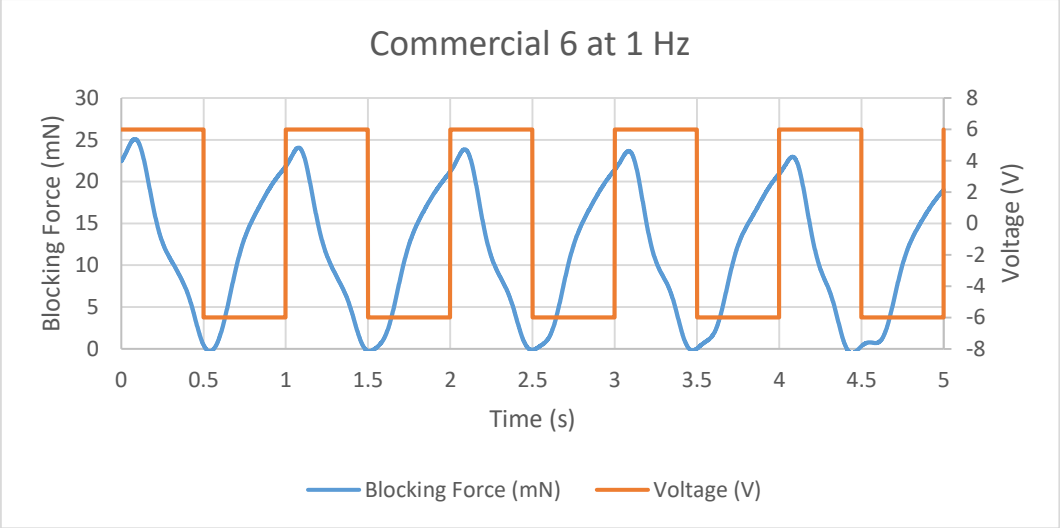

Figure 11.59 Blocking Force of Commercial 6 IPMC at 1 Hz

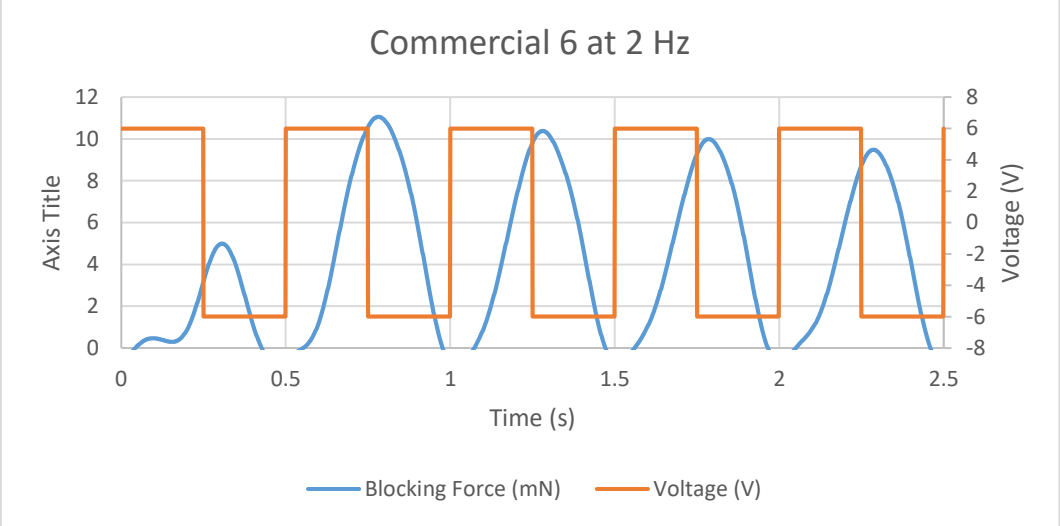

Figure 11.60 Blocking Force of Commercial 6 IPMC at 2 Hz

2.7 Strathclyde 1

Figure 11.61 to **Figure 11.64** show the blocking force diagram of Strathclyde 1 IPMC.

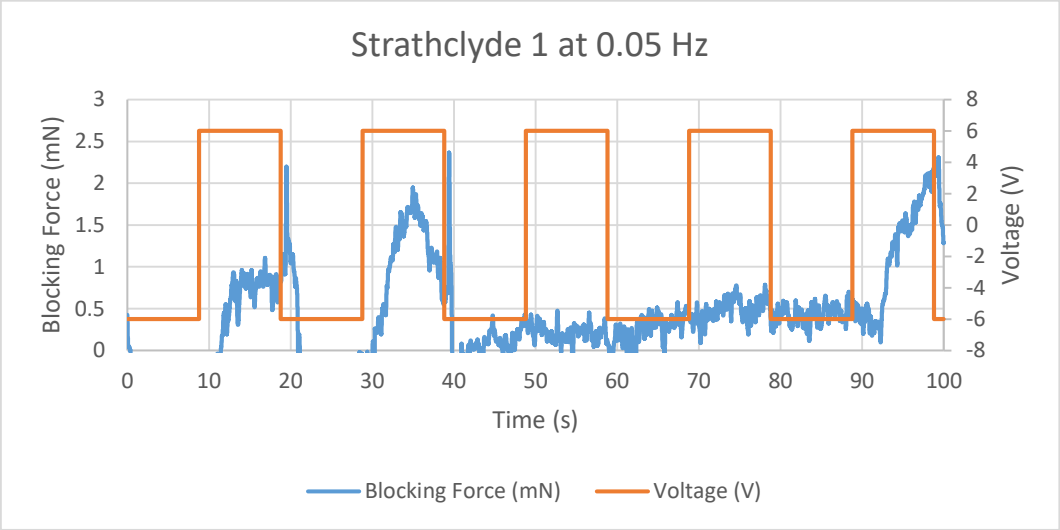

Figure 11.61 Blocking Force of Strathclyde 1 IPMC at 0.05 Hz

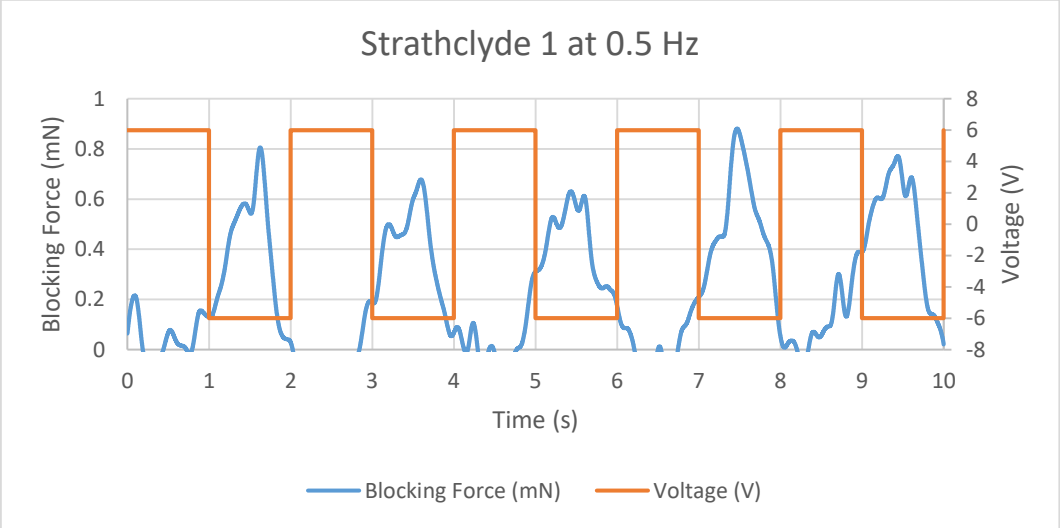

Figure 11.62 Blocking Force of Strathclyde 1 IPMC at 0.5 Hz

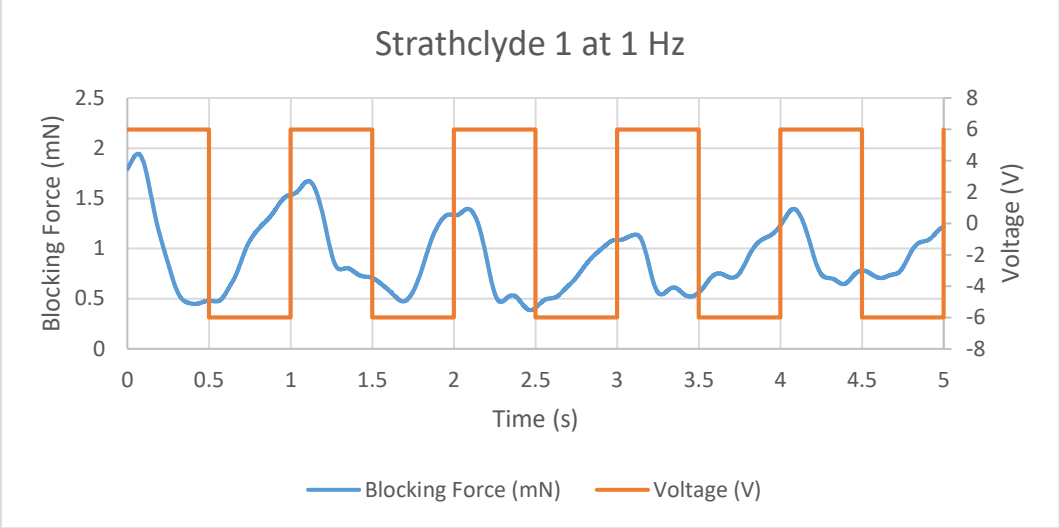

Figure 11.63 Blocking Force of Strathclyde 1 IPMC at 1 Hz

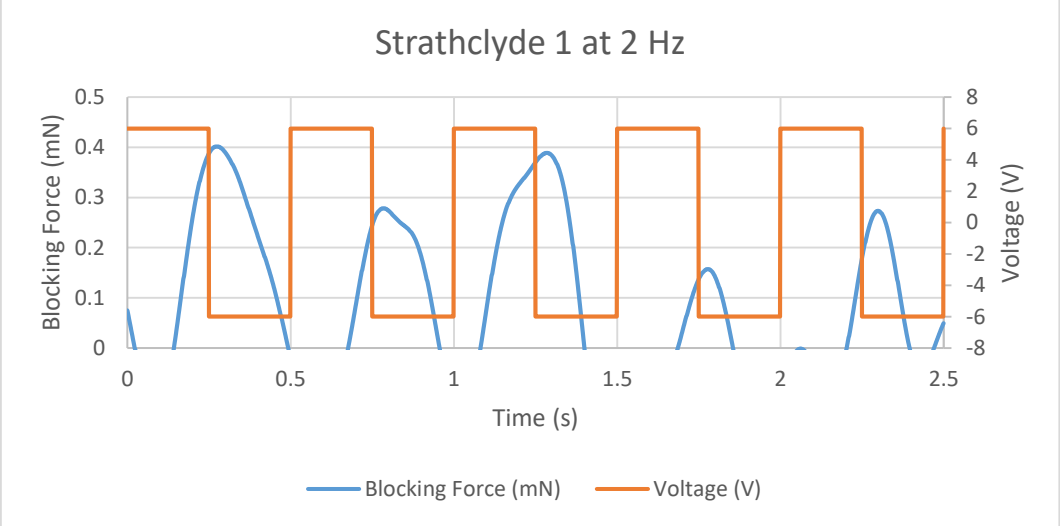

Figure 11.64 Blocking Force of Strathclyde 1 IPMC at 2 Hz

2.8 Strathclyde 2

Figure 11.65 to **Figure 11.68** show the blocking force diagram of Strathclyde 2 IPMC.

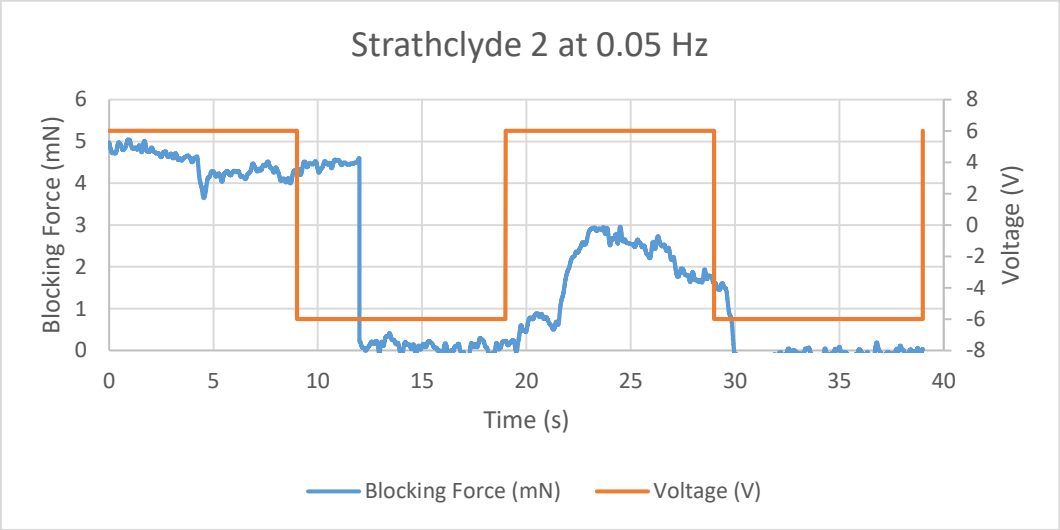

Figure 11.65 Blocking Force of Strathclyde 2 IPMC at 0.05 Hz

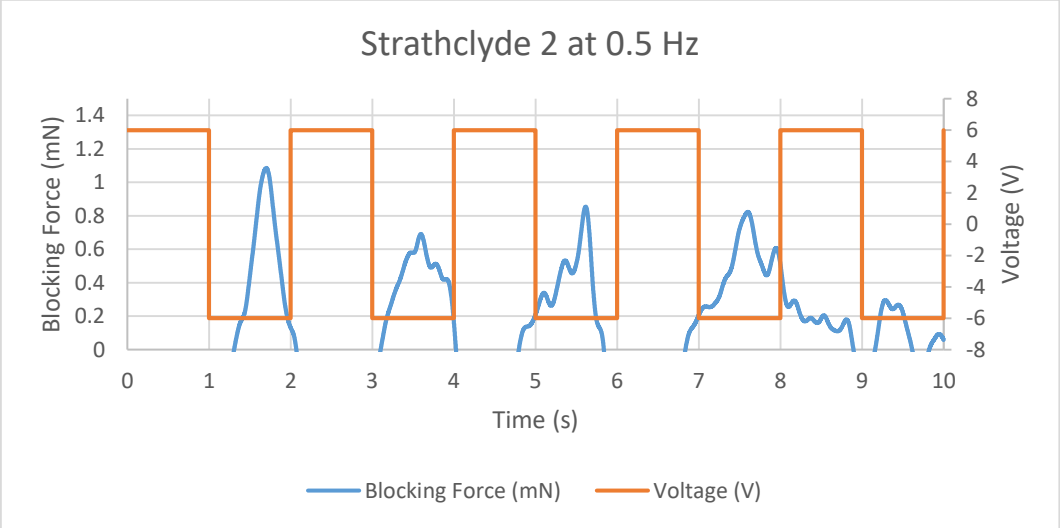

Figure 11.66 Blocking Force of Strathclyde 2 IPMC at 0.5 Hz

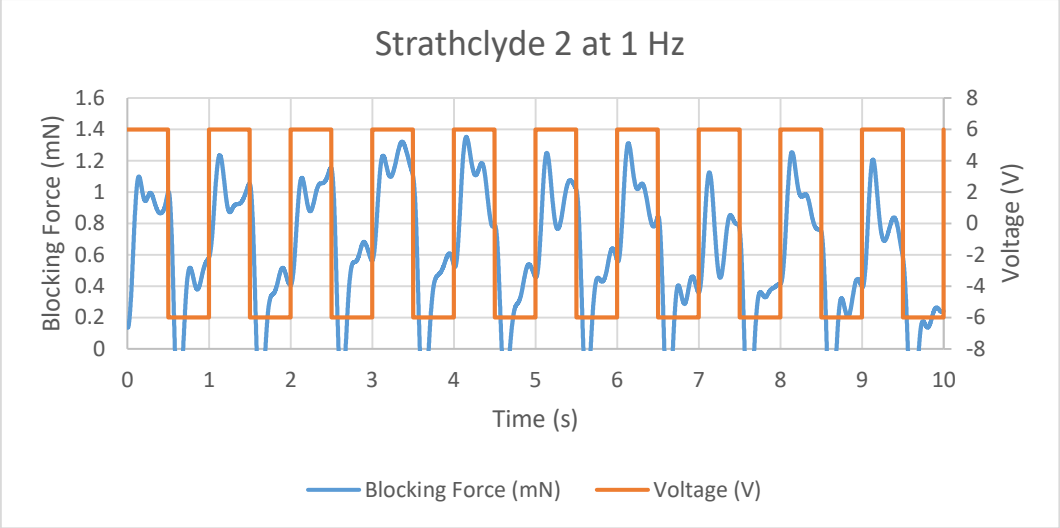

Figure 11.67 Blocking Force of Strathclyde 2 IPMC at 1 Hz

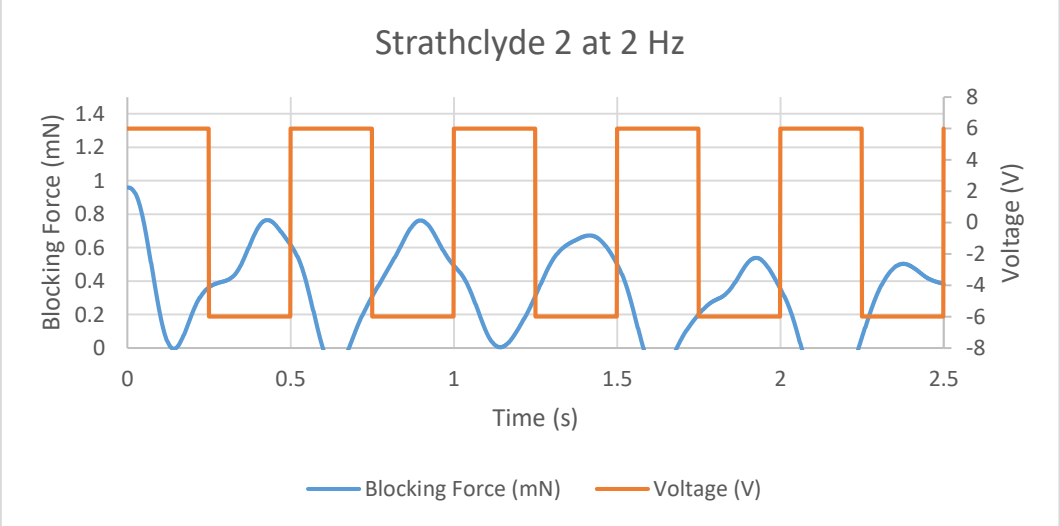

Figure 11.68 Blocking Force of Strathclyde 2 IPMC at 2 Hz

2.9 Strathclyde 3

Figure 11.69 to **Figure 11.72** show the blocking force diagram of Strathclyde 3 IPMC.

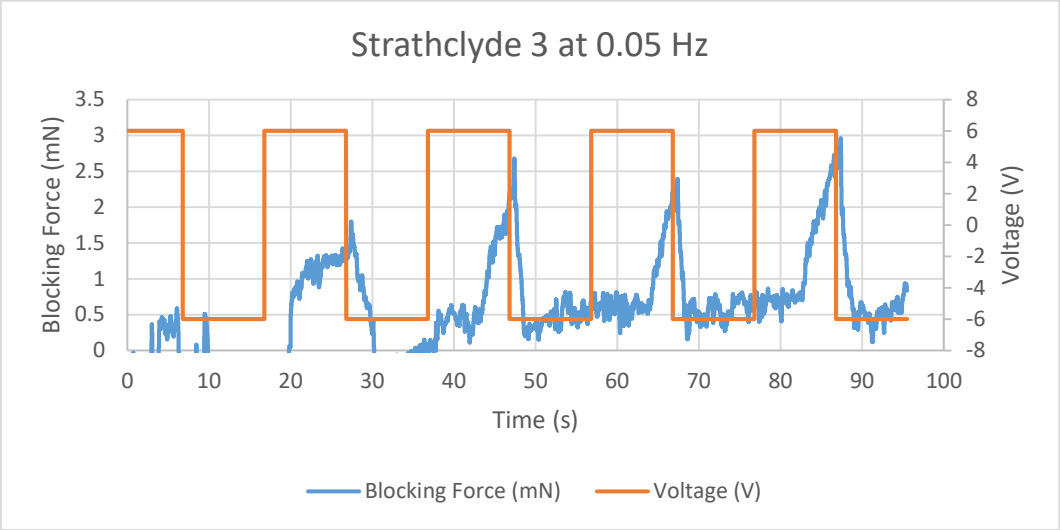

Figure 11.69 Blocking Force of Strathclyde 3 IPMC at 0.05 Hz

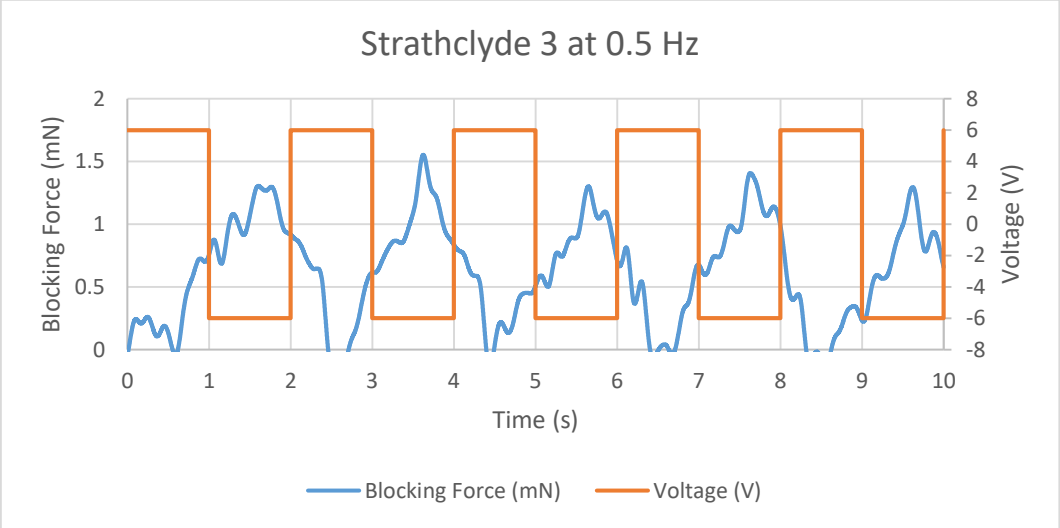

Figure 11.70 Blocking Force of Strathclyde 3 IPMC at 0.5 Hz

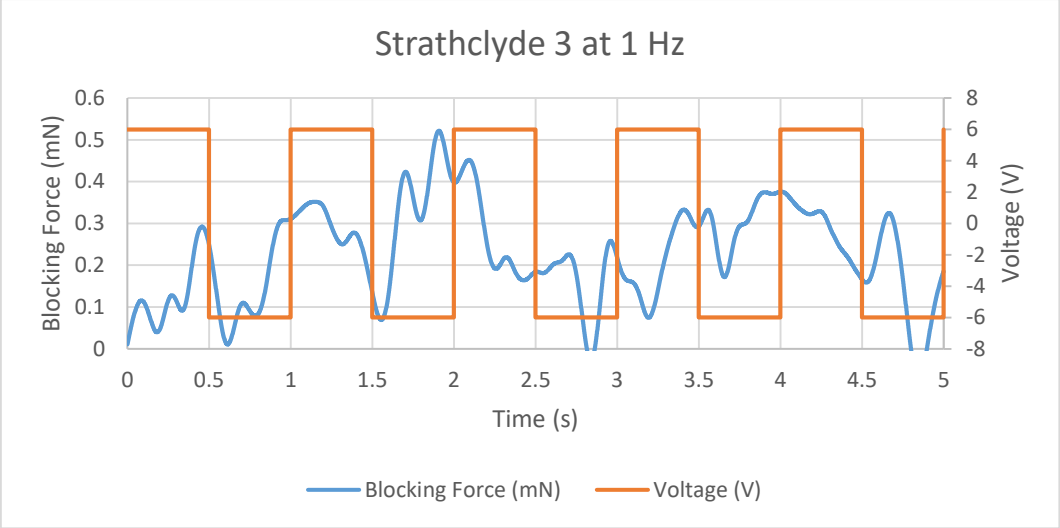

Figure 11.71 Blocking Force of Strathclyde 3 IPMC at 1 Hz

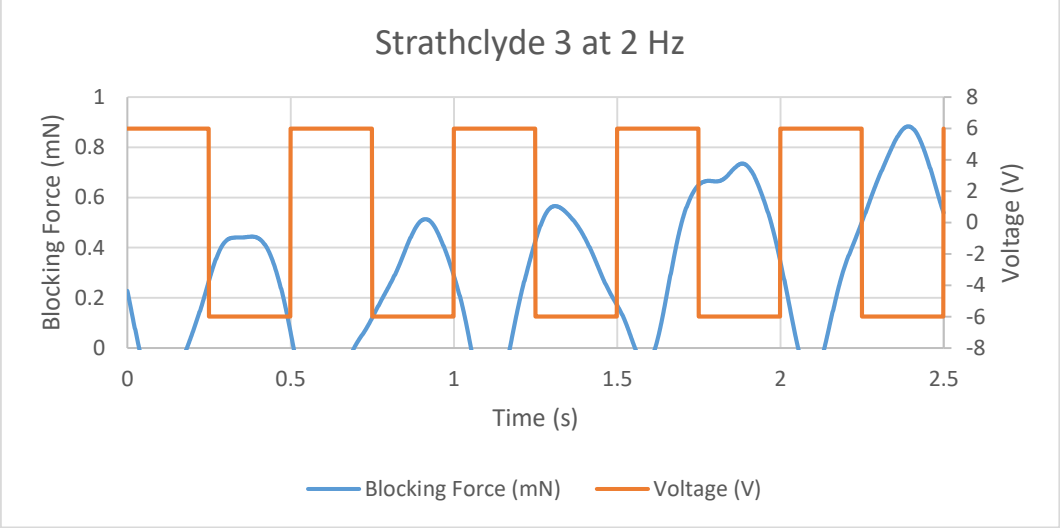

Figure 11.72 Blocking Force of Strathclyde 3 IPMC at 2 Hz

2.10 Strathclyde 4

Figure 11.73 to **Figure 11.76** show the blocking force diagram of Strathclyde 4 IPMC.

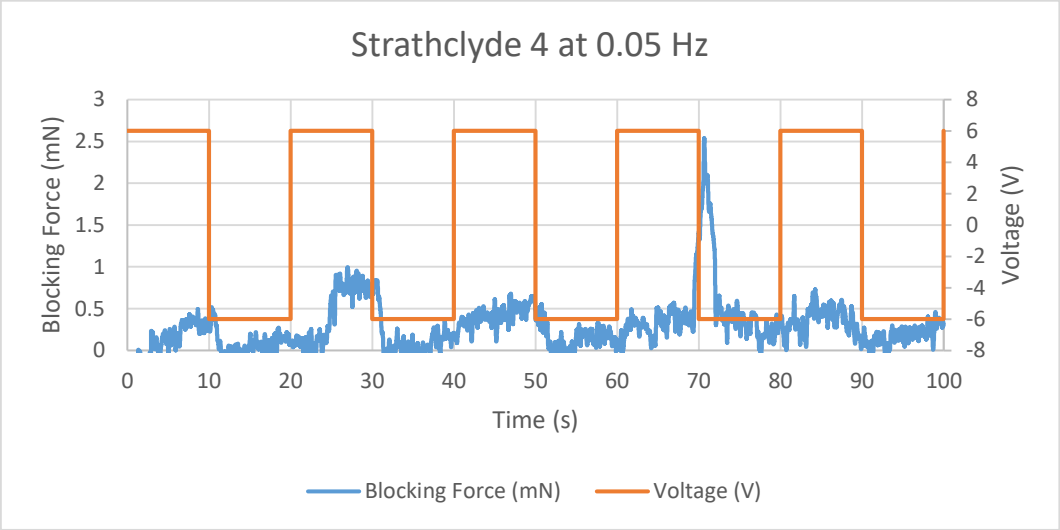

Figure 11.73 Blocking Force of Strathclyde 4 IPMC at 0.05 Hz

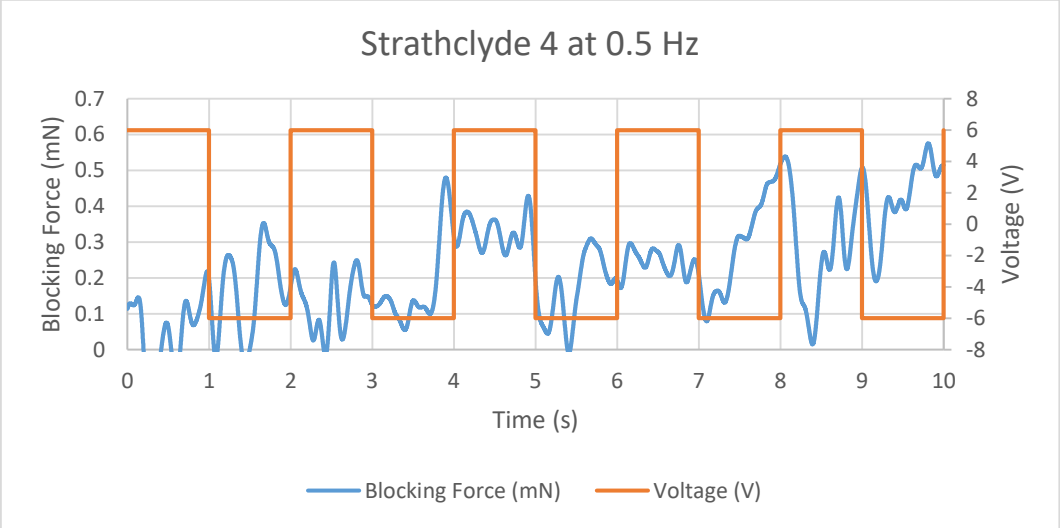

Figure 11.74 Blocking Force of Strathclyde 4 IPMC at 0.5 Hz

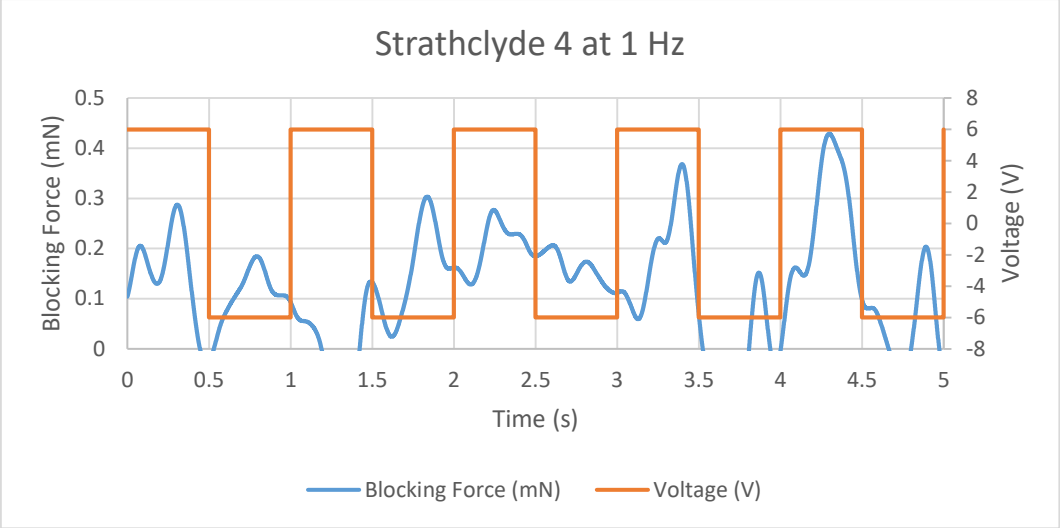

Figure 11.75 Blocking Force of Strathclyde 4 IPMC at 1 Hz

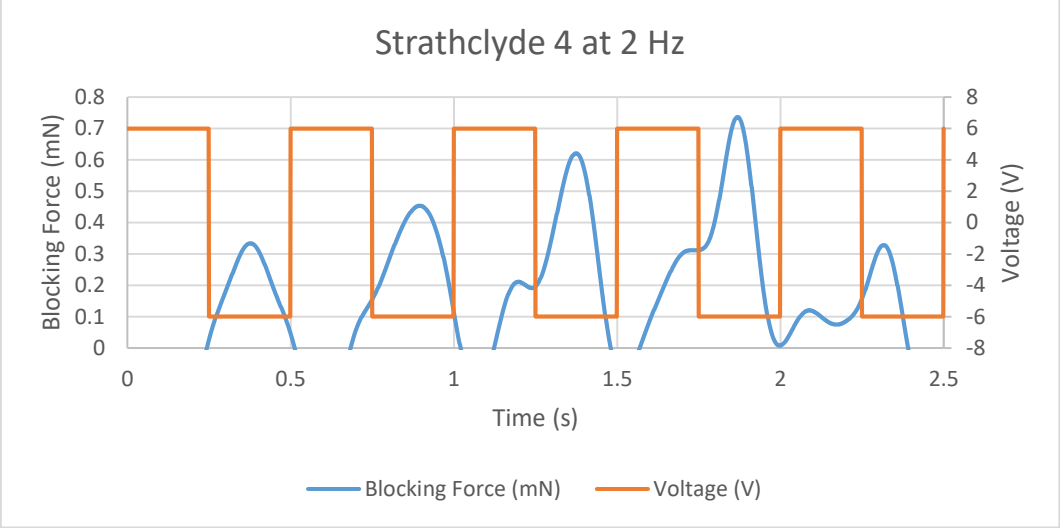

Figure 11.76 Blocking Force of Strathclyde 4 IPMC at 2 Hz

2.11 Strathclyde 5

Figure 11.77 to **Figure 11.80** show the blocking force diagram of Strathclyde 5 IPMC.

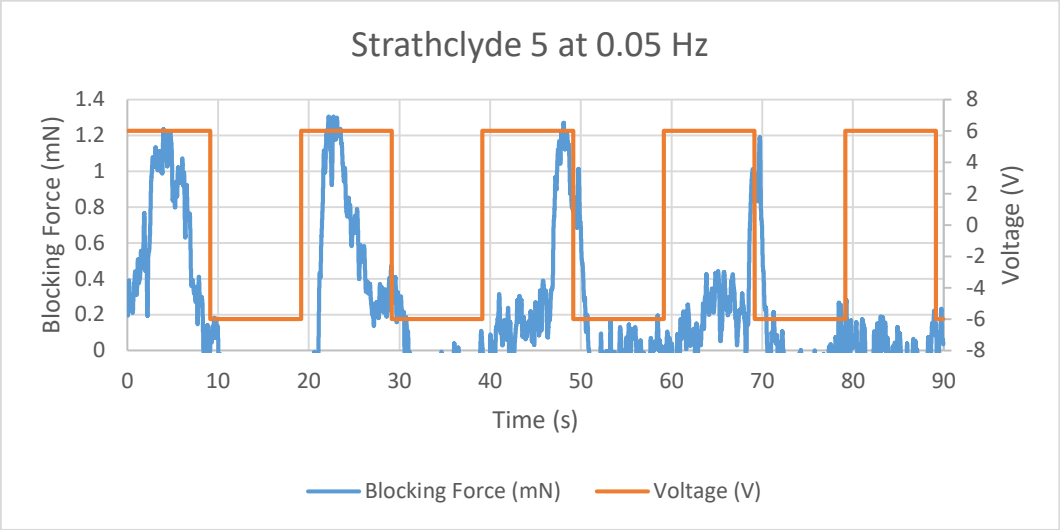

Figure 11.77 Blocking Force of Strathclyde 5 IPMC at 0.05 Hz

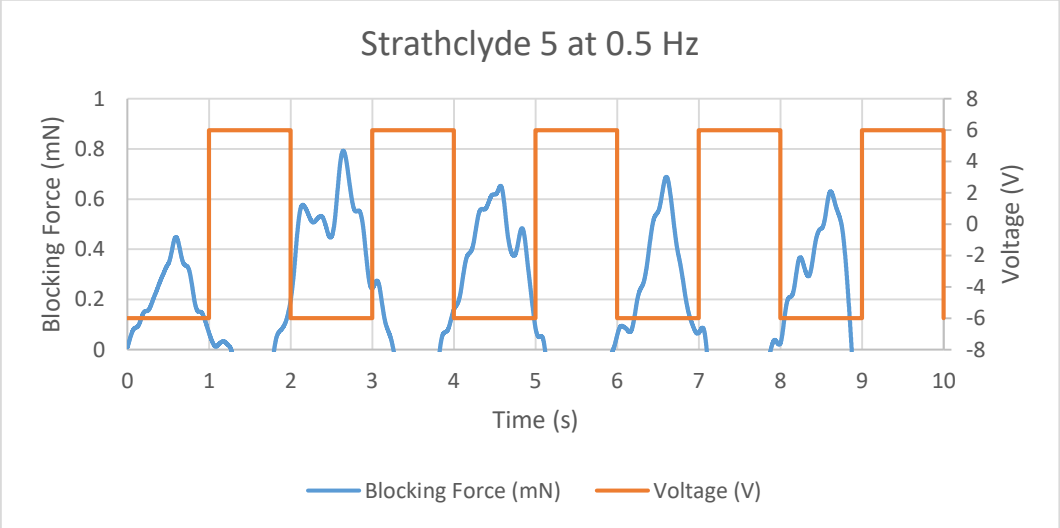

Figure 11.78 Blocking Force of Strathclyde 5 IPMC at 0.5 Hz

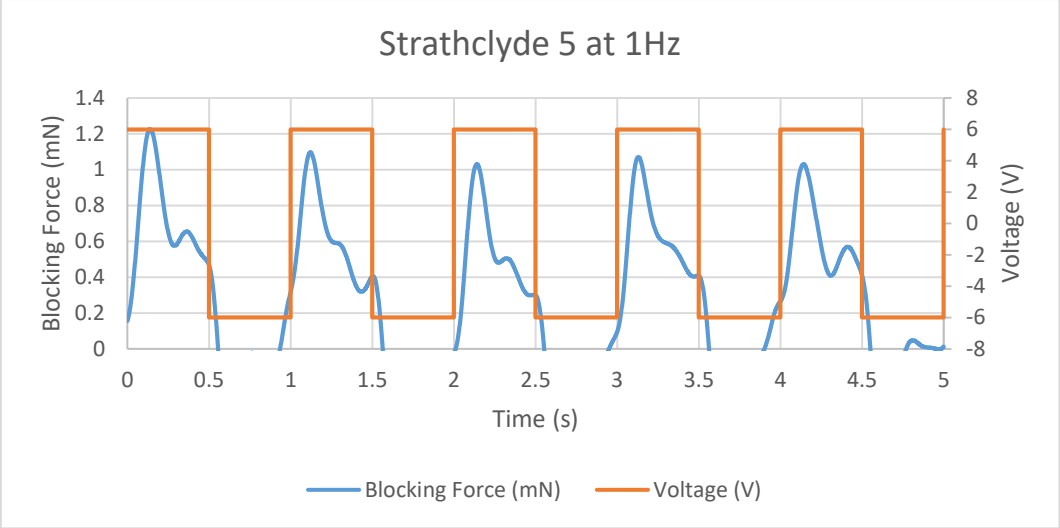

Figure 11.79 Blocking Force of Strathclyde 5 IPMC at 1 Hz

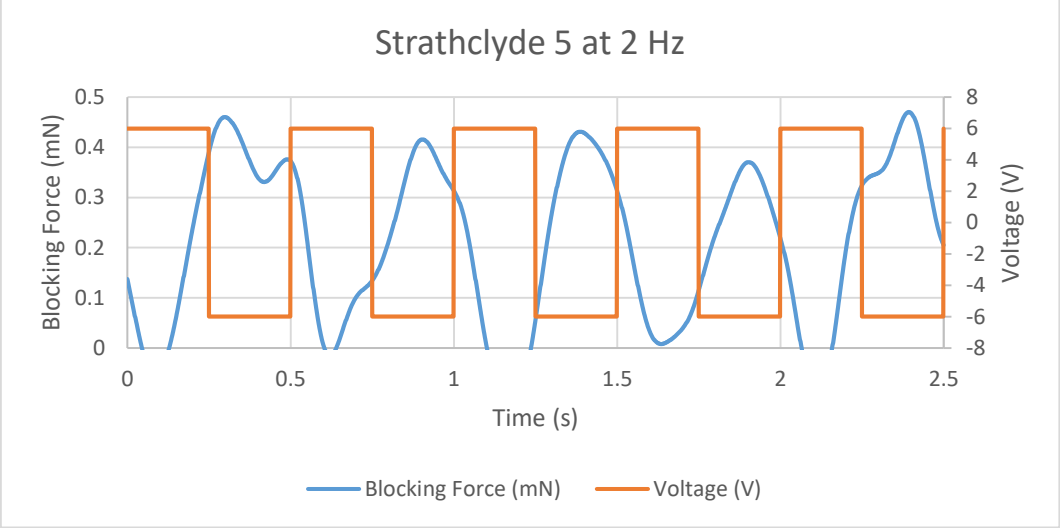

Figure 11.80 Blocking Force of Strathclyde 5 IPMC at 2 Hz

2.12 Strathclyde 6

Figure 11.81 to **Figure 11.84** show the blocking force diagram of Strathclyde 6 IPMC.

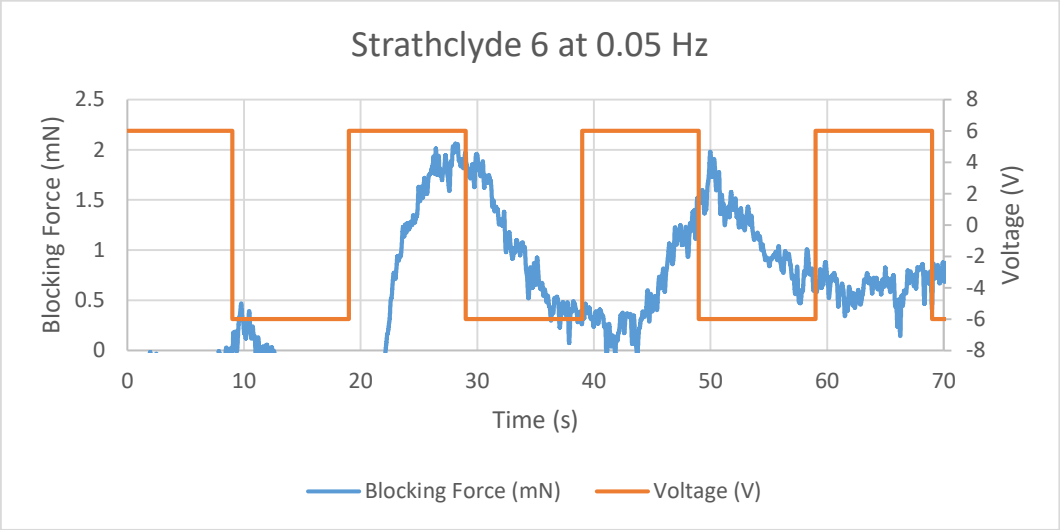

Figure 11.81 Blocking Force of Strathclyde 6 IPMC at 0.05 Hz

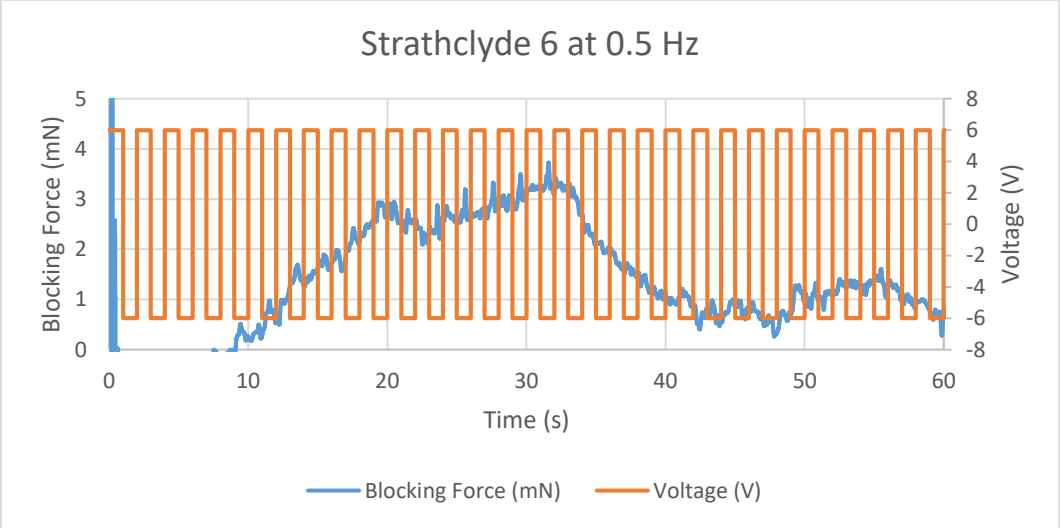

Figure 11.82 Blocking Force of Strathclyde 6 IPMC at 0.5 Hz

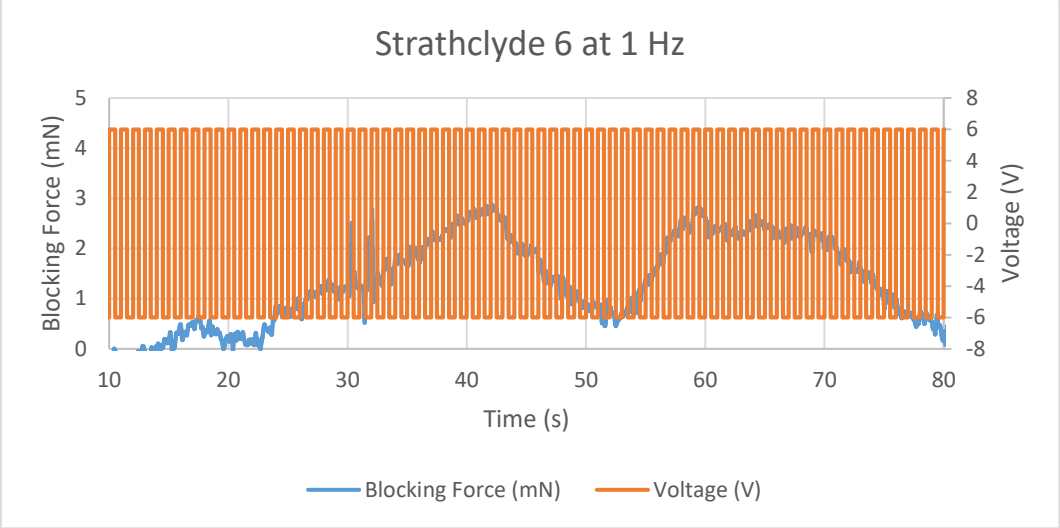

Figure 11.83 Blocking Force of Strathclyde 6 IPMC at 1 Hz

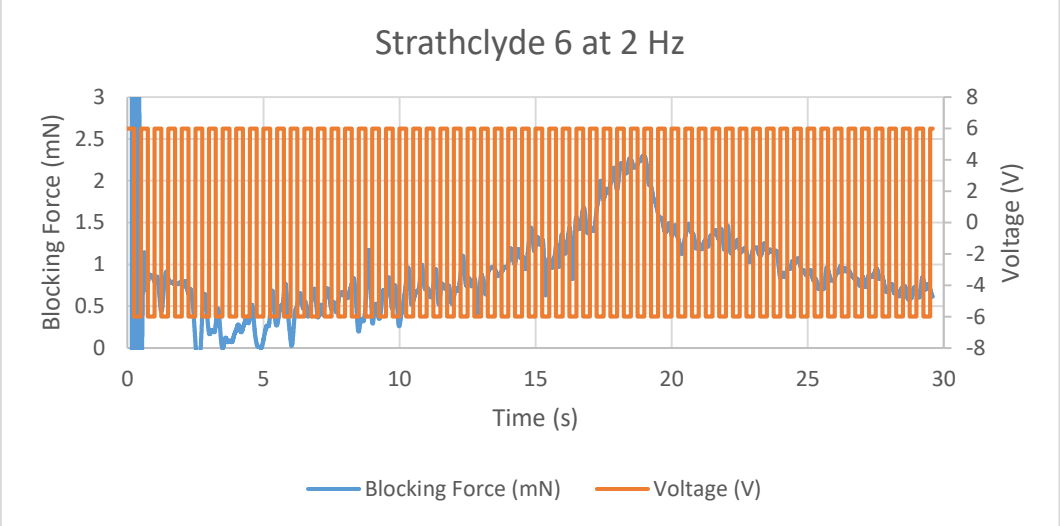

Figure 11.84 Blocking Force of Strathclyde 6 IPMC at 2 Hz

2.13 Strathclyde 7

Figure 11.85 to **Figure 11.88** show the blocking force diagram of Strathclyde 7 IPMC.

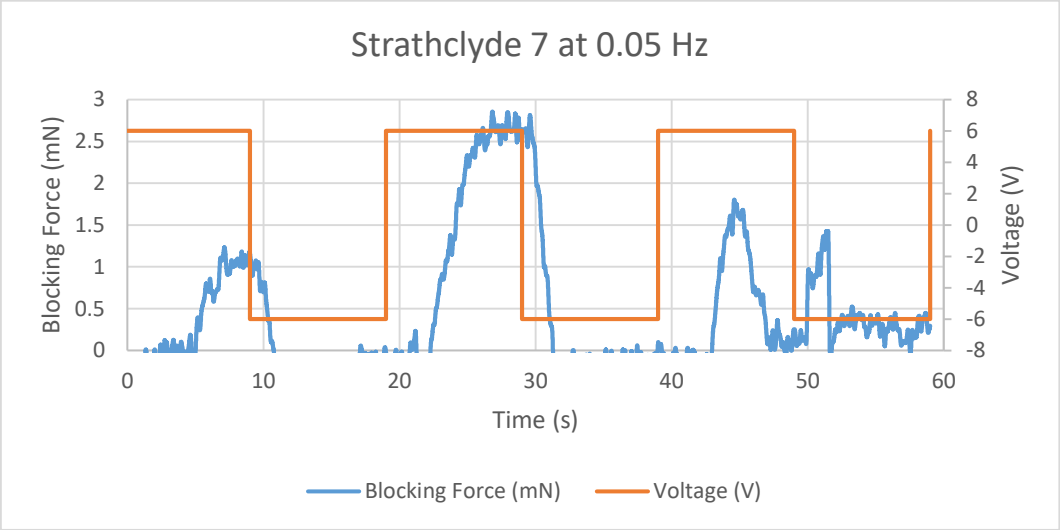

Figure 11.85 Blocking Force of Strathclyde 7 IPMC at 0.05 Hz

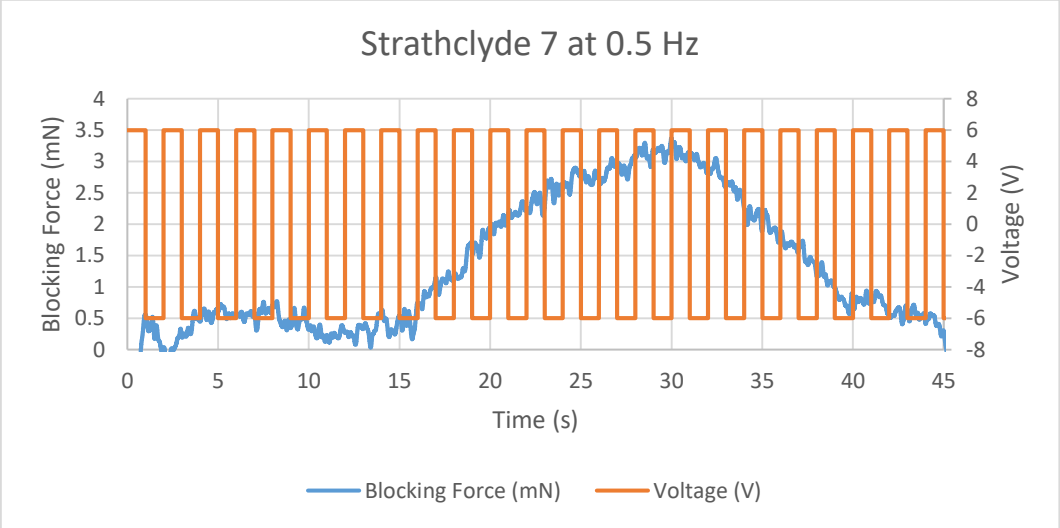

Figure 11.86 Blocking Force of Strathclyde 7 IPMC at 0.5 Hz

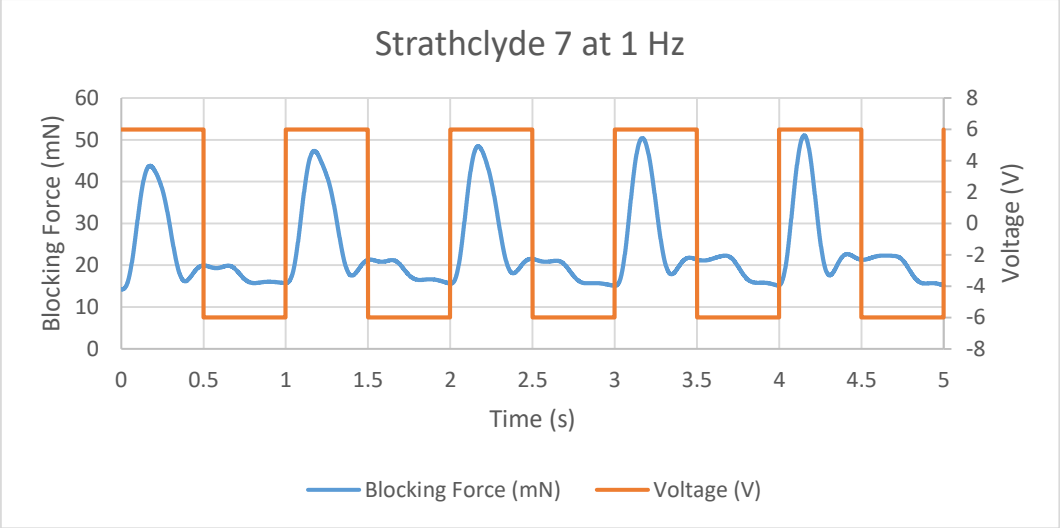

Figure 11.87 Blocking Force of Strathclyde 7 IPMC at 1 Hz

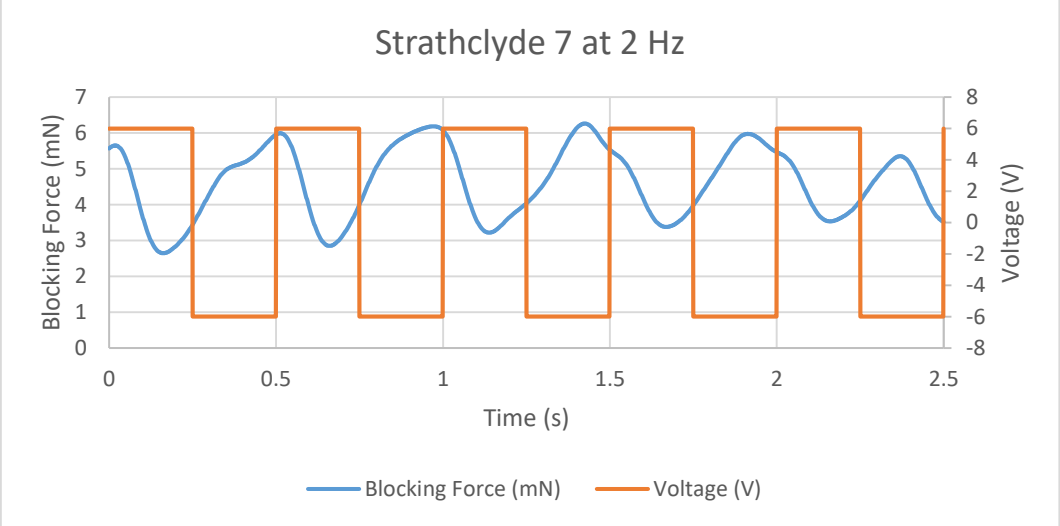

Figure 11.88 Blocking Force of Strathclyde 7 IPMC at 2 Hz

2.14 Strathclyde 8

Figure 11.89 to **Figure 11.91** show the blocking force diagram of Strathclyde 8 IPMC

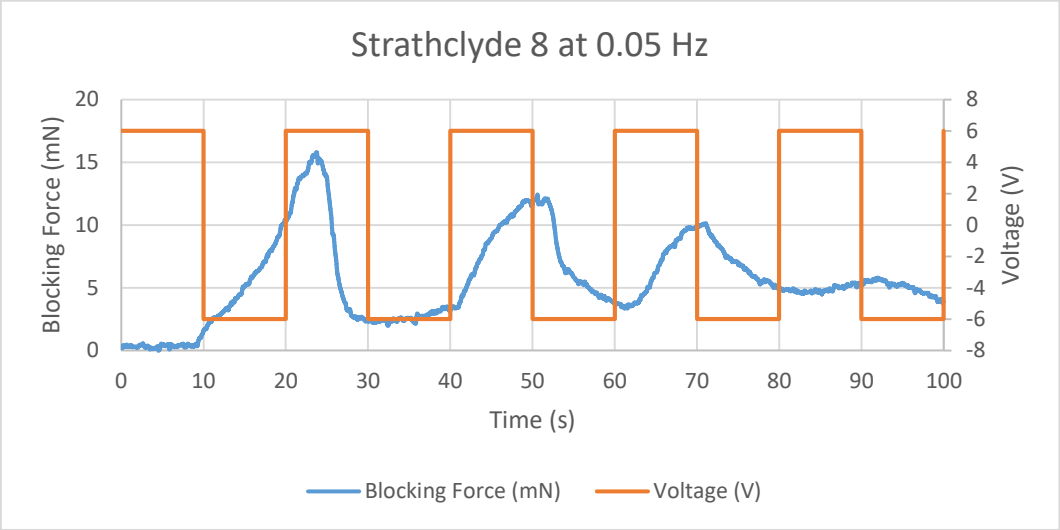

Figure 11.89 Blocking Force of Strathclyde 8 IPMC at 0.05 Hz

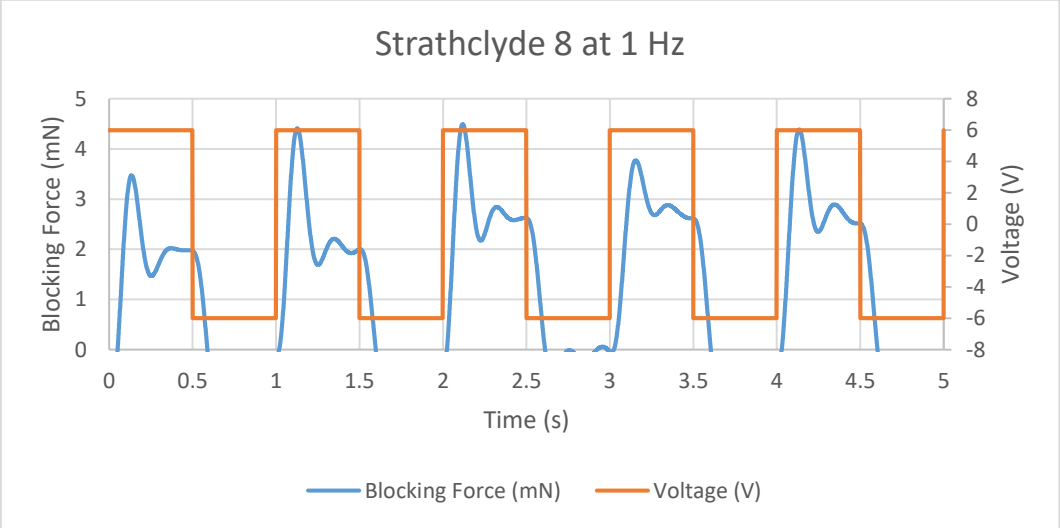

Figure 11.90 Blocking Force of Strathclyde 8 IPMC at 1 Hz

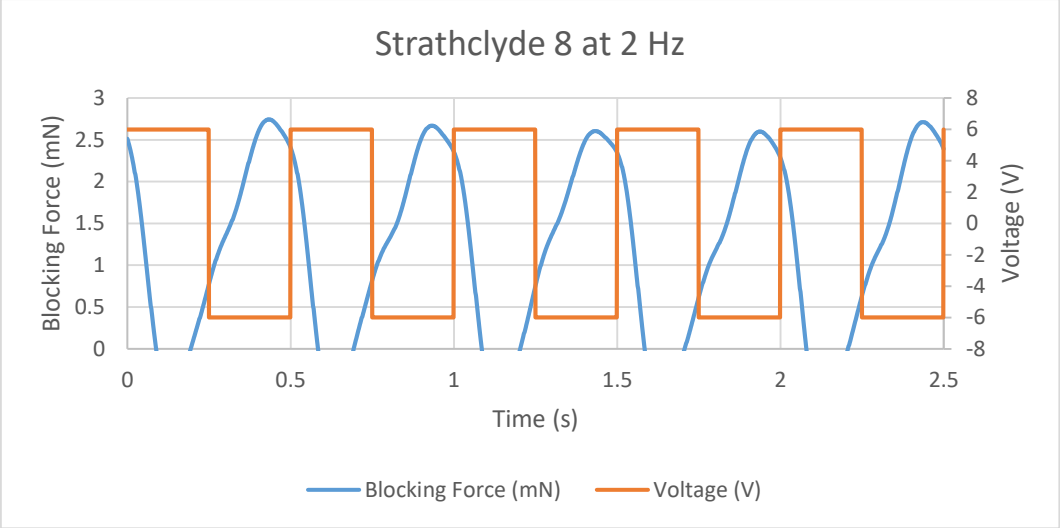

Figure 11.91 Blocking Force of Strathclyde 8 IPMC at 2 Hz

2.15 Strathclyde 9

Figure 11.92 to **Figure 11.95** show the blocking force diagram of Strathclyde 9 IPMC.

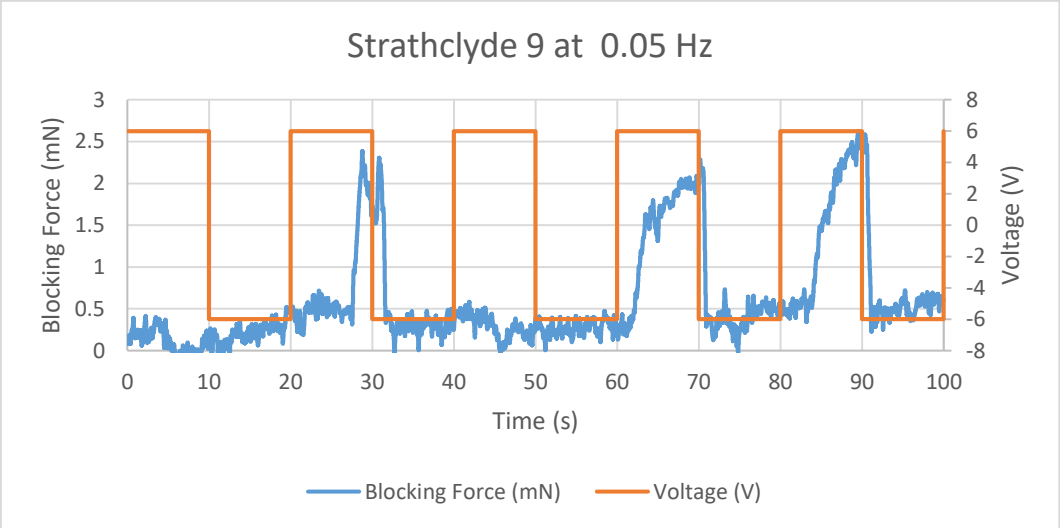

Figure 11.92 Blocking Force of Strathclyde 9 IPMC at 0.05 Hz

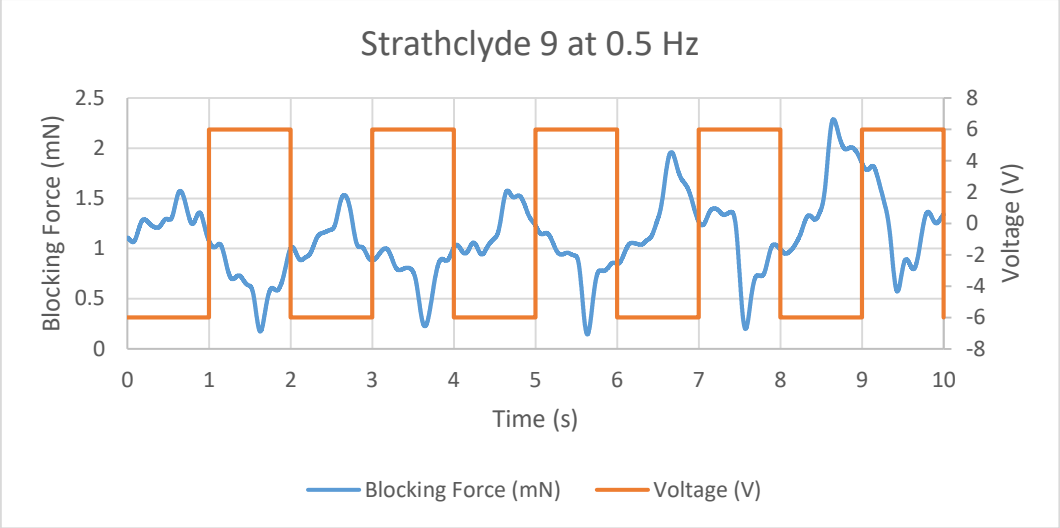

Figure 11.93 Blocking Force of Strathclyde 9 IPMC at 0.5 Hz

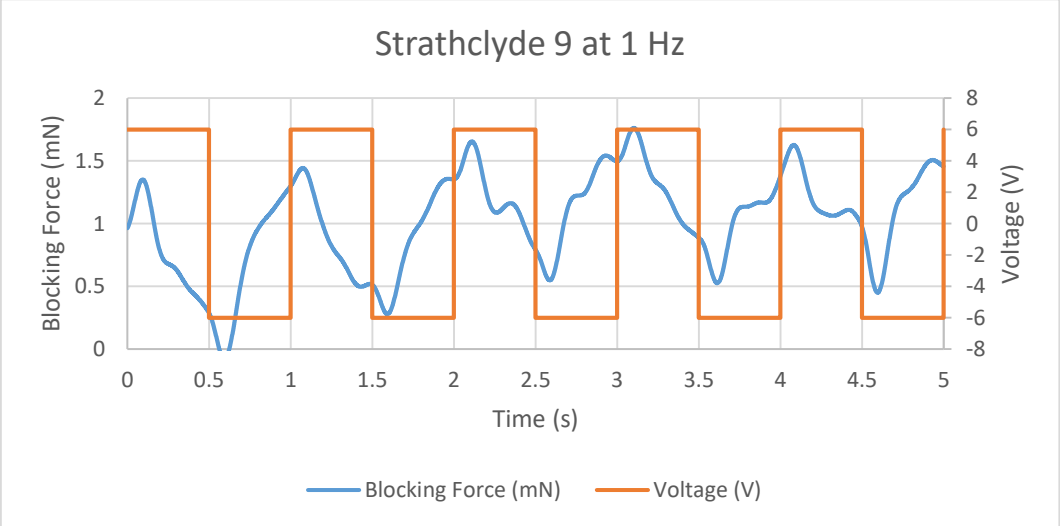

Figure 11.94 Blocking Force of Strathclyde 9 IPMC at 1 Hz

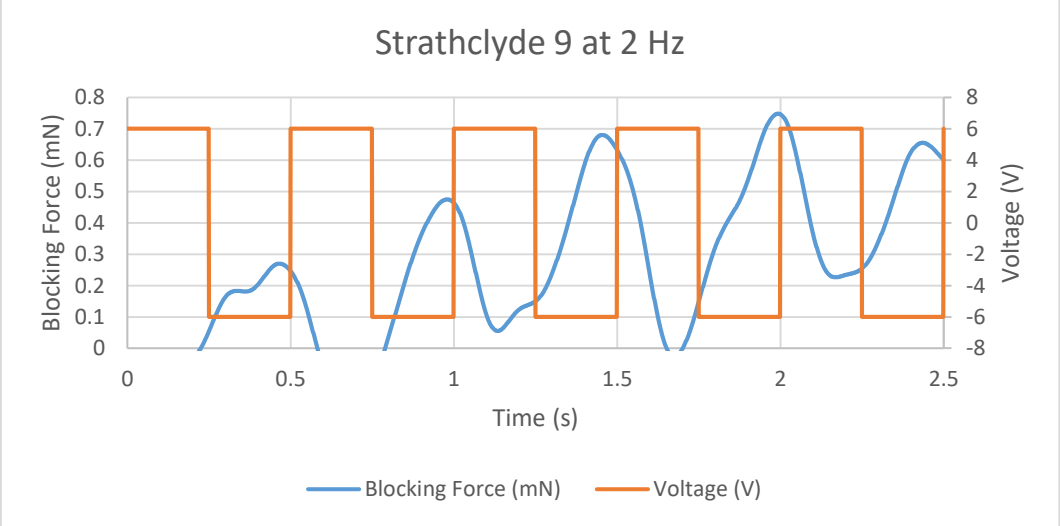

Figure 11.95 Blocking Force of Strathclyde 9 IPMC at 2 Hz

2.16 Strathclyde 10

Figure 11.96 to **Figure 11.99** show the blocking force diagram of Strathclyde 10 IPMC.

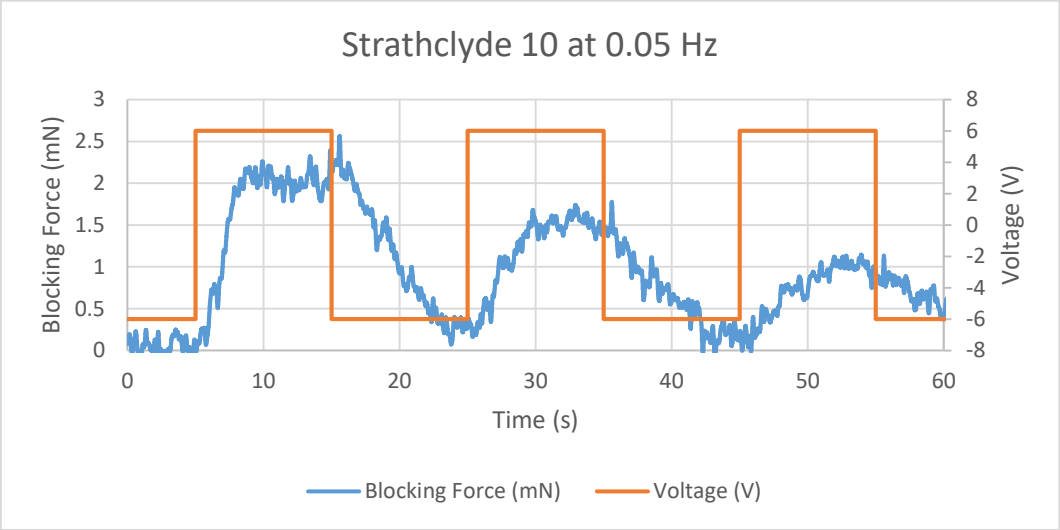

Figure 11.96 Blocking Force of Strathclyde 10 IPMC at 0.05 Hz

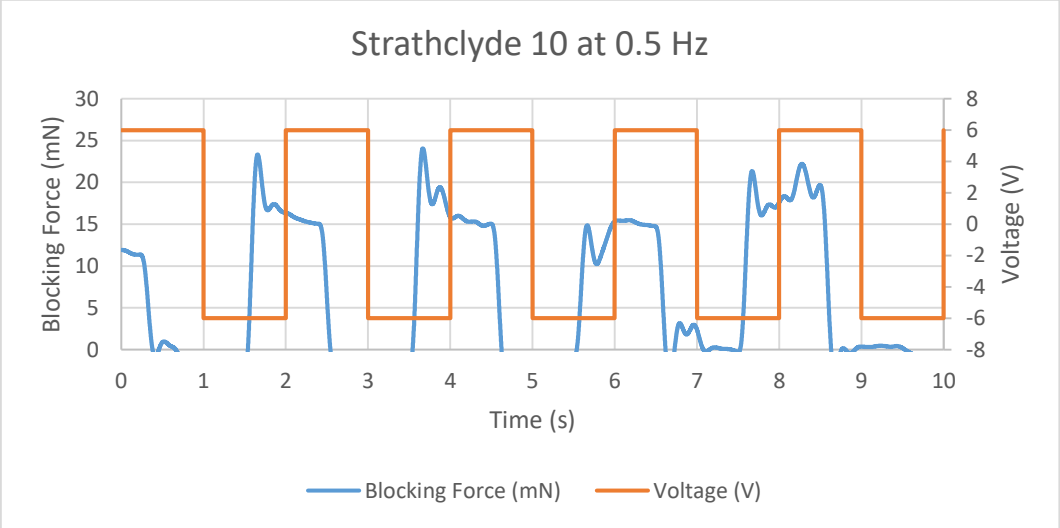

Figure 11.97 Blocking Force of Strathclyde 10 IPMC at 0.5 Hz

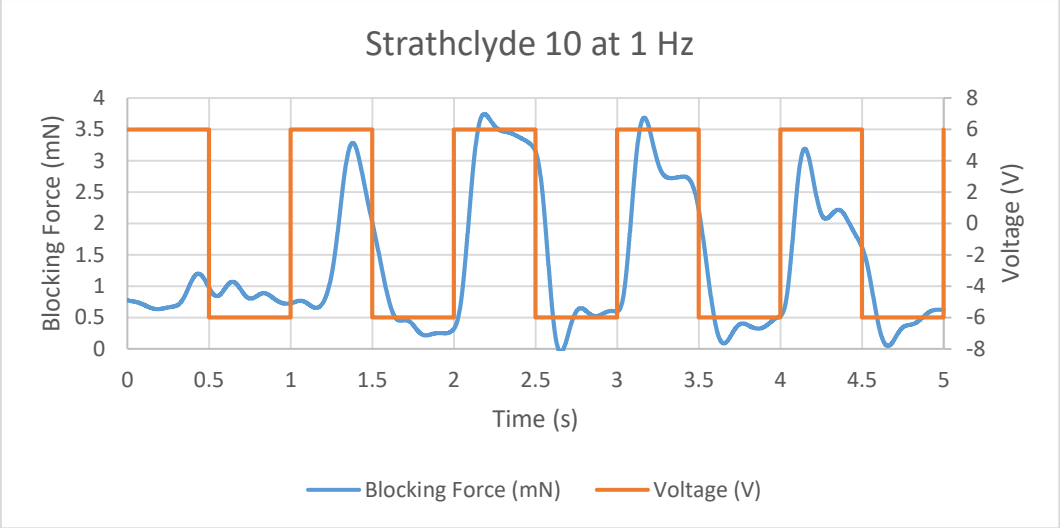

Figure 11.98 Blocking Force of Strathclyde 10 IPMC at 1 Hz

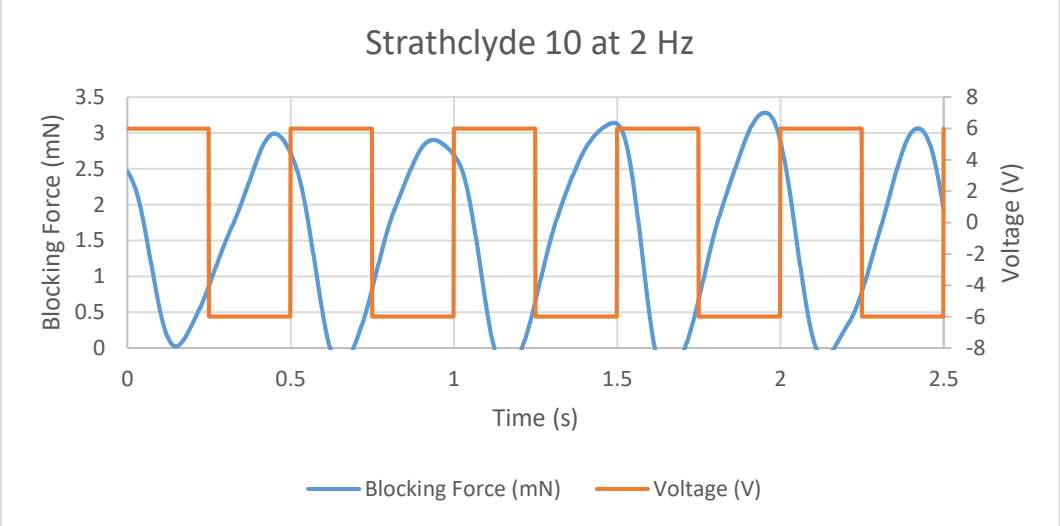

Figure 11.99 Blocking Force of Strathclyde 10 IPMC at 2 Hz

2.17 Strathclyde 11

Figure 11.100 to **Figure 11.103** show the blocking force diagram of Strathclyde 11 IPMC.

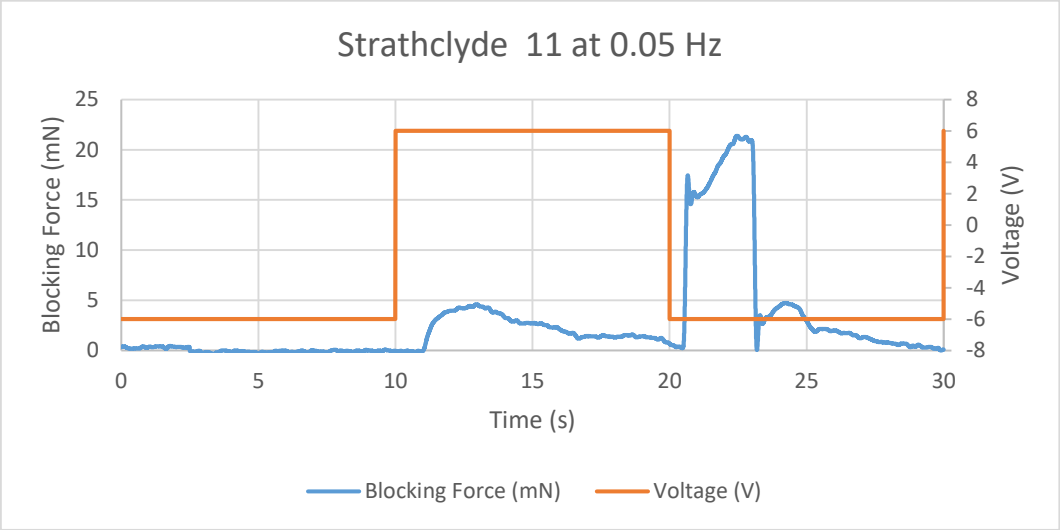

Figure 11.100 Blocking Force of Strathclyde 11 IPMC at 0.05 Hz

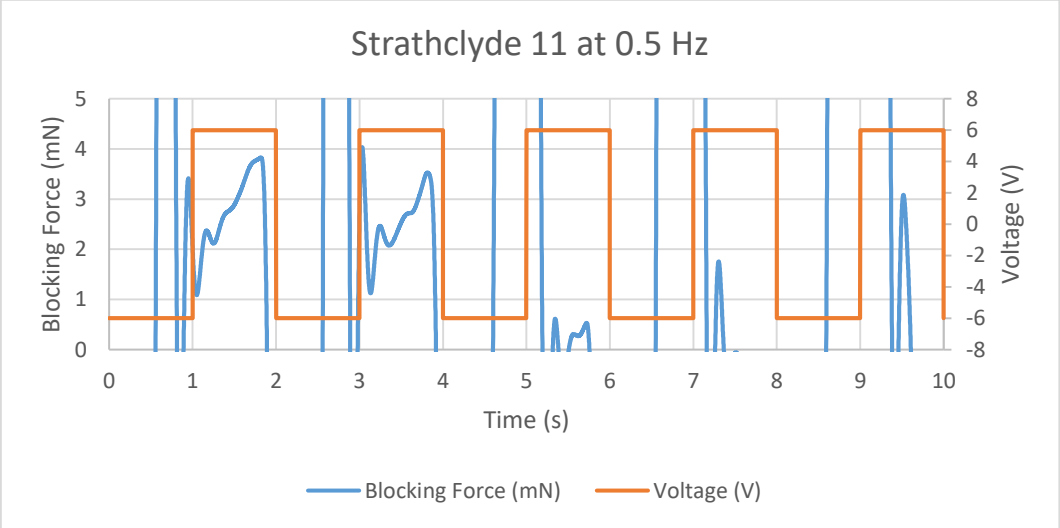

Figure 11.101 Blocking Force of Strathclyde 11 IPMC at 0.5 Hz

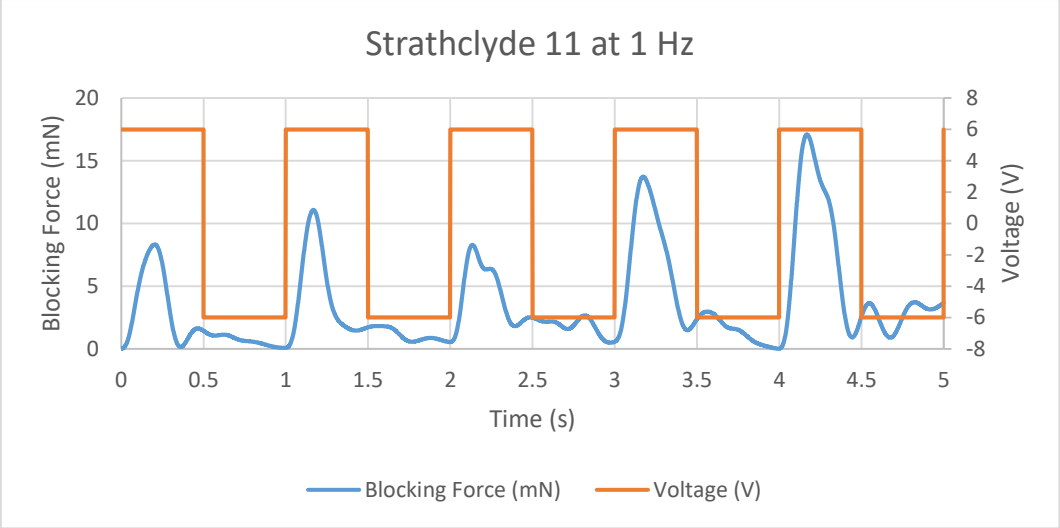

Figure 11.102 Blocking Force of Strathclyde 11 IPMC at 1 Hz

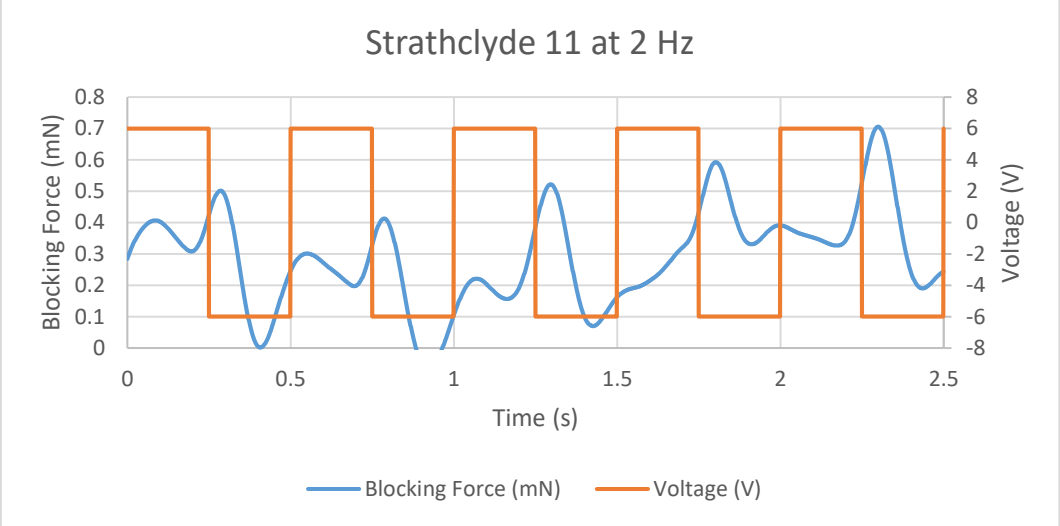

Figure 11.103 Blocking Force of Strathclyde 11 IPMC at 2 Hz

11.6 Power Harvesting Diagrams

Figure 11.104 shows the generated voltage from IPMC Commercial 1.

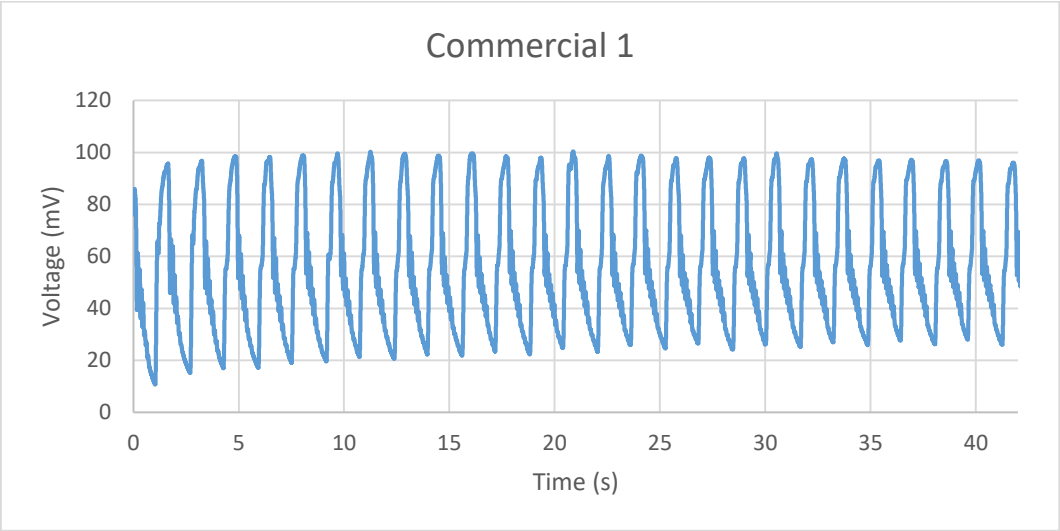

Figure 11.104 Voltage generated from Commercial 1

Figure 11.105 shows the generated voltage from IPMC Commercial 2.

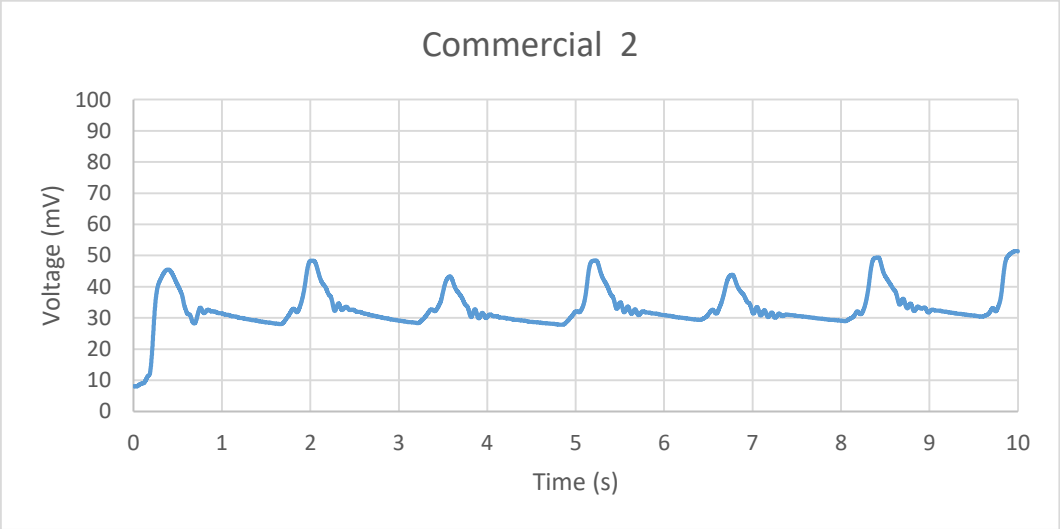

Figure 11.105 Voltage generated from Commercial 2

Figure 11.106 shows the generated voltage from IPMC Commercial 3.

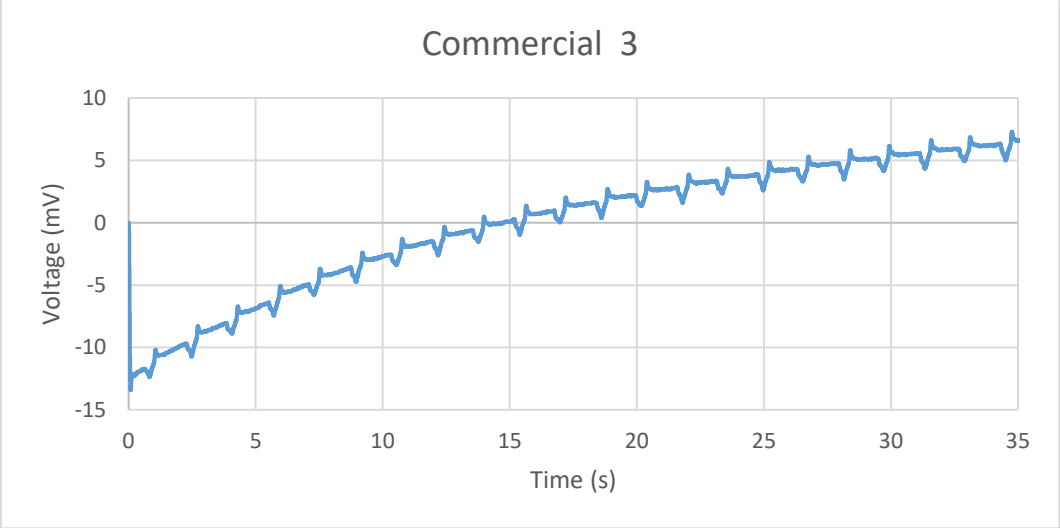

Figure 11.106 Voltage generated from Commercial 3

Figure 11.107 shows the generated voltage from IPMC Commercial 4.

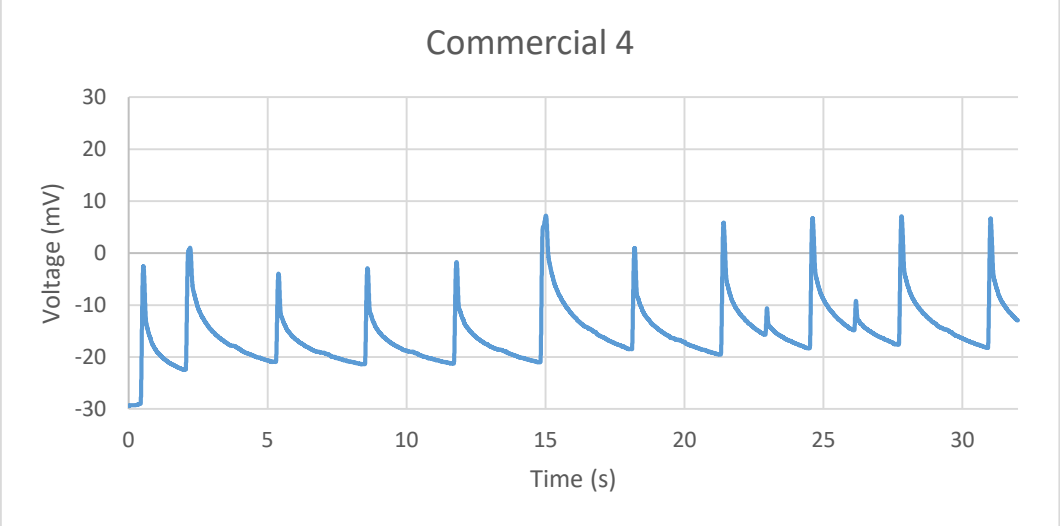

Figure 11.107 Voltage generated from Commercial 4

Figure 11.108 shows the generated voltage from IPMC Commercial 5.

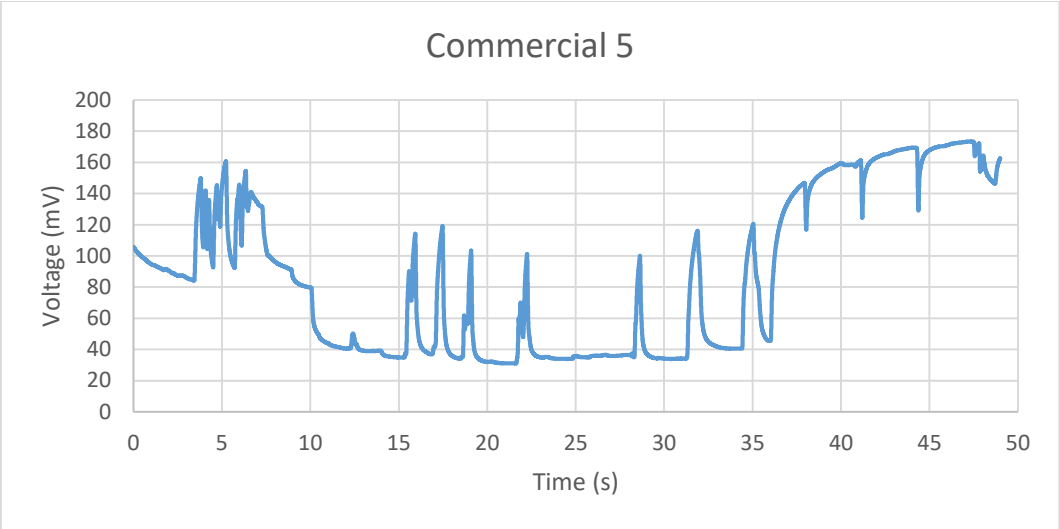

Figure 11.108 Voltage generated from Commercial 5

Figure 11.109 shows the generated voltage from IPMC Commercial 6.

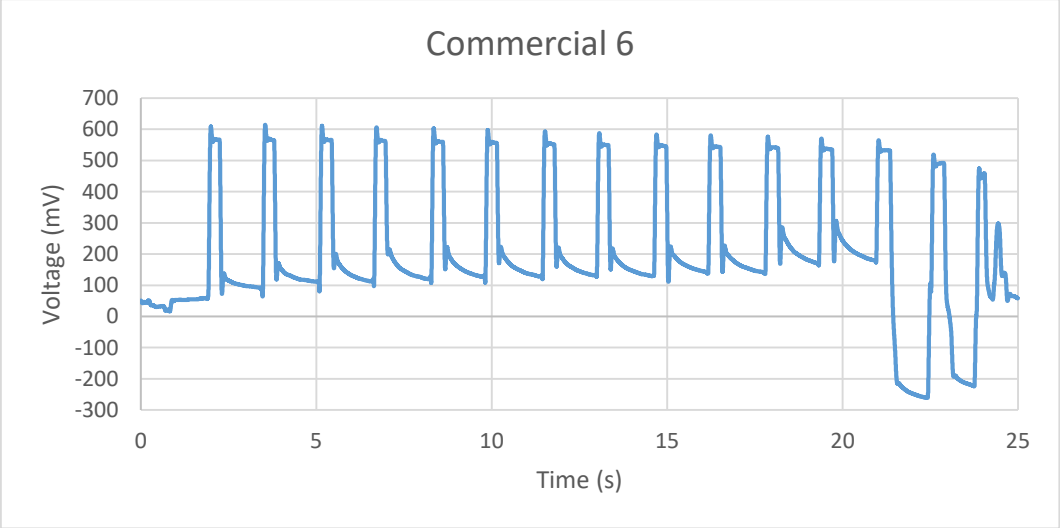

Figure 11.109 Voltage generated from Commercial 6

Figure 11.110 shows the generated voltage from IPMC Strathclyde 1.

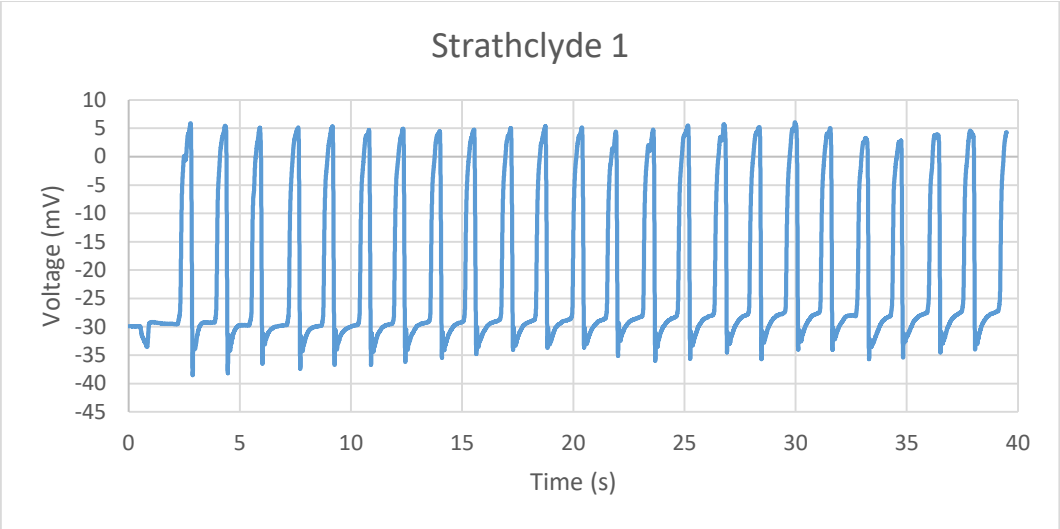

Figure 11.110 Voltage generated from Strathclyde 1

Figure 11.111 shows the generated voltage from IPMC Strathclyde 2.

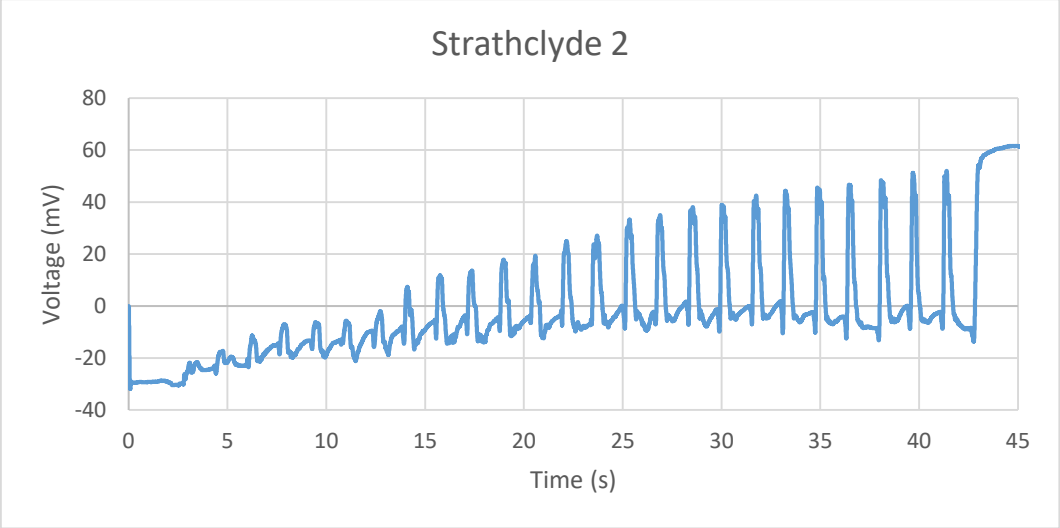

Figure 11.111 Voltage generated from Strathclyde 2

Figure 11.112 shows the generated voltage from IPMC Strathclyde 3.

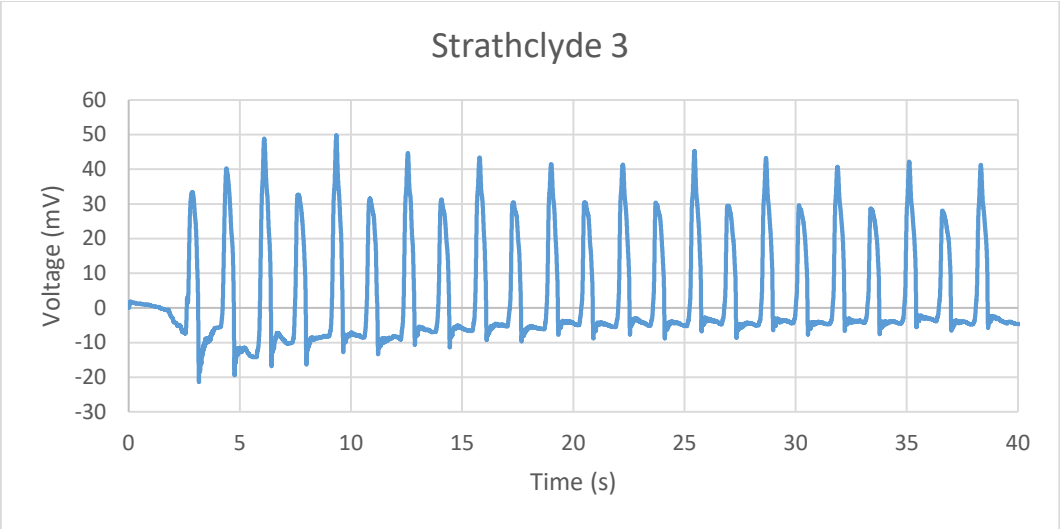

Figure 11.112 Voltage generated from Strathclyde 3

Figure 11.113 shows the generated voltage from IPMC Strathclyde 4.

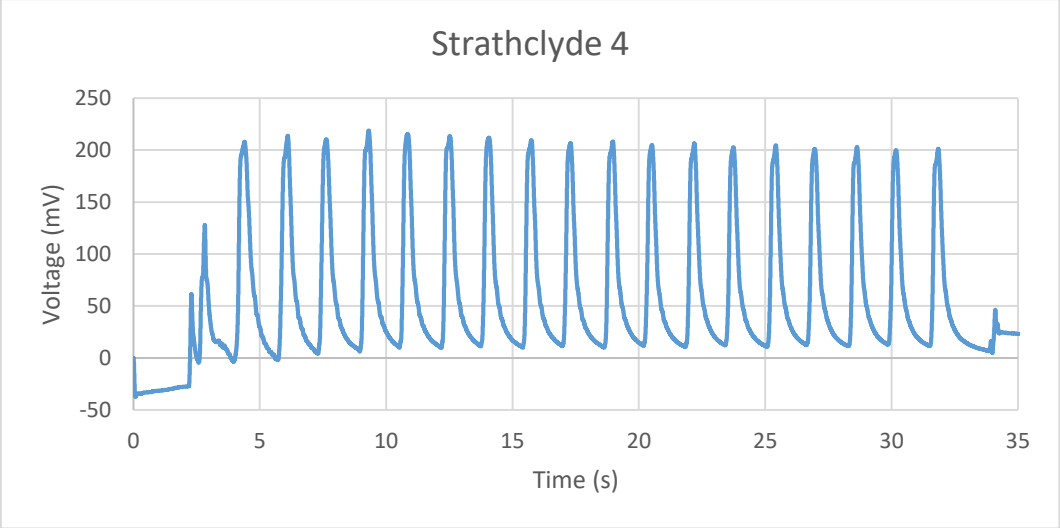

Figure 11.113 Voltage generated from Strathclyde 4

Figure 11.114 shows the generated voltage from IPMC Strathclyde 5.

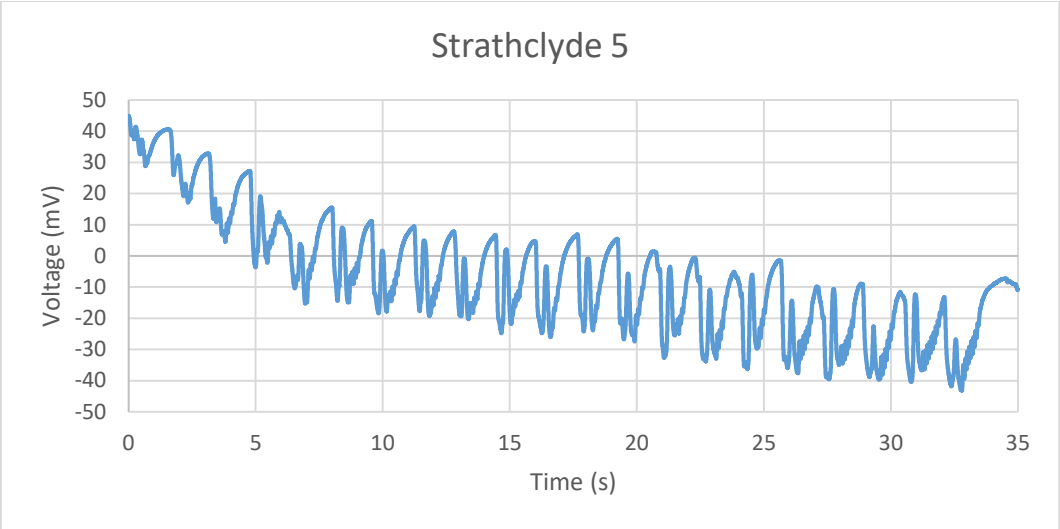

Figure 11.114 Voltage generated from Strathclyde 5

Figure 11.115 shows the generated voltage from IPMC Strathclyde 6.

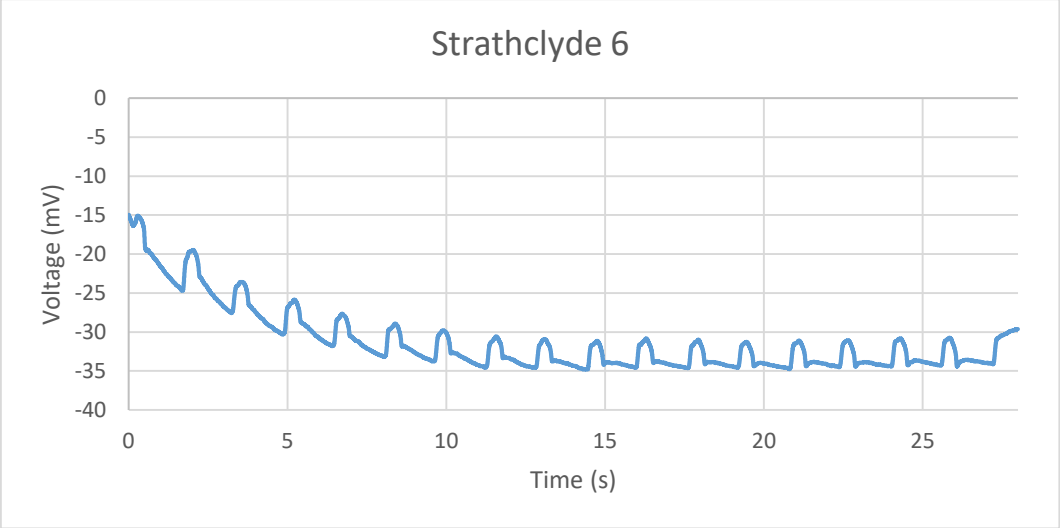

Figure 11.115 Voltage generated from Strathclyde 6

Figure 11.116 shows the generated voltage from IPMC Strathclyde 7.

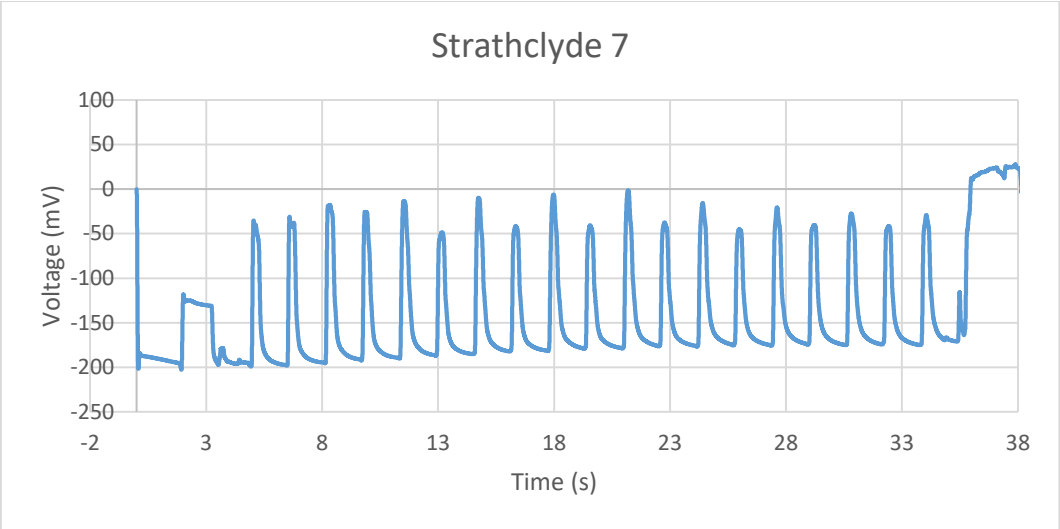

Figure 11.116 Voltage generated from Strathclyde 7

Figure 11.117 shows the generated voltage from IPMC Strathclyde 8.

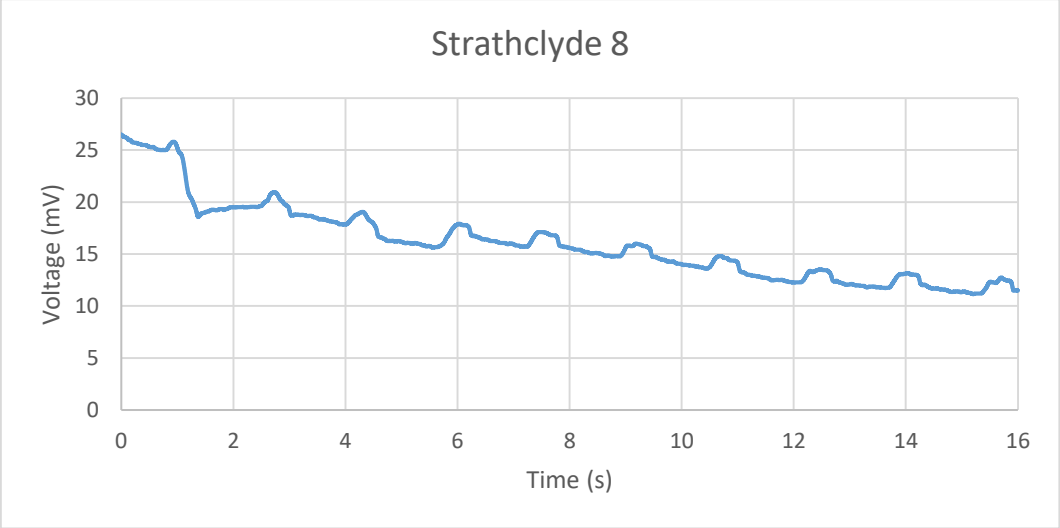

Figure 11.117 Voltage generated from Strathclyde 8

Figure 11.118 shows the generated voltage from IPMC Strathclyde 9.

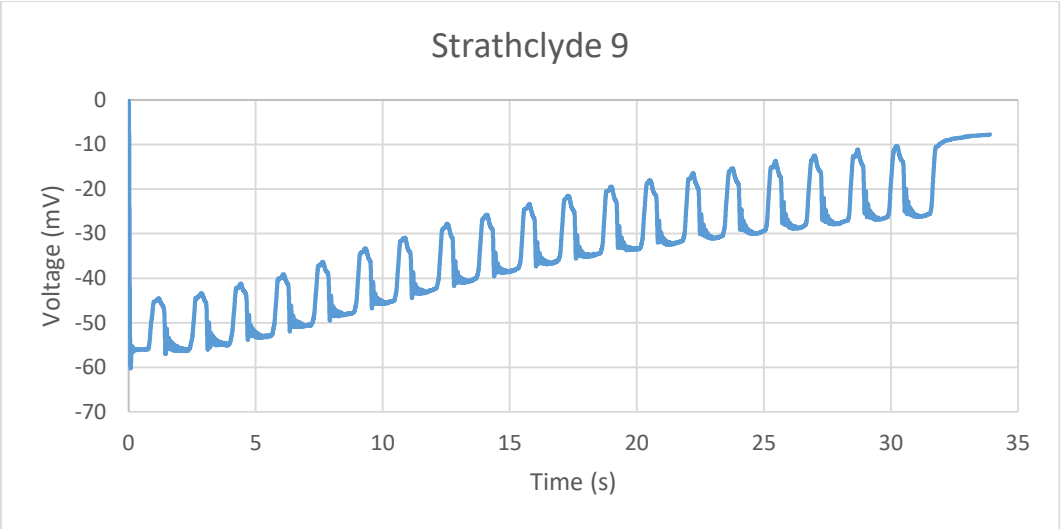

Figure 11.118 Voltage generated from Strathclyde 9

Figure 11.119 shows the generated voltage from IPMC Strathclyde 10.

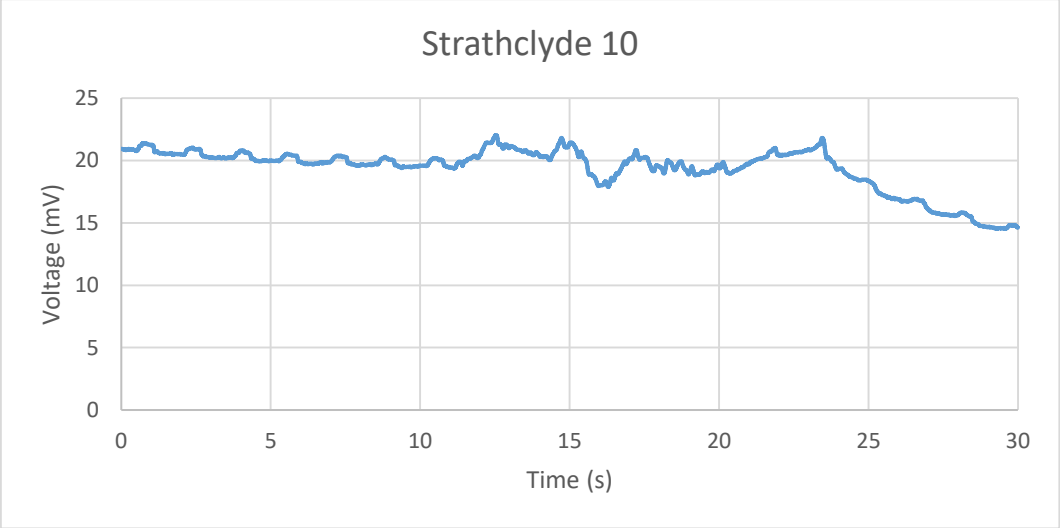

Figure 11.119 Voltage generated from Strathclyde 10

Figure 11.120 shows the generated voltage from IPMC Strathclyde 11.

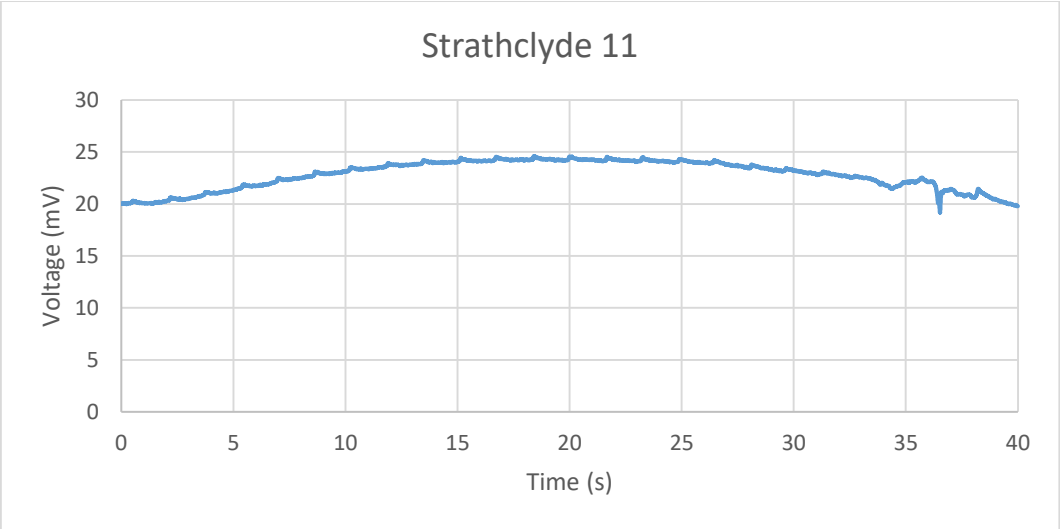

Figure 11.120 Voltage generated from Strathclyde 11

11.7 Power Balance

Table 11.2 showed a comparison between the generated and consumed current, voltage, and power of all IPMC samples

	Current generated (µA)	Current consumed (mA)	V_{rms} Generated (mV)	Voltage Consumed (V)	Power Generated (mW)	Power consumed (mW)
Commercial 1	2	100	56.56	6	0.113	600
Commercial 2	5	100	14.14	6	0.070	600
Commercial 3	12	110	1.41	6	0.016	660
Commercial 4	14	200	17.68	6	0.247	1200
Commercial 5	56	150	56.56	6	3.167	900
Commercial 6	100	500	353.50	6	35.350	3000
Strathclyde 1	15	200	28.28	6	0.424	1200
Strathclyde 2	65	100	42.42	6	2.757	600
Strathclyde 3	65	60	49.49	6	3.216	360
Strathclyde 4	74	40	141.40	6	10.46	240
Strathclyde 5	72	180	21.21	6	1.527	1080
Strathclyde 6	32	200	3.54	6	0.113	1200
Strathclyde 7	20	120	127.26	6	2.545	720
Strathclyde 8	4	150	2.12	6	0.008	900
Strathclyde 9	52	200	10.61	6	0.551	1200
Strathclyde 10	21	50	1.41	6	0.029	300
Strathclyde 11	15	300	1.41	6	0.021	1800

Table 11.2 Comparison between the generated and consumed electrical parameters

11.8 Force Sensor Datasheet

IPR – INSTITUT DE PRODUCTION & ROBOTIQUE

LABORATOIRE DE PRODUCTION MICROTECHNIQUE (LPM)
Thomas Maeder
CH-1015 LAUSANNE, Switzerland
☎: +41 21 693 58 23
Fax : +41 21 693 38 91
thomas.maeder@epfl.ch
http://ipr.epfl.ch

ÉCOLE POLYTECHNIQUE
FÉDÉRALE DE LAUSANNE

MilliNewton EPFL E.doc

Millinewton – generic OEM force sensor

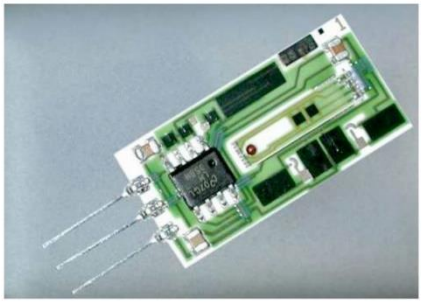

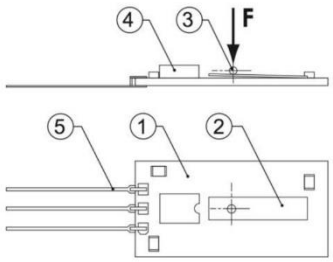

1 Base
2 Cantilever beam
3 Force centring ball
4 Amplifier
5 Contacts

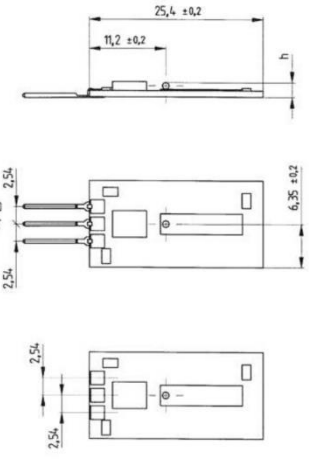

Highlights

- Force sensor for 400…2'000 mN in thick-film technology
- Amplified ratiometric output
- Entirely calibrated
  - Offset ± 1%
  - Span ± 1%
- Temperature compensated
- Base 25.4 x 12.7 mm

Applications

- Robotics
- Assembly
- Yarn tension measurement
- Indirect pressure measurement

Description

The MilliNewton force sensor is a simple and advantageous solution for the measurement of small forces.

The force is measured through bending of a cantilever beam, which carries a piezoresistive bridge. The electronics on the base carry out the signal amplification and deliver a voltage output which is a linear function of the force.

The sensor is entirely made in thick-film technology, which guarantees exceptional stability. Its design allows automated fabrication and calibration using standard production equipment.

Specifications (supply at U_s = 5.00V)

Parameter	Value	Unit
Environment	Air and non-aggressive gases	
Temperature range	0…70	°C
Humidity	0…80	%
Nominal force (short-term overload)	0… 400 (1'000) 0…1'000 (2'000) 0…2'000 (3'000)	mN
Offset: output at zero force	0.50 (10)	V (%U_s)
Span: output difference between nominal and zero force	3.00 (60)	V (%U_s)
Precision of offset	±1	% Span
Precision of span	±1	%
Temperature coefficient of offset	±0.02 (typical) ±0.05 (maximal)	%FS/K
Temperature coefficient of span	-0.02 (typical)	%/K
Response time	<10	ms
Weigth	1.4	g
Allowed electrical load	>50 <10	kΩ nF
Supply current	<3	mA

Variants

MilliNewton - X - XXXX - X - X - X

Type	13x3 beam	A			
	Others	B			
Force ranges	400 mN		0400		
	1'000 mN		1000		
	2'000 mN		2000		
Contacts	SIL pins			L	
	Contact pads			P	
Temperature	Compensated				C
	Uncompensated				U
Supply & output	5.00±0.25 V DC ratiométrique				A